

# Teleoperated and cooperative robotics : a performance oriented control design

**Citation for published version (APA):**

Denasi, A. (2015). *Teleoperated and cooperative robotics : a performance oriented control design*. [Phd Thesis 1 (Research TU/e / Graduation TU/e), Mechanical Engineering]. Technische Universiteit Eindhoven.  
<https://doi.org/10.6100/IR782390>

**DOI:**

[10.6100/IR782390](https://doi.org/10.6100/IR782390)

**Document status and date:**

Published: 20/01/2015

**Document Version:**

Publisher's PDF, also known as Version of Record (includes final page, issue and volume numbers)

**Please check the document version of this publication:**

- A submitted manuscript is the version of the article upon submission and before peer-review. There can be important differences between the submitted version and the official published version of record. People interested in the research are advised to contact the author for the final version of the publication, or visit the DOI to the publisher's website.
- The final author version and the galley proof are versions of the publication after peer review.
- The final published version features the final layout of the paper including the volume, issue and page numbers.

[Link to publication](#)

**General rights**

Copyright and moral rights for the publications made accessible in the public portal are retained by the authors and/or other copyright owners and it is a condition of accessing publications that users recognise and abide by the legal requirements associated with these rights.

- Users may download and print one copy of any publication from the public portal for the purpose of private study or research.
- You may not further distribute the material or use it for any profit-making activity or commercial gain
- You may freely distribute the URL identifying the publication in the public portal.

If the publication is distributed under the terms of Article 25fa of the Dutch Copyright Act, indicated by the "Taverne" license above, please follow below link for the End User Agreement:

[www.tue.nl/taverne](http://www.tue.nl/taverne)

**Take down policy**

If you believe that this document breaches copyright please contact us at:

[openaccess@tue.nl](mailto:openaccess@tue.nl)

providing details and we will investigate your claim.

# Teleoperated and cooperative robotics: a performance oriented control design

Teleoperated and cooperative robotics: a performance oriented control design

Alper Denasi

Alper Denasi



## INVITATION



You are cordially invited  
to the public defense of  
my PhD thesis

**Teleoperated and  
cooperative robotics:  
a performance oriented  
control design**

Date: **Tuesday,  
January 20, 2015**

Time: **16:00 hrs**

Place: **Auditorium  
Collegezaal 4  
Eindhoven University of  
Technology**

**Alper Denasi**  
alperden15@gmail.com

# Teleoperated and cooperative robotics: a performance oriented control design

Alper Denasi



The research reported in this thesis is part of the research program of the Dutch Institute of Systems and Control (DISC). The author has successfully completed the educational program of the Graduate School DISC.

This research was supported partially by the Remote Robotics project funded from a Pieken in de Delta grant of the Dutch Ministry of Economy.

Teleoperated and cooperative robotics: a performance oriented control design  
by Alper Denasi – Eindhoven University of Technology, 2015 – PhD thesis.

A catalogue record is available from the Eindhoven University of Technology Library.  
ISBN: 978-90-386-3738-9  
NUR: 992

Cover Design: Oscar Peña Ramírez.  
Reproduction: Ipskamp Drukkers B.V., Enschede, The Netherlands.

Copyright ©2015 by A. Denasi. All rights reserved.

# Teleoperated and cooperative robotics: a performance oriented control design

PROEFSCHRIFT

ter verkrijging van de graad van doctor  
aan de Technische Universiteit Eindhoven,  
op gezag van de rector magnificus prof.dr.ir. C.J. van Duijn,  
voor een commissie aangewezen door het College voor Promoties,  
in het openbaar te verdedigen  
op dinsdag 20 januari 2015 om 16.00 uur

door

Alper Denasi

geboren te Istanbul, Turkije

Dit proefschrift is goedgekeurd door de promotoren en de samenstelling van de promotiecommissie is als volgt:

voorzitter : prof.dr. L.P.H. de Goey  
promotor : prof.dr. H. Nijmeijer  
copromotoren : dr. A. Saccon  
: dr.ir. D. Kostić  
leden : Prof.Dr.-Ing. S. Hirche (Technische Universität München)  
: prof.dr. M. Kinnaert (Université Libre de Bruxelles)  
: prof.dr. K.M. van Hee  
: prof.dr. F.C.T. van der Helm (Technische Universiteit Delft)

*Dedicated to my parents  
and my sister:*

*Ester, Samson, and Lara*

*To the memory of my mother:*

*Ester Denasi*





# Contents

	<b>Summary</b>	<b>xi</b>
<b>1</b>	<b>Introduction</b>	<b>1</b>
1.1	The robot-environment interaction problem and teleoperation . . .	1
1.1.1	Control of contact tasks . . . . .	2
1.1.2	Cooperative manipulation . . . . .	5
1.1.3	Teleoperation. . . . .	11
1.2	Thesis overview . . . . .	12
1.2.1	Motivation. . . . .	12
1.2.2	Problem statement and contributions . . . . .	13
1.3	Outline . . . . .	16
<b>2</b>	<b>A hybrid impedance controller with finite-time stability characteristics</b>	<b>17</b>
2.1	Introduction. . . . .	17
2.2	Homogeneity of vector fields and finite-time stability . . . . .	19
2.3	Manipulator and contact dynamics model . . . . .	23
2.3.1	Manipulator kinematics and dynamics . . . . .	23
2.3.2	Environment model. . . . .	25
2.4	A hybrid impedance controller with finite-time stability characteristics . . . . .	26
2.5	Stability analysis for contact phase . . . . .	31
2.6	Robust stability analysis . . . . .	32
2.6.1	Uncertainty modelling . . . . .	33
2.6.2	Perturbed system stability analysis . . . . .	38
2.7	Illustrative simulations . . . . .	40
2.8	Experiments. . . . .	49
2.8.1	Experimental setup . . . . .	49
2.8.2	Experimental results . . . . .	51
2.9	Concluding remarks . . . . .	55

<b>3</b>	<b>Impedance controller for cooperative manipulation</b>	<b>59</b>
3.1	Introduction . . . . .	59
3.2	Modelling of cooperative manipulation systems . . . . .	61
3.2.1	Fixed grasp . . . . .	63
3.2.2	Non-fixed grasp . . . . .	65
3.3	A cascade controller for fixed grasps . . . . .	71
3.3.1	Motion control . . . . .	72
3.3.2	Internal force-based impedance control . . . . .	75
3.3.3	External force-based impedance control . . . . .	84
3.4	Numerical simulations . . . . .	87
3.4.1	Fixed grasp . . . . .	87
3.4.2	Non-fixed grasp . . . . .	89
3.5	Concluding remarks . . . . .	90
<b>4</b>	<b>Time-delay compensation using Internal Model Principle and Control Together</b>	<b>95</b>
4.1	Introduction . . . . .	95
4.2	Bilateral teleoperation architectures . . . . .	98
4.2.1	Position error, $(P_b - P_b)$ . . . . .	99
4.2.2	Kinesthetic force feedback, $(P - p_b F)$ . . . . .	100
4.2.3	Four channel, $(P_b F_b - P_b F_b)$ . . . . .	100
4.3	Internal Model Principle and Control Together (IMPACT) . . . . .	100
4.3.1	Control structure . . . . .	103
4.3.2	Controller design . . . . .	104
4.3.3	Robustness analysis . . . . .	108
4.4	Numerical simulations . . . . .	110
4.5	Experiments . . . . .	114
4.5.1	Experimental setup . . . . .	114
4.5.2	Illustrative simulations . . . . .	115
4.5.3	Experimental results . . . . .	119
4.6	Concluding remarks . . . . .	124
<b>5</b>	<b>Conclusions and recommendations</b>	<b>127</b>
5.1	Conclusions . . . . .	127
5.2	Recommendations . . . . .	129
<b>A</b>	<b>Proofs for hybrid impedance control with finite-time stability characteristics</b>	<b>131</b>
A.1	Proof of Proposition 2.14 . . . . .	131
A.2	Derivation of the bound $\rho(x, t)$ in (2.90) . . . . .	134
A.3	Investigation of a strict Lyapunov function for (2.97) . . . . .	137
A.4	Proof of Lemma 2.23 . . . . .	139
A.5	Proof of Lemma 2.24 . . . . .	140

---

<b>B</b>	<b>Additional simulation and experimental results for hybrid impedance control with finite-time stability characteristics</b>	<b>141</b>
B.1	Additional simulation results . . . . .	141
B.2	Additional experimental results . . . . .	144
<b>C</b>	<b>Technical drawings and force sensor calibration</b>	<b>149</b>
C.1	Force sensor calibration . . . . .	149
C.2	Technical drawings for mechanical interface . . . . .	150
<b>D</b>	<b>Further information about unilateral constraints</b>	<b>155</b>
D.1	Set-valued force laws for frictional contact . . . . .	155
D.2	Impact . . . . .	158
D.3	Modelling nonlinear mechanical systems with dry friction and impact using measure differential inclusions . . . . .	160
<b>E</b>	<b>Impedance controller for cooperative manipulation: Lemmas</b>	<b>163</b>
<b>F</b>	<b>Impedance controller for cooperative manipulation: Additional Simulations</b>	<b>167</b>
<b>G</b>	<b>Reference trajectory</b>	<b>171</b>
	<b>Bibliography</b>	<b>173</b>
	<b>Samenvatting</b>	<b>187</b>
	<b>Acknowledgements</b>	<b>189</b>
	<b>Curriculum Vitae</b>	<b>191</b>



# Summary

## **Teleoperated and cooperative robotics: a performance oriented control design**

---

This thesis deals with two important subfields of robotics, namely interaction control and telerobotics. Interaction control is studied in two different settings, where a single robot is used in the first one and multiple robots are used in the second one. The latter is also known as the cooperative manipulation problem. Teleoperated systems have been a popular research subject in the robotics community for several decades. They are utilized in applications that take place in hazardous environments such as nuclear power plants for nuclear waste disposal, in hospitals to perform minimally invasive surgery, in space to perform repair of orbital modules. Recently, in rapidly aging societies there is also an increasing effort towards integrating robots into domestic environments. Cooperative manipulation, on the other hand, deals with tasks such as assembly, transportation of large or heavy objects which single manipulators most likely fail to execute.

The problem of finite time control of interaction control tasks is addressed in the first part of this thesis. Robotic tasks such as cooperative manipulation are comprised of multiple subtasks such as approaching a given object and grasping it. A suitable reference trajectory is designed for each phase to execute the complete task. Good measures of performance for the subtasks are the convergence speed of the actual trajectories to the desired ones and ultimate bound on the error between them. Depending on the characteristics of the closed-loop equation, different settling times can be obtained. A specific case is when this settling time is finite, and thus the error vanishes in finite-time. Such a strategy can be beneficial, since it guarantees that the task is performed exactly as it is commanded. For this pur-

pose, a continuous finite-time stable force tracking impedance control algorithm is proposed. The manipulator rotational kinematics is described by using a suitable quaternion representation. The case when the environment can be modelled as a linear spring with unknown constant stiffness coefficient and rest position, is investigated. The robustness of the algorithm against uncertainties in the robot dynamic model is analyzed.

In the second part of the thesis, cooperative manipulation of a rigid object handled by non-redundant robots, with stiff links and joints located on a fixed base, is investigated. Control design for such cooperative systems is more complicated compared to controlling a single manipulator, since the interaction between the object, manipulators, and the environment with which the object is in contact, should also be considered. For safe and successful execution of the task, besides the motion of the object and contact forces induced by the environment, internal forces which are a good measure of the object's mechanical stresses, should be accommodated. Two different modelling approaches are investigated. In the first approach the manipulators hold the object via fixed grasp points, where it is assumed that there is no relative motion between the object and the manipulators. The second approach takes into account the relative motion between the manipulators and the object at the contact points. A cascade control law, comprised of motion control, internal and object impedance control loops is designed for the first case. Guidelines are provided on how to tune the parameters of the internal and object impedance relationships. Special attention is given to prove the uniqueness of the solutions of the closed-loop system when investigating its asymptotic stability.

The last part of this thesis focuses on time delay compensation and disturbance rejection in a commonly used bilateral teleoperation architecture. In a teleoperated scenario, the actual task is carried out by a slave manipulator located at a remote environment where it receives commands sent by a human operator through a communication channel. Even though teleoperation is beneficial to remove the operator's presence from the environment, it comes with a price to pay. Since the operator's commands to and the sensor signals from the remote robot to improve his/her awareness are transmitted through a communication channel, they would be subject to communication delay. Time delays can hamper the stability of the telerobotic system, if not accounted for in the control design. For this purpose, a predictor based algorithm, which is robust with respect to model uncertainty and external disturbances, is designed. The design is based on the combination of an internal model control and internal model principle. A pragmatic rationale is applied in the design of local controllers which is based on frequency response function measurements and a pole placement method. The approach is validated experimentally on a setup comprised of two industrial robots.

# Chapter I

## Introduction

**Abstract** The interaction problems for single and multi robot systems as well as teleoperation are introduced first in this chapter. Then, the cases for single and multiple manipulators and teleoperation are detailed separately in the following sections. The chapter ends with the formulation of the research objective and main contributions of this thesis.

### 1.1 The robot-environment interaction problem and teleoperation

The second half of the twentieth century witnessed the rise of robotic and automated systems in industry. In the last decade or so, with the advance of computers and with the reduction of the costs of related hardware and software, robots find use in different fields such as agriculture, underwater and recently in households. Robots used in the industry were initially only able to execute simple tasks (e.g. pick and place), due to the lack of advanced sensing capabilities. Thanks to the progress in sensor technologies, robotic systems are becoming more intelligent, and the environments in which they can operate are gradually shifting from static towards dynamic ones. Examples of such sensors are tactile and force sensors and vision systems (e.g. a camera). As robotic systems become widespread in different domains, they are expected to execute diverse and challenging tasks. In order to successfully accomplish them, such systems should be robust and safe and they should demonstrate a sufficient level of flexibility. A robotic or an automated system is considered to be robust, if it is capable to operate under varying operating conditions without changing its initial structure. Robots used in industrial applications should be safe in the sense that they should neither damage themselves nor the objects present in their environments. Furthermore, for applications concerning the robots working nearby humanbeings, the safety of the humans has to be insured. Flexibility of a robotic system is its ability to be reassigned quickly and easily in the case of changing manufacturing demands. One particular class of

the aforementioned systems is robotic manipulators, which are mechanisms composed by a chain of rigid bodies (i.e. the links) connected by joints [158]. In this thesis, considering the previously mentioned notions of robustness and flexibility, particular aspects of

1. control of contact tasks, e.g. grinding, mechanical assembly,
2. cooperative manipulation,
3. teleoperation

for robotic manipulators are addressed.

An important class of manipulation tasks that involve physical interaction between the manipulator and environment are the contact tasks. To successfully accomplish such tasks, the manipulators should have improved sensory capabilities (e.g. sensing interaction forces) [132]. In the case of cooperative manipulation, a task is carried out by multiple manipulators rather than by a single one. Teleoperation refers to robotic systems that are commanded from a distance. These systems may have different applications, such as supporting humans in the execution of tasks that are dangerous or even impossible by conventional means.

In the following subsections, control of contact tasks, cooperative manipulation and teleoperation are explained in more detail.

### 1.1.1 Control of contact tasks

Following the successful applications of manipulators in tasks where physical interaction with the environment is not the main intention, such as spot-welding, spray painting and palletizing, it has become logical to start investigation of robot applications in contact tasks. Control of contact tasks has been investigated in the last three decades [132, 157], with a particular desire to enhance autonomy of manipulators operating in unstructured (or semi-structured) environments. In a structured environment, configuration of objects with which the robot interacts is known precisely, unintended collisions do not occur, the ambient conditions (e.g. lighting, temperature) do not vary significantly, and etc. Applications like spot-welding and spray painting can be executed using pre-planned motion profiles. Robot control strategies that consider only desired motion profiles are less suitable to utilize in unstructured environments. This is due to the fact that the success of this strategy depends heavily on accurate modelling of the manipulator and the environment. Any modelling error or uncertainty eventually result in less



accurate motion planning and consequently unexpected contact forces/moments may arise. In classical motion control, high bandwidth servo control designs are used to increase robustness against modeling and parameter uncertainties and disturbances. However, when both the manipulator and the environment are very stiff, the contact forces/moments can reach very high values causing damage of either one or both.

Risks of damage can be reduced if the manipulator can comply with the environment, i.e. if it can modify its response based on the contact force/moments. Compliant behavior can be achieved either by mechanical design or by analog/digital control or both. Grinding (see Figure 1.1(a)), polishing, deburring and mechanical assembly (see Figure 1.1(b)) are examples of industrial applications that require a manipulator to be in contact with the environment most of the time. Manipulators in domestic applications (i.e. home robotics), that attract ever increasing attention in the recent years, are also used to execute contact tasks such as wiping surfaces (see Figure 1.1(c)) and opening doors (see Figure 1.1(d)).

Contact forces can be actively controlled in two different ways, indirectly or directly [157]. Indirect schemes use motion control as an implicit mean to regulate the contact forces whereas direct schemes utilize explicit force feedback loops [132]. Indirect techniques are impedance (or admittance) control [66] and stiffness (or compliance) control (a simplified type of impedance control) [124]. The direct techniques include hybrid motion/force control [117], inner/outer motion/force control [41] and parallel position/force control [35]. Detailed modelling of the environment can be avoided if indirect schemes are used, however the position tracking performance can deteriorate [132]. Among the direct methods, hybrid motion/force control is quite common, where its success depends on whether explicit constraint equations defining the environment geometry exist [157]. Another challenge for hybrid controllers is to establish contact with the environment in a stable way [170].

In a complete contact task there are three phases, free motion, contact motion and the transition phases. As the name suggests the first one refers to the case where the manipulator moves in spaces free of obstacles, the second one is related to motion along certain surfaces, whereas the last one considers the transitions to and from free and contact motion phases which involve impact phenomena [25]. An important problem associated with the control of contact tasks is the transition phase in which the manipulator comes from free motion into contact with the environment. Successfully completing the transition phase is important to execute a complete contact task.

There are many factors that affect the robustness and performance of a manipulator in contact tasks. These are in general related with availability of different

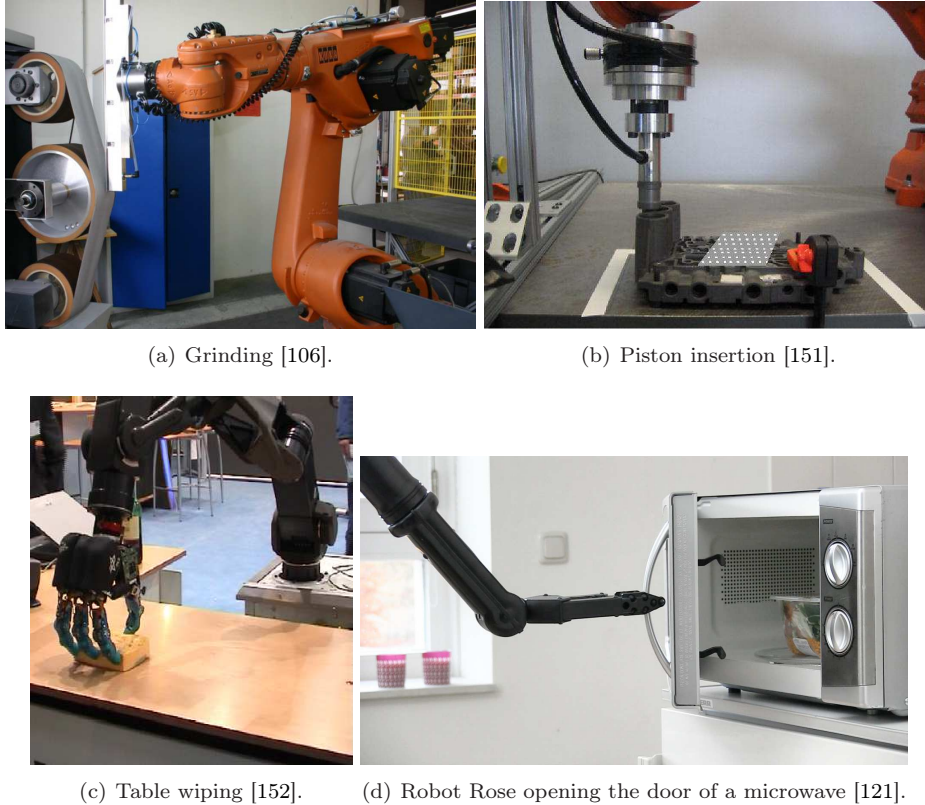


**Figure 1.1** Examples related to contact tasks.

sensory feedback data, and knowledge of models of the manipulator and the environment. Many variants of indirect and direct contact force control algorithms can be found in the control literature. Control algorithms for contact tasks can be classified as non-model (or model free) based, model-based, adaptive, robust and robust-adaptive schemes as shown in the Table 1.1. This classification is made based on several criteria. First, the properties of the dynamic model of the manipulator used in the stability analysis are determined. Whether, how and to what extent such a model is used in the control design is investigated. Second, the mechanical properties of the end-effector used in this model are determined. This is done by checking whether the effect of compliance, be it due to a force sensor or another source such as a soft cover is included to the model. Third, they are classified into categories depending on the way they define the desired trajectories (known-distorted-modified) and/or they decompose the task space (estimate-measured online-identified online) [72]. Next, the mechanical and geometric prop-

erties of the environment the manipulator is supposed to make contact with are classified. This classification is done based on whether the environment is modeled as compliant or (idealized) rigid one. After that whether special attention is given to the rotational parameterizations is determined. This is important for contact tasks that consider not only contact forces but also contact moments (or torques) since characterization of rotational contact parameters (e.g. stiffness) is not as straightforward as for translational ones [30]. Next considerations are type of measurements/estimations and whether the effect of measurement noise or estimation error is taken into account in the control design and stability analysis. The achieved stability results are classified regarding free and contact motion, and transition phases of the contact task. A final item is related to whether experimental results are presented and on what type of surfaces these experiments are done.

In the last decade, there has been an increasing interest on intentionally introducing mechanical compliance in the design of manipulators for service applications. This is driven by the desire to increase safety, to damp the impact forces and to provide a better force/torque transmission to the manipulators' joints by reducing the effects backlash, dry friction, etc. Examples of such designs that can be found in the literature are series elastic actuators (SEA) and variable stiffness/damping/impedance actuators (see [155]). These devices usually have additional internal control loops to regulate the torques delivered to the joints, or joint stiffness/damping/impedances. The control of such devices is beyond the scope of this thesis.

### 1.1.2 Cooperative manipulation

Multi-arm robotic systems are a popular subject of active research in recent years [31, 147]. These systems become required due to limited payload capacity of single-arm systems in certain tasks and need for additional equipment (e.g. fixtures) besides the single arm manipulators. Practical examples are heavy payload transportation (see Figure 1.2(a) and Figure 1.2(b)) and fixtureless multi-part assembly in industry (see Figure 1.2(c)) and in space (see Figure 1.2(d)), or folding of cloths and preparing meals in the domestic domain (see Figure 1.2(e) and Figure 1.2(f)). Cooperative manipulators can have significant advantages compared to a single robot. If multiple manipulators are used to carry a heavy or large payload, for example, the weight can be distributed among several smaller and cheaper robots and the payload can be handled more safely. Mechanical assembly, an important process in many industries (e.g. automotive), can be performed faster and flexibly. Special fixtures whose main purpose are to support certain parts of the assembly are often used in this process. With the help of multiple manipulators where one

or more play the role of the fixture, the number of special fixtures can be reduced or ultimately their use can be eliminated completely. In many cooperative tasks, the manipulators grasp a common object and also bring it into contact with the

**Table 1.1** Overview of literature related to control of contact tasks

Prop.\Alg.	Non-model based	Model based	Adaptive	Robust	Robust-adaptive
Dyn. model					
Rig. link	[14]	[110, 111] [91, 144] [87, 164]	[38, 127, 159] [39, 40, 45] [6]	[165, 167]	[36, 169]
Flex. link	[76]				
Flex. joint			[39]		
Act. model			[40]		
Known struc.		[110, 111] [91, 144] [87, 164]	[6]	[165, 167]	[36, 169]
Part. known structure			[38, 127, 159] [39, 40, 45]		
Kno. prm.		[110, 111] [91, 144] [87, 164]	[45]		
Unkno. prm.	[14]		[38, 127, 159] [6, 39, 40]		[36, 169]
Uncer. prm.				[165, 167]	
Ext. dist.			[38, 159]	[165, 167]	[36, 169]
End-effector					
Rigid	[14]	[110, 111] [91, 144] [87, 164]	[38, 39, 159] [6, 40]	[165, 167]	[36, 169]
Compliant	[14]		[45, 127]		
Pos. target					
Known		[110, 111] [91]	[38, 39, 127] [6, 40, 159]	[165]	[169]
Modified		[91, 164]			
Distorted			[45]	[167]	[36]
Setpoint	[76]	[110]	[38, 39, 159]		
			[45]		
Time-vary.	[14]	[91, 111]	[38, 39, 127]	[165, 167]	[36, 169]
Continued on Next Page...					

Table 1.1 – Continued					
Prop.\Alg.	Non-model based	Model based	Adaptive	Robust	Robust-adaptive
traject.		[87, 164]			
Nrm. vect.					
Measured		[164]			
Estimated		[91]			
Const. est.	[14, 76]	[110, 111]	[38, 39, 127] [6, 40, 159]	[165, 167]	[36, 169]
Identified			[45]		
Cont. type					
Sing. pnt.	[14, 76]	[110, 111] [91, 164]	[38, 39, 127] [40, 45, 159]	[165, 167]	[36, 169]
Mult. pnt.					
Cont. fric.	[14]	[91, 164] [87]	[45]	[167]	[36, 169]
Rigid					
Known loc.		[110, 111]		[165]	
Uncer. loc.		[91]		[167]	[36]
Compliant					
Known struc.	[76]		[38, 39, 127] [6, 159]	[165]	[169]
Part. known structure					
Unkno. struc.	[14]				
Kno. prm.			[159]	[165]	
Unkno. prm.	[14]		[38, 39, 127]	[165]	[169]
Uncer. prm.					
Cont. surf. geometry					
Curved			[39, 45]		
Planar	[14]	[144]	[38, 39, 127] [6, 159]		
Mov. plan.		[91]			
General	[76]	[110, 111] [91]		[165, 167]	[36, 169]
Rotat. prm.		[87]			
Measurements					
Position	[14, 76]	[110, 111] [91, 144]	[38, 39, 127] [40, 159]	[165, 167]	[36, 169]
Continued on Next Page...					

Table 1.1 – Continued					
Prop.\Alg.	Non-model based	Model based	Adaptive	Robust	Robust-adaptive
		[87, 164]	[6, 45]		
Velocity	[14, 76]	[110, 111] [91, 144]	[39, 40, 45] [6]	[165, 167]	[36, 169]
Accel.		[144]			
Cont. force	[14, 76]	[91, 111] [144, 164]	[38, 39, 127] [40, 159]	[165, 167]	[36, 169]
Estimations					
Position					
Velocity			[38]		
Accel.					
Cont. force			[6]		
Meas. noise, est. error					
Stab. result					
Free mot. ph.					
Bounded.					
Asymp. stab.					
Exp. stab.		[111]			
Fin.-time stab.					
Contact trans. phase					
Sim./Exp.			[38, 39, 159]		
Expon. stab.		[111]			
Fin.-time stab.		[110]			
Contact ph.					
Bounded.	[14]		[38, 39, 159] [40]	[167]	[169]
Asymp. stab.		[91, 164]	[6, 45, 127]	[165]	
Exp. stab.		[111]			
Fin.-time stab.		[110]			
Exp. results					
Curved		[164]			
Planar	[76]	[111, 164]	[38, 159]		
Moving planar					
General					

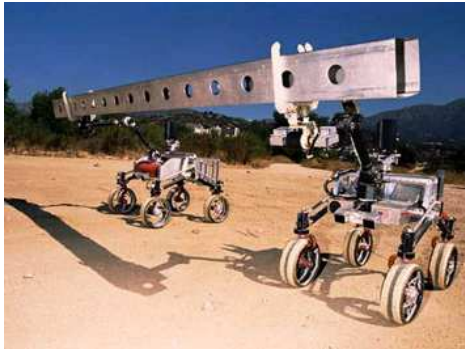
environment. Some examples are scribing, painting, grinding, polishing, contour following, and object aligning.

Although in cooperative manipulation usually a commonly grasped object is considered, in [135] a distinction is made between non-coordinated (i.e. each arm performs different tasks), coordinated (i.e. each arm performs a different part of the same task) and bimanual (in the case of two manipulators) manipulation. The analysis and control of the first class is the same as in the case of individual manipulators for which there is an abundance of literature.

Cooperative manipulation tasks can be categorized according to the grasp points as fixed and non-fixed [135]. In the first case, it is assumed that the object is rigidly attached to the manipulators, thus the contact constraints are bilateral. In the latter case, relative motion between the object and the manipulators is possible, thus the contact constraints are unilateral. Although contact cannot be broken when considering bilateral constraints, it is still possible to model holding an object using grippers with fixed grasp points if the object has specific features (e.g. the ear of a coffee mug). In such a case contact can be broken if the grippers are opened.

Different control laws have been developed for cooperative manipulators such as master/slave, hybrid position/force, input-output and input-state linearization, impedance and passivity based control. In master/slave control, one manipulator (master) is motion controlled and in charge of imposing the desired motion of the object, whereas the others (slaves) are force controlled and required to follow the motion imposed by the master. Problems such as the requirement for the slave(s) to be sufficiently compliant and how to assign the roles of master and slave(s) to the manipulators dynamically for certain tasks are commonly found in literature [149]. Hybrid position/force control is one of the first non-master/slave control algorithms used for cooperative manipulation [62, 150]. It considers transforming the motion and force variables of the end-effectors of the manipulators into object motion and internal/external forces, such that they can be controlled separately [148, 149]. The drawbacks of this controller are related to the incorrect use of orthogonality [46] and contact compliance [57].

Input-output and input-state linearization are model-based compensation methods which realize a decoupled linear system that can be controlled using well known linear techniques. Using this technique controllers have been designed in the joint space [143] and in the operational (or task) space [34, 74, 75]. In [79], a reduced order dynamical model is obtained by constraint elimination which is used to design a controller that decouples the force and motion controlled degrees of freedom.



(a) Two NASA rovers handling a large beam [106].



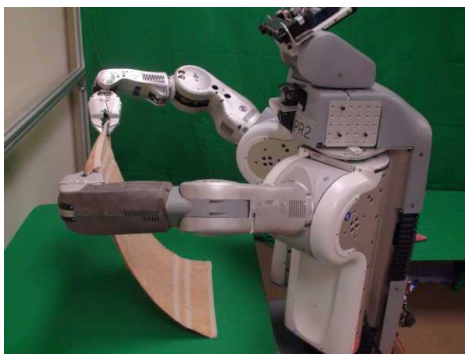
(b) Model of two Stanford Assistant Mobile Manipulators handling a large object [151].



(c) Motoman SDA10 assembling a chair [120].



(d) Cooperative Manipulation Testbed of the Robonaut program [104].



(e) PR2 folding towels [95].



(f) Robot Rose preparing a meal [121].

**Figure 1.2** Examples related to cooperative manipulation.



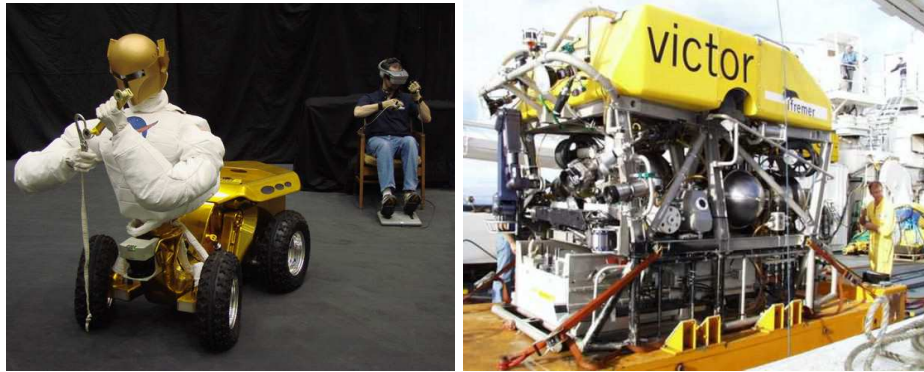
Impedance control is another very widely used technique for controlling cooperative manipulation tasks. Its use in cooperative manipulation can be categorized into three groups; by enforcing an impedance relationship between the grasped object and the external environment or by enforcing an impedance relationship between the grasped object and the manipulators or a combination of both. The approaches in the first category consider controlling the external forces that arise from the contact of the grasped object with the environment and usually require the knowledge of object accelerations (either by measurement or by estimation) and an object's inertial parameters [99, 126]. For the second type, the emphasis is on controlling the internal forces of the grasped object instead of controlling the external forces [23, 78]. Only very few geometric parameters of the object are required for the operation of this type of controllers, knowledge of object inertial parameters are usually not required. The last category considers controlling both the internal forces of the object and contact forces between the object and an external environment. The impedance controllers for regulating internal forces [23] and external forces [126] are combined in [28, 32].

Besides the previously mentioned approaches, passivity based [160] or adaptive [103, 139] or robust control algorithms [168] for cooperative manipulators also exist in the literature.

### 1.1.3 Teleoperation

Started as a means to allow for safety purposes, a human operator to perform a given task without being physically present on the location where the task is executed, teleoperation can be considered as one of the earliest applications of robotics [107, 128]. Teleoperation is utilized in research domains such as medicine (e.g. surgery), underwater, space, agriculture, search and rescue, and nuclear. The prefix *tele* means "at a distance" and in its all generality refers to the separation of the user from the environment where the task is executed [107]. This separation can be desired due to the fact that the environment is dangerous or it is larger (e.g. excavation [142]) or smaller (e.g. microassembly [21]) in comparison to the user such that he/she can manipulate it. Consequently, teleoperated systems can be separated into two sites, the local (the operator) and the remote (the environment). In Figure 1.3, two examples of teleoperated systems from two diverse fields are shown.

In some teleoperation applications further human intervention may be required [107]. Based on the level autonomy or intelligence they possess, teleoperated systems can be categorized into three groups; direct control, shared control, supervisory control. These control architectures are summarized in Figure 1.4.



(a) Robonaut [106].

(b) Remotely operated vehicle, Victor 6000 [151].

**Figure 1.3** Examples related to teleoperated systems.

Among these categories, direct control has the lowest level of autonomy, whereas supervisory control has the highest one. Many different architectures exist for direct control which are explained in greater detail in Section 4.2. In a direct control architecture, the operator uses a device called master manipulator, which is often a joystick, to provide motion commands to a slave manipulator which executes the actual task at the remote side.

## 1.2 Thesis overview

### 1.2.1 Motivation

Time efficiency of the execution of contact tasks is not well explored in the research community. Control systems designed to execute such tasks are usually constructed in a hierarchical manner. For the successful execution of the task, it is required to complete each subtask in finite time, which guarantees that the task is performed exactly as it is commanded. A way to accomplish this goal is to design the low-level controllers in the hierarchy to have finite-time convergence.

As explained in Section 1.1.2, since there are two main categories of cooperative manipulation tasks, the methods for modelling them are also different. In the case of cooperative manipulation with non-fixed grasp points, for which relative motion is permissible, a general model which is capable of describing the transitions to and from non-contact and contact is required. Concerning the cooperative

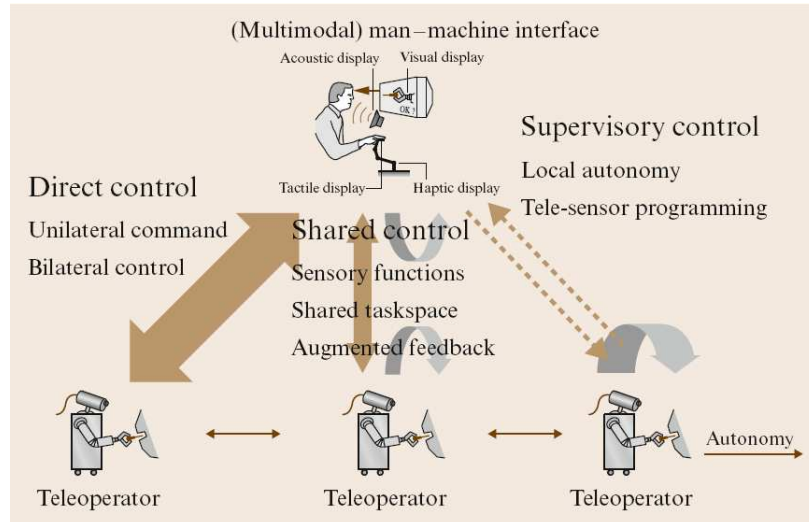


**Figure 1.4** Different concepts for telerobotic control architectures [107].

manipulation tasks with fixed-grasp points, contact can be established once by very slowly approaching the object and after grasp is achieved, detachment will unlikely occur. Therefore, investigation of complex modelling approaches for this case is not required. In this case, the most relevant problems to be studied are the ones described in Section 1.1.2, following desired motion trajectories for the grasped object and controlling the internal and external forces which act on the object.

Time delays in the communication channel due to for instance long distances complicate the controller design for bilateral teleoperated systems. They can reduce the performance of teleoperated systems or ultimately destabilize them. Another factor that can affect the performance of a teleoperated system is the disturbance acting on the slave manipulator located at the remote site.

### 1.2.2 Problem statement and contributions

In the scope of robotics problems described in the previous section, this thesis focuses on control design strategies for the following problems:

1. robust and fast tracking of desired motion and force trajectories designed for a manipulator executing contact tasks.

2. cooperative manipulation of a common object held via fixed-grasp points which can come in contact with an external environment.
3. time-delay compensation and disturbance rejection in bilaterally teleoperated manipulators.

Furthermore, this thesis investigates suitable modelling approaches for cooperative manipulation tasks with non-fixed grasp points.

For the given research focus, the main contributions of this work may be stated as follows:

1. The existing approaches in the literature for controlling contact tasks are classified according to the control methods, certain characteristics of the manipulator and environment and some practical issues. This classification is carried out from control theory perspective.
2. The finite-time stability concept is integrated into a hybrid impedance control algorithm. Suitable impedance characteristics are selected in accordance with the constraints of the environment, in order to track desired position and force trajectories. The position and force tracking performance is improved by means of an inverse-dynamics based finite time convergent impedance control law. Finite time convergence is achieved by means of an input chattering-free continuous controller. The contact transitions are executed using a non-switching controller. The control law is capable of dealing with the unknown constant stiffness coefficient and rest position of the environment.
3. This thesis presents approaches for modelling cooperative manipulators in the case of fixed and non-fixed grasps. For the non-fixed grasp case, the transitions from free motion to constrained motion and vice versa are discussed with the help of unilateral constraints. For the fixed grasp case, a cascade controller is designed that is capable of controlling the motion, internal forces and external forces acting on an object. The inner loop of this cascade control scheme contains individual inverse dynamics controllers to track reference trajectories for each manipulator. An impedance controller driven by internal forces and desired object trajectories determines the reference trajectories for the inverse dynamics controllers. An external force based impedance controller determines the desired object trajectories. One of the main contributions of this work is the stability proof. It is shown that, using the proposed object impedance controller, any desired contact force can be achieved.

4. The time-delay compensation and disturbance rejection in position error based bilateral teleoperation is addressed. The combination of internal model control and internal model principle is applied to the aforementioned problem. The benefits of this approach are robustness against model uncertainties and external disturbances. The master and slave manipulators contain non-linear compensators in their local feedback controllers which allows us to deal with some practical issues such as friction or gravity compensation. A pragmatic rationale is applied in the design of local controllers which is based on frequency response function measurements and a pole placement method. The number of controller parameters is kept small for easy tuning of the controller. Robust stability of the designed controller is analysed by means of the Nyquist criterion. The effectiveness of the approach is demonstrated in experiments.

The following list of publications summarizes the main results obtained during this PhD project:

#### **Journal article**

- Denasi, A., Kostić, D. and Nijmeijer, H. (2013). Time delay compensation in bilateral teleoperations using IMPACT. *IEEE Transactions on Control Systems Technology*, 21(3), 704-715. [44]

#### **Journal article in preparation**

- Denasi, A., Kostić, D., Saccon, A. and Nijmeijer, H. A hybrid impedance controller with finite-time stability characteristics (Chapter 2).

#### **Conference proceedings**

- Denasi, A., Kostić, D. and Nijmeijer, H. (2010). An application of IMPACT structure to bilateral teleoperations. In *49th IEEE Conference on Decision and Control (CDC)*, pages 1985-1990, dec. 2010. [43]
- Heck, D.J.F., Kostić D., Denasi A. and Nijmeijer H. (2013). Internal and external force-based impedance control for cooperative manipulation. In *Proceedings of the European Control Conference (ECC 2013)*, July 17-19, 2013, pages 2299-2304. [63]

- Pena Ramirez, J., Denasi, A., Rodriguez-Angeles, A., Alvarez, J., Nijmeijer, H. and Aihara, K. (2014). Controlled Synchronization: A Huygens' Inspired Approach. The 19th World Congress of the International Federation of Automatic Control, Cape Town, South Africa, 24-29 August 2014. [118]

### 1.3 Outline

The thesis is organized as follows. In Chapter 2, an impedance controller is proposed which is capable of tracking a desired position and contact force in finite time. The control algorithm is validated through extensive simulations and experiments.

Chapter 3 introduces two different categories of cooperative manipulation tasks, namely grasps with fixed points and non-fixed points and suitable modelling approaches for them. Furthermore, for the first category a cascaded control algorithm is proposed which is capable of controlling the motion and internal forces of the object, and the contact forces between the object and an external environment.

In Chapter 4, a controller is proposed which is capable of compensating for the time-delays in bilateral teleoperations. It can also reject disturbances from a known class that act at the output of the slave manipulator. The control algorithm is validated through extensive simulations and experiments.

Finally, concluding remarks and recommendations for future research directions are presented in Chapter 5.

## Chapter 2

# A hybrid impedance controller with finite-time stability characteristics

**Abstract** Hybrid impedance control is a suitable technique to perform interaction tasks. In this chapter, we propose a hybrid continuous contact-force-tracking impedance control law with finite-time stability characteristics. We investigate our approach on non-redundant manipulators with rigid links and non-flexible joints. A quaternion representation is used for the rotational part of the impedance controller. The controller gains are designed based on the knowledge of the environment geometry. The algorithm is illustrated in simulations with a well-known Puma 560 robot manipulator. Furthermore, experimental results on a three degrees of freedom robot are presented.

### 2.1 Introduction

The ability to handle interaction between manipulator and environment is one of the key elements for a successful manipulation task [157]. A sole motion control algorithm may not be adequate for such tasks, since modelling errors and uncertainties, mostly related to the environment, can result in high contact forces. These can cause damage to the manipulator and environment. Therefore, it is necessary to control both the positions and forces.

The interaction control strategies can mainly be categorized into two groups: indirect force control and direct force control [131]. Among indirect force control approaches, impedance control is commonly used to perform manipulation tasks including complex ones such as multiple robots performing cooperative manipulation [23]. In impedance control, a desired dynamic relationship between the motion and contact force of the end-effector of the manipulator and the environment is achieved, instead of controlling them separately [66]. This dynamic relationship is analogous to a linear six degrees of freedom second order mechanical system

characterized by desired inertia, damping and stiffnesses. Hybrid position/force control is among the common direct force control approaches in which the configuration space of the manipulator is divided into position and force controlled subspaces [117]. A combination of these two approaches called hybrid impedance control was first proposed in [7] which applies impedance control in the position controlled subspace contrary to hybrid position/force control. The algorithm also allows to introduce desired inertia and damping in the force controlled subspace and does not switch during contact transition [92].

Robotic tasks such as cooperative manipulation and grasping are generally comprised of multiple subtasks. These subtasks have to be executed chronologically and/or simultaneously. Control systems designed to execute such tasks are usually constructed in a hierarchical manner. Therefore, for the successful execution of the task, it is required to complete each subtask in finite time, which guarantees that the task is performed exactly as it is commanded. However, this cannot be achieved by using an asymptotically stable linear second order closed-loop dynamics, even though it converges exponentially (i.e. fast) to its equilibrium [16]. Therefore, we investigate non-Lipschitz dynamical systems in order to provide finite-time convergence to the desired dynamical behavior, which would guarantee zero tracking error after a finite time. Furthermore, for practical purposes, it is preferable to use continuous control laws that do not exhibit chattering in the input signals. Another appeal of finite-time convergent controllers is their high precision tracking performance [140]. The concept of continuous finite-time control is first investigated by Haimo in [58] although earlier attempts to obtain finite-time response systems exist [119]. Bhat and Bernstein established a rigorous framework on finite-time stability of continuous autonomous systems in [18]. Further results on this topic with a particular application to robotics related problems can be found in the references [71, 140, 141]. Finite-time convergence concept is also applied to force control tasks by using a dynamical terminal sliding mode control law in [112]. The type of impedance models used in this chapter are actually not uncommon in the literature where in [59] the stiffness of human fingertips tissue is modeled using a nonlinear model (fractional power of its argument) and also in [163] damping of limb motion is again modelled using fractional powers.

Sliding mode control theory is applied to impedance control, to achieve the desired impedance behavior in the presence of perturbations and disturbances, in [33, 52]. However, in these implementations, the desired dynamics on the sliding surface is represented by a linear system. Therefore, even when the sliding surfaces are reached in finite time, the position and force errors will go to zero in infinite time.

In this chapter, we propose a continuous finite-time stable force tracking impedance control algorithm which is designed in Cartesian space. We investigate our approach on non-redundant manipulators with rigid-links and joints without flex-



ibilities. The rotational part of the impedance controller is designed using the quaternion representation. It is assumed that the environment with which the robot interacts, can be represented as a linear spring. The controller stiffness, damping and inertias are selected in accordance with the constraints of the environment. Furthermore, the desired trajectory is designed such that the desired force and position are tracked in constrained and unconstrained directions, simultaneously. The control law is capable of dealing with the unknown constant stiffness coefficient and rest position of the environment. The robustness of the algorithm against uncertainties in the robot dynamic model is investigated in simulations and experiments and guidelines are presented how to investigate the uniform ultimate boundedness of the tracking error trajectories.

The main contributions of this chapter are: i) the original, to the best of the author's knowledge, integration of the finite-time stability concept to a hybrid impedance control algorithm, ii) the design of suitable impedance characteristics in accordance with the constraints of the environment, in order to track desired position and force trajectories, iii) improvement of the position and force tracking performance by means of an inverse-dynamics based finite time convergent impedance control law, iv) achievement of finite time convergence by means of an input chattering-free continuous control, v) executing contact transitions with a non-switching controller.

This chapter is organized as follows. Important lemma's, theorems, definitions and properties related to finite-time stability are introduced in Section 2.2. In Section 2.3, we present the relevant background information about manipulator modeling and the environment with which it interacts. A hybrid impedance control algorithm with finite-time stability characteristics is proposed in Section 2.4. The stability analysis for the controller is presented in Section 2.5. Guidelines to analyze the robust stability of the closed-loop system are given in Section 2.6. An illustrative simulation case study on a Puma 560 manipulator is given in Section 2.7. Experimental results related to a three degrees of freedom robot arm are introduced in Section 2.8. Conclusions are discussed in Section 2.9.

## 2.2 Homogeneity of vector fields and finite-time stability

In this section, homogeneity of continuous vector fields and finite-time stability of continuous autonomous systems are introduced. These concepts are used in the following sections in the stability proofs. Consider the system of differential equations [17, 18],

$$\dot{x}(t) = f(x(t)), \quad (2.1)$$

where  $f : \mathcal{D} \rightarrow \mathbb{R}^n$  is continuous on an open neighborhood  $\mathcal{D} \subseteq \mathbb{R}^n$  of the origin and  $f(0) = 0$ . A continuously differentiable ( $\mathcal{C}^1$ ) function  $x : I \rightarrow \mathcal{D}$  is called a *so-*

lution of (2.1) on the interval  $I \subseteq \mathbb{R}$  if  $x$  satisfies (2.1) for all  $t \in I$ . We assume that (2.1) possesses unique solutions in *forward time* for all initial conditions [18]. This assumption together with the continuity of  $f$  guarantees the continuous dependency of the solution on initial conditions. We denote by  $\varphi(\cdot, x_0)$  or, alternatively,  $\varphi^{x_0}(\cdot)$  the unique solution of (2.1) satisfying  $\varphi(0, x_0) = x_0$ . Sufficient conditions for forward-time uniqueness of non-Lipschitzian systems can be found in [2], [37], [48] (e.g. Peano's uniqueness theorem, not to be confused with Peano's existence theorem). The following definition of finite-time stability appears in [18].

**Definition 2.1.** *The origin of (2.1) is called a finite-time-stable equilibrium, if there exists an open neighborhood  $\mathcal{N} \subseteq \mathcal{D}$  of the origin and a settling-time function  $T : \mathcal{N} \setminus \{0\} \rightarrow (0, \infty)$ , such that the following statements hold:*

- (i) *Finite-time convergence: For every  $x_0 \in \mathcal{N} \setminus \{0\}$ ,  $\varphi^{x_0}$  is defined on  $[0, T(x_0))$ ,  $\varphi^{x_0}(t) \in \mathcal{N} \setminus \{0\}$  for all  $t \in [0, T(x_0))$ , and  $\lim_{t \rightarrow T(x_0)} \varphi^{x_0}(t) = 0$ .*
- (ii) *Lyapunov stability: For every open neighborhood  $\mathcal{U}_\varepsilon$  of 0 there exists an open subset  $\mathcal{U}_\delta$  of  $\mathcal{N}$  containing 0 such that, for every  $x_0 \in \mathcal{U}_\delta \setminus \{0\}$ ,  $\varphi^{x_0}(t) \in \mathcal{U}_\varepsilon$  for all  $t \in [0, T(x_0))$ .*

The origin is said to be a globally finite-time-stable equilibrium if it is a finite-time-stable equilibrium with  $\mathcal{D} = \mathcal{N} = \mathbb{R}^n$ .

The sufficient conditions for finite-time stability obtained by using a Lyapunov function involving a scalar differential inequality (i.e. comparison lemma) can be summarized in the following lemma.

**Lemma 2.2.** *Suppose there exists a continuous function  $V : \mathcal{D} \rightarrow \mathbb{R}$  such that the following conditions hold:*

- (i)  *$V$  is positive definite.*
- (ii) *There exist real numbers  $c > 0$  and  $\alpha \in (0, 1)$  and an open neighborhood  $\mathcal{V} \subseteq \mathcal{D}$  of the origin such that*

$$\dot{V}(x) + c(V(x))^\alpha \leq 0, \quad x \in \mathcal{V} \setminus \{0\}. \quad (2.2)$$

Then the origin is a finite-time-stable equilibrium of (2.1). Moreover, if  $\mathcal{N}$  is as in Definition 2.1 and  $T$  is the settling-time function, then

$$T(x) \leq \frac{1}{c(1-\alpha)} V(x)^{1-\alpha}, \quad x \in \mathcal{N}, \quad (2.3)$$

and  $T$  is continuous on  $\mathcal{N}$ . If in addition  $\mathcal{D} = \mathbb{R}^n$ ,  $V$  is proper, and  $\dot{V}$  is negative in  $\mathbb{R}^n \setminus \{0\}$ , then the origin is a globally finite-time-stable equilibrium of (2.1).

Investigation of the literature related to finite-time stability and stabilization indicates that besides the sliding-mode techniques, concepts related to homogeneous systems are often employed [19, 70, 88]. The necessity for such an approach arises due to the difficulty of using Lemma 2.2 to prove finite-time stability of the system (2.1) which requires finding an explicit Lyapunov function  $V(x)$  (also known as a strict Lyapunov function in the literature). The properties of homogeneous systems introduced in this section are used to investigate the nominal stability of the closed-loop system as explained in Section 2.5.

**Definition 2.3** (Dilation). *Dilation  $\Delta_\lambda^r$  is a mapping depending on positive definite dilation coefficients  $r = (r_1, r_2, \dots, r_n)$  ( $r_i > 0, 1 \leq i \leq n$ ), which assigns to every  $\lambda > 0$  a global diffeomorphism*

$$\Delta_\lambda^r(x) = (\lambda^{r_1}x_1, \dots, \lambda^{r_n}x_n)^T, \quad (2.4)$$

where  $(x_1, \dots, x_n)$  are suitable coordinates on  $\mathbb{R}^n$ .

**Definition 2.4** (Homogeneity). *Let  $(r_1, \dots, r_n) \in \mathbb{R}^n$  with  $r_i > 0, i = 1, \dots, n$ . Let  $V : \mathbb{R}^n \rightarrow \mathbb{R}$  be a continuous function.  $V$  is said to be homogeneous of degree  $\sigma \in \mathbb{R}$  with respect to the dilation  $\Delta_\lambda^r(x_1, \dots, x_n) = (\lambda^{r_1}x_1, \dots, \lambda^{r_n}x_n)$ , if, for any given  $\lambda > 0$ ,*

$$V(\lambda^{r_1}x_1, \dots, \lambda^{r_n}x_n) = \lambda^\sigma V(x), \quad \forall x \in \mathbb{R}^n. \quad (2.5)$$

Let  $f(x) = (f_1(x), \dots, f_n(x))^T$  be a continuous vector field.  $f(x)$  is said to be homogeneous of degree  $\kappa \in \mathbb{R}$  with respect to the dilation  $\Delta_\lambda^r(x_1, \dots, x_n) = (\lambda^{r_1}x_1, \dots, \lambda^{r_n}x_n)$  if, for any given  $\lambda > 0$ ,

$$f_i(\lambda^{r_1}x_1, \dots, \lambda^{r_n}x_n) = \lambda^{\kappa+r_i} f_i(x), \quad i = 1, \dots, n, \quad \forall x \in \mathbb{R}^n. \quad (2.6)$$

System (2.1) is said to be homogeneous if  $f(x)$  is homogeneous.

**Definition 2.5** (Homogeneous norm). *A homogeneous norm is a map  $x \rightarrow \|x\|_{r,p}$  of degree 1 with respect to the dilation  $\Delta_\lambda^r$  and satisfies the following equation:*

$$\|x\|_{r,m} = \left( |x_1|^{\frac{m}{r_1}} + \dots + |x_n|^{\frac{m}{r_n}} \right)^{\frac{1}{m}} \quad (2.7)$$

where  $m > \max\{r_1, \dots, r_n\}$ .

**Lemma 2.6.** *Suppose that the system (2.1) is homogeneous of degree  $\kappa$ . Then the origin of the system is finite-time stable if it is asymptotically stable, and  $\kappa < 0$ .*

According to the theorems of Rosier [122] and Zubov [172] the existence of a strict homogeneous Lyapunov function for the dynamics (2.1) is guaranteed which is introduced in [70] with the following lemma.

**Lemma 2.7.** *Suppose that the system (2.1) is homogeneous of degree  $\kappa$  w.r.t. the dilation  $\Delta_\lambda^r(x_1, \dots, x_n) = (\lambda^{r_1}x_1, \dots, \lambda^{r_n}x_n)$ ,  $f$  is continuous and  $x = 0$  is its asymptotically stable equilibrium. Then, for any positive integer  $j$  and any real number  $\sigma_0 > j \cdot \max\{r_1, \dots, r_n\}$ , there is a  $C^j$  homogeneous function  $V$  of degree  $\sigma_0$  with the same dilation such that  $V$  is positive definite, radially unbounded, and  $\dot{V}(x) < 0$  for all  $x \neq 0$ .*

**Lemma 2.8.** *Suppose  $V_1$  and  $V_2$  are continuous real-valued functions on  $\mathbb{R}^n$ , homogeneous with respect to  $\nu$  of degrees  $l_1 > 0$  and  $l_2 > 0$ , respectively, and  $V_1$  is positive definite. Then, for every  $x \in \mathbb{R}^n$ ,*

$$\left[ \min_{\{z:V_1(z)=1\}} V_2(z) \right] [V_1(x)]^{\frac{l_2}{l_1}} \leq V_2(x) \leq \left[ \max_{\{z:V_1(z)=1\}} V_2(z) \right] [V_1(x)]^{\frac{l_2}{l_1}}. \quad (2.8)$$

**Lemma 2.9.** *Consider the following system*

$$\dot{\xi} = f(\xi) + \widehat{f}(\xi), \quad f(0) = 0, \quad \xi \in \mathbb{R}^n, \quad (2.9)$$

where  $f(\xi)$  is a continuous homogeneous vector field of degree  $\kappa < 0$  with respect to the dilation  $\Delta_\lambda^r(\xi_1, \dots, \xi_n) = (\lambda^{r_1}\xi_1, \dots, \lambda^{r_n}\xi_n)$ , and  $\widehat{f}$  satisfies  $\widehat{f}(0) = 0$ . Assume  $\xi = 0$  is an asymptotically stable equilibrium of the system  $\dot{\xi} = f(\xi)$ . Then  $\xi = 0$  is a locally finite-time stable equilibrium of the system (2.9) if

$$\lim_{\lambda \rightarrow 0} \frac{\widehat{f}_i(\lambda^{r_1}\xi_1, \dots, \lambda^{r_n}\xi_n)}{\lambda^{\kappa+r_i}} = 0, \quad i = 1, \dots, n, \quad \forall \xi \neq 0. \quad (2.10)$$

**Lemma 2.10.** *Global asymptotic stability and local finite-time stability of the closed-loop system imply global finite-time stability [71, 140].*

The following inequality is commonly used when investigating the finite-time stability of control systems. The next property is useful for skew-symmetric matrices.

**Lemma 2.11.** [60] *For  $y \in \mathbb{R}^n$  and  $\alpha \in \mathbb{R}$  with  $\alpha \geq 1$ , the following inequality holds,*

$$\left( \sum_{i=1}^n |y_i| \right)^{\frac{1}{\alpha}} \leq \sum_{i=1}^n |y_i|^{\frac{1}{\alpha}} \leq n^{\frac{\alpha-1}{\alpha}} \left( \sum_{i=1}^n |y_i| \right)^{\frac{1}{\alpha}} \quad (2.11)$$

where  $|\cdot|$  denotes the absolute value.

**Property 2.12.** [49] *Given two vectors  $x, y \in \mathbb{R}^n$ , the following relationship holds,*

$$S(x)S(y) = yx^T - x^T yI \quad (2.12)$$

$$S(S(x)y) = S(S(x)y) = S(x)S(y) - S(y)S(x) \quad (2.13)$$

where  $S(x)$  is the skew-symmetric matrix of  $x$ .

## 2.3 Manipulator and contact dynamics model

In this section, the kinematic and dynamic equations are introduced for a non-redundant serial manipulator in contact with a compliant environment. We assume the manipulator to possess 6 independent degrees of freedom such that the 3 positions and 3 orientations can be specified for the end-effector, hence the robot arm is non-redundant. In the following derivation, a superscript is only used to refer matrix and vector quantities to a frame other than the fixed base frame.

### 2.3.1 Manipulator kinematics and dynamics

The links of the manipulators are assumed to be rigid while the joints exhibit no flexibility. The end-effector position  $p_e \in \mathbb{R}^3$  and orientation represented by the rotation matrix  $R_e \in \text{SO}(3)$  of the manipulator are related to the joint variables,  $\theta \in \mathbb{R}^6$  via the forward kinematics map (i.e.  $p_e(\theta)$ ,  $R_e(\theta)$ ). A common way to derive this map is by using Denavit-Hartenberg convention [131, 136]. The end-effector velocities are related to the joint velocities by the geometric Jacobian,

$$v_e = J(\theta)\dot{\theta} \quad (2.14)$$

where  $v_e = [\dot{p}_e^T \ \dot{\omega}_e^T]^T$ ,  $\dot{p}_e \in \mathbb{R}^3$  and  $\dot{\omega}_e \in \mathbb{R}^3$  are the translational and the angular velocities expressed w.r.t. the base frame, respectively. The translational and angular accelerations w.r.t. the base frame follow from (2.14) as,

$$\dot{v}_e = J(\theta)\ddot{\theta} + \dot{J}(\theta)\dot{\theta} \quad (2.15)$$

where  $\dot{v}_e = [\ddot{p}_e^T \ \ddot{\omega}_e^T]^T$ . It is common to use a suitable parameterization for the orientation of the end-effector with less parameters than the rotation matrix (which has 9 parameters) in order to reduce computational complexity for the implementation of the control algorithm and trajectory planning [29, 89]. A minimal parameterization of the three dimensional rotation group  $SO(3)$  requires 3 parameters [131]. Examples of such representations are Euler angles, exponential parameterization, etc. A problem with minimal parameterizations is that they cannot be both global (in the sense of a 1-1 map between the parameters and the rotation matrix) and nonsingular [138]. Ad hoc solutions such as redefining the inertial frame or switching to a different parameterization can in principle deal with these singularities [94]. Unit quaternions, a non-minimal parameterization, are selected to compute the orientation error, since they are computationally efficient and can properly represent a large range of orientation angles [29, 89]. Given the rotation matrix  $R_e$ , its four parameter singularity-free representation is given by the following unit quaternion,  $q_e = [\eta_e, \epsilon_e^T]^T \in \mathbb{S}^3$ ,

$$\eta_e = \cos \frac{\gamma_e}{2}, \quad \epsilon_e = \beta_e \sin \frac{\gamma_e}{2} \quad (2.16)$$

with  $\gamma_e \in \mathbb{R}$  and  $\beta_e \in \mathbb{S}^2$  being the rotation angle and unit vector of an equivalent angle/axis representation of the rotation matrix satisfying the unit norm constraint

$$\eta_e^2 + \epsilon_e^T \epsilon_e = 1 \quad (2.17)$$

and  $\eta_e \geq 0$  when  $\gamma_e \in [-\pi, \pi]$ . The time derivative of the unit quaternion  $q_e$  is related to the spatial angular velocity  $\omega_e$  by,

$$\dot{q}_e = \begin{bmatrix} \dot{\eta}_e \\ \dot{\epsilon}_e \end{bmatrix} = \frac{1}{2} T(q_e) \omega_e = \frac{1}{2} \begin{bmatrix} -\epsilon_e^T \\ E(\eta_e, \epsilon_e) \end{bmatrix} \omega_e = \frac{1}{2} \begin{bmatrix} -\epsilon_e^T \\ \eta_e I_3 - S(\epsilon_e) \end{bmatrix} \omega_e \quad (2.18)$$

where  $S(\epsilon_e)$  is a skew-symmetric matrix and the following relations

$$E^T(\eta_e, \epsilon_e) E(\eta_e, \epsilon_e) = I_3 - \epsilon_e \epsilon_e^T, \quad (2.19)$$

$$T^T(\eta_e, \epsilon_e) T(\eta_e, \epsilon_e) = I_3, \quad (2.20)$$

$$T(\eta_e, \epsilon_e) T^T(\eta_e, \epsilon_e) = I_4 - q_e q_e^T, \quad (2.21)$$

are satisfied. The relation between the rotation matrix and unit quaternion is given by the Rodrigues' formula,

$$R_e(\eta_e, \epsilon_e) = (\eta_e^2 - \epsilon_e^T \epsilon_e) I_3 + 2\epsilon_e \epsilon_e^T + 2\eta_e S(\epsilon_e) \quad (2.22)$$

where  $R_e(\eta_e, \epsilon_e) = R_e(-\eta_e, -\epsilon_e)$  which follows from the fact that  $\mathbb{S}^3$  is a double cover of  $SO(3)$  (i.e. the map from quaternions to rotation matrices is two-to-one).

### Quaternion error kinematics

Let  $R_d$  and  $q_d$  denote the desired rotation matrix and its corresponding unit quaternion referred w.r.t. the base frame. The orientation error between desired and actual end-effector frames is described by the rotation matrix

$$R_d^e = R_e^T R_d \quad (2.23)$$

with its time-derivative computed as

$$\dot{R}_d^e = S(\Delta\omega_{de}^e) R_d^e \quad (2.24)$$

where

$$\Delta\omega_{de}^e = \omega_d^e - \omega_e^e = R_e^T(\omega_d - \omega_e) \quad \text{and} \quad \Delta\omega_{de} = \omega_d - \omega_e$$

where  $\Delta\omega_{de}^e$  and  $\omega_d^e$  are the angular velocity error and desired angular velocity, respectively referred w.r.t. the end-effector frame. The unit quaternion corresponding to  $R_d^e$  given by (2.23) can be extracted either by using (2.22) or from

$$\eta_{de} = \eta_e \eta_d + \epsilon_e^T \epsilon_d \quad (2.25)$$

$$\epsilon_{de}^e = \eta_e \epsilon_d - \eta_d \epsilon_e - S(\epsilon_e) \epsilon_d \quad (2.26)$$

using the knowledge of the desired  $(\eta_d, \epsilon_d)$  and actual  $(\eta_e, \epsilon_e)$  quaternions. Since the desired orientation trajectory  $q_d = [\eta_d \ \epsilon_d^T]^T$  must correspond to a rotation, it should satisfy the unit norm constraint  $q_d^T q_d = 1$ . The time derivative of the quaternion error (2.25)-(2.26) is computed as

$$\dot{\eta}_{de} = -\frac{1}{2} (\epsilon_{de}^e)^T \Delta\omega_{de}^e \quad (2.27)$$

$$\dot{\epsilon}_{de}^e = \frac{1}{2} E(\eta_{de}, \epsilon_{de}^e) \Delta\omega_{de}^e = \frac{1}{2} [\eta_{de} I_3 - S(\epsilon_{de}^e)] \Delta\omega_{de}^e \quad (2.28)$$

where the Property 2.12 is used. Equations (2.27) and (2.28) can be referred w.r.t. the base frame as

$$\dot{\eta}_{de} = -\frac{1}{2} (R_e^T \epsilon_{de})^T R_e^T \Delta\omega_{de} = -\frac{1}{2} \epsilon_{de}^T \Delta\omega_{de} \quad (2.29)$$

$$\dot{\epsilon}_{de} = \dot{R}_e \epsilon_{de}^e + R_e \dot{\epsilon}_{de}^e = \frac{1}{2} E(\eta_{de}, \epsilon_{de}) \omega_d - \frac{1}{2} E^T(\eta_{de}, \epsilon_{de}) \omega_e \quad (2.30)$$

where  $E(\eta_{de}, \epsilon_{de}) = \eta_{de} I_3 - S(\epsilon_{de})$ . It can be shown that the quaternion vector  $(\eta_{de}, \epsilon_{de})$  can be extracted from the rotation matrix  $R_{de} = R_d R_e^T$  [29]. In Section 2.4 the time derivative of (2.30) given by

$$\ddot{\epsilon}_{de} = \frac{1}{2} \dot{E} \omega_d + \frac{1}{2} E \dot{\omega}_d - \frac{1}{2} \dot{E}^T \omega_e - \frac{1}{2} E^T \dot{\omega}_e \quad (2.31)$$

is used to derive a suitable feedback law in a similar way compared to the controller based on the approximation of the angle-axis parameterization [29].

The dynamic equations of motion of the manipulator are obtained using Euler-Lagrange equations as,

$$M(\theta) \ddot{\theta} + C(\theta, \dot{\theta}) \dot{\theta} + \tau_f(\dot{\theta}) + g(\theta) = \tau - J^T(\theta) F_e \quad (2.32)$$

where  $M(\theta) \in \mathbb{R}^{6 \times 6}$ ,  $C(\theta, \dot{\theta}) \dot{\theta} \in \mathbb{R}^6$ ,  $\tau_f(\dot{\theta}) \in \mathbb{R}^6$  and  $g(\theta) \in \mathbb{R}^6$  are the inertia matrix, a vector containing Coriolis and centrifugal terms, joint friction and gravity vector, respectively. Here, the friction torques/forces are modelled using a static mapping, although more sophisticated models with internal dynamics exist (e.g. LuGre [42], generalized Maxwell-slip [3], etc.). Furthermore,  $\tau \in \mathbb{R}^6$ ,  $F_e \in \mathbb{R}^6$  represent the actuator torques, and environment contact forces/moments w.r.t. the base frame, which are given as,  $F_e = [f_e^T \ \mu_e^T]^T$  with  $f_e \in \mathbb{R}^3$  contact forces and  $\mu_e \in \mathbb{R}^3$  contact moments.

### 2.3.2 Environment model

Consider the end-effector making contact with an elastic surface described by [105],

$$\varphi(p_e) = h \quad (2.33)$$

where  $\varphi(\cdot)$  is an at least twice differentiable function in its domain of definition and  $h$  parameterizes the surface deflection (or deformation). The surface is assumed to be sufficiently smooth and convex. Common examples of such surfaces are planar,

$$\varphi(p_e) = n^T (p_e - p_o)$$

where  $p_e = [p_{e,x} \ p_{e,y} \ p_{e,z}]^T$ ,  $n \in \mathbb{R}^3$  and  $p_o \in \mathbb{R}^3$  are the Cartesian coordinates, the normal to the plane and the offset of the plane from the origin and spherical,

$$\varphi(p_e) = \|p_e - p_o\| - r_o$$

where  $p_o \in \mathbb{R}^3$  and  $r_o \in \mathbb{R}_{>0}$  represent the position of its center and radius [20]. For a frictionless and compliant surface, the normal component of the contact force exerted by the end-effector on the surface is modeled as,

$$f_{e,n} = \begin{cases} -k_e h, & \text{if } h \leq 0 \\ 0, & \text{if } h > 0 \end{cases} \quad (2.34)$$

where  $k_e$  characterizes the stiffness of the surface. This model is known in the literature as the Kelvin model [53]. The complete contact force vector exerted by the end-effector on the surface is given by,

$$f_e = n(p_e) f_{e,n}, \quad \text{where } n(p_e) = \left( \frac{\partial \varphi(p_e)}{\partial p_e} \right)^T \quad (2.35)$$

where  $f_e \in \mathbb{R}^3$  and  $n(p_e) \in \mathbb{R}^3$  is the normal direction of the surface. The effect of contact friction can also be included in the model by considering the tangential components of the contact force

$$f_e = n(p_e) f_{e,n} + t(p_e) f_{e,t} \quad (2.36)$$

where  $t(p_e) \in \mathbb{R}^{3 \times 2}$  represent the tangential directions of the surface and  $f_{e,t} \in \mathbb{R}^2$  the friction force which depends on the magnitude of the normal force (i.e.  $|f_{e,n}|$ ) and velocity of the end-effector [166]. In the following analysis, we only consider the case  $h \leq 0$ , when the robot is in contact with the environment (i.e. contact motion phase) and assume that the surface is frictionless. The assumption on the absence of contact friction is solely motivated by theoretical reasons and the effect of contact friction is left as a perturbation to the nominal closed-loop system which is introduced in the following sections. The behavior of the closed-loop system with the hybrid impedance controller during contact transition and in the presence of contact friction is investigated in simulations and experiments.

## 2.4 A hybrid impedance controller with finite-time stability characteristics

In this section, an impedance controller having finite-time stability characteristics is designed. The controller is designed in such a way that it can track the desired



force and motion (translation/orientation) trajectories defined in a suitable set of coordinates. Furthermore, under certain assumptions, it should be capable of tracking constant reference trajectories perfectly in finite time. Before deriving the equations for the controller, a suitable set of coordinates for the position, known as the task space coordinates [105, 166], are selected

$$r_e = \Gamma(p_e) = \begin{bmatrix} r_{e,n} \\ r_{e,t} \end{bmatrix} = \begin{bmatrix} \varphi(p_e) \\ \psi(p_e) \end{bmatrix} \quad (2.37)$$

where  $\varphi(p_e) \in \mathbb{R}$  and  $\psi(p_e) \in \mathbb{R}^2$  are mutually independent, such that the Jacobian of the mapping  $\Gamma(p_e)$  should be nonsingular. The task space coordinates (2.37) can be extended to contain the orientation variables by using the unit quaternion (2.16) described in Section 2.3.1 as

$$x_e = \begin{bmatrix} r_e \\ q_e \end{bmatrix} = \begin{bmatrix} \Gamma(p_e) \\ q_e \end{bmatrix} \quad (2.38)$$

and furthermore the end-effector velocity is expressed using task coordinates

$$v = \begin{bmatrix} J_r(p_e) & 0_{3,3} \\ 0_{3,3} & I_3 \end{bmatrix} v_e = \mathbb{J}_r(\theta) J(\theta) \dot{\theta} \quad (2.39)$$

where

$$\mathbb{J}_r(\theta) = \begin{bmatrix} J_r(p_e) & 0_{3,3} \\ 0_{3,3} & I_3 \end{bmatrix} \quad \text{and} \quad \mathbb{J}(\theta) = \mathbb{J}_r(\theta) J(\theta) \quad (2.40)$$

with  $0_{3,3}$  and  $I_3$  are the  $3 \times 3$  zero and identity matrices, respectively, and  $J_r(p_e)$  is the Jacobian of the mapping  $\Gamma(p_e)$ . By using the Jacobian  $J_r(p_e)$ , the contact forces can also be written in terms of task coordinates as

$$f_r = J_r^{-1}(p_e) f_e = \begin{bmatrix} f_{e,n} \\ 0_{2,1} \end{bmatrix} \quad (2.41)$$

where  $0_{2,1}$  is the 2-dimensional null vector due to the assumption on the absence of contact friction. The task space accelerations are derived using (2.39)

$$\dot{v} = \mathbb{J}(\theta) \ddot{\theta} + \dot{\mathbb{J}}(\theta) \dot{\theta}. \quad (2.42)$$

Under the assumption that the manipulator is away from kinematic singularities, equation (2.42) can be used to derive the manipulator dynamic model in terms of task coordinates as

$$M_c(\theta) \dot{v} + C_c(\theta, \dot{\theta}) v + F_f(\theta, \dot{\theta}) + g_c(\theta) = F_c - F_r \quad (2.43)$$

where

$$\begin{aligned}
M_c(\theta) &= \mathbb{J}^{-T}(\theta)M(\theta)\mathbb{J}^{-1}(\theta) \\
C_c(\theta, \dot{\theta})v &= \mathbb{J}^{-T}(\theta) \left( C(\theta, \dot{\theta}) - M(\theta)\mathbb{J}^{-1}(\theta)\dot{\mathbb{J}}(\theta) \right) \mathbb{J}^{-1}(\theta)v \\
F_f(\theta, \dot{\theta}) &= \mathbb{J}^{-T}(\theta)\tau_f(\dot{\theta}) \\
g_c(\theta) &= \mathbb{J}^{-T}(\theta)g(\theta) \\
F_c &= \mathbb{J}^{-T}(\theta)\tau \\
F_r &= \mathbb{J}^{-T}(\theta)F_e
\end{aligned}$$

are the equivalent (or effective) inertia matrix, vector of Coriolis and centrifugal forces, friction forces and gravity forces. Since, the end-effector position  $p_e(\theta)$  and orientation  $R_e(\theta)$  and (2.37) are locally invertible maps,  $\theta$  can simply be eliminated from (2.43) (pg. 197 of [102]). However, since for most robots  $\theta$  is measured directly and forward kinematics map is computed, it is convenient to leave  $\theta$  dependence explicit. Furthermore,  $F_c \in \mathbb{R}^6$  and  $F_r \in \mathbb{R}^6$  are the equivalent actuator forces and the contact force/moment vector in the task coordinates. For the environment model considered in Section 2.3.2, the contact force/moment vector is  $F_r = [f_r^T \ 0_{3,1}^T]^T$ . In order to achieve the desired finite-time tracking characteristics described at the beginning of this section an inverse-dynamics based controller is selected. This controller is designed in terms of the task coordinates,

$$F_c = M_c(\theta)u + C_c(\theta, \dot{\theta})v + F_f(\theta, \dot{\theta}) + g_c(\theta) + F_r \quad (2.44)$$

where,  $u$  is a new control input. The actual joint torques applied to the manipulator that correspond to the actuator forces, (2.44) are given by

$$\tau = M(\theta)\mathbb{J}^{-1}(\theta) \left( u - \dot{\mathbb{J}}(\theta)\dot{\theta} \right) + C(\theta, \dot{\theta})\dot{\theta} + \tau_f(\dot{\theta}) + g(\theta) + J^T(\theta)F_e \quad (2.45)$$

where it is assumed that the contact force and moment measurements are available to compensate for  $F_e$ . Furthermore, for the time-being it is assumed that the dynamic model of the manipulator and geometric properties of the environment are exactly known. In Section 2.6, the effect of uncertainties in the manipulator dynamics and in geometric properties of the environment are analyzed. By substituting (2.44) into the manipulator dynamics (2.43) we obtain,

$$M_c(\theta)(\dot{v} - u) = 0 \quad (2.46)$$

where the new control input is selected as  $u = [u_r^T \ u_\phi^T]^T$ , where  $u_r \in \mathbb{R}^3$  and  $u_\phi \in \mathbb{R}^3$  are the translational and rotational parts of the controller, respectively. The translational part,  $u_r$ , is given as,

$$u_r = \ddot{r}_d + M_{d,r}^{-1} (B_{d,r}\text{Sig}(\dot{r}_d - \dot{r}_e)^{\alpha_2} + K_{d,r}\text{Sig}(r_d - r_e)^{\alpha_1} - K_{f,r}(f_r - f_d)) \quad (2.47)$$

where  $r_d$ ,  $\dot{r}_d$ ,  $\ddot{r}_d$  and  $f_d$  represent the desired position, velocity, acceleration and force trajectories expressed in the constraint frame and  $0 < \alpha_1 < 1$  and  $\alpha_2 = 2\alpha_1/(\alpha_1 + 1)$ . Here, the following vector function is used,

$$\text{Sig}(\xi)^\alpha = [\text{sig}(\xi_1)^\alpha, \dots, \text{sig}(\xi_n)^\alpha]^T = [|\xi_1|^\alpha \text{sgn}(\xi_1), \dots, |\xi_n|^\alpha \text{sgn}(\xi_n)]^T \quad (2.48)$$

where  $\xi = [\xi_1, \dots, \xi_n]^T \in \mathbb{R}^n$ ,  $0 < \alpha < 1$ , and  $\text{sgn}(\cdot)$  being the standard signum function defined as

$$\text{sgn}(\xi_i) = \begin{cases} 1, & \xi_i > 0 \\ 0, & \xi_i = 0, \\ -1 & \xi_i < 0 \end{cases}$$

for  $\xi_i \in \mathbb{R}$ . Furthermore,  $M_{d,r}$ ,  $B_{d,r}$ ,  $K_{d,r}$ , and  $K_{f,r}$  are the desired inertia, damping, stiffness, and proportional force feedback matrices selected as

$$M_{d,r} = m_{d,t}(I_3 - \Sigma) + m_{d,n}\Sigma, \quad (2.49)$$

$$B_{d,r} = b_{d,t}(I_3 - \Sigma) + b_{d,n}\Sigma, \quad (2.50)$$

$$K_{d,r} = k_{d,t}(I_3 - \Sigma) + k_{d,n}\Sigma, \quad (2.51)$$

$$K_{f,r} = k_{f,r}I_3. \quad (2.52)$$

This selection ensures proper impedance characteristics for unconstrained and constrained directions, with  $\Sigma = \text{diag}[1 \ 0 \ 0]$  being a suitable selection matrix. Here,  $m_{d,t}$ ,  $b_{d,t}$  and  $k_{d,t}$  are the desired inertia, damping and stiffness coefficients for unconstrained (tangential) directions, and  $m_{d,n}$ ,  $b_{d,n}$  and  $k_{d,n}$  are the desired inertia, damping and stiffness coefficients for constrained (normal) directions, respectively. The rotational part of the new control input,  $u_\phi$  is designed analogously to [89] by using only the vector part of the quaternion error,  $\epsilon_{de}$  which is a minimal parameterization. By using (2.31), a suitable feedback law can be derived such as to obtain a decoupled closed-loop relationship. Since from the rotational part of (2.46)  $\dot{\omega}_e = u_\phi$  is obtained,  $u_\phi$ , can be selected as,

$$u_\phi = E^{-T} \left( \dot{E}\omega_d + E\dot{\omega}_d - \dot{E}^T\omega_e + 2M_{d,\phi}^{-1} (B_{d,\phi}\text{Sig}(\dot{\epsilon}_{de})^{\alpha_2} + K_{d,\phi}\text{Sig}(\epsilon_{de})^{\alpha_1}) \right) \quad (2.53)$$

where,  $M_{d,\phi}$ ,  $B_{d,\phi}$  and  $K_{d,\phi}$  are positive definite control gain matrices. Here,  $E^{-T}$  becomes singular when  $\eta_{de} = 0$  which is due to the fact that a minimal parameterization is selected. However, this singularity can be avoided by using the method described in [89], which is based on checking whether the scalar component of the quaternion approaches zero (i.e.  $\eta_{de} = 0$ ). When the manipulator is away from kinematic singularities (i.e.  $\det(J(\theta)) \neq 0$ ) and the singularity due to minimal

parameterization (i.e.  $\eta_{de} \neq 0$ ), by using the controller (2.47)-(2.53) the closed-loop can be written as,

$$M_{d,r}\ddot{e}_r + B_{d,r}\text{Sig}(\dot{e}_r)^{\alpha_2} + K_{d,r}\text{Sig}(e_r)^{\alpha_1} = K_{f,r}e_f \quad (2.54)$$

$$M_{d,\phi}\ddot{\epsilon}_{de} + B_{d,\phi}\text{Sig}(\dot{\epsilon}_{de})^{\alpha_2} + K_{d,\phi}\text{Sig}(\epsilon_{de})^{\alpha_1} = 0 \quad (2.55)$$

where  $e_r = r_d - r_e$ , and  $e_f = f_r - f_d$ . Since the stiffness coefficient of the contacted environment,  $k_e$  given in (2.34) is usually not known in advance in practice, the desired stiffness of the controller and the desired velocity and acceleration trajectories in the constrained direction can be set to  $k_{d,n} = 0$  and  $\dot{r}_{d,n} = \ddot{r}_{d,n} = 0$  and consequently (2.47) is modified

$$u_r = \ddot{r}_d + M_{d,r}^{-1} (B_{d,r}\text{Sig}(\dot{e}_r)^{\alpha_2} + K_{d,r}\text{Sig}(e_r)^{\alpha_1} - K_{f,r}(e_f + \text{Sig}(e_f)^{\alpha_1})) \quad (2.56)$$

to obtain,

$$M_{d,r}\ddot{e}_r + B_{d,r}\text{Sig}(\dot{e}_r)^{\alpha_2} + K_{d,r}\text{Sig}(e_r)^{\alpha_1} = K_{f,r}(e_f + \text{Sig}(e_f)^{\alpha_1}) \quad (2.57)$$

instead of (2.54) so that the desired force,  $f_d$  can be tracked for any constant  $k_e$  at the steady state. For any given desired constant force  $f_{d,n}$ , it is possible to find a constant  $k_e > 0$  and  $r_{d,n}$  (i.e.  $\dot{r}_{d,n} = \ddot{r}_{d,n} = 0$ ) such that

$$f_{d,n} = k_e r_{d,n} \quad (2.58)$$

is satisfied. Here, it should be realized that the expression (2.58) is not used in the actual implementation of the controller, but it is used to prove stability. Therefore, the knowledge of the values of  $k_e$  and  $r_{d,n}$  is not necessary, and can be unknown. Consequently, for the translational part we have the following closed-loop equation,

$$M_{d,r}\ddot{e}_r + B_{d,r}\text{Sig}(\dot{e}_r)^{\alpha_2} + \bar{K}_{d,r}\text{Sig}(e_r)^{\alpha_1} + K_e e_r = 0 \quad (2.59)$$

where the matrices  $M_{d,r}$  and  $B_{d,r}$  are the same as in (2.49)-(2.50) whereas  $K_e$  and  $\bar{K}_{d,r}$  are given by,

$$\bar{K}_{d,r} = k_{d,t}(I_{3 \times 3} - \Sigma) + k_{f,r}(k_e)^{\alpha_1} \Sigma, \quad K_e = k_e \Sigma \quad (2.60)$$

by reformulating the force error as the position error using (2.34). Another property of this strategy is that it can be used to bring the manipulator into contact, when it starts from non-contact (or free) motion phase. Since in free motion phase (i.e.  $f_{e,n} = 0$ ) in the normal direction, the control law is given by

$$m_{d,n}\ddot{r}_{e,n} + b_{d,n}\text{sig}(\dot{r}_{e,n})^{\alpha_2} = -k_{f,r}(f_d + \text{sig}(f_d)^{\alpha_1}) \quad (2.61)$$

which is a mass and nonlinear damping element driven by the external force at the right-hand side of (2.61).

**Remark 2.13.** *It can be realized from the impedance relationship given by (2.54) that, since nonlinear stiffness and damping functions are used, the resultant stiffness and damping are a function of the error and its derivative respectively. Varying the force-feedback coefficient  $K_{f,r}$  scales the impedance parameters on the LHS of equation (2.54). When the fractional power is selected as  $0 < \alpha_1 < 1$  in the stiffness term, for the same gain  $K_{d,r}$  a higher stiffness compared to  $\alpha_1 = 1$  is obtained for errors smaller than 1 (i.e.  $|e_i| < 1$  for  $i = 1, \dots, 3$ ).*

## 2.5 Stability analysis for contact phase

In this section the stability of the closed-loop system given by the equations (2.55) and (2.59) is investigated. Furthermore, for the sake of simplicity, it is assumed that  $M_{d,\phi}$ ,  $B_{d,\phi}$  and  $K_{d,\phi}$  are diagonal matrices. The sketch of the stability proof when the manipulator is in the contact phase is provided in this section, and the complete proof can be found in Appendix A. Lemmas 2.6 and 2.9 are used for this purpose. Denote by  $\mathcal{W}$  the region in which the manipulator operates, which is a subset of the finite workspace from which kinematic and representation singularities are removed. Then, the state-space for the closed-loop system is given by  $\mathfrak{C}_s := \mathcal{W} \times \mathbb{R}^6$  where  $\mathbb{R}^6$  stands for the velocity errors. The asymptotic stability of the origin of the closed-loop system (2.55) and (2.59) in  $\mathfrak{C}_s$  is shown using the following positive definite  $C^1$  candidate Lyapunov function

$$\begin{aligned} V(e_r, \dot{e}_r, \epsilon_{de}, \dot{\epsilon}_{de}) &= \frac{1}{2} \dot{e}_r^T \dot{e}_r + \frac{1}{\alpha_1 + 1} e_r^T M_{d,r}^{-1} \bar{K}_{d,r} \text{Sig}(e_r)^{\alpha_1} + \frac{1}{2} e_r^T M_{d,r}^{-1} K_e e_r \\ &\quad + \frac{1}{2} \dot{\epsilon}_{de}^T \dot{\epsilon}_{de} + \frac{1}{\alpha_1 + 1} \epsilon_{de}^T M_{d,\phi}^{-1} K_{d,\phi} \text{Sig}(\epsilon_{de})^{\alpha_1} \end{aligned} \quad (2.62)$$

together with LaSalle's invariance principle, since the time derivative of (2.62) is negative semi-definite. Due to the fact that the translational part of the closed-loop equations (2.59) is not homogeneous, Lemma 2.6 cannot be applied directly to this problem. Therefore, with the help of Lemma 2.9 the closed-loop vector field is first separated into its homogeneous and non-homogeneous parts. The closed-loop system is represented in state-space form by selecting  $x_1 = e_r$ ,  $x_2 = \dot{e}_r$ ,  $x_3 = \epsilon_{de}$ ,  $x_4 = \dot{\epsilon}_{de}$  and  $x = [x_1^T \ x_2^T \ x_3^T \ x_4^T]^T$  as follows,

$$\dot{x} = f(x) + \hat{f}(x) \quad (2.63)$$

where

$$f(x) = \begin{bmatrix} x_2 \\ M_{d,r}^{-1} (-\bar{K}_{d,r} \text{Sig}(x_1)^{\alpha_1} - B_{d,r} \text{Sig}(x_2)^{\alpha_2}) \\ x_4 \\ M_{d,\phi}^{-1} (-K_{d,\phi} \text{Sig}(x_3)^{\alpha_1} - B_{d,\phi} \text{Sig}(x_4)^{\alpha_2}) \end{bmatrix}, \quad \hat{f}(x) = \begin{bmatrix} 0 \\ -M_{d,r}^{-1} K_e x_1 \\ 0 \\ 0 \end{bmatrix} \quad (2.64)$$

are the homogeneous part of degree  $\kappa = \alpha_1 - 1 < 0$  and the perturbation which satisfies  $\widehat{f}(0) = 0$ , respectively. The asymptotic stability of the homogeneous part is shown with the following Lyapunov function candidate,

$$V_2 = \frac{1}{2}x_2^T x_2 + \frac{1}{\alpha_1 + 1} \sum_{i=1}^3 \frac{\bar{k}_{d,r,i}}{m_{d,r,i}} |x_{1,i}|^{\alpha_1+1} + \frac{1}{2}x_4^T x_4 + \frac{1}{\alpha_1 + 1} \sum_{i=1}^3 \frac{k_{d,\phi,i}}{m_{d,\phi,i}} |x_{3,i}|^{\alpha_1+1} \quad (2.65)$$

and using LaSalle's invariance principle. According to Lemma 2.6 it follows that the homogeneous part  $f(x)$  in (2.64) is finite-time stable, since it is asymptotically stable and its degree is negative. Furthermore, the non-homogeneous part of the vector field  $\widehat{f}(x)$  in (2.64) satisfies the condition (2.10) given in Lemma 2.9 (see Appendix A for details). This implies the local finite-time stability of the closed-loop system (2.55) and (2.59). The main result of this section is summarized with the following proposition.

**Proposition 2.14.** *Consider the manipulator dynamics described by (2.43) in terms of the task space variables and the environment represented by the model (2.34) with  $h \leq 0$  which corresponds to the case when the manipulator is in the contact phase. The following control law*

$$F_c = M_c(\theta)u + C_c(\theta, \dot{\theta})v + F_f(\theta, \dot{\theta}) + g_c(\theta) + F_r \quad (2.66)$$

with  $u$  given by

$$u = \begin{bmatrix} \ddot{r}_d + M_{d,r}^{-1} (B_{d,r} \text{Sig}(\dot{e}_r)^{\alpha_2} + K_{d,r} \text{Sig}(e_r)^{\alpha_1} - K_{f,r} (e_f + \text{Sig}(e_f)^{\alpha_1})) \\ E^{-T} \left( \dot{E}\omega_d + E\dot{\omega}_d - \dot{E}^T \omega_e + 2M_{d,\phi}^{-1} (B_{d,\phi} \text{Sig}(\dot{\epsilon}_{de})^{\alpha_2} + K_{d,\phi} \text{Sig}(\epsilon_{de})^{\alpha_1}) \right) \end{bmatrix} \quad (2.67)$$

where  $e_r = r_d - r_e$ ,  $\epsilon_{de} = R_e \epsilon_{de}^e$  given by (2.26) and  $e_f = f_r - f_d$  achieves finite-time tracking of the desired translation  $r_d$  and orientation  $\epsilon_d$  and force trajectories  $f_d$  in the case when the environment stiffness  $k_e$  and location of the surface are unknown. Here, the powers  $\alpha_1$  and  $\alpha_2$  are given by  $0 < \alpha_1 < 1$  and  $\alpha_2 = 2\alpha_1 / (\alpha_1 + 1)$ . The matrices  $M_{d,r}$ ,  $B_{d,r}$  and  $K_{f,r}$  are positive definite and  $K_{d,r}$  is positive semi-definite whereas  $M_{d,\phi}$ ,  $B_{d,\phi}$  and  $K_{d,\phi}$  are positive definite.

*Proof.* The detailed proof of this proposition is given in Appendix A.1.  $\square$

## 2.6 Robust stability analysis

In this section, the guidelines to investigate the effect of a mismatch between the actual robot parameter values and those used in the model-based compensation (2.44), or (2.45) its joint space version, are presented.

### 2.6.1 Uncertainty modelling

When the compensation terms used in the controller (2.44) are not known perfectly, the controller can be rewritten as

$$F_c = \widehat{M}_c(\theta)u + \widehat{C}_c(\theta, \dot{\theta})v + \widehat{F}_f(\theta, \dot{\theta}) + \widehat{g}_c(\theta) + F_r \quad (2.68)$$

with the uncertain terms  $\widehat{\bullet}$  given by,

$$\begin{aligned} \widehat{M}_c(\theta) &= \mathbb{J}^{-T}(\theta)\widehat{M}(\theta)\mathbb{J}^{-1}(\theta) \\ \widehat{C}_c(\theta, \dot{\theta})v &= \mathbb{J}^{-T}(\theta) \left( \widehat{C}(\theta, \dot{\theta}) - \widehat{M}(\theta)\mathbb{J}^{-1}(\theta)\dot{\mathbb{J}}(\theta) \right) \mathbb{J}^{-1}(\theta)v \\ \widehat{F}_f(\theta, \dot{\theta}) &= \mathbb{J}^{-T}(\theta)\widehat{\tau}_f(\theta, \dot{\theta}) \\ \widehat{g}_c(\theta) &= \mathbb{J}^{-T}(\theta)\widehat{g}(\theta) \end{aligned}$$

where it is assumed that the uncertainty is only due to the terms of the dynamic model of the manipulator.

**Remark 2.15.** *The effect of the uncertainty (either in the parameters or the structure or both) in the task-space variables (2.37) characterizing the contacted surface can be included to this by following the approach from [65] by considering the Jacobian  $\mathbb{J}(\theta)$  to be uncertain, due to  $\widehat{\mathbb{J}}_r(\theta)$  in (2.39). Another way to deal with this type of uncertainty is by using the force and position sensor readings to online estimate the local shape of the surface which is done in [87, 171]. Furthermore, the effect of contact friction can be included as a part of the uncertain friction term in  $\widehat{F}_f(\theta, \dot{\theta})$  (see [112] for more details).*

When the controller (2.68) is substituted into (2.43) we obtain,

$$M_c(\theta)\dot{v} = M_c(\theta)u - \delta M_c(\theta)u - \delta C_c(\theta, \dot{\theta})v - \delta F_f(\theta, \dot{\theta}) - \delta g_c(\theta) \quad (2.69)$$

where  $\delta\bullet = \bullet - \widehat{\bullet}$  represents the modelling error for each term. By assuming that the manipulator is away from kinematic singularities, equation (2.69) can be rewritten as,

$$\dot{v} = u + \Xi(\theta, \dot{\theta}, u) \quad (2.70)$$

where  $\Xi(\theta, \dot{\theta}, u)$  represents the nonlinear uncertainty function given by

$$\Xi = \begin{bmatrix} \Xi_r \\ \Xi_\phi \end{bmatrix} = -M_c^{-1}(\theta) \left( \delta M_c(\theta)u + \delta C_c(\theta, \dot{\theta})v + \delta F_f(\theta, \dot{\theta}) + \delta g_c(\theta) \right) \quad (2.71)$$

where  $\Xi_r \in \mathbb{R}^3$  and  $\Xi_\phi \in \mathbb{R}^3$  are the parts that affect translational and rotational parts of the closed-loop dynamics, respectively. After some manipulation and

substitution of  $u_r$  and  $u_\phi$  into (2.70), the error dynamics in the presence of the uncertainty can be written as follows

$$\ddot{e}_r = -M_{d,r}^{-1} (B_{d,r} \text{Sig}(\dot{e}_r)^{\alpha_2} + \bar{K}_{d,r} \text{Sig}(e_r)^{\alpha_1} + K_e e_r) + \Xi_r \quad (2.72)$$

$$\ddot{e}_{de} = -M_{d,\phi}^{-1} (B_{d,\phi} \text{Sig}(\dot{e}_{de})^{\alpha_2} + K_{d,\phi} \text{Sig}(e_{de})^{\alpha_1}) + \frac{1}{2} E^T \Xi_\phi \quad (2.73)$$

which can be expressed in the state-space by selecting  $x = [x_1^T \ x_2^T]^T = [e^T \ \dot{e}^T]^T = [e_r^T \ \epsilon_{de}^T \ \dot{e}_r^T \ \dot{\epsilon}_{de}^T]^T$  with  $e = [e_r^T \ \epsilon_{de}^T]^T$  being the error as follows

$$\begin{aligned} \dot{x}_1 &= x_2 \\ \dot{x}_2 &= -M_d^{-1} K_d \text{Sig}(x_1)^{\alpha_1} - M_d^{-1} B_d \text{Sig}(x_2)^{\alpha_2} - M_d^{-1} K_E x_1 + \tilde{\Xi} \end{aligned} \quad (2.74)$$

where  $M_d = \text{diag}\{M_{d,r}, M_{d,\phi}\}$ ,  $B_d = \text{diag}\{B_{d,r}, B_{d,\phi}\}$ ,  $K_d = \text{diag}\{\bar{K}_{d,r}, K_{d,\phi}\}$ ,  $K_E = \text{diag}\{K_e, 0_{3,3}\}$  and  $\tilde{\Xi} = \mathfrak{T} \Xi$  with  $\mathfrak{T} = \text{diag}\{I_3, \frac{1}{2} E^T\}$  where the arguments of  $E^T$  and  $\mathfrak{T}$  are omitted for brevity. Therefore, the uncertainty term that affects the error dynamics (2.74) is given by,

$$\tilde{\Xi} = -\mathfrak{T} M_c^{-1}(\theta) \left( \delta M_c(\theta) u + \delta C_c(\theta, \dot{\theta}) v + \delta F_f(\theta, \dot{\theta}) + \delta g_c(\theta) \right) \quad (2.75)$$

whose norm can be shown to be bounded from above by a scalar and possibly time-varying function  $\varrho(x, t) \geq 0$  as

$$\|\tilde{\Xi}(\theta, \dot{\theta}, u)\| \leq \varrho(x, t). \quad (2.76)$$

**Remark 2.16.** Here, it can be concluded that the uncertainty term  $\tilde{\Xi}(\theta, \dot{\theta}, u)$  depends on the control input  $u$  and consequently on its gains. Using the uncertainty representation derived above to design a robust control algorithm with an additional control input depending on  $\varrho(x, t)$  such as the ones designed in [130, 131], is not easy since increasing the gains in  $u$  to improve performance would result in an increase of  $\varrho(x, t)$ . In [13], a method to deal with this problem is introduced which structures the uncertainty differently.

The following properties are important for derivation of the bound  $\varrho(x, t)$  on the uncertainty  $\tilde{\Xi}(\theta, \dot{\theta}, u)$ .

**Property 2.17.** For manipulators with all revolute joints,  $M(\theta)$ ,  $C(\theta, \dot{\theta})$ , and  $g(\theta)$  satisfy,

$$0 < M_m \leq \|M(\theta)\| \leq M_M, \quad \forall \theta \quad (2.77)$$

$$\|C(\theta, \dot{\theta})\| \leq C_M \|\dot{\theta}\|, \quad \forall \theta, \dot{\theta} \quad (2.78)$$

$$\|g(\theta)\| \leq G_M, \quad \forall \theta \quad (2.79)$$



where it is assumed that  $M_m$ ,  $M_M$ ,  $C_M$ , and  $G_M$  are known. Furthermore, it is also assumed that the joint friction torques can be bounded by

$$\|\tau_f(\dot{\theta})\| \leq \mathcal{F}_1 + \mathcal{F}_2 \|\dot{\theta}\|, \quad \forall \theta, \dot{\theta} \quad (2.80)$$

where it is assumed that  $\mathcal{F}_1$  and  $\mathcal{F}_2$  are known. The nominal values of the Coriolis and centrifugal terms, the gravity and joint friction torque vectors  $\widehat{C}(\theta, \dot{\theta})$ ,  $\widehat{g}(\theta)$ ,  $\widehat{\tau}_f(\theta, \dot{\theta})$  are selected such that they satisfy inequalities similar to (2.78), (2.79) and (2.80) with their bounds indicated as  $\widehat{\bullet}$  (e.g.  $\widehat{G}_M$ ). The desired trajectory signals are designed such that they satisfy,

$$\sup_{t \geq 0} \|\ddot{r}_d\| < \mathcal{A}_M, \quad \sup_{t \geq 0} \|\dot{r}_d\| < \mathcal{V}_M, \quad (2.81)$$

$$\sup_{t \geq 0} \|\dot{\omega}_d\| < \mathcal{K}_M, \quad \sup_{t \geq 0} \|\omega_d\| < \mathcal{O}_M. \quad (2.82)$$

The Jacobian matrices  $J(\theta)$ ,  $J_r(\theta)$  and their time derivative  $\dot{J}(\theta)$ ,  $\dot{J}_r(\theta)$  are bounded from above by,

$$\|J(\theta)\| \leq J_M, \quad \|J_r(\theta)\| \leq J_{r,M}, \quad \forall \theta \quad (2.83)$$

$$\|\dot{J}(\theta)\| \leq \bar{J}_M \|\dot{\theta}\|, \quad \|\dot{J}_r(\theta)\| \leq \bar{J}_{r,M} \|\dot{\theta}\|, \quad \forall \theta, \dot{\theta} \quad (2.84)$$

which consequently results in boundedness of  $\mathbb{J}(\theta)$  and  $\dot{\mathbb{J}}(\theta)$ .

**Property 2.18.** The norm of the matrix  $E^T$  can be calculated using (2.19) as follows,

$$\begin{aligned} \|E^T\| &= \sqrt{\lambda_{\max}(EE^T)} = \sqrt{\lambda_{\max}(I_3 - \epsilon_{de}\epsilon_{de}^T)} = \sqrt{\lambda_{\max}(I_3 - \sin^2 \theta_{de} r_{de} r_{de}^T)} \\ &= \sqrt{\lambda_{\max}(R_{de}(I_3 - \text{diag}\{\sin^2 \theta_{de}, 0, 0\})R_{de}^T)} = 1 \end{aligned} \quad (2.85)$$

with  $\lambda_{\max}$  the maximum eigenvalue and where  $\epsilon_{de} = r_{de} \sin \frac{\theta_{de}}{2}$  is the vector part of the quaternion extracted from the rotation matrix  $R_{de} = R_d R_e^T$  with  $\theta_{de}$  and  $r_{de}$  its angle/axis parameterization [29]. The norm of the matrix  $\mathfrak{T}$  can be calculated

$$\|\mathfrak{T}\| = \sqrt{\lambda_{\max}(\mathfrak{T}^T \mathfrak{T})} = \sqrt{\lambda_{\max}\left(\begin{bmatrix} I_3 & 0_{3,3} \\ 0_{3,3} & \frac{1}{4}EE^T \end{bmatrix}\right)} = 1 \quad (2.86)$$

with  $\lambda_{\max}$  the maximum eigenvalue of the matrix  $\mathfrak{T}^T \mathfrak{T}$ , where (2.85) is used.

**Remark 2.19.** Due to the fact that the Jacobian matrix  $J(\theta)$  can become singular for certain values of  $\theta$ , it is mathematically impossible to obtain an upper bound on  $\|J^{-1}(\theta)\|$ . This problem can be resolved if the inverse is computed using methods which are robust against kinematic singularities, with one common example being

the damped least squares Jacobian inverse [131]. With the help of such techniques it is possible to bound the inverse of the Jacobian matrix

$$\|J^{-1}(\theta)\| \leq \tilde{J}_M \quad (2.87)$$

and since  $\mathbb{J}_r(\theta)$  in (2.40) is by definition non-singular

$$\|\mathbb{J}^{-1}(\theta)\| \leq \|\mathbb{J}_r^{-1}(\theta)J^{-1}(\theta)\| \leq \tilde{J}_{r,M}\tilde{J}_M \quad (2.88)$$

where  $\|\mathbb{J}_r^{-1}(\theta)\| \leq \tilde{J}_{r,M}$ .

**Remark 2.20.** Since the manipulator in question is assumed to be non-redundant and has 6 d.o.f., with the help of the Remark 2.19 the term  $M_c^{-1}(\theta)\delta M_c(\theta)$  in (2.75) can be shown to satisfy

$$\begin{aligned} M_c^{-1}(\theta)\delta M_c(\theta) &= (\mathbb{J}^{-T}(\theta)M(\theta)\mathbb{J}^{-1}(\theta))^{-1}(\mathbb{J}^{-T}(\theta)\delta M(\theta)\mathbb{J}^{-1}(\theta)) \\ &= \mathbb{J}(\theta)M^{-1}(\theta)\mathbb{J}^T(\theta)\mathbb{J}^{-T}(\theta)\left(M(\theta) - \widehat{M}(\theta)\right)\mathbb{J}^{-1}(\theta) \\ &= \mathbb{J}(\theta)\left(I - M^{-1}(\theta)\widehat{M}(\theta)\right)\mathbb{J}^{-1}(\theta). \end{aligned} \quad (2.89)$$

By selecting the estimated inertia matrix  $\widehat{M}(\theta)$  as

$$\widehat{M}(\theta) = \frac{2}{M_m + M_M}I_6$$

with  $M_m$  and  $M_M$  given in (2.77), it can be shown that

$$\alpha_M := \left\|I - M^{-1}(\theta)\widehat{M}(\theta)\right\| \leq \frac{M_M - M_m}{M_M + M_m} < 1.$$

By selecting more accurate values for  $\widehat{M}(\theta)$ , e.g. obtained by an identification experiment, would result in a lower bound on the norm.

By using the Properties 2.17 and 2.18 and following the Remarks 2.19 and 2.20, the norm bound on the uncertainty term (2.75) is computed as,

$$\left\|\tilde{\Xi}\right\| \leq \varrho(x, t) = \rho_4 \|x\|^2 + \rho_3 \|x\| + \rho_2 \|x\|^{\alpha_2} + \rho_1 \|x\|^{\alpha_1} + \rho_0 \quad (2.90)$$

where  $\rho_0$ ,  $\rho_1$ ,  $\rho_2$ ,  $\rho_3$  and  $\rho_4$  are given by,

$$\begin{aligned} \rho_0 &= \max(J_{r,M}, 1) \alpha_M \tilde{J}_M \tilde{J}_{r,M} \|\mathfrak{F}^{-1}\| \left( \sqrt{\mathcal{A}_M^2 + \aleph_M^2} + \|\dot{\mathfrak{F}}\| \sqrt{\mathcal{V}_M^2 + \Omega_M^2} \times \right. \\ &\quad \left. (1 + \|\mathfrak{F}^{-1}\|) \right) + \max(J_{r,M}, 1) \frac{J_M}{M_m} \left( G_M + \widehat{G}_M \right) + \max(J_{r,M}, 1) \frac{J_M}{M_m} \times \end{aligned}$$

$$\begin{aligned} & \left( \mathcal{F}_1 + \widehat{\mathcal{F}}_1 + (\mathcal{F}_2 + \widehat{\mathcal{F}}_2) \tilde{J}_M \tilde{J}_{r,M} \|\mathfrak{T}^{-1}\| \sqrt{\mathcal{V}_M^2 + \Omega_M^2} \right) + \max(J_{r,M}, 1) J_M \times \\ & \left( M_M C_M + \alpha_M \tilde{J}_M \tilde{J}_{r,M} (\bar{J}_{r,M} J_M + \max(J_{r,M}, 1) \bar{J}_M) \right) \times \\ & \tilde{J}_M \tilde{J}_{r,M} \|\mathfrak{T}^{-1}\|^2 \mathcal{V}_M^2 + \Omega_M^2 \end{aligned} \quad (2.91)$$

$$\rho_1 = 6^{\frac{1-\alpha_1}{2}} \max(J_{r,M}, 1) \alpha_M \tilde{J}_M \tilde{J}_{r,M} \|\mathfrak{T}^{-1}\| \max_{i=1,\dots,6} \left( \frac{k_{d,i}}{m_{d,i}} \right) \quad (2.92)$$

$$\rho_2 = 6^{\frac{1-\alpha_2}{2}} \max(J_{r,M}, 1) \alpha_M \tilde{J}_M \tilde{J}_{r,M} \|\mathfrak{T}^{-1}\| \max_{i=1,\dots,6} \left( \frac{b_{d,i}}{m_{d,i}} \right) \quad (2.93)$$

$$\begin{aligned} \rho_3 = & \max(J_{r,M}, 1) \alpha_M \tilde{J}_M \tilde{J}_{r,M} \|\mathfrak{T}^{-1}\| \left( \|\dot{\mathfrak{z}}\| \|\mathfrak{T}^{-1}\| + k_{f,r} (k_e)^{\alpha_1} \max_{i=1,\dots,6} \left( \frac{1}{m_{d,i}} \right) \right) \\ & + \max(J_{r,M}, 1) \frac{J_M}{M_m} \left( \mathcal{F}_1 + \widehat{\mathcal{F}}_1 + (\mathcal{F}_2 + \widehat{\mathcal{F}}_2) \tilde{J}_M \tilde{J}_{r,M} \|\mathfrak{T}^{-1}\| \right) \\ & + 2 \max(J_{r,M}, 1) J_M \left( M_M C_M + \alpha_M \tilde{J}_M \tilde{J}_{r,M} (\bar{J}_{r,M} J_M \right. \\ & \left. + \max(J_{r,M}, 1) \bar{J}_M) \right) \tilde{J}_M \tilde{J}_{r,M} \|\mathfrak{T}^{-1}\|^2 \sqrt{\mathcal{V}_M^2 + \Omega_M^2} \end{aligned} \quad (2.94)$$

$$\begin{aligned} \rho_4 = & \max(J_{r,M}, 1) J_M \left( M_M C_M + \alpha_M \tilde{J}_M \tilde{J}_{r,M} (\bar{J}_{r,M} J_M \right. \\ & \left. + \max(J_{r,M}, 1) \bar{J}_M) \right) \tilde{J}_M \tilde{J}_{r,M} \|\mathfrak{T}^{-1}\|^2 \end{aligned} \quad (2.95)$$

The details of the computation of each term are given in the Appendix A.2.

**Remark 2.21.** *It can be noticed that the bound derived in (2.90) contains a term  $\|\mathfrak{T}^{-1}\|$  which directly depends on  $\|E^{-T}\|$  where  $E^{-T}(\eta_{de}, \epsilon_{de})$  can be computed as*

$$E^{-T}(\eta_{de}, \epsilon_{de}) = \eta_{de} I - S(\epsilon_{de}) + \frac{1}{\eta_{de}} \epsilon_{de} (\epsilon_{de})^T \quad (2.96)$$

where  $\eta_{de} = \pm \sqrt{1 - \epsilon_{de}^T \epsilon_{de}}$  can become infinite when  $\eta_{de} \rightarrow 0$  or equivalently  $\epsilon_{de}^T \epsilon_{de} \rightarrow 1$ . Therefore, a finite upper bound (either constant or state dependent) on the norm of  $E^{-T}$  cannot be computed. This is a consequence of using a minimal parameterization for the orientation part of the controller. Although the singularity can be dealt with in the approach mentioned in Section 2.4, it is not useful for analyzing the boundedness of the error dynamics. Derivation of ultimate bounds on the error trajectory usually leads to conservative results. Because the norm of the inverse of a matrix is used in the calculation of uncertainty, the results would be even more conservative. Furthermore, to reduce the effect of this problem, if we take a smaller domain to calculate reasonable bounds on the uncertainty term, then outside this region the controller would still be able work (although it will require large control inputs) whereas this would be neglected by the stability analysis.

Considering the discussion in Remark 2.21, in the following section the stability of

the perturbed system is analyzed by considering only the translational part of the closed-loop system and assuming that the manipulator possesses three independent degrees of freedom such that the end-effector positions can be specified. In this case, the uncertainty term and its upper bound would be similar to the one derived in (2.90) but it would be simpler and it would not involve any terms  $\|\mathfrak{T}^{-1}\|$ . Therefore, in the following section the stability of the translational part of the error dynamics (2.72) in the presence of uncertainties is investigated.

### 2.6.2 Perturbed system stability analysis

Since the homogeneous part of the closed-loop system (2.59) denoted by the first six rows (since  $x_1, x_2 \in \mathbb{R}^3$ ) of  $f(x)$  in (2.63) is locally finite-time convergent, according to Lemma 2.7 there exists a strict Lyapunov function that satisfies Lemma 2.8 with the same dilation of  $f(x)$  in (2.63) where  $V_2(x)$  is the Lyapunov function and  $V_1(x)$  is the corresponding homogeneous norm expressed by Definition 2.5. Furthermore, since (2.59) is locally finite-time convergent, the Lyapunov function for the homogeneous part can be expanded with additional terms for (2.59). Finding such an explicit function is known to be a challenging problem, even though there are certain examples in the literature [15, 71].

**Remark 2.22.** *It is shown here that for the scalar version of the system (i.e. when  $x_1, x_2 \in \mathbb{R}$ )*

$$\begin{aligned}\dot{x}_1 &= x_2 \\ \dot{x}_2 &= -l_1 \text{sig}(x_1)^{\alpha_1} - l_2 \text{sig}(x_2)^{\alpha_2}\end{aligned}\quad (2.97)$$

with  $l_1, l_2 > 0$ , the functions proposed in [15, 71] are not strict Lyapunov functions. A generalized version of the Lyapunov function proposed in [71] is,

$$V(x_1, x_2) = \frac{2}{3 + \alpha_1} c_1 |x_1|^{\frac{3+\alpha_1}{2}} + \frac{1 + \alpha_1}{3 + \alpha_1} c_2 |x_2|^{\frac{3+\alpha_1}{1+\alpha_1}} + c_3 x_1 x_2 \quad (2.98)$$

where  $c_1, c_2$  and  $c_3$  are constants (in [71] these are  $c_3 = (l_1/l_2)^{1/\alpha_1}$ ,  $c_1 = (1 + c_3^{(3+\alpha_1)/2})$ ,  $c_2 = 1$ ) and the Lyapunov function proposed in [15]

$$\begin{aligned}V(x_1, x_2) &= \frac{c_1}{2} x_1^2 + \frac{1 + \alpha_1}{4} c_2 |x_2|^{\frac{4}{1+\alpha_1}} + c_3 x_1 \text{sig}(x_2)^{\frac{2}{1+\alpha_1}} \\ &= \begin{bmatrix} x_1 \\ \text{sig}(x_2)^{\frac{2}{1+\alpha_1}} \end{bmatrix}^T \underbrace{\begin{bmatrix} \frac{c_1}{2} & \frac{c_3}{2} \\ \frac{c_3}{2} & \frac{1+\alpha_1}{4} c_2 \end{bmatrix}}_P \begin{bmatrix} x_1 \\ \text{sig}(x_2)^{\frac{2}{1+\alpha_1}} \end{bmatrix}\end{aligned}\quad (2.99)$$

which is homogeneous with respect to the dilation vector of the system (2.97) with  $P = P^T$  whose positive definiteness can be satisfied by checking the principal minors, are not strict Lyapunov functions. The proofs of these statements are given in Appendix A.3. They make use of the following two lemmas.

**Lemma 2.23.** *The function  $f_1(\xi_1, \xi_2) = \text{sig}(\xi_1)^{\frac{2}{1+\alpha_1}} \xi_2$  can be lower and upper bounded on the circle  $\mathbb{S} = \{(\xi_1, \xi_2) : \xi_1^2 + \xi_2^2 = 1\}$  as*

$$-M_1 \leq f_1(\xi_1, \xi_2) \leq M_1 \quad (2.100)$$

where  $M_1 = \left(\frac{2}{3+\alpha_1}\right)^{\frac{1}{1+\alpha_1}} \left(\frac{1+\alpha_1}{3+\alpha_1}\right)^{\frac{1}{2}}$ .

*Proof.* The proof of this Lemma is given in the Appendix A.4.  $\square$

**Lemma 2.24.** *The functions  $f_2(\xi_1, \xi_2) = \text{sig}(\xi_1)^{\frac{2\alpha_1}{1+\alpha_1}} \text{sig}(\xi_2)^{\frac{2}{1+\alpha_1}}$  and  $f_3(\xi_1, \xi_2) = \text{sig}(\xi_1)^{\frac{2}{1+\alpha_1}} \text{sig}(\xi_2)^{\frac{2\alpha_1}{1+\alpha_1}}$  can be lower and upper bounded on the circle  $\mathbb{S} = \{(\xi_1, \xi_2) : \xi_1^2 + \xi_2^2 = 1\}$  as follows,*

$$-M_2 \leq f_2(\xi_1, \xi_2) \leq M_2 \quad (2.101)$$

$$-M_2 \leq f_3(\xi_1, \xi_2) \leq M_2 \quad (2.102)$$

with  $M_2 = \left(\frac{1}{1+\alpha_1}\right)^{\frac{1}{1+\alpha_1}} \left(\frac{\alpha_1}{1+\alpha_1}\right)^{\frac{\alpha_1}{1+\alpha_1}}$ . For  $0 < \alpha_1 < 1$ ,  $M_2$  varies in  $0.5 < M_2 < 1$ .

*Proof.* The proof of this Lemma is given in the Appendix A.5.  $\square$

Since a strict Lyapunov function has not been found, we can only show here how the analysis can be completed when such a function is found. Since the first six rows of  $f(x)$  in (2.64) are homogeneous of degree  $\kappa = \alpha_1 - 1$  (see the proof of Lemma 2.9 in [69, 70] for more details), according to Lemma 2.7 there exists a  $C^j$  homogeneous Lyapunov function of degree  $\sigma_0 > j \cdot \max\{r_1, \dots, r_n\}$  for the system  $\dot{x} = f(x)$ . This Lyapunov function,  $V(x)$  satisfies

$$c_1 \|x\|_{r,m}^{\sigma_0} \leq V(x) \leq c_2 \|x\|_{r,m}^{\sigma_0} \quad (2.103)$$

with  $\|x\|_{r,m}$  the homogeneous norm according to Definition 2.5,  $c_1 = \min_{z \in S_0} V(z)$  and  $c_2 = \max_{z \in S_0} V(z)$  where  $S_0 = \{x \in \mathbb{R}^6 \mid \|x\|_{r,m} = 1\}$ . Since both the Lyapunov function  $V(x)$  and the first six rows of  $f(x)$  in (2.64) are homogeneous, it can be shown that the time derivative of this Lyapunov function is also homogeneous (of degree  $\sigma_0 + \kappa$ ) and satisfies

$$-\hat{c}_2 \|x\|_{r,p}^{\sigma_0+\kappa} \leq \dot{V}(x) \leq -\hat{c}_1 \|x\|_{r,p}^{\sigma_0+\kappa} \quad (2.104)$$

with  $c_1 = \min_{z \in S_0} -\dot{V}(z)$  and  $c_2 = \max_{z \in S_0} -\dot{V}(z)$ . It is shown (see [69] for more details) that the derivative of this Lyapunov function along the trajectory of system (2.63) satisfies

$$\dot{V}(x) = \frac{\partial V}{\partial x} \left( f(x) + \hat{f}(x) \right) \leq -\frac{c_0}{2} V(x)^{\frac{\sigma_0+\kappa}{\sigma_0}} \quad (2.105)$$

in a neighborhood of the origin  $\widehat{U} = \{x \in \mathbb{R}^6 : x_i = \lambda^{r_i} z_i, i = 1, \dots, n, 0 \leq \lambda < \lambda_0, z = (z_1, \dots, z_6)^T, \|x\|_{r,m} = 1\}$  with sufficiently small  $\lambda_0$ , where  $r_i$  are the dilation coefficients (see (A.16) for more details). If we consider the case which takes into account the system with the uncertainty term  $\Xi_r(x)$ , the time derivative of this Lyapunov function along the solutions of (2.72) is given by

$$\begin{aligned} \dot{V}(x) &= \frac{\partial V}{\partial x} \left( f(x) + \widehat{f}(x) + \Xi_r(x) \right) \\ &\leq -\frac{c_0}{2} V(x)^{\frac{\sigma_0 + \kappa}{\sigma_0}} + \left\| \frac{\partial V}{\partial x} \right\| \|\Xi_r(x)\| \\ &\leq -\frac{c_0}{2} V(x)^{\frac{\sigma_0 + \kappa}{\sigma_0}} + \left\| \frac{\partial V}{\partial x} \right\| \left( \rho_4 \|x\|^2 + \rho_3 \|x\| + \rho_2 \|x\|^{\alpha_2} + \rho_1 \|x\|^{\alpha_1} + \rho_0 \right) \end{aligned} \quad (2.106)$$

which can be used to compute ultimate bounds on the error trajectory if a strict Lyapunov function is known. Consequently, we conjecture that the error dynamics in the presence of the uncertainty given by (2.72) is uniformly ultimately bounded.

## 2.7 Illustrative simulations

Simulation results for the hybrid impedance controller with finite-time stability characteristics are given in this section. We consider a Puma 560, a 6 degrees of freedom manipulator with revolute joints having no flexibility and with rigid links. The kinematic and dynamic parameters of this manipulator can be found in [9]. We assume that the stiffness of the environment is  $k_E = 10^5$  [N/m]. The environment used in simulations is a hyperplane defined by the following line equation,

$$\varphi(p_e) = a_1 p_{e,x} + a_2 p_{e,y} + a_3 p_{e,z} + a_4 = 0 \quad (2.107)$$

where  $a_1 = 0$ ,  $a_2 = 1$ ,  $a_3 = 0$  and  $a_4 = 0.6$ , respectively. The environment geometry described by equation (2.107), corresponds to a plane parallel w.r.t. to  $x - z$  plane of the fixed world frame placed at  $y = -0.6$  [m]. The base frame of the Puma 560 is located at the coordinates  $[0 \ 0 \ 0]^T$ . An illustration of the simulation setup is shown in Figure 2.1.

Two different simulation studies are carried out. In the first one, the setpoint regulation and contact transition performance of the hybrid impedance controller with finite-time stability characteristics are investigated under the uncertainty of the robot dynamic model. Additional simulation results for the case when there is no uncertainty are given in the Appendix B.1, which show that perfect tracking is achieved in the absence of the uncertainty. The simulations are done in Matlab

with an implicit Euler solver with a fixed time step size of 0.0005 seconds. The end-effector is initially located at  $[0.17 \ -0.55 \ 0.014]^T$  in the first case. In the second case study the trajectory tracking performance is investigated for time-varying reference signals when the manipulator starts already from the contact

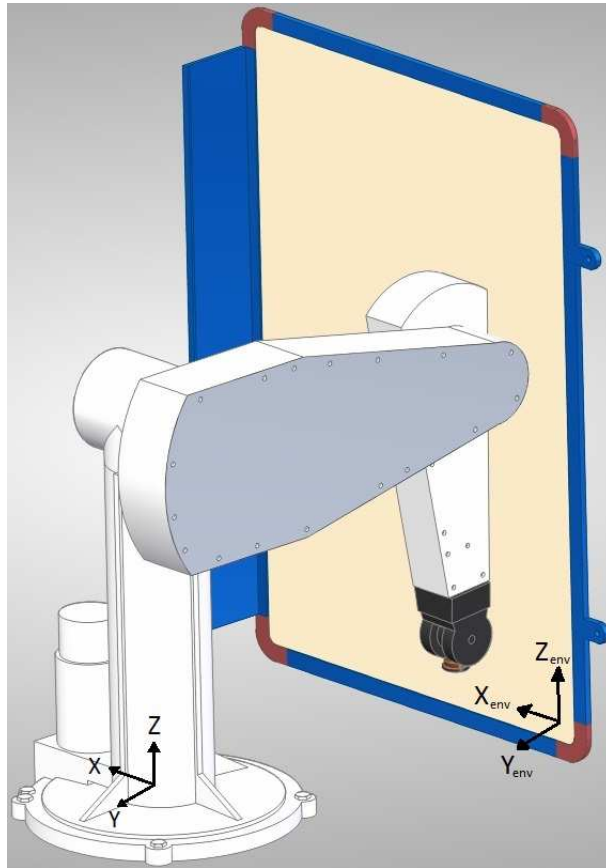


**Figure 2.1** A Puma 560 manipulator together with a whiteboard.

phase. The results for the case of a linear hybrid impedance controller are also presented for comparison purposes (e.g. like in [20]). This can be achieved by setting the exponential powers in the feedback terms of (2.47) and (2.53) to  $\alpha_1 = 1$  and consequently  $\alpha_2 = 1$ . For the first simulation, a constant desired contact force of  $f_{d,n} = -10$  [N] is used in the normal direction. The final desired quaternion for the rotational part of the closed-loop is selected randomly while satisfying the unit norm constraint. For both simulation studies, it is assumed that the masses of the links, their center of masses and inertias have 50% uncertainty, which is exaggerated with the purpose to investigate the performance of the hybrid impedance

controller. Furthermore, each joint is affected by viscous and asymmetric Coulomb friction given by  $\tau_f(\dot{\theta}_i) = \tau_{\text{cou},1}\text{sgn}(\dot{\theta}_i) + \tau_{\text{cou},2} + \tau_{\text{visc}}\dot{\theta}_i$ , which are not compensated by the controllers, i.e.  $\hat{\tau}_f(\dot{\theta}_i) = 0$ . The effect of actuator saturation is also present in the simulation model where the numerical values of the limits are taken from [9]. The parameters of both control laws are selected as  $k_{d,t} = 100$ ,  $k_{d,n} = 0$ ,  $b_{d,t} = 20$ ,  $b_{d,n} = 20$ ,  $m_{d,t} = 1$ ,  $m_{d,n} = 1$  and  $K_{f,r} = I_3$  for the translational part and  $M_{d,\phi} = I_3$ ,  $B_{d,\phi} = 10\sqrt{2}I_3$  and  $K_{d,\phi} = 50I_3$  with the sole difference of the exponential powers of the feedback terms. The powers of the nonlinear feedback terms are  $\alpha_1 = 2/5$  and  $\alpha_2 = 2\alpha_1/(\alpha_1 + 1) = 4/7$ . The results of the first simulation study are shown in Figure 2.2 and Figure 2.4 where the linear hybrid impedance controller is used and in Figure 2.3 and 2.5 where the hybrid impedance controller with finite time stability characteristics is used. The initial value of the actual end-effector quaternion vector is  $[\eta_e(0) \ \epsilon_e^T(0)]^T = [-0.5 \ 0.5 \ 0.5 \ 0.5]^T$ , whereas the desired one is given by  $[\eta_d \ \epsilon_d^T]^T = [-0.0970 \ 0.8789 \ -0.2313 \ -0.4058]^T$ . When Figures 2.4 and 2.5 are compared it can be observed that a zero steady-state error is not achieved due to the presence of uncertainty in the robot model. However, the steady state position error in the tangential directions and orientation errors are a lot smaller for the finite-time controller compared to the linear one and convergence speed is higher. The steady-state force error obtained using the finite-time stable controller is slightly less compared to the linear one. The magnitude of the contact force peaks and the contact transition duration are lower for the finite-time controller. However, this can be due to the specific type of damping function used in the controller, since energy loss and consequently contact force peaks at impacts are primarily related to damping [26]. It can be seen in Figures 2.2 and 2.3 that actuator torque limits are reached at a few instances. Furthermore, Figure 2.3 shows that the actuator torques are not chattering since finite time convergent controller is continuous. The desired position trajectories in the tangential directions used for the second simulations are generated by

$$r_{d,t}(t) = \begin{cases} r_{d,t}(0), & t \leq 0 \\ a_5t^5 + a_4t^4 + a_3t^3 + a_2t^2 + a_1t + a_0, & 0 \leq t \leq t_1 \\ r_{d,t}(t_1) + 0.075(1 - \cos(t - t_1)), & t_1 \leq t \end{cases}$$

where the coefficients  $a_i$  for  $i = 1, \dots, 5$  of the 5<sup>th</sup> order polynomial are computed using with  $r_{d,t}(0)$  and  $r_{d,t}(t_1)$  being the initial and final points of the first segment of the reference. The desired force trajectory in the normal direction is given by

$$f_{d,n}(t) = -10 \cdot (1 + 0.5 \sin(t)).$$

The desired trajectory for the quaternion is obtained by integrating the following differential equation

$$\dot{q}_d = \frac{1}{2}T(q_d)\omega_d + \frac{\gamma}{2}(1 - q_d^T q_d)q_d \quad (2.108)$$



where the second term is a nonlinear feedback or normalization term with  $\gamma > 0$  being a design parameter which helps preserving the unity of quaternion norm (see [50] for more details). In (2.108), the following desired angular velocity

$$\omega_d(t) = 0.2 \cos(0.5t) \left(1 - e^{-0.1t^3}\right) + 0.1 \sin(0.5t) \left(1 - e^{-0.1t^3}\right)$$

is used and its time derivative,  $\dot{\omega}_d$  represents the desired angular acceleration signal. The parameters of both control laws are selected as  $k_{d,t} = 100$ ,  $k_{d,n} = 0$ ,  $b_{d,t} = 20$ ,  $b_{d,n} = 20$ ,  $m_{d,t} = 1$ ,  $m_{d,n} = 1$  and  $K_{f,r} = I_3$  and  $M_{d,\phi} = I_3$ ,  $B_{d,\phi} = 10\sqrt{2}I_3$  and  $K_{d,\phi} = 50I_3$ . The powers of the nonlinear feedback terms are given as  $\alpha_1 = 2/5$  and  $\alpha_2 = 2\alpha_1/(\alpha_1 + 1) = 4/7$ . The results of the second simulation study are given in Figures 2.6 and 2.7 when the linear hybrid impedance controller is used and in Figures 2.8 and 2.9 where the hybrid impedance controller with finite time stability characteristics is used. In Table 2.1, we show the maximum values, the integrated absolute values (IAE) and the integrated square values (ISE) of the quaternion difference (i.e.  $\eta_d - \eta_e$ ), the position errors in the tangent directions, and the contact force errors in the normal directions. Here, the integrated absolute values (IAE) and the integrated square values (ISE) of the aforementioned errors are defined by,

$$\text{IAE} = \int_0^{\infty} |e(t)| dt \quad \text{ISE} = \int_0^{\infty} (e(t))^2 dt$$

where  $e(t)$  is the error variable of interest (position, force, etc.). Furthermore, maximum values and the root mean square of the norm of the actuator torque vector ( $\tau$ ) are also presented in Table 2.1. It can be seen that the difference between the desired and actual quaternions and the position errors are a lot lower for the finite-time convergent controller compared to the linear one.

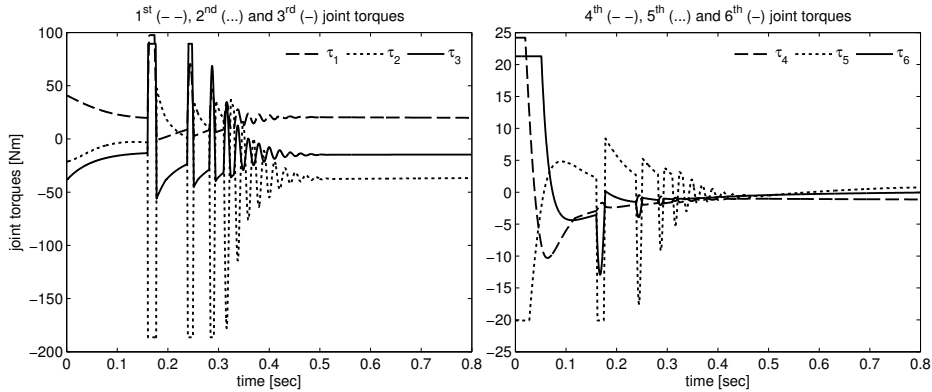


**Figure 2.2** Joint torques when the actuator saturation is applied and the linear hybrid impedance controller is used.

The force errors for the controller with finite-time stability characteristics are lower compared to the linear one, however, the difference is not as high as is the case with the other errors. Furthermore, it can be observed from the maximum value and root mean square of the norm of the actuator torques that the power usage for both controllers are similar to each other. Similar to the previous simulation study, the actuator torques for the controller with finite-time convergence characteristics do not chatter since it is continuous. Moreover, since the environment used during the simulations is not a perfectly rigid one, an infinite number of bounces in a finite time interval, also known as the Zeno behavior, does not occur.

**Table 2.1** Comparison of tracking errors and control signals achieved with two control laws

Quantity/Cont.	Hyb. imp. cont. lin.	Hyb. imp. cont. fin. tim.
Max. quat. diff.	0.1462	0.0077
IAE quat. diff.	1.2411	0.0586
ISE quat. diff.	0.1255	$2.9197 \cdot 10^{-4}$
Max. pos. error [m]	0.0727	0.0010
IAE pos. error [m]	0.7994	0.0108
ISE pos. error [m]	0.0489	$8.4690 \cdot 10^{-6}$
Max. for. error [N]	2.9914	1.7613
IAE for. error [N]	20.3435	10.4002
ISE for. error [N]	37.9485	11.4069
Max. abs. cont. inp. [Nm]	48.8722	51.3070
RMS cont. inp. [Nm]	38.3976	41.3312

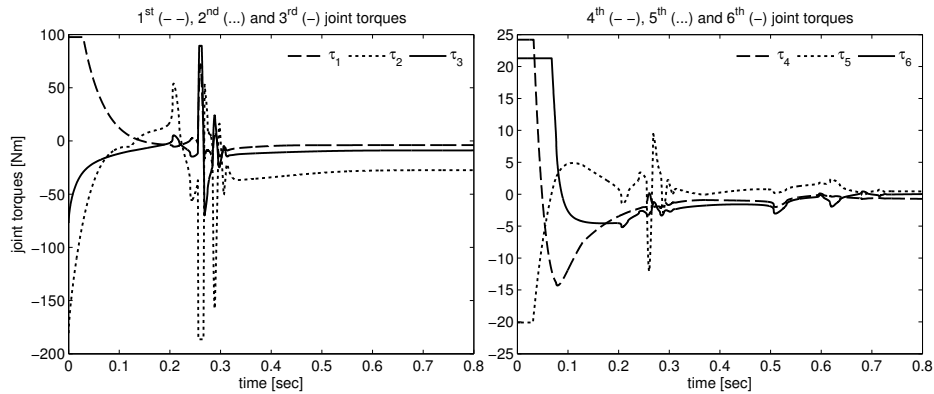


**Figure 2.3** Joint torques when the actuator saturation is applied and the finite-time stable hybrid impedance controller is used.

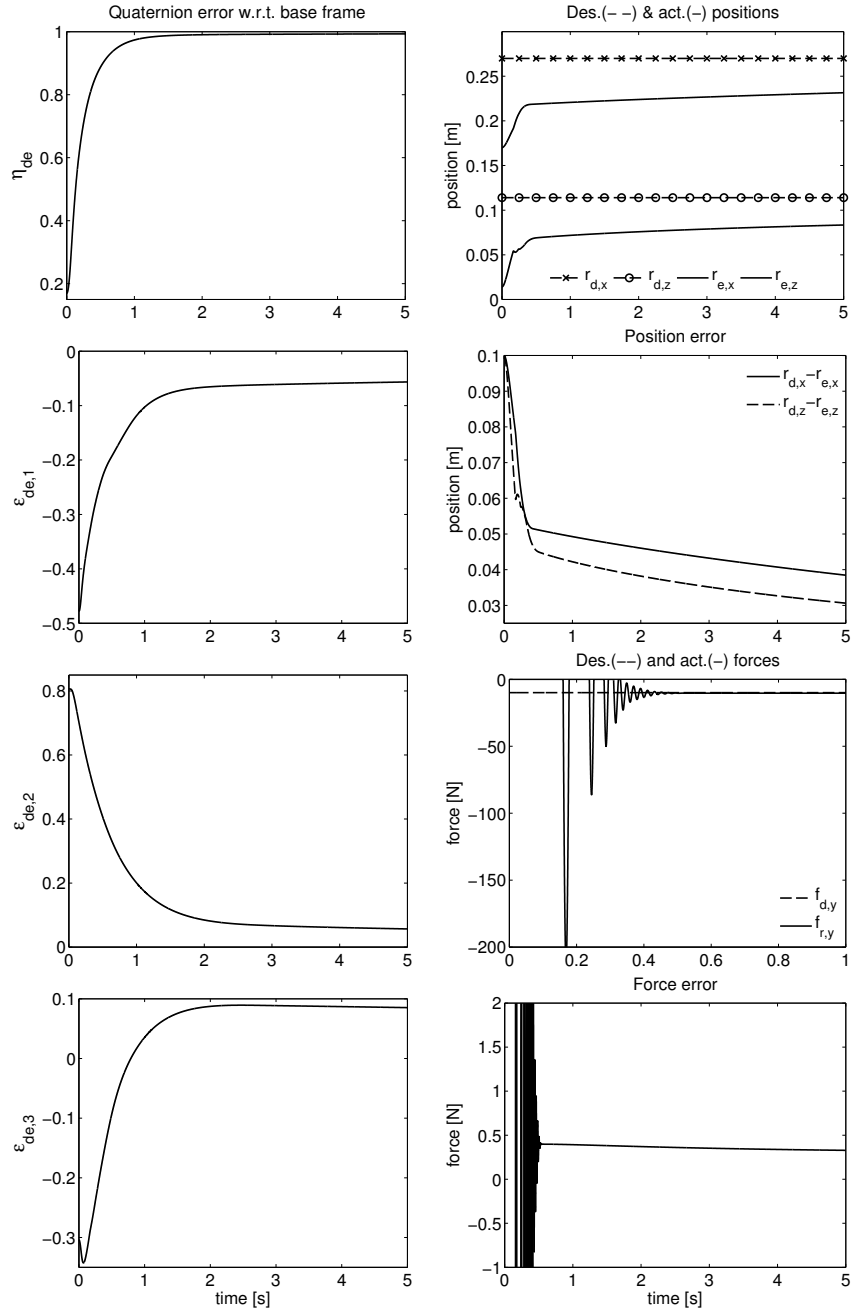


**Figure 2.4** Quaternion error ( $\eta_{de}, \epsilon_{de,1}, \epsilon_{de,2}, \epsilon_{de,3}$ ) expressed w.r.t. base frame (left), desired  $r_{d,t}$  and actual  $r_{e,t}$  tangential end-effector positions (top right), and their difference ( $2^{nd}$  from right), desired  $f_{d,n}$  and actual  $f_{r,n}$  normal contact forces ( $3^{rd}$  from right) and their difference (bottom right) with the linear hybrid impedance controller.

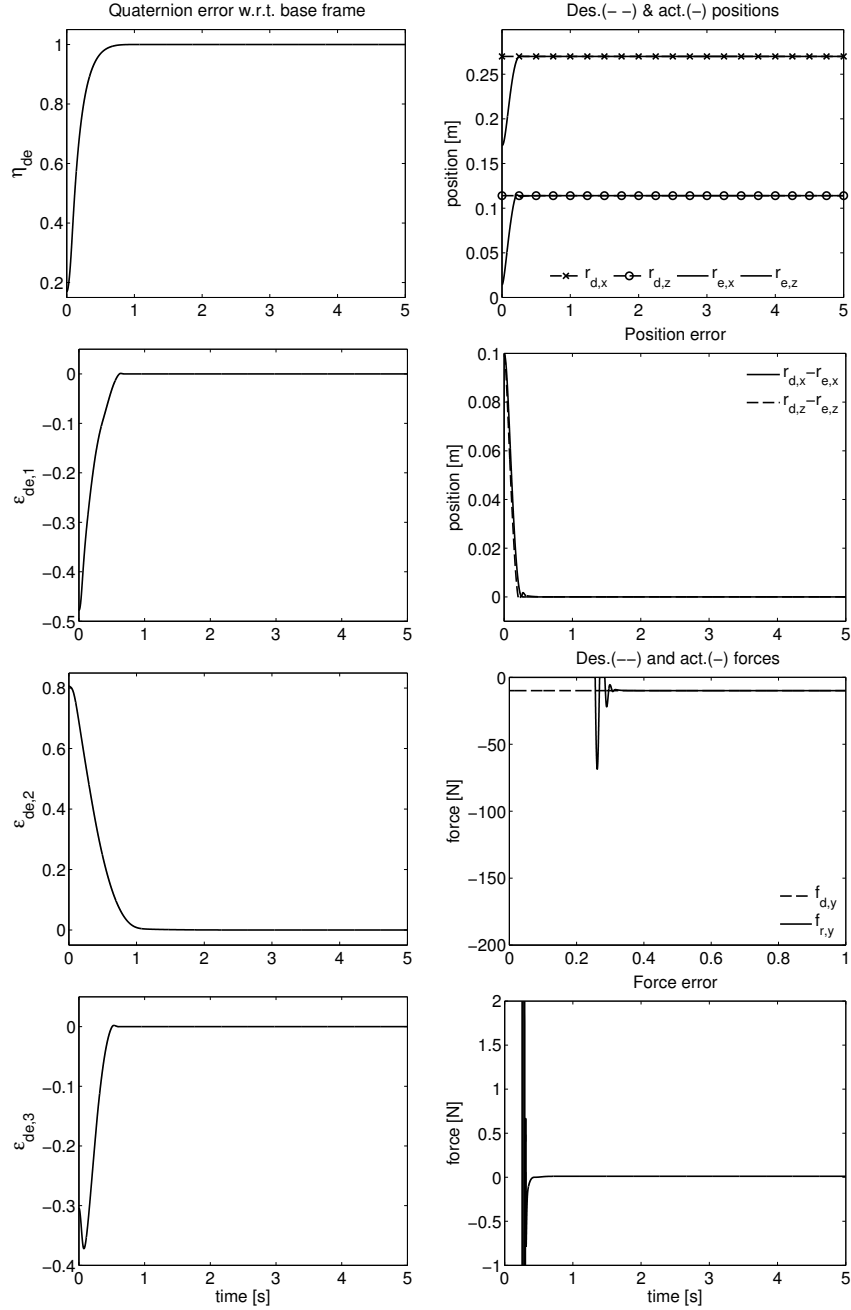


**Figure 2.5** Quaternion error ( $\eta_{de}, \epsilon_{de,1}, \epsilon_{de,2}, \epsilon_{de,3}$ ) expressed w.r.t. base frame (left), desired  $r_{d,t}$  and actual  $r_{e,t}$  tangential end-effector positions (top right), and their difference ( $2^{nd}$  from right), desired  $f_{d,n}$  and actual  $f_{r,n}$  normal contact forces ( $3^{rd}$  from right) and their difference (bottom right) with the finite-time stable hybrid impedance controller.

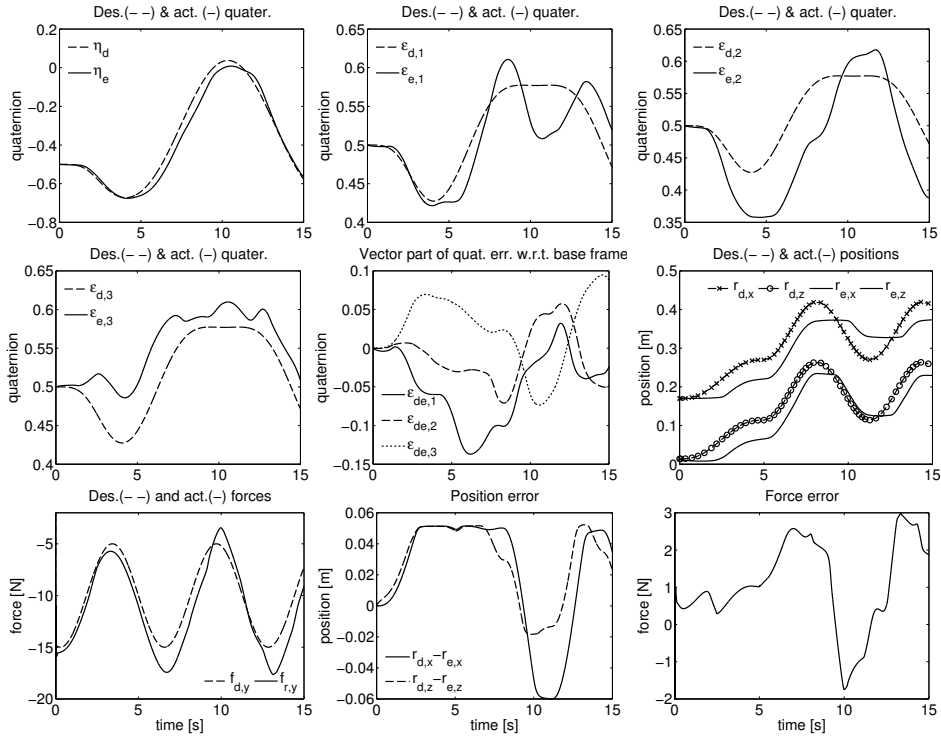


**Figure 2.6** Linear hybrid impedance controller. Desired and actual quaternions ( $1^{st}$  row, left plot of  $2^{nd}$  row), vector part of quaternion error w.r.t. base frame (middle plot of  $2^{nd}$  row), desired and actual positions (right plot of  $2^{nd}$  row), desired and actual forces (left plot of  $3^{rd}$  row), position error (middle plot of  $3^{rd}$  row), force error (right plot of  $3^{rd}$  row)

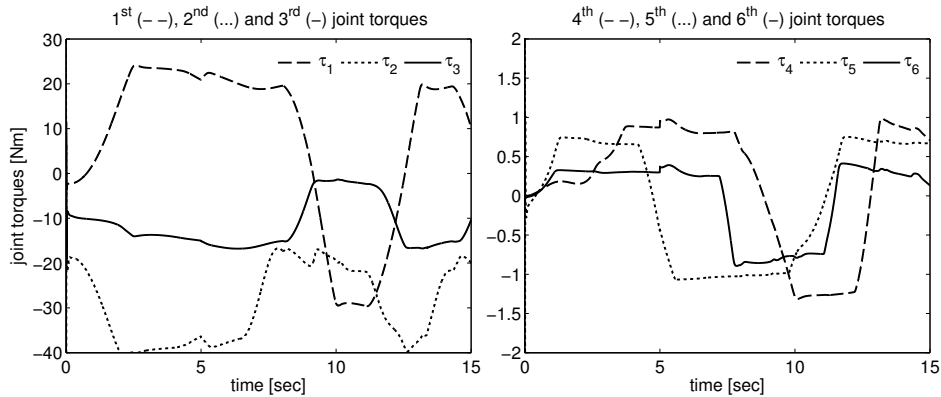


**Figure 2.7** Joint torques when the actuator saturation is applied and the linear hybrid impedance controller is used.

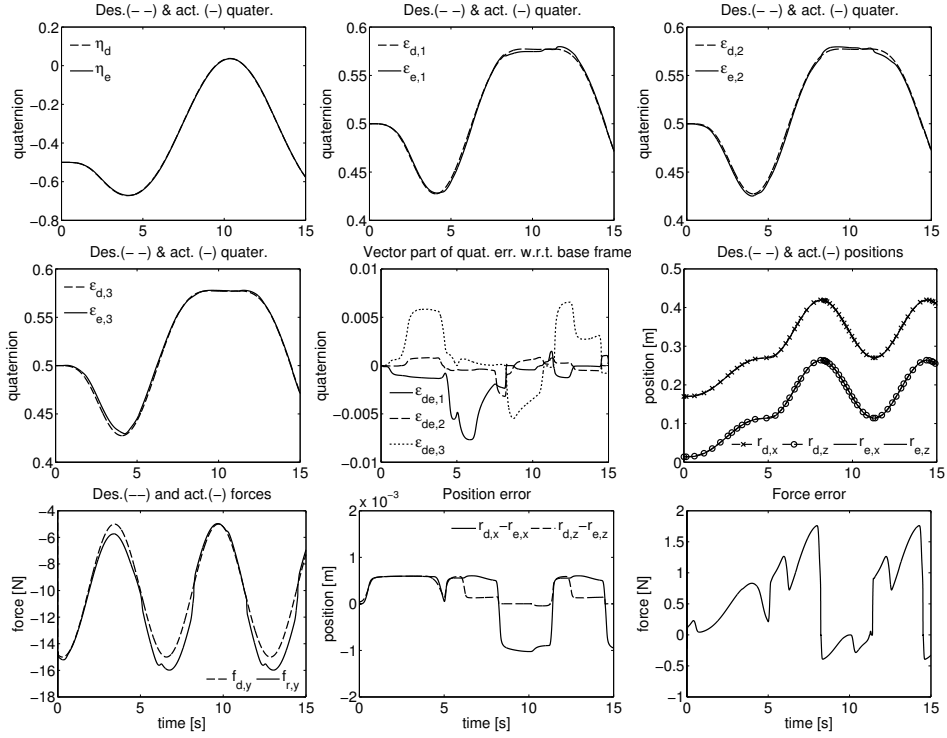


**Figure 2.8** Finite-time stable hybrid impedance controller. Desired and actual quaternions (1<sup>st</sup> row, left plot of 2<sup>nd</sup> row), vector part of quaternion error w.r.t. base frame (middle plot of 2<sup>nd</sup> row), desired and actual positions (right plot of 2<sup>nd</sup> row), desired and actual forces (left plot of 3<sup>rd</sup> row), position error (middle plot of 3<sup>rd</sup> row), force error (right plot of 3<sup>rd</sup> row)

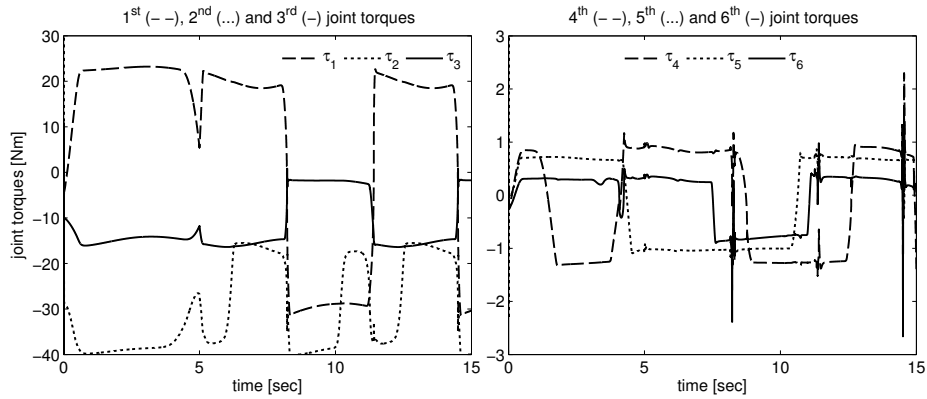


**Figure 2.9** Joint torques when the actuator saturation is applied and the finite-time stable hybrid impedance controller is used.

## 2.8 Experiments

In this section, the experimental results obtained using a three degrees-of-freedom manipulator are presented.

### 2.8.1 Experimental setup

The experimental setup consists of the robot arm shown in Figure 2.10 and a portable whiteboard. Three revolute degrees-of-freedom (RRR kinematics) of the robot arm are implemented as waist, shoulder, and elbow. Similar kinematics is very common in industry. The first three degrees-of-freedom of the PUMA 560 robot, for instance, are implemented in a similar fashion. The robot mechanism is

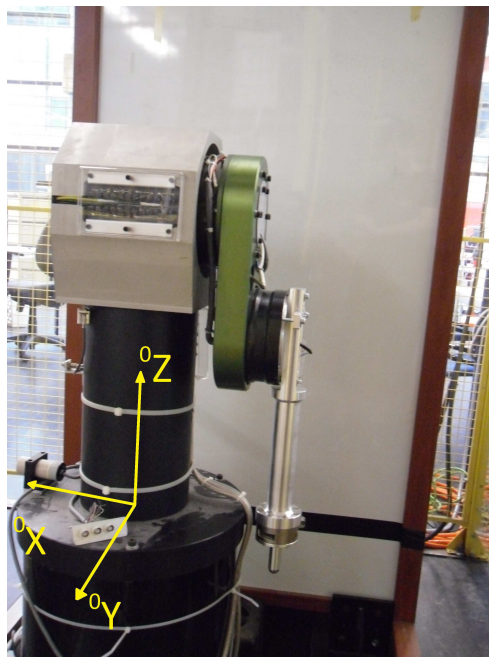


**Figure 2.10** The RRR robot arm together with the whiteboard environment.

actuated by brushless DC direct-drive motors from Dynaserv DM-series [153], with nominal torques of 60, 30, and 15 [Nm], respectively. Motors are of outer-rotor type with internal encoders and bearings, and each of them is directly coupled to the corresponding robot link. Since no gearboxes are used for the coupling, the RRR robot belongs to the class of direct-drive robots [10]. Integrated optical encoders provide 655360 pulses per revolution, which is equivalent to the angular resolution of approximately  $10^{-5}$  [rad]. The motors are driven by power amplifiers

with built-in current controllers. Both encoders and amplifiers are connected to a PC-based control system. This system consists of a MultiQ-PCI board for data acquisition and control [115], combined with a real time Windows application Wincon [116] that runs Simulink generated code using Real-Time Workshop on a PC. Such system facilitates the design and real-time implementation of controllers in Simulink. The controllers run at a sampling frequency of  $f_s = 2000$  [Hz] ( $T_s = 0.5$  [ms]). The power electronics ensure linearity between the commanded voltages  $u_i$  at the output of the MultiQ-PCI board (control voltage) and the torques  $\tau_i$  generated by the motors

$$\tau_i = k_i^{\tau u} u_i \quad (2.109)$$

where the gains are  $k_1^{\tau u} = 12$  [N/V],  $k_2^{\tau u} = 9$  [N/V],  $k_3^{\tau u} = 3$  [N/V] which are taken from [80]. As is the case with any power amplifier, the relation between the torques and voltages is not perfectly linear. This can have some influence on the performance of the controller. Because of the direct-drive actuation, the dynamics of the RRR robot are highly nonlinear and coupled (see [10] for more details). The joints of the robot arm are influenced by friction including severe stick-slip phenomena. Aside from rigid-body dynamics and friction, several other effects can be excited, e.g. vibrations at the robot base and high frequency resonances. The kinematic and dynamic models of the RRR robot can be found in [81]. In the derivation of the forward kinematics, Denavit-Hartenberg (DH) convention is used. The base frame ( ${}^0X^0Y^0Z$ ) used in this convention is shown on the physical robot in Figure 2.10. The experimental setup has been modified w.r.t. to the one considered in [81] such that a drawing task on the whiteboard shown in Figure 2.10 can be executed. For this purpose, an ATI SI-65-5 Gamma model force/torque sensor (transducer) is used to measure the contact forces. The transducer is a compact, rugged, monolithic structure that converts force and torque into analog strain gage signals [12]. The measured analog voltage signals are sent to the PC using six A/D converters of the MultiQ-PCI board. In order to mount the force sensor to the robot arm, a suitable mechanical interface (i.e. the last link) is designed and manufactured using aluminum. The length and weight of this mechanical interface are close to the original last link of the robot arm [81]. Furthermore, in order to make contact with the whiteboard a probe is manufactured comprised of an aluminum hollow cylinder body and a bearing ball. The details of the mechanical design of the last link and the probe can be found in the Appendix C.2. The controller developed in this chapter is derived in terms of Cartesian (or task) space variables, that are expressed w.r.t. a base frame denoted by '0' (see the frame  ${}^0X^0Y^0Z$  shown in Figure 2.10). Therefore, for the proper execution of the controller, a homing procedure for the RRR manipulator is required. Due to malfunctioning of the existing homing sensors at the RRR manipulator, automatic homing was not possible at the time experiments have been carried out. Instead, the arm has been manually placed to its initial configuration. Manual homing is



not as precise as using the homing sensors, which also influences the accuracy of any function or map (e.g. end-effector position  $p_e(\theta)$ , inertia matrix  $M(\theta)$ , etc.) that is calculated using the joint coordinates  $\theta$ . The velocities are not measured directly, but are calculated by numerical differentiation of the low-pass filtered encoder measurements. A 4<sup>th</sup> order Butterworth low-pass filter with a cut-off frequency of 80 [Hz] is used for this purpose.

### 2.8.2 Experimental results

The experimental results related to a drawing task on a whiteboard are presented in this subsection. The purpose of the experiment is to draw half of a circle on the whiteboard while controlling the force normal to it. Additional experimental results are presented in Appendix B.2, where the desired half circle trajectory in the contact phase is designed to be executed faster than the one given in this section. This is done in order to highlight the effect of stick-slip friction phenomena present in the experiments. The whiteboard is placed parallel to the  ${}^0X$ - ${}^0Z$  plane of the base frame of the RRR robot (see the frame  ${}^0X{}^0Y{}^0Z$  shown in Figure 2.10). For the configuration shown in Figure 2.10, the  ${}^0Y$  axis coincides with the normal vector of the whiteboard. The environment (i.e. the whiteboard) geometry is similar to the one described by (2.107), although it is not a perfectly planar wall, where the coefficients are  $a_1 \approx 0$ ,  $a_2 \approx 1$ ,  $a_3 \approx 0$  and  $a_4 \approx 0.426$  [m]. For the environment geometry under consideration, the task space variables are selected as  $r_{e,n} = p_{e,y}$  (i.e. y-axis) for the normal direction,  $r_{e,t} = [p_{e,x} \ p_{e,z}]^T$  (i.e. x,z axes) for the tangent directions. Since the sole whiteboard is not that stiff and can tilt around an axis parallel to  ${}^0X$ , it is stiffened by fixing cardboard boxes to its back and placing a portable file cabinet behind it. The force sensor readings are affected by factors other than the actual contact force arising from the contact with the environment, such as the weight of the probe and tool plate of the sensor (not the weight of the whole sensor). Therefore, prior to the experiment, the calibration routine introduced in [145] is performed to compensate for influences of these weights. The calibrated force sensor readings are filtered using a 4<sup>th</sup> order Butterworth low-pass filter with a cut-off frequency of 50 [Hz]. The controller (2.45), (2.56) for the case of unknown contact stiffness and location derived in this chapter drives the end-effector with a constant velocity in a given direction to make contact with the whiteboard. The manipulator is brought to the vicinity of the whiteboard using a joint space inverse dynamics controller. This controller is enabled to bring the RRR robot from its initial configuration  $\theta = [\frac{3}{2}\pi \ -\frac{1}{2}\pi \ 0]^T$  which corresponds to the end-effector position  $p_e = [p_{e,x} \ p_{e,y} \ p_{e,z}]^T = [-0.2615 \ 0 \ -0.0585]^T$  to the configuration  $\theta = [\frac{3}{2}\pi \ \frac{1}{6}\pi \ -\frac{2}{3}\pi]^T$  which corresponds to the end-effector position  $p_e = [p_{e,x} \ p_{e,y} \ p_{e,z}]^T = [-0.2615 \ -0.1732 \ 0.2415]^T$  in 5 seconds using a reference trajectory defined by,

$$\theta_{\text{des}}(t) = \frac{\theta_{\text{fin}} - \theta_{\text{ini}}}{t_f} \left( t - \frac{\sin\left(\frac{2\pi}{t_f}t\right)}{\frac{2\pi}{t_f}} \right) + \theta_{\text{ini}} \quad (2.110)$$

where  $\theta_{\text{ini}}$ ,  $\theta_{\text{fin}}$  and  $t_f$  are the initial and final angular positions and total travel time between them, respectively. The next  $t = 2.5$  [s] the robot arm is brought from the configuration  $\theta = [\frac{3}{2}\pi \ \frac{1}{6}\pi \ -\frac{2}{3}\pi]^T$  to the vicinity of the whiteboard at the configuration  $\theta = [\frac{3}{2}\pi \ \frac{1}{6}\pi \ -\frac{1}{2}\pi]^T$  which corresponds to the end-effector position  $p_e = [p_{e,x} \ p_{e,y} \ p_{e,z}]^T = [-0.2615 \ -0.3825 \ 0.2976]^T$ . Here, once again the reference trajectory (2.110) is used. The plots of the reference and actual joint trajectories for this part of the experiment are shown in Figure 2.11. It can be realized from Figure 2.11 that the tracking performance of the third joint

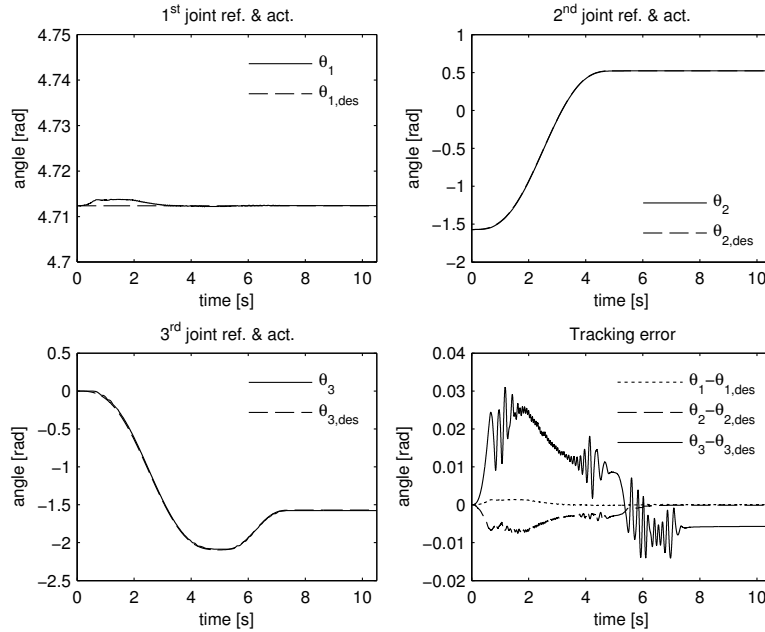


**Figure 2.11** Reference (- -) and actual (-) joint angular positions for moving from  $\theta = [\frac{3}{2}\pi, -\frac{1}{2}\pi, 0]^T$  to  $\theta = [\frac{3}{2}\pi, \frac{1}{6}\pi, -\frac{1}{2}\pi]^T$ .

is the worst and it suffers the most from stick-slip oscillations. The influence of these stick-slip oscillations are also visible in the end-effector force plots, see the vibrations recorded by the force sensor between  $t = 1$  [s] and  $t = 8.5$  [s] in Figure 2.14 for example. Since the force sensor is quite sensitive, it also picks up those vibrations. The tracking errors remaining at the end of this reference trajectory after the manipulator comes to stand-still are given by  $\theta_1 - \theta_{1,\text{des}} = 3.8 \cdot 10^{-5}$

[rad],  $\theta_2 - \theta_{2,des} = 1.5 \cdot 10^{-4}$  [rad] and  $\theta_3 - \theta_{3,des} = 5.7 \cdot 10^{-3}$  [rad], respectively. Starting from  $t = 8.5$ , [s] the manipulator is commanded to hold its position until  $t = 13.5$  [s] such that it can switch from the inverse dynamics controller to the controller (2.45), (2.56) with  $f_d = 0$  and  $k_{d,n} \neq 0$ . The gains for the controller (2.45), (2.56) are selected as,  $M_{d,r} = 2I_3$ ,  $B_{d,r} = 27I_3$ ,  $K_{d,r} = 1100I_3$  and  $K_{f,r} = \text{diag}\{0.9, 0.35, 0.35\}$  and the powers are selected as  $\alpha_1 = 4/5$  and  $\alpha_2 = 8/9$ . This selection is done by trial and error based on achieved position and force tracking errors. The feedback gains are increased and the power  $\alpha_1$  is decreased until low position and force tracking errors are obtained. The switching takes place at  $t = 11.5$  [s] which can be noticed from the small peaks in the joint torque plots in Figure 2.12. At  $t = 13.5$  [s], the reference force is switched from  $f_{d,n} = 0$  to  $f_{d,n} = -10$  [N] and the stiffness gain is switched from  $k_{d,n} = 1100$  to  $k_{d,n} = 0$  which drives the end-effector with a (approximately) constant velocity until it makes contact with the whiteboard. From the switching instant on, the end-effector position in the normal direction (y-direction in this case) is monitored during the whole time interval when  $k_{d,n} = 0$  and this position is taken as the reference one for the normal direction. Note that the position tracking error in the normal (y-) direction shown in Figure 2.16 between  $t = 13.5$  [s] and  $t = 36$  [s] are not relevant, since  $k_{d,n} = 0$  holds in that whole time interval and the force tracking error is then the relevant variable. It can be observed from Figure 2.14 that contact with the whiteboard is established approximately at  $t = 14.7$  [s]. This can also be verified from the spikes observed in the end-effector forces in the tangential directions in Figure 2.13. The spikes in the forces in the tangential (x-,z-) directions settle approximately around a value of 0 [N]. The end-effector force in the normal (y-) direction settles at  $f_{e,n} = -1.5$  [N], which is not that close to the desired end-effector force. This is due to the static friction in the joints and probably the inaccurate knowledge of the actuator gain (2.109). Three seconds after contact is made, at  $t = 18$  [s], the end-effector is commanded to draw a half circle of radius  $R_{\text{circ}} = 0.0625$  [m] twice on the whiteboard in the tangential directions. The total duration of this half circle trajectory is 12.254 [s]. The desired end-effector position  $r_{d,t}(t)$ , velocity  $\dot{r}_{d,t}(t)$  and acceleration  $\ddot{r}_{d,t}(t)$  describing the half circle trajectory are generated by

$$\begin{aligned} r_{d,t}(t) &= \begin{bmatrix} r_{1,c} - R_{\text{circ}} \cos(\varpi_0 + \varsigma(t)) \\ r_{2,c} + R_{\text{circ}} (1 + \sin(\varpi_0 + \varsigma(t))) \end{bmatrix}, \\ \dot{r}_{d,t}(t) &= \begin{bmatrix} R_{\text{circ}} \dot{\varsigma}(t) \sin(\varpi_0 + \varsigma(t)) \\ R_{\text{circ}} \dot{\varsigma}(t) \cos(\varpi_0 + \varsigma(t)) \end{bmatrix}, \\ \ddot{r}_{d,t}(t) &= \begin{bmatrix} R_{\text{circ}} \ddot{\varsigma}(t) \sin(\varpi_0 + \varsigma(t)) + R_{\text{circ}} \dot{\varsigma}^2(t) \cos(\varpi_0 + \varsigma(t)) \\ R_{\text{circ}} \ddot{\varsigma}(t) \cos(\varpi_0 + \varsigma(t)) - R_{\text{circ}} \dot{\varsigma}^2(t) \sin(\varpi_0 + \varsigma(t)) \end{bmatrix} \end{aligned}$$

where  $R_{\text{circ}}$ ,  $\varpi_0$ ,  $r_{1,c}$  and  $r_{2,c}$  are the radius of the circle, the initial angle defining the initial point on the circle and the coordinates of the initial point in Cartesian

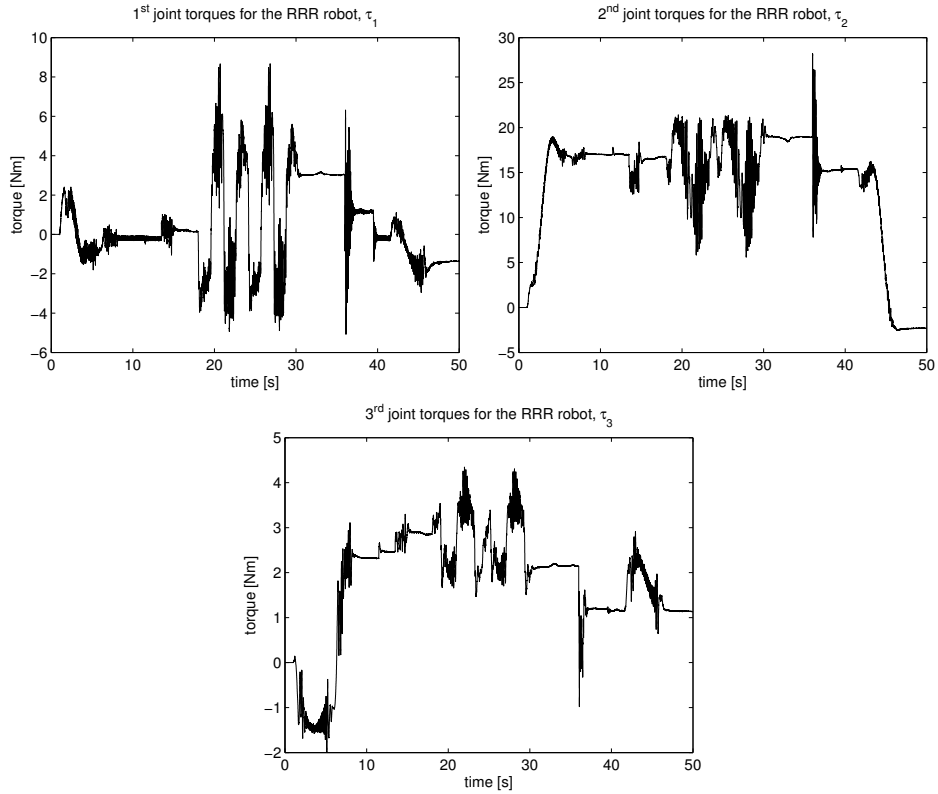


**Figure 2.12** Joint torques for the finite-time stable hybrid impedance controller.

space, respectively. Furthermore, the angle  $\zeta(t)$  and its time derivatives  $\dot{\zeta}(t)$  and  $\ddot{\zeta}(t)$  are generated by the 3<sup>rd</sup> order profile with constant jerk, constant acceleration and constant velocity intervals described by the equations given in the Appendix G. It can be realized from the Figure 2.15 that between the time instants  $t = 18$  [s] and  $t = 30.254$  [s] the tracking performance in x-direction is better than compared to the one in z-direction. The plots of the reference and actual half circles drawn by the robot on the whiteboard are shown in Figure 2.17. The high frequency oscillations visible in Figure 2.15 are due to a combination of the friction (mainly stick-slip phenomena) effects in the joints and the friction between the tip of the probe and the whiteboard. The effect of the contact friction is also visible in the end-effector force plots in the time interval  $t = 18$  [s] and  $t = 30.254$  [s] shown in Figure 2.13. See that the direction of the forces is changing according to the motion direction in these figures. Furthermore, some oscillations and spikes are also present in the end-effector force in the normal (y-) direction which are most likely due to joint friction (mainly stick-slip phenomena) and/or some parasitic

dynamics (flexibilities in the manipulator structure). It should be noted that such an effect is not uncommon in experiments reported in the literature related to motion on a surface while staying in contact with it (see Figures 5 and 6 in [156] for example). After the half circle trajectory is completed, the end-effector returns to approximately the initial position it made contact with the whiteboard for the first time (at  $t = 14.7$  [s]) and rests in that position until  $t = 36$  [s]. The end-effector force in the normal ( $y$ -) direction settles at  $f_{e,n} = -2.5$  [N]. The end-effector forces in the tangential directions settle at  $f_{e,t,1} = -0.42$  [N] and  $f_{e,t,2} = -0.7$  [N] which are most likely due to static friction between the probe and the whiteboard. At  $t = 36$  [s] the RRR robot is commanded a reference force of  $f_{d,n} = 10$  [N] for 0.5 [s] to break contact with the environment. The influence of the step type changes in the force reference can also be noticed in the joint torques in Figure 2.12. At  $t = 66.5$  [s] the reference force is switched from  $f_{d,n} = 10$  [N] to  $f_{d,n} = 0$  [N] and the stiffness is switched from  $k_{d,n} = 0$  to  $k_{d,n} = 1100$ . Since the end-effector position in the normal ( $y$ -) direction was logged during the time interval  $k_{d,n} = 0$ , its value at  $t = 36.5$  [s] is used as the setpoint. At  $t = 39.5$  [s], the manipulator is switched from the hybrid impedance controller to the joint space inverse dynamics controller. From that time instant on, the manipulator is driven back to the starting point of the experiment at  $\theta = [\frac{3}{2}\pi \quad -\frac{1}{2}\pi \quad 0]^T$  which corresponds to the end-effector position  $p_e = [p_{e,x} \quad p_{e,y} \quad p_{e,z}]^T = [-0.2615 \quad 0 \quad -0.0585]^T$  with a reference trajectory given by (2.110). It can be noticed from Figure 2.12 that no chattering phenomenon is present in the joint torques sent to the actuators since the control law is continuous.

## 2.9 Concluding remarks

In this chapter, a hybrid impedance controller with finite-time stability characteristics is derived. The controller is designed based on task space robot variables. The controller contains model based compensation terms based on manipulator dynamic model. The homogeneity principle for vector fields is used to achieve finite-time stability. The controller for rotational variables is designed using unit quaternions. Stability of the closed-loop system subject to this controller is analyzed assuming no uncertainty in the model based compensation terms. Guidelines for the robust stability analysis when manipulator dynamics is not perfectly known are also provided. The performance of the algorithm is tested in simulations with a Puma 560 robot. Furthermore, experimental results on a three degrees-of-freedom robot manipulator are provided. From the simulation results, it can be concluded that for similar amplitudes of the control signals, much better position and orientation tracking errors are achieved using the finite-time stable hybrid impedance controller as compared to the linear one, whereas this difference is not high for force tracking errors. Experimental results further demonstrate the tracking performance of the designed controller.

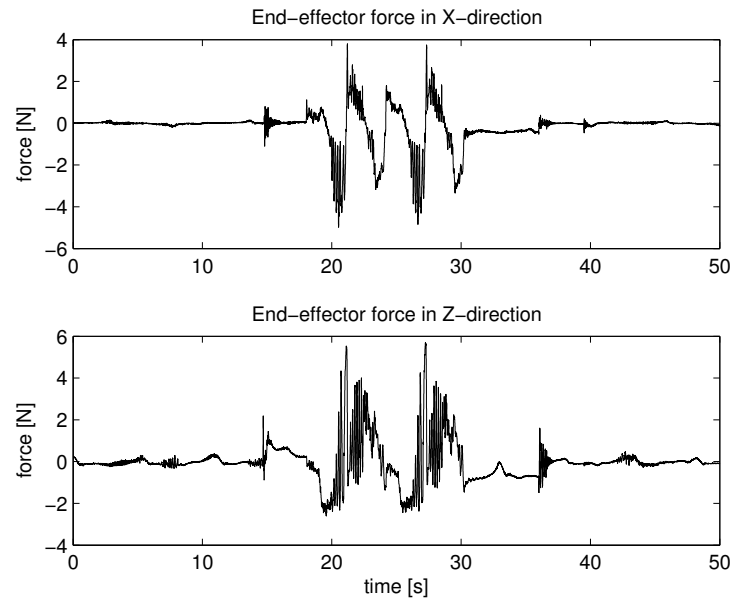


Figure 2.13 End-effector forces in tangential x-(top) and z-(bottom) directions.

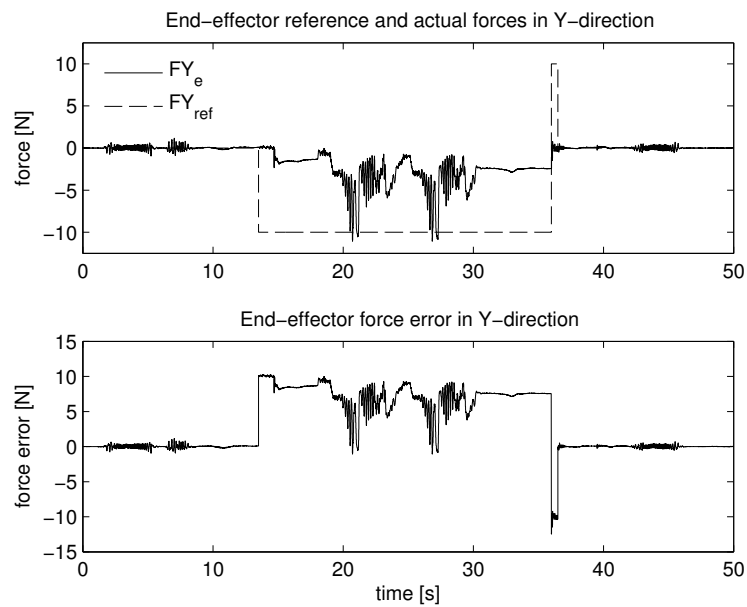
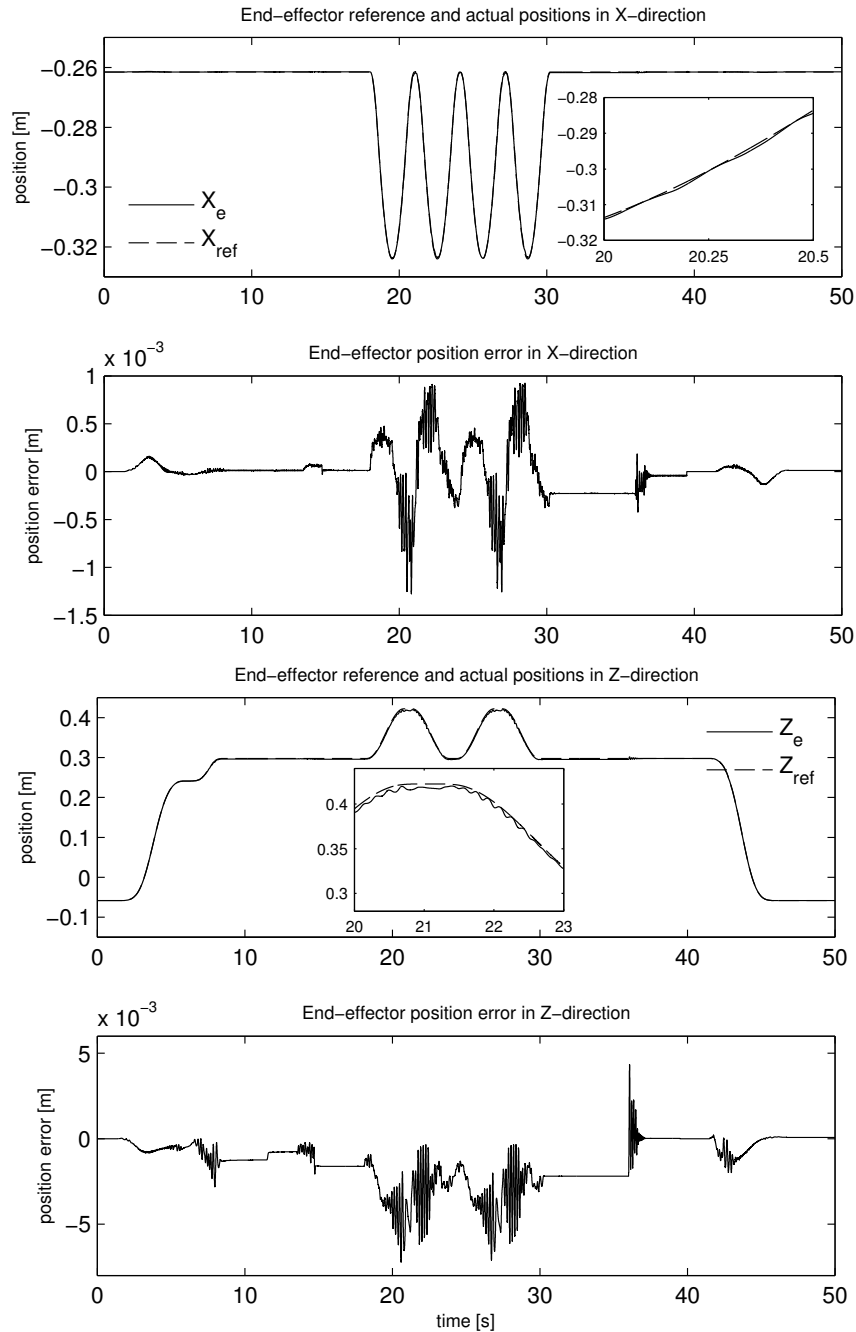


Figure 2.14 Reference (---), actual (—) end-effector forces in normal (y-) direction.



**Figure 2.15** Reference (- -) and actual (-) positions and error in tangential (x-,z-) directions.

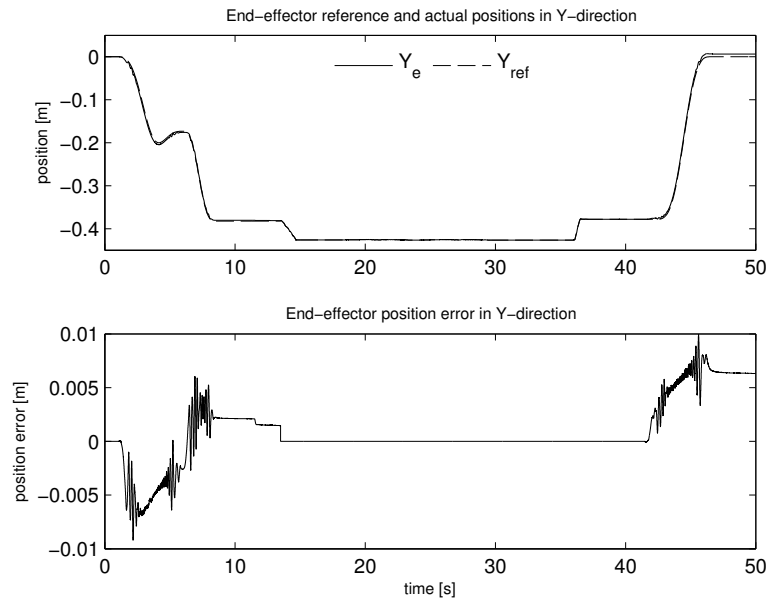


Figure 2.16 Reference (- -), actual (-) end-effector positions in normal (y-) direction.

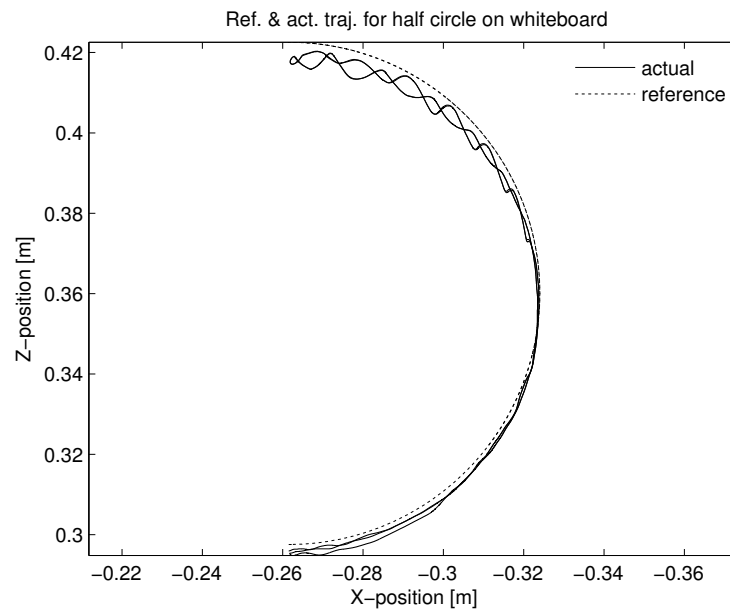


Figure 2.17 Reference ( $\cdots$ ), actual (-) end-effector positions for half circle part of trajectory.



# Chapter 3

## Impedance controller for cooperative manipulation

**Abstract** Cooperative manipulation enables multiple robot manipulators to work together to execute a common task. Two different modelling approaches are investigated for cooperative manipulation. The first one is applicable when the grasp is rigid such that there is no relative motion between the manipulators and the object at the contact points. The second one is applicable when relative motion exists at the contact points. A cascade controller is proposed for cooperative manipulation of an object for the rigid grasp case. This algorithm controls motion and internal forces of a grasped object together with contact forces between the object and environment. Only knowledge of the kinematics of the manipulated object is required, since the interaction forces and moments between the object and manipulators are measured. The internal stresses in the object are controlled based on enforced impedance relationships between the object and each manipulator. The internal forces and moments are computed using the object kinematics. Contact with the environment is controlled with an enforced impedance relationship between the object and the environment. For both internal and external forces, reference trajectories can be specified. Asymptotic stability of each controller is proven using Lyapunov stability theory and LaSalle's invariance principle. Guidelines are suggested to compute the parameters of the internal impedance controller. Merits of the control algorithm are demonstrated in simulations.

### 3.1 Introduction

Cooperative manipulation enables multiple robotic manipulators to work together towards executing a common task, thereby extending the domain of possible robotic applications. It is especially important for execution of tasks that are difficult, if not impossible, by single robots. Over the past few years, tasks exe-

cuted by multiple manipulators get more attention, because the costs for robotic hardware, processing power, and software continue to decrease. As already discussed in Chapter 1, cooperative manipulators can have significant advantages compared to single robots when they are used in tasks such as carrying heavy or large payloads and mechanical assembly.

The individual manipulators belonging to a cooperative system do not necessarily have to be identical. For example, one manipulator can have a fixed base and another can be mounted on a mobile base, or their end-effectors can be different. Provided that they have enough degrees of freedom for the desired task, they can cooperate. The properties of the manipulated object can also differ. It can be rigid or flexible or it can have extra degrees of freedom. Its geometry and its time-invariant or time-varying dynamics can be a priori known or unknown. The grasp between the manipulators and the object can be modelled in two different ways; fixed grasps and non-fixed grasps [135]. In the first modelling approach the manipulators hold the object via fixed grasp points, and no relative motion occurs between the object and the manipulators. The combined object-manipulator system forms a closed kinematic chain. This is the case, for example, for objects that have handles. The absence of relative motion between the object and the manipulators is also known in the literature as a rigid or tight grasp [31]. The second modelling approach takes into account the relative motion between the manipulators and the object at the contact points [125, 135].

For cooperative manipulation tasks, it is important to simultaneously control the motion of the system comprised of the manipulators and the object, the interaction forces between the object and the manipulators (internal forces), and the contact forces between the object and the environment (external forces). Over the past decades, several control algorithms have been proposed for cooperative manipulators (see [31] or, for a more recent overview [135]). The algorithms that can control both forces and motion can be divided into hybrid position/force control [62, 149] schemes and impedance/admittance control [23, 28, 123, 126] schemes. In the hybrid control schemes, the coordination space is decoupled into motion and force controlled directions, using a predefined and fixed selection matrix. Unexpected contact in motion controlled directions can lead to damage of the object and manipulators, since the force in these directions is not controlled [35]. In the impedance control schemes the dynamic relation between the forces and motion of the system is taken into account. Using impedance control, the task can be executed without leading to contact instability in the absence of precise knowledge of the contact directions. However, to achieve a satisfactory level of position/force tracking performance, the precise knowledge of contact directions is still required.

In this chapter, the modelling of cooperative manipulators is addressed in the case of fixed and non-fixed grasps. Furthermore, for the non-fixed grasp case, the

transitions from free motion to constrained motion and vice versa are also discussed. The non-fixed grasp is modelled as a Lagrangian complementarity system [27]. The concept of unilateral constraints is discussed for this case. For the fixed grasp case, the control architecture of [23] is adapted to control the motion and interaction forces, and it is combined with the cascade architecture of [28] and an extension of the impedance controller of [126] to control the contact (or external) forces of the object and the environment. The inner loop of this cascade control scheme contains individual inverse dynamics controllers to control the motion of each manipulator. An impedance controller driven by internal forces and desired object trajectories determines the reference trajectories for the inverse dynamics controllers. An external force based impedance controller determines the desired object trajectories. As one of the main contributions of this chapter, we complement the asymptotic stability analysis of the internal force-based impedance controller of [23]. We propose guidelines on how to tune the parameters of the internal force-based impedance relationship. Finally we show that, using the proposed object impedance controller, any required contact force can be achieved. A preliminary version of this work appears in [63].

This chapter is organized as follows. The modelling of cooperative manipulation systems for fixed and non-fixed grasps is described in Section 3.2. The aforementioned cascade control architecture and its inner motion control loop are presented in Sections 3.3 and 3.3.1, respectively. The outer loop of this cascade architecture which is comprised of internal and external force based impedance control laws are explained in Sections 3.3.2 and 3.3.3. Simulation results are presented in Section 3.4. Conclusions and final remarks are given in Section 3.5.

## 3.2 Modelling of cooperative manipulation systems

Consider a system composed of  $n$  non-redundant manipulators interacting with a rigid object. The links of the manipulators are assumed to be rigid while the joints exhibit no flexibility. The grasp on the object can be modelled in two different ways. In the first case, the grasp is fixed and no degrees of freedom (DOF) are present between the end effectors of the manipulators and the object: manipulators can exert both forces and moments on the object. In the second case, a relative motion between the end-effectors and the grasped object is possible. For example, rolling or sliding of the object on the end-effector surface is allowed. In this case, the effect of non-contact to contact transitions and vice versa is also taken into account. Schematic representations of both cases are shown in Figures 3.1(a) and 3.1(b) for the case of fixed and non-fixed grasps, respectively.

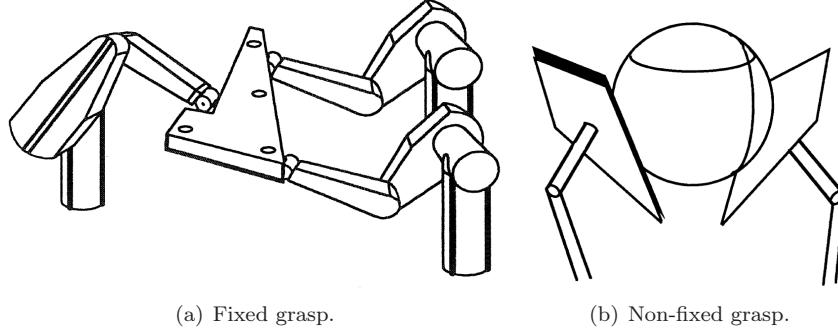


**Figure 3.1** Different modelling approaches in cooperative manipulation.

Before detailing fixed and non-fixed grasps, we briefly review the kinematics and dynamics of a manipulator. We consider each manipulator to possess six independent degrees of freedom such that the three positions and three orientations can be specified for the end-effector, hence the robot arms are nonredundant. The end-effector position  $\chi_i \in \mathbb{R}^3$  and orientation represented by the rotation matrix  $R_i \in \text{SO}(3)$  of each manipulator  $i \in \{1, 2, \dots, n\}$  are related to the joint angles,  $q_i \in \mathbb{R}^6$  via the forward kinematics. The translational  $\dot{\chi}_i \in \mathbb{R}^3$  and spatial angular  $\omega_i \in \mathbb{R}^3$  velocities are related to the joint velocities  $\dot{q}_i \in \mathbb{R}^6$  by means of the *geometric* manipulator Jacobian  $J_i(q_i) \in \mathbb{R}^{6 \times 6}$  [131]

$$\begin{bmatrix} \dot{\chi}_i \\ \omega_i \end{bmatrix} = J_i(q_i) \dot{q}_i. \quad (3.1)$$

By differentiating (3.1) with respect to time, the relation between the joint space and task space accelerations can be obtained

$$\begin{bmatrix} \ddot{\chi}_i \\ \dot{\omega}_i \end{bmatrix} = \dot{J}_i(q_i) \dot{q}_i + J_i(q_i) \ddot{q}_i, \quad \text{with} \quad \dot{J}_i(q_i) = \sum_{j=1}^6 \frac{\partial J_i(q_i)}{\partial q_{i,j}} \dot{q}_{i,j} \quad (3.2)$$

where  $q_{i,j}$  is the  $j^{\text{th}}$  element of the  $i^{\text{th}}$  manipulator's vector of joint angles and  $\ddot{\chi}_i \in \mathbb{R}^3$  and  $\dot{\omega}_i \in \mathbb{R}^3$  are the translational and the angular accelerations, respectively. The dynamics of the  $i^{\text{th}}$  manipulator, described in the joint space, is given by

$$M_i(q_i) \ddot{q}_i + C_i(q_i, \dot{q}_i) \dot{q}_i + g_i(q_i) = \tau_i - J_i^T(q_i) h_i. \quad (3.3)$$

In (3.3),  $M_i(q_i) \in \mathbb{R}^{6 \times 6}$  is the inertia matrix of manipulator  $i$ ,  $C_i(q_i, \dot{q}_i) \dot{q}_i \in \mathbb{R}^6$  the Coriolis and centrifugal force vector,  $g_i(q_i) \in \mathbb{R}^6$  the vector of gravitational forces,  $\tau_i \in \mathbb{R}^6$  the vector of applied joint torques, and  $h_i \in \mathbb{R}^6$  the vector of contact forces and moments at the end-effector of manipulator  $i$ . The vector  $h_i$  is given by

$$h_i = \begin{bmatrix} f_i \\ \mu_i \end{bmatrix} \quad (3.4)$$

where  $f_i \in \mathbb{R}^3$  are the contact forces and  $\mu_i \in \mathbb{R}^3$  are the contact moments. The dynamics (3.3) of the individual manipulators can be combined into

$$M(q)\ddot{q} + C(q, \dot{q})\dot{q} + g(q) = \tau - J^T(q)h \quad (3.5)$$

where  $M = \text{diag}(M_1, \dots, M_n)$ ,  $C = \text{diag}(C_1, \dots, C_n)$ ,  $g = [g_1^T, \dots, g_n^T]^T$ ,  $\tau = [\tau_1^T, \dots, \tau_n^T]^T$ ,  $J = \text{diag}(J_1, \dots, J_n)$ ,  $h = [h_1^T, \dots, h_n^T]^T$  and  $q = [q_1^T, \dots, q_n^T]^T$ . In the next section, the kinematic and dynamic equations for both cases are derived.

### 3.2.1 Fixed grasp

A schematic representation for the case of fixed grasp with two manipulators is shown in Figure 3.2. Let  $O$  be a fixed point on the manipulated object (e.g., the center of mass) with a coordinate frame  $\mathcal{T}_o$  centered on it and fixed relatively to the body. Furthermore, let  $\mathcal{T}_i$ ,  $i = \{1, 2\}$ , be two coordinate frames attached to the end-effectors of each manipulator and  $\mathcal{T}_w$  denote the world (common base) frame. The vectors  $p_i = R_i p_i^i$ ,  $i = \{1, 2\}$ , called the *virtual sticks* determine the position of  $\mathcal{T}_o$  with respect to  $\mathcal{T}_i$  expressed in the world frame [148, 149]. Note that  $p_i^i \in \mathbb{R}^3$  is a constant vector from frame  $\mathcal{T}_i$  to  $\mathcal{T}_o$ , since it is expressed in frame  $\mathcal{T}_i$ . The position

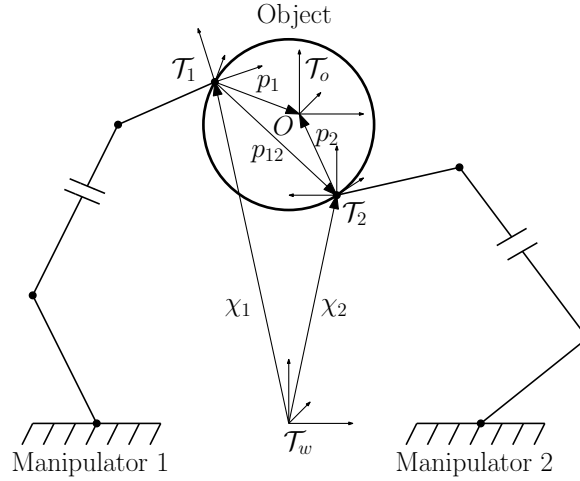


**Figure 3.2** Two cooperative manipulators handling a spherical object.

and orientation of the frame  $\mathcal{T}_o$  relative to the ground fixed frame  $\mathcal{T}_w$  are given by, the vector  $\chi_o \in \mathbb{R}^3$  and matrix  $R_o \in \text{SO}(3)$ , respectively. The translational  $\dot{\chi}_i$  and angular  $\omega_i$  end-effector velocities are related to the translational  $\dot{\chi}_o \in \mathbb{R}^3$  and

angular  $\omega_o \in \mathbb{R}^3$  object velocities by

$$\begin{bmatrix} \dot{\chi}_i \\ \omega_i \end{bmatrix} = J_{oi} \begin{bmatrix} \dot{\chi}_o \\ \omega_o \end{bmatrix} = \begin{bmatrix} I_3 & \Lambda(p_i) \\ O_3 & I_3 \end{bmatrix} \begin{bmatrix} \dot{\chi}_o \\ \omega_o \end{bmatrix} \quad (3.6)$$

where  $J_{oi} \in \mathbb{R}^{6 \times 6}$  is the object Jacobian related to the  $i^{\text{th}}$  end-effector. Here,  $\Lambda(p_i)$  is a skew symmetric matrix of the virtual stick  $p_i = R_i p_i^i \in \mathbb{R}^3$ . To obtain a relation between the translational  $\ddot{\chi}_i$  and angular  $\dot{\omega}_i$  end-effector accelerations and the translational  $\ddot{\chi}_o \in \mathbb{R}^3$  and angular  $\dot{\omega}_o \in \mathbb{R}^3$  object accelerations, equation (3.6) is differentiated with respect to time

$$\begin{bmatrix} \ddot{\chi}_i \\ \dot{\omega}_i \end{bmatrix} = \dot{J}_{oi} \begin{bmatrix} \dot{\chi}_o \\ \omega_o \end{bmatrix} + J_{oi} \begin{bmatrix} \ddot{\chi}_o \\ \dot{\omega}_o \end{bmatrix}. \quad (3.7)$$

By using a local parameterization of  $R_o \in \text{SO}(3)$ , the dynamics of the object can be written in the task space

$$M_o(x_o)\ddot{x}_o + C_o(x_o, \dot{x}_o)\dot{x}_o + g_o(x_o) = h_o \quad (3.8)$$

where  $M_o(x_o) \in \mathbb{R}^{6 \times 6}$  is the inertia matrix of the object,  $C(x_o, \dot{x}_o)\dot{x}_o \in \mathbb{R}^6$  is the vector of Coriolis and centrifugal forces,  $g_o(x_o) \in \mathbb{R}^6$  is the vector of the object gravitational forces, and  $h_o = [f_o^T \ \mu_o^T]^T \in \mathbb{R}^6$  are the net forces  $f_o \in \mathbb{R}^3$  and moments  $\mu_o \in \mathbb{R}^3$  acting on the object, expressed in the world frame (see pg. 276-277 of [102] for further details). The forces and moments acting on the object  $h_o$  are related to the vector of stacked object/manipulator contact forces  $h = [h_1^T, h_2^T, \dots, h_n^T]^T \in \mathbb{R}^{6n}$  via

$$h_o = J_o^T h \quad (3.9)$$

with  $J_o = [J_{o1}^T, J_{o2}^T, \dots, J_{on}^T]^T \in \mathbb{R}^{6n \times 6}$ . The dynamics of the manipulators and object are modeled using  $6n + 6$  equations of motion separately. However, the combined system of  $n$  manipulators and the object has only 6 DOF (translation and rotation of the object), so  $6n$  constraints have to be specified in order to complete the model. Since the grasp between each manipulator and the object is assumed to be tight, there is no relative motion between the end-effectors and object. Thus, the velocities at the contact points between object and the end-effector of manipulator  $i$  from equations (3.1) and (3.6) are equal, leading to the following constraint equations

$$J_{oi} \begin{bmatrix} \dot{\chi}_o \\ \omega_o \end{bmatrix} = J_i(q_i)\dot{q}_i. \quad (3.10)$$

Combining the constraint equations for all manipulators leads to the  $6n$  constraints

$$J_o \begin{bmatrix} \dot{\chi}_o \\ \omega_o \end{bmatrix} = J(q)\dot{q} \quad (3.11)$$

where  $J(q) = \text{diag}(J_1(q_1), \dots, J_n(q_n)) \in \mathbb{R}^{6n \times 6n}$  and  $q = [q_1^T, \dots, q_n^T]^T \in \mathbb{R}^{6n}$ .

### Internal force

The vector of stacked contact forces  $h$  can be decomposed into a motion inducing component  $h_M = [h_{M1}^T, h_{M2}^T, \dots, h_{Mn}^T]^T \in \mathbb{R}^{6n}$  and an internal component  $h_I = [h_{I1}^T, h_{I2}^T, \dots, h_{In}^T]^T \in \mathbb{R}^{6n}$  that does not contribute to the object's motion [23, 123]

$$h = h_M + h_I. \quad (3.12)$$

The motion inducing force  $h_M$  can be determined from  $h_o$  using (3.9)

$$h_M = (J_o^T)^\# h_o \quad (3.13)$$

where  $(J_o^T)^\#$  is the generalized inverse of transpose of object Jacobian given by

$$(J_o^T)^\# = \frac{1}{n} \begin{bmatrix} I_3 & O_3 \\ \Lambda(p_1) & I_3 \\ \vdots & \vdots \\ I_3 & O_3 \\ \Lambda(p_n) & I_3 \end{bmatrix} = \frac{1}{n} \begin{bmatrix} J_{o1}^{-T} \\ \vdots \\ J_{on}^{-T} \end{bmatrix} \quad (3.14)$$

with  $n$  being the number of manipulators [23]. Substitution of (3.9) leads to

$$h_M = (J_o^T)^\# J_o^T h \quad (3.15)$$

where  $(J_o^T)^\# J_o^T \in \mathbb{R}^{6n \times 6n}$  has rank 6, since  $J_o$  has rank 6. In fact, the part of the measured contact force  $h$  that lies in the null space of  $J_o^T$  does not contribute to the object's motion

$$J_o^T h_I = 0.$$

This part of the contact force is defined as the internal force  $h_I$ . The internal force  $h_I$  can be determined from equations (3.12) and (3.15)

$$h_I = \left( I - (J_o^T)^\# J_o^T \right) h. \quad (3.16)$$

#### 3.2.2 Non-fixed grasp

When multiple manipulators grasp an object without using fixed grasp points, relative motion between the end-effectors and the grasped object is possible while rolling or sliding of the object on the end-effector surface is allowed [135]. In this case, the contact can be characterized as either rolling or sliding, depending on the friction condition being at stick or slip. When the contact condition is pure rolling,

the constraint is holonomic for two-dimensional case and non-holonomic for the three-dimensional one [98, 125]. Consider two manipulators and an object which initially may or may not be stationary. Assume that surfaces of this object are convex and smooth, at least in a neighborhood of a potential contact point between the object and the manipulators. Here, the convexity assumption is required for uniqueness. The schematic of such a situation is shown in Figure 3.3. The notation and formulation for the kinematic analysis in this section is borrowed from [54], whereas the notation and formulation for the dynamic model is taken from [85, 86].

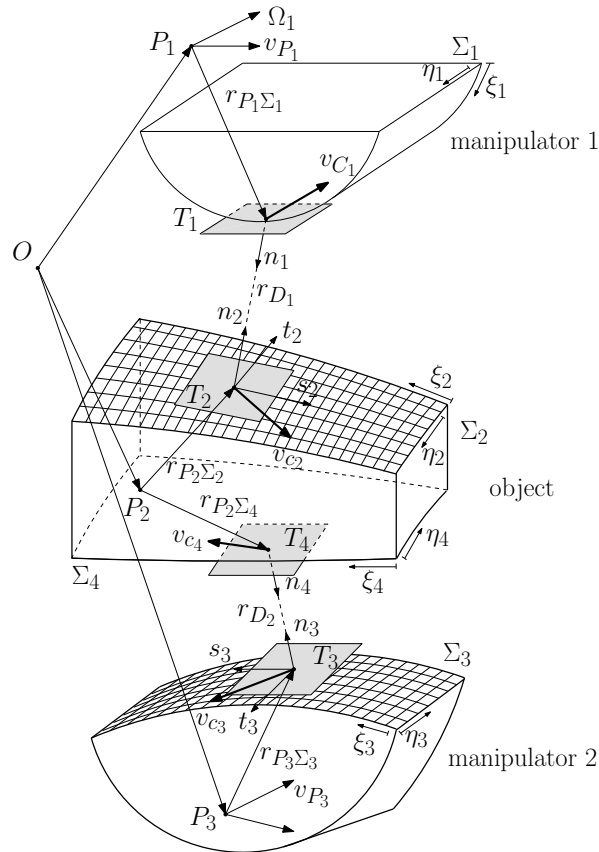


**Figure 3.3** Two cooperative manipulators handling an object (drawing produced similar to [54, 85]).

**Remark 3.1.** *In the following, the contact kinematics and dynamics are introduced for the three dimensional (spatial) case. The derivation of these equations for the planar case can be done in a similar fashion.*



In Figure 3.3, the points  $P_1$  and  $P_3$  represent body-fixed points that belong to the first and second manipulators, respectively and point  $P_2$  is a body-fixed point which belongs to the object and at point  $O$  the inertial frame is located. The linear and angular velocities of each body-fixed frame is given by  $v_{P_i}$  and  $\Omega_i$  for  $i = 1, 2, 3$ , respectively. The surfaces of each manipulator and each side of the object close to the respective manipulator are parameterized with  $r_{P_i\Sigma_j} = r_{P_i\Sigma_j}(q_i, \xi_j, \eta_j)$  for  $(i, j) = \{(1, 1), (2, 2), (2, 4), (3, 3)\}$ . If  $r_{P_i\Sigma_j}$  is referred to the body fixed frame, it only depends on the surface parameters  $\xi_j$  and  $\eta_j$ . The additional dependence on the generalized coordinates  $q_j$  is observed if arbitrary frames are used. For each contact pair between the object and the respective manipulator, an orthonormal basis  $(u_j, v_j, n_j)$  is defined by the tangents  $s_j := \partial r_{P_i\Sigma_j} / \partial \xi_j$ ,  $t_j := \partial r_{P_i\Sigma_j} / \partial \eta_j$  such that

$$u_j := \frac{s_j}{|s_j|}, \quad v_j := \frac{t_j}{|t_j|}, \quad n_j := \frac{s_j \times t_j}{|s_j \times t_j|} \quad (3.17)$$

where  $(\xi_j, \eta_j)$  are ordered such that  $n_j$  becomes the outward normal for  $j = 1, 2, 3, 4$ .

**Remark 3.2.** For the spatial contact case, it is possible to define an additional contact coordinate besides the surface parameters  $\xi_j, \eta_j$  for each contact pair as done in [98, 125]. This additional parameter is called the angle of contact. It is defined as the angle between the vectors  $v_1$  and  $v_2$  considering the object and the 1<sup>st</sup> manipulator pair and the angle between the vectors  $v_3$  and  $v_4$  considering the object and the 2<sup>nd</sup> manipulator pair.

**Remark 3.3.** Once either one of both manipulators make contact with the object, it is possible to obtain relations between the first and second time derivatives of the contact coordinates and the relative velocities and accelerations of the manipulators and the object [98, 125].

The time derivatives of the contour vector  $r_{P_i\Sigma_j}$  and the 3-tuple  $(u_j, v_j, n_j)$  are given by

$$\begin{aligned} \dot{r}_{P_i\Sigma_j} &= \Omega_i \times r_{P_i\Sigma_j} + \Phi_j \dot{\zeta}_j \quad \text{with} \quad \Phi_j = \frac{\partial r_{P_i\Sigma_j}}{\partial \zeta_j} = (s_j, t_j) \\ \dot{k}_j &= \Omega_i \times k_j + K_j \dot{\zeta}_j \quad \text{with} \quad K_j = \frac{\partial k_j}{\partial \zeta_j} \end{aligned} \quad (3.18)$$

where  $\zeta_j = (\xi_j, \eta_j)^T$  and  $(k_j, K_j)$  is any of the respective tangential or normal directions  $(u_j, U_j)$ ,  $(v_j, V_j)$  or  $(n_j, N_j)$  for  $j = 1, 2, 3, 4$ . The velocity  $v_{\Sigma_j}$  of a point moving on the surface in terms of the rigid body motion  $(v_{P_i}, \Omega_i)$  is thus given by  $v_{\Sigma_j} = v_{P_i} + \dot{r}_{P_i\Sigma_j}$  resulting in

$$v_{\Sigma_j} = v_{C_j} + \Phi_j \dot{\zeta}_j \quad \text{with} \quad v_{C_j} = v_{P_i} + \Omega_i \times r_{P_i\Sigma_j} \quad (3.19)$$

where  $v_{C_j}$  denotes the rigid body velocity portion of  $v_{\Sigma_j}$ . Similarly, the acceleration  $a_{C_j} = \dot{v}_{C_j}$  can be obtained by differentiating the second equation of (3.19)

$$a_{C_j} = a_{Q_j} + \Omega_i \times \Phi_j \dot{\zeta}_j \quad \text{with} \quad a_{Q_j} = a_{P_j} + \dot{\Omega}_i \times r_{P_i \Sigma_j} + \Omega_i \times (\Omega_i \times r_{P_i \Sigma_j}). \quad (3.20)$$

Finally,  $v_{C_j}$  and  $a_{C_j}$  can be represented as a function of the time derivatives of the generalized coordinates  $q$ , i.e.  $\dot{q}$  and  $\ddot{q}$

$$v_{C_j} = J_{C_j} \dot{q} + \hat{l}_{C_j}, \quad a_{C_j} = J_{C_j} \ddot{q} + \bar{l}_{C_j} \quad (3.21)$$

where  $\bar{l}_{C_j} = \dot{J}_{C_j} \dot{q} + \dot{\hat{l}}_{C_j}$ , and  $J_{C_j}$  is the Jacobian of the respective contact point.

The main equations of contact kinematics between the two manipulators and the object can be derived with the help of the equations introduced previously in this subsection. These are the definition of contact points, their distance, their relative velocities and accelerations along the normal and tangential directions. The first step in the derivation of these relative expressions is the introduction of distance vectors,

$$r_{D_1} = r_{O\Sigma_2} - r_{O\Sigma_1}, \quad (3.22)$$

$$r_{D_2} = r_{O\Sigma_4} - r_{O\Sigma_3} \quad (3.23)$$

where  $r_{O\Sigma_j}$  are vectors pointing from a common inertially fixed point  $O$  to the surfaces under consideration. Then, the corresponding pair of tangent planes spanned by  $(u_j, v_j)$  are adjusted parallel to each other such that the distance vectors of the respective contact pairs become parallel to each other. The surface parameters  $(\zeta_1^*, \zeta_2^*, \zeta_3^*, \zeta_4^*)$  which correspond to that situation solve the following eight nonlinear equations

$$\begin{aligned} n_1^T u_2 = 0, \quad n_1^T v_2 = 0, \quad r_{D_1}^T u_1 = 0, \quad r_{D_1}^T v_1 = 0 \\ n_3^T u_4 = 0, \quad n_3^T v_4 = 0, \quad r_{D_2}^T u_3 = 0, \quad r_{D_2}^T v_3 = 0. \end{aligned} \quad (3.24)$$

These parameters are called the contact parameters and the corresponding points at the surfaces given by  $r_{P_i \Sigma_j}(\zeta_j^*)$  are called the contact points. When the manipulators and the object are moving the conditions (3.24) for the contact points should not change, which implies that the following must hold

$$\begin{aligned} \dot{n}_1^T u_2 + n_1^T \dot{u}_2 = 0, \quad \dot{r}_{D_1}^T u_1 + r_{D_1}^T \dot{u}_1 = 0 \\ \dot{n}_1^T v_2 + n_1^T \dot{v}_2 = 0, \quad \dot{r}_{D_1}^T v_1 + r_{D_1}^T \dot{v}_1 = 0 \\ \dot{n}_3^T u_4 + n_3^T \dot{u}_4 = 0, \quad \dot{r}_{D_2}^T u_3 + r_{D_2}^T \dot{u}_3 = 0 \\ \dot{n}_3^T v_4 + n_3^T \dot{v}_4 = 0, \quad \dot{r}_{D_2}^T v_3 + r_{D_2}^T \dot{v}_3 = 0. \end{aligned} \quad (3.25)$$

Expression (3.25) constitutes a system of eight linear equations in  $\dot{\zeta}_j^*$  when substituting  $(\dot{n}_j, \dot{u}_j, \dot{v}_j)$  from (3.18) and  $v_{\Sigma_j}$  from (3.19) with  $\dot{r}_{D_1} = v_{\Sigma_2} - v_{\Sigma_1}$ ,  $\dot{r}_{D_2} = v_{\Sigma_4} - v_{\Sigma_3}$ . After the solution  $(\zeta_1^*, \zeta_2^*, \zeta_3^*, \zeta_4^*)$  of (3.25) is found, the distances  $g_{N_1}$  and  $g_{N_2}$  of the contact points can be calculated as,

$$g_{N_1} = n_1^T r_{D_1}, \quad g_{N_2} = n_2^T r_{D_2}. \quad (3.26)$$

The respective manipulator and the surface of the object close to it are separated when  $g_N > 0$ , are in contact when  $g_N = 0$ , and penetrate each other when  $g_N < 0$ . The relative velocities of the contact points at both side of the object with respect to the three directions  $(u_1, v_1, n_1)$  and  $(u_3, v_3, n_3)$  are given as,

$$\begin{aligned} \dot{g}_{K_1} &= (v_{C_2} - v_{C_1})^T k_1, & (K_1, k_1) &= (U_1, u_1), (V_1, v_1), (N_1, n_1) \\ \dot{g}_{K_2} &= (v_{C_4} - v_{C_3})^T k_3, & (K_2, k_3) &= (U_2, u_3), (V_2, v_3), (N_2, n_3) \end{aligned} \quad (3.27)$$

where (3.27) can be obtained after (3.26) is differentiated for  $(K_1, k_1) = (N_1, n_1)$  and  $(K_2, k_2) = (N_2, n_3)$ . The time derivatives of the relative velocities  $\dot{g}_{K_1}$  and  $\dot{g}_{K_2}$  in (3.27) are computed as

$$\begin{aligned} \ddot{g}_{K_1} &= (a_{C_2} - a_{C_1})^T k_1 + (v_{C_2} - v_{C_1})^T \dot{k}_1 \\ \ddot{g}_{K_2} &= (a_{C_4} - a_{C_3})^T k_2 + (v_{C_4} - v_{C_3})^T \dot{k}_2 \end{aligned} \quad (3.28)$$

where  $a_{C_j}$  is given in (3.20),  $\dot{k}_1$  and  $\dot{k}_3$  is obtained from (3.18), and  $\zeta_j^*$  in  $a_{C_j}$ ,  $\dot{k}_1$  and  $\dot{k}_3$  is the solution of (3.25). Substituting  $v_{C_j}$  and  $a_{C_j}$  from (3.21) into (3.27) and (3.28) yields a representation of the relative velocities and accelerations in the form,

$$\dot{g}_{K_1} = w_{K_1}^T \dot{q} + \hat{w}_{K_1}, \quad \ddot{g}_{K_2} = w_{K_2}^T \ddot{q} + \bar{w}_{K_1} \quad (3.29)$$

$$\dot{g}_{K_2} = w_{K_2}^T \dot{q} + \hat{w}_{K_2}, \quad \ddot{g}_{K_2} = w_{K_2}^T \ddot{q} + \bar{w}_{K_2} \quad (3.30)$$

with  $w_{K_1} = (J_{C_2} - J_{C_1})^T k_1$ ,  $w_{K_2} = (J_{C_4} - J_{C_3})^T k_3$ ,  $\hat{w}_{K_1} = (\hat{c}_{C_2} - \hat{c}_{C_1})^T k_1$ ,  $\hat{w}_{K_2} = (\hat{c}_{C_4} - \hat{c}_{C_3})^T k_3$ ,  $\bar{w}_{K_1} = \dot{w}_{K_1}^T \dot{q} + \hat{w}_{K_1}$  and  $\bar{w}_{K_2} = \dot{w}_{K_2}^T \dot{q} + \hat{w}_{K_2}$ . Finally we arrange the two normal relative velocities in the vector  $\dot{g}_N^T := (g_{N_1}, g_{N_2})$  and the four tangential relative velocities in the vector  $\dot{g}_T^T := (\dot{g}_{U_1}, \dot{g}_{V_1}, \dot{g}_{U_2}, \dot{g}_{V_2})$  which gives the sliding direction of the contact points in the common tangent plane. With the abbreviations  $W_N := (w_{N_1}, w_{N_2})$ ,  $W_T := (w_{U_1}, w_{V_1}, w_{U_2}, w_{V_2})$ ,  $\hat{w}_T^T = (\hat{w}_{U_1}, \hat{w}_{V_1}, \hat{w}_{U_2}, \hat{w}_{V_2})$  and  $\bar{w}_T^T = (\bar{w}_{U_1}, \bar{w}_{V_1}, \bar{w}_{U_2}, \bar{w}_{V_2})$ , (3.29) and (3.30) can be rewritten in the following form

$$\dot{g}_N = W_N^T \dot{q} + \hat{w}_N, \quad \dot{g}_T = W_T^T \dot{q} + \hat{w}_T \quad (3.31)$$

$$\ddot{g}_N = W_N^T \ddot{q} + \bar{w}_N, \quad \ddot{g}_T = W_T^T \ddot{q} + \bar{w}_T \quad (3.32)$$

which provides the contact kinematic equations that will be used in the derivation of the dynamic equations. Mechanical systems with unilateral constraints such as

Coulomb friction, contact and impact can be modelled using measure differential inclusions [85, 86]. This formulation is capable of describing the discontinuous nature of the friction forces together with the impulsive nature of the impact laws. This framework can also be used to model the cooperative manipulation system for the non-fixed grasp case considered in this section. The equations of motion of this system in the contact phase with friction and without impulsive loads (impact-free) can be formulated using the Lagrangian approach,

$$M(q)\dot{u} - h(q, u, t) - W_N(q)\lambda_N - W_T(q)\lambda_T = 0, \quad (3.33)$$

for almost all  $t$ , where  $q \in \mathbb{R}^n$  represent the generalized coordinates and  $u(t) = \dot{q}(t)$ ,  $\forall t$  represent the generalized velocities.  $M(q) = M^T(q) > 0$  is the mass matrix,  $h(q, u, t)$  is a column vector of all generalized forces such as gyroscopic, gravitational and time-dependent actuator forces, etc., except friction and contact forces. The friction and contact forces are introduced using  $\lambda_T$  and  $\lambda_N$ , respectively, with the matrices  $W_T(q)$  and  $W_N(q)$  given in (3.32). In order to distinguish between the possible contacts between each manipulator and the object the following index sets can be introduced,

$$\begin{aligned} I_G &= \{1, \dots, n_C\} && \text{the set of all contacts,} \\ I_N &= \{i \in I_G \mid g_{N_i}(q) = 0\} && \text{the set of all closed contacts,} \end{aligned} \quad (3.34)$$

where the force and impact laws for each contact are elaborated in Appendices D.1 and D.2 and normal contact distances  $g_{N_i}(q)$  are collected in the vector  $g_N(q)$ . For each closed contact  $i \in I_N$ , the set-valued normal contact force  $\lambda_{N_i}$  and friction force  $\lambda_{T_i}$  can be derived from non-smooth potentials (see Appendix D.1),

$$-\lambda_{N_i} \in \partial\Psi_{C_N}^*(\gamma_{N_i}), \quad -\lambda_{T_i} \in \partial\Psi_{C_T}^*(\gamma_{T_i}) \quad (3.35)$$

where  $\gamma_{N_i}$  and  $\gamma_{T_i}$  are the corresponding columns of the normal and tangential velocities given in (3.31). The following Filippov type differential inclusion

$$M(q)\dot{u} - h(q, u) \in - \sum_{i \in I_N} W_{N_i}(q)\partial\Psi_{C_N}^*(\gamma_{N_i}) - W_{T_i}(q)\partial\Psi_{C_T}^*(\gamma_{T_i}) \quad (3.36)$$

describes the behavior of the cooperative manipulation system for impact free motion for almost all  $t$ . The effect of impacts can be included using the inclusions

$$\Lambda_{N_i} \in \partial\Psi_{C_N}^*(\xi_{N_i}), \quad \Lambda_{T_i} \in \partial\Psi_{C_T}^*(\xi_{T_i}), \quad i \in I_N, \quad (3.37)$$

with

$$\xi_{N_i} = \gamma_{N_i}^+ + e_{N_i}\gamma_{N_i}^-, \quad \xi_{T_i} = \gamma_{N_i}^+ + e_{N_i}\gamma_{N_i}^- \quad (3.38)$$

in which  $e_{N_i}$  and  $e_{T_i}$  are the normal and tangential restitution coefficients, respectively. In order to correctly describe impulsive forces, (3.36) are turned into the following measure differential equations,

$$M(q)du - h(q, u)dt = W_N(q)d\Lambda_N + W_T(q)d\Lambda_T, \quad \forall t \quad (3.39)$$

where the differential measure of the contact impulses  $d\Lambda_N$  and  $d\Lambda_T$  contains a Lebesgue measurable part  $\lambda dt$  and an atomic part  $\Lambda d\eta$

$$d\Lambda_N = \lambda_N dt + \Lambda_N d\eta, \quad d\Lambda_T = \lambda_T dt + \Lambda_T d\eta, \quad (3.40)$$

that can be expressed as inclusions

$$\begin{aligned} -d\Lambda_{N_i} &\in \partial\Psi_{C_N}^*(\xi_{N_i})(dt + d\eta), \\ -d\Lambda_{T_i} &\in \partial\Psi_{C_{T_i}(\lambda_{N_i})}^*(\xi_{T_i})dt + \partial\Psi_{C_{T_i}(\Lambda_{N_i})}^*(\xi_{T_i})d\eta. \end{aligned} \quad (3.41)$$

Equations (3.39) and (3.41) describe the time-evolution of the cooperative manipulation system in the case of non-fixed grasps with discontinuities in the generalized velocities arising from impact. They can be solved using methods such as time-stepping. More details of the derivation of this model are given in Appendix D.

### 3.3 A cascade controller for fixed grasps

In this section, a cascade controller for cooperative manipulation in the case of fixed grasps is introduced. The block diagram of this controller is shown in Figure 3.4. A motion controller is at the lowest level of this scheme. Compared to the controller suggested in [23], the inner motion control loop is added to improve the tracking performance. The reference for this motion control law is obtained from an impedance relationship driven by the internal force error which is presented in Section 3.3.2. The desired trajectory for each manipulator is obtained from the kinematic constraints between the object and the respective manipulator. Finally, the desired object motion is obtained from the external force based impedance controller which is presented in Section 3.3.3.

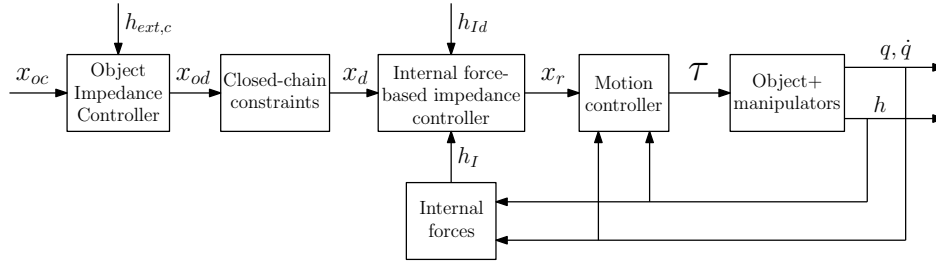


Figure 3.4 Control architecture of the cooperative manipulators.

### 3.3.1 Motion control

An inverse dynamics based controller is applied to each manipulator to asymptotically track a reference trajectory  $x_{ir} = \{\chi_{ir} \in \mathbb{R}^3, R_{ir} \in SO(3)\}$  in Cartesian space [29]. In (3.3) we apply the following control input

$$\tau_i = C_i(q_i, \dot{q}_i) \dot{q}_i + g_i(q_i) + J_i(q_i)^T h_i + M_i(q_i) J_i^{-1}(q_i) \left\{ u_i - \dot{J}_i(q_i) \dot{q}_i \right\}. \quad (3.42)$$

By taking relationship (3.2) into account, we obtain

$$\begin{bmatrix} \ddot{\chi}_i \\ \dot{\omega}_i \end{bmatrix} = u_i \quad (3.43)$$

where  $u_i \in \mathbb{R}^6$  is the new control input. Its first three elements are used for tracking the translational part of the reference trajectory (i.e.  $\chi_{ir} \in \mathbb{R}^3$ ) whereas its last three elements are used for tracking the rotational part of the reference trajectory (i.e.  $R_{ir} \in SO(3)$ ) for the end-effector of the  $i^{th}$  manipulator. It is assumed that the manipulator dynamics is perfectly known for this control law and the robot is operating in a region outside of kinematic singularities. Depending on the parameterization of the rotation matrices, the rotational part of  $u_i$  can be designed in different ways [29]. In order to obtain linear decoupled closed-loop dynamics, an approximation of the angle/axis parameterization is selected (see [93] for further details). Using this approximation for the orientation error, the error  $\Delta x_i \in \mathbb{R}^6$  of the end-effector of manipulator  $i$  given by

$$\Delta x_i = \begin{bmatrix} \Delta \chi_i \\ \xi_i \end{bmatrix} = \begin{bmatrix} \chi_{ir} - \chi_i \\ \frac{1}{2} (n_i \times n_{ir} + s_i \times s_{ir} + a_i \times a_{ir}) \end{bmatrix} \quad (3.44)$$

is valid when  $n_i^T n_{ir} > 0$ ,  $s_i^T s_{ir} > 0$  and  $a_i^T a_{ir} > 0$ . Here,  $\Delta \chi_i \in \mathbb{R}^3$  is the translational error and  $\xi_i \in \mathbb{R}^3$  is the orientation error. The vectors  $n_i, s_i, a_i$ , and  $n_{ir}, s_{ir}, a_{ir}$  are the columns of actual and reference rotation matrices  $R_i$  and  $R_{ir}$ ,

$$R_i = [ n_i \quad s_i \quad a_i ], \quad R_{ir} = [ n_{ir} \quad s_{ir} \quad a_{ir} ]. \quad (3.45)$$

The velocity error of the end-effector of  $i^{th}$  manipulator is defined as [29],

$$\Delta \dot{x}_i = \begin{bmatrix} \Delta \dot{\chi}_i \\ \dot{\xi}_i \end{bmatrix} = \begin{bmatrix} \dot{\chi}_{ir} - \dot{\chi}_i \\ L_i^T \omega_{ir} - L_i \omega_i \end{bmatrix} \quad (3.46)$$

where  $\Delta \dot{\chi}_i$  is the time derivative of the translational part of (3.44),  $\dot{\xi}_i$  the time derivative of the orientational part of (3.44) and  $\dot{\chi}_{ir} \in \mathbb{R}^3$  and  $\omega_{ir} \in \mathbb{R}^3$  are the translational and angular reference velocities, respectively. The matrix  $L_i \in \mathbb{R}^{3 \times 3}$  depends on the columns of the rotation matrices  $R_i$  and  $R_{ir}$  and is given by [29]

$$L_i = -\frac{1}{2} (\Lambda(n_{ir})\Lambda(n_i) + \Lambda(s_{ir})\Lambda(s_i) + \Lambda(a_{ir})\Lambda(a_i)) \quad (3.47)$$

where  $\Lambda(x) \in \mathbb{R}^{3 \times 3}$  is the skew symmetric matrix of the vector  $x \in \mathbb{R}^3$ . The acceleration errors are defined as the time derivatives of (3.46),

$$\Delta \ddot{x}_i = \begin{bmatrix} \Delta \ddot{\chi}_i \\ \dot{\xi}_i \end{bmatrix} = \begin{bmatrix} \ddot{\chi}_{ir} - \ddot{\chi}_i \\ \dot{L}_i^T \omega_{ir} + L_i^T \dot{\omega}_{ir} - \dot{L}_i \omega_i - L_i \dot{\omega}_i \end{bmatrix} \quad (3.48)$$

where  $\ddot{\chi}_{ir} \in \mathbb{R}^3$  and  $\dot{\omega}_{ir} \in \mathbb{R}^3$  are the translational and angular reference accelerations, respectively, and  $\dot{L}_i \in \mathbb{R}^{3 \times 3}$  is the time derivative of  $L_i$  whose explicit formula is given in [90]. Based on (3.48), the new control input  $u_i$  in (3.42) is selected as [29]

$$u_i = \begin{bmatrix} \ddot{\chi}_{ir} + K_{vi,t} \Delta \dot{\chi}_i + K_{pi,t} \Delta \chi_i \\ L_i^{-1} \left( \dot{L}_i^T \omega_{ir} + L_i^T \dot{\omega}_{ir} - \dot{L}_i \omega_i + K_{vi,\alpha} \dot{\xi}_i + K_{pi,\alpha} \xi_i \right) \end{bmatrix} \quad (3.49)$$

where  $K_{pi,t}, K_{vi,t}, K_{pi,\alpha}, K_{vi,\alpha} \in \mathbb{R}^{3 \times 3}$  are positive definite matrices, representing the proportional and derivative gains of the feedback controller in translational and orientational directions.

Here, the feasibility of the controller (3.42) and (3.49) is discussed. The vector of joint positions,  $q_i$  for each manipulator can be measured using e.g. incremental encoders, whereas the joint velocities  $\dot{q}_i$  can either be measured by tachometers [157] or computed from joint positions via numerical differentiation (possibly with filtering) or reconstructed using observers. The forward kinematic maps,  $\chi_i(q_i)$  and  $R_i(q_i)$  and the geometric Jacobian  $J_i(q_i)$  of the manipulators can be derived using the Denavit-Hartenberg convention [136]. Thus, the translational  $\Delta \chi_i$  and rotational  $\xi_i$  errors can be computed since reference trajectories,  $\chi_{ir}$  and  $R_{ir}$  are known. Using (3.1), the translational and angular velocities  $\dot{\chi}_i$  and  $\omega_i$  are computed and used to calculate the time derivatives of the translational and rotational errors  $\Delta \dot{\chi}_i$  and  $\dot{\xi}_i$ , since the reference trajectories  $\omega_{ir}$  and  $R_{ir} = [n_{ir} \ s_{ir} \ a_{ir}]$  are known. Furthermore,  $L_i$  and  $\dot{L}_i$  can be computed since  $R_i, R_{ir}, \dot{R}_i$  and  $\dot{R}_{ir}$  are known. Consequently, the new control input (3.49) is feasible to implement. The manipulator dynamic equation (3.3) can be derived using standard techniques and its parameters can be identified for instance using offline identification techniques which can be used to compute the terms of (3.42) [131]. The end-effector forces/moments,  $h_i$  can be measured for instance using 6-axis force sensors. Consequently, the implementation of (3.42) is feasible.

When (3.42) is substituted into (3.3) and (3.1) is used, after some algebraic manipulations, the following closed-loop error dynamics,

$$\Delta \ddot{x}_i + K_{vi} \Delta \dot{x}_i + K_{pi} \Delta x_i = 0 \quad (3.50)$$

is obtained where  $K_{pi} = \text{diag} \{K_{pi,t}, K_{pi,\alpha}\}$  and  $K_{vi} = \text{diag} \{K_{vi,t}, K_{vi,\alpha}\}$ . In the derivation of (3.50), it is assumed that  $J_i$  is far away from kinematic singularities.

The equations (3.50) for  $i = 1, \dots, n$  can be combined into

$$\Delta\ddot{x} + K_v\Delta\dot{x} + K_p\Delta x = 0 \quad (3.51)$$

where  $\Delta x = [\Delta x_1^T, \Delta x_2^T, \dots, \Delta x_n^T]^T \in \mathbb{R}^{6n}$  and  $K_p = \text{diag}\{K_{p1}, K_{p2}, \dots, K_{pn}\} \in \mathbb{R}^{6n \times 6n}$ . Stability of the system (3.51) is investigated using Lyapunov's stability theorem [73]. Consider the following candidate Lyapunov function

$$V_1 = \frac{1}{2}\Delta\dot{x}^T\Delta\dot{x} + \frac{1}{2}\Delta x^T K_p \Delta x \quad (3.52)$$

where  $\Delta x$  and  $K_p$  are as given before. Calculating the time derivative  $\dot{V}_1$  gives

$$\dot{V}_1 = \Delta\dot{x}^T [\Delta\ddot{x} + K_p\Delta x]. \quad (3.53)$$

Using the error dynamics of (3.50), it can be shown that  $\dot{V}_1$  is semi-negative definite

$$\dot{V}_1 = -\Delta\dot{x}^T K_v \Delta\dot{x} \leq 0 \quad (3.54)$$

where  $K_v = \text{diag}\{K_{v1}, K_{v2}, \dots, K_{vn}\} \in \mathbb{R}^{6n \times 6n}$ . So for  $t \rightarrow \infty$ ,  $\Delta\dot{x} \rightarrow 0$ , thus for  $t \rightarrow \infty$ ,  $\Delta x \rightarrow c$ , with  $c$  a constant value. From (3.54) it can be concluded that the system is stable. Asymptotic stability of the equilibrium  $\Delta x = \Delta\dot{x} = 0$  is investigated using LaSalle's invariance principle [73]. The radially unbounded set  $\Omega_1$  is defined as

$$\Omega_1 = \{\Delta x, \Delta\dot{x} \in \mathbb{R}^{6n} | V_1(\Delta x, \Delta\dot{x}) \leq \infty\}. \quad (3.55)$$

The set  $E_1$  in  $\Omega_1$  is defined as

$$E_1 = \{\Delta x, \Delta\dot{x} \in \Omega_1 | \dot{V}_1 = 0\} = \{\Delta x, \Delta\dot{x} \in \Omega_1 | \Delta\dot{x} = 0\}. \quad (3.56)$$

The set  $M_1$  is defined as the largest invariant set in  $E_1$ . Using  $\Delta\dot{x} = 0$  and  $\Delta\ddot{x} = 0$  in the closed loop dynamics (3.50), results in

$$K_p\Delta x = 0. \quad (3.57)$$

Since  $K_p$  is block-diagonal, it can be concluded that

$$K_{pi}\Delta x_i = 0. \quad (3.58)$$

The matrix  $K_{pi}$  is positive definite, since it is a block diagonal matrix with positive definite submatrices  $K_{pi,t}$  and  $K_{pi,\alpha}$ , hence

$$\Delta x_i = 0. \quad (3.59)$$

Thus, the largest invariant set  $N_1$  in  $E_1$  becomes

$$N_1 = \{\Delta x, \Delta\dot{x} \in E_1 | \Delta x = 0\}. \quad (3.60)$$

From LaSalle's invariance principle it can be concluded that for  $t \rightarrow \infty$ ,  $\Delta x \rightarrow 0$  and thus that the equilibrium point  $\Delta x = \Delta\dot{x} = 0$  is asymptotically stable.



### 3.3.2 Internal force-based impedance control

Using the motion controller of (3.42), the end-effector positions and orientations (and thus the position and orientation of the object) can be controlled. However, controlling only the motion during object manipulation can result in internal forces and moments in the object such as, compression, tension, bending and torsion. A possible way to control the internal forces and moments of the object is to enforce an impedance relationship between the manipulator end-effectors and the object. The idea is to compute the manipulator end-effector reference trajectory  $x_{ir} = \{\chi_{ir} \in \mathbb{R}^3, R_{ir} \in SO(3)\}$  for the motion controller (3.42) from the desired end-effector trajectory  $x_{id} = \{\chi_{id} \in \mathbb{R}^3, R_{id} \in SO(3)\}$ , based on the internal force error  $\Delta h_{Ii}$  [28, 32]. The impedance relationship for each manipulator reads

$$D_i \Delta \ddot{x}_i + B_i \Delta \dot{x}_i + S_i \Delta \tilde{x}_i = \Delta h_{Ii} \quad (3.61)$$

where  $D_i, B_i, S_i \in \mathbb{R}^{6 \times 6}$  are positive definite matrices, representing the desired inertia, damping and stiffness matrices, respectively. Here,  $\Delta h_{Ii} = h_{Iid} - h_{Ii}$  represents the internal force/moment error of the end-effector of the  $i^{th}$  manipulator, with  $h_{Ii} = [f_{Ii}^T \ \mu_{Ii}^T]^T \in \mathbb{R}^6$  being the internal forces ( $f_{Ii} \in \mathbb{R}^3$ ) and moments ( $\mu_{Ii} \in \mathbb{R}^3$ ) and  $h_{Iid} \in \mathbb{R}^6$  being the desired internal forces ( $f_{Iid} \in \mathbb{R}^3$ ) and moments ( $\mu_{Iid} \in \mathbb{R}^3$ ). The error  $\Delta \tilde{x}_i$  between the desired  $x_{id}$  and reference  $x_{ir}$  trajectories of end-effector  $i$ , is expressed as

$$\Delta \tilde{x}_i = \begin{bmatrix} \Delta \tilde{\chi}_i \\ \tilde{\xi}_i \end{bmatrix} = \begin{bmatrix} \chi_{id} - \chi_{ir} \\ \frac{1}{2} (n_{ir} \times n_{id} + s_{ir} \times s_{id} + a_{ir} \times a_{id}) \end{bmatrix} \quad (3.62)$$

where  $\chi_{id}$  is the desired position of the end-effector of manipulator  $i$  and  $n_{id}$ ,  $s_{id}$  and  $a_{id}$  are the columns of the rotation matrix  $R_{id}$ . The orientation error is formulated analogously to (3.46). The first and second time derivatives of  $\Delta \tilde{x}_i$  are

$$\Delta \dot{\tilde{x}}_i = \begin{bmatrix} \Delta \dot{\tilde{\chi}}_i \\ \dot{\tilde{\xi}}_i \end{bmatrix} = \begin{bmatrix} \dot{\chi}_{id} - \dot{\chi}_{ir} \\ \tilde{L}_i^T \omega_{id} - \tilde{L}_i \omega_{ir} \end{bmatrix} \quad (3.63)$$

$$\Delta \ddot{\tilde{x}}_i = \begin{bmatrix} \Delta \ddot{\tilde{\chi}}_i \\ \ddot{\tilde{\xi}}_i \end{bmatrix} = \begin{bmatrix} \ddot{\chi}_{id} - \ddot{\chi}_{ir} \\ \dot{\tilde{L}}_i^T \omega_{id} + \tilde{L}_i^T \dot{\omega}_{id} - \dot{\tilde{L}}_i \omega_{ir} - \tilde{L}_i \dot{\omega}_{ir} \end{bmatrix} \quad (3.64)$$

where  $\dot{\chi}_{id}$  and  $\ddot{\chi}_{id}$  are the translational desired velocity and acceleration while  $\omega_{id}$  and  $\dot{\omega}_{id}$  are the angular desired velocity and acceleration for the end-effector of manipulator  $i$ . The matrix  $\tilde{L}_i$  is given by

$$\tilde{L}_i = -\frac{1}{2} (\Lambda(n_{id})\Lambda(n_{ir}) + \Lambda(s_{id})\Lambda(s_{ir}) + \Lambda(a_{id})\Lambda(a_{ir})). \quad (3.65)$$

From the impedance relationship of (3.61), the reference trajectory for the motion controller of the previous section can be obtained. In the remaining part of this subsection stability of the impedance relationship is investigated.

### Stability analysis

The main result of this subsection is presented with the following proposition.

**Proposition 3.4.** *If the matrices  $K_{pi}$ ,  $K_{di}$ ,  $D_i$ ,  $B_i$  and  $S_i$  are selected positive definite, and the orientation errors  $\xi_i$  are sufficiently small, then the system described by (3.50) and (3.61) is locally asymptotically stable, i.e.  $\Delta x, \Delta \tilde{x} \rightarrow 0$  for  $t \rightarrow \infty$ .*

*Proof.* The stability of the system described by (3.50) and (3.61), is investigated with the following candidate Lyapunov function

$$V_2 = V_1 + \frac{1}{2} \Delta \dot{x}^T D \Delta \dot{x} + \frac{1}{2} \Delta \tilde{x}^T S \Delta \tilde{x} \quad (3.66)$$

where  $\Delta \tilde{x} = [\Delta \tilde{x}_1^T, \Delta \tilde{x}_2^T, \dots, \Delta \tilde{x}_n^T]^T \in \mathbb{R}^{6n}$ ,  $D = \text{diag}\{D_1, D_2, \dots, D_n\} \in \mathbb{R}^{6n \times 6n}$  and  $S = \text{diag}\{S_1, S_2, \dots, S_n\} \in \mathbb{R}^{6n \times 6n}$ . Calculating the time derivative  $\dot{V}_2$  gives

$$\dot{V}_2 = \dot{V}_1 + \Delta \dot{x}^T [D \Delta \ddot{x} + S \Delta \dot{\tilde{x}}] \quad (3.67)$$

and using the internal force-based impedance controller of (3.61)

$$\dot{V}_2 = -\Delta \dot{x}^T K_v \Delta \dot{x} + \Delta \dot{x}^T [\Delta h_I - B \Delta \dot{x}] \quad (3.68)$$

where  $\Delta h_I = [\Delta h_{I1}, \Delta h_{I2}, \dots, \Delta h_{In}]^T \in \mathbb{R}^{6n}$  and  $B = \text{diag}\{B_1, B_2, \dots, B_n\} \in \mathbb{R}^{6n \times 6n}$ . Using (3.6) the relation between the object and manipulator velocity in the error space can be obtained

$$\begin{bmatrix} \dot{\chi}_{id} - \dot{\chi}_{ir} \\ \omega_{id} - \omega_{ir} \end{bmatrix} = J_{oi,d} \begin{bmatrix} \dot{\chi}_{od} \\ \omega_{od} \end{bmatrix} - J_{oi,r} \begin{bmatrix} \dot{\chi}_{or} \\ \omega_{or} \end{bmatrix} \quad (3.69)$$

where  $J_{oi,d} \in \mathbb{R}^{6 \times 6}$  ( $J_{oi,r} \in \mathbb{R}^{6 \times 6}$ ) relates the desired (reference) translational  $\dot{\chi}_{od}$  and angular  $\omega_{od}$  object velocities to desired (reference) translational  $\dot{\chi}_{id}$  and angular  $\omega_{id,t}$  manipulator velocities. The impedance relationship (3.61) depends on the actual state of the system ( $\Delta h_{Ii} = \Delta h_{Ii}(q_i, \dot{q}_i, h_i)$ ), but it is assumed that with sufficiently high gains  $D_i$ ,  $B_i$  and  $S_i$ , the orientation error  $\tilde{\xi}_i$  (hence  $R_{id} \approx R_{ir}$ ) can be kept small. For small orientation errors, the two terms on the right hand side of (3.69) can be combined, since for  $p_{id} \approx p_{ir}$ ,  $J_{oi,d} \approx J_{oi,r}$

$$\begin{bmatrix} \dot{\chi}_{id} - \dot{\chi}_{ir} \\ \omega_{id} - \omega_{ir} \end{bmatrix} = J_{oi,r} \begin{bmatrix} \dot{\chi}_{od} - \dot{\chi}_{or} \\ \omega_{od} - \omega_{or} \end{bmatrix} \quad (3.70)$$

is obtained. For a small orientation error  $\tilde{\xi}_i$  the matrix  $\tilde{L}_i \approx I$  (see (3.65)), so that the velocity error  $\Delta \dot{\tilde{x}}_i$  of (3.63) reduces to

$$\Delta \dot{\tilde{x}}_i = \begin{bmatrix} \dot{\chi}_{id} - \dot{\chi}_{ir} \\ \omega_{id} - \omega_{ir} \end{bmatrix}. \quad (3.71)$$

Combining equations (3.70) and (3.71) results in

$$\Delta \dot{\tilde{x}}_i = J_{oi,r} \begin{bmatrix} \dot{\chi}_{od} - \dot{\chi}_{or} \\ \omega_{od} - \omega_{or} \end{bmatrix} \quad (3.72)$$

and combined for all manipulators

$$\Delta \dot{\tilde{x}} = J_{o,r} \begin{bmatrix} \dot{\chi}_{od} - \dot{\chi}_{or} \\ \omega_{od} - \omega_{or} \end{bmatrix} \quad (3.73)$$

where  $J_{o,r} = [J_{o1,r}^T, \dots, J_{on,r}^T]^T \in \mathbb{R}^{6n \times 6}$ . Substituting (3.73) into (3.68) gives

$$\dot{V}_2 = \underbrace{-\Delta \dot{x}^T K_v \Delta \dot{x}}_{\leq 0} + \underbrace{\begin{bmatrix} \dot{\chi}_{od} - \dot{\chi}_{or} \\ \omega_{od} - \omega_{or} \end{bmatrix}^T J_{o,r}^T \Delta h_I}_{=0} \underbrace{-\Delta \dot{\tilde{x}}^T B \Delta \dot{\tilde{x}}}_{\leq 0} \leq 0. \quad (3.74)$$

The first and third term on the right hand side are non-positive, since  $K_v$  and  $B$  are positive definite. The second term is equal to zero, because the internal forces (and thus the internal force error) are in the null space of  $J_{o,r}^T$  (it was previously proven that for  $t \rightarrow \infty$ ,  $\Delta x \rightarrow 0$ , so  $\Delta x_o \rightarrow 0$  and  $J_o \rightarrow J_{o,r}$ ). Thus, for  $t \rightarrow \infty$ ,  $\Delta \dot{x} \rightarrow 0$  and  $\Delta \dot{\tilde{x}} \rightarrow 0$ . This means that  $\Delta x \rightarrow c_1$  and  $\Delta \tilde{x} \rightarrow c_2$ , with  $c_1$  and  $c_2$  constant parameters. So from (3.74) local stability can be concluded.

Previously it was proved that  $\Delta x = \Delta \dot{x} = 0$  is asymptotically stable. Using LaSalle's invariance principle, asymptotic stability of the equilibrium point  $\Delta x = \Delta \tilde{x} = \Delta \dot{x} = \Delta \dot{\tilde{x}} = 0$  is investigated. The set  $\Omega_2$  is defined as

$$\Omega_2 = \{ \Delta x, \Delta \dot{x}, \Delta \tilde{x}, \Delta \dot{\tilde{x}} \in \mathbb{R}^{6n} \mid V_2(\Delta x, \Delta \dot{x}, \Delta \tilde{x}, \Delta \dot{\tilde{x}}) \leq \infty \}. \quad (3.75)$$

The set  $E_2$  in  $\Omega_2$  is defined as

$$E_2 = \left\{ \Delta x, \Delta \dot{x}, \Delta \tilde{x}, \Delta \dot{\tilde{x}} \in \Omega_2 \mid \dot{V}_2 = 0 \right\} = \left\{ \Delta x, \Delta \dot{x}, \Delta \tilde{x}, \Delta \dot{\tilde{x}} \in \Omega_2 \mid \Delta \dot{x} = \Delta \dot{\tilde{x}} = 0 \right\}. \quad (3.76)$$

The set  $N_2$  is defined as the largest invariant set in  $E_2$ . Substituting  $\Delta \dot{\tilde{x}} = 0$  and  $\Delta \ddot{\tilde{x}} = 0$  in (3.61) and premultiplication with  $J_{o,r}^T$  results in

$$J_{o,r}^T S \Delta \tilde{x} = J_{o,r}^T \Delta h_I = 0, \quad (3.77)$$

since  $\Delta h_I$  is in the null space of  $J_{o,r}^T$ . The left-hand side of (3.77) can be rewritten considering the terms for each individual manipulator as

$$J_{o1,r}^T S_1 \Delta \tilde{x}_1 + J_{o2,r}^T S_2 \Delta \tilde{x}_2 + \dots + J_{on,r}^T S_n \Delta \tilde{x}_n = 0. \quad (3.78)$$

To prove asymptotic stability, the two-arm case ( $i \in \{1, 2\}$ ), like in [23], is considered for ease of analysis. The results may be extended to multiple arms. In the

following analysis all vectors are expressed in the world frame, unless a superscript defines otherwise.

For the two-arm case, (3.78) reduces to

$$J_{o1,r}^T S_1 \Delta \tilde{x}_1 + J_{o2,r}^T S_2 \Delta \tilde{x}_2 = 0. \quad (3.79)$$

This relationship consists of 6 equations and 12 unknowns ( $\Delta \tilde{x}_{1r}$  and  $\Delta \tilde{x}_{2r}$ ). To determine a unique solution, 6 constraint equations have to be identified. These constraint equations can be obtained from the assumption that the manipulators have a tight grasp on the object. The first 3 constraints are related to the closed kinematic chain formed by the two manipulators and the object. From Figure 3.2 the following relation between the positions of the end-effectors  $\chi_i$  can be obtained

$$\chi_1 + R_1 p_{12}^1 = \chi_2 \quad (3.80)$$

with  $p_{12}^1$  a constant vector from frame  $\mathcal{T}_1$  to  $\mathcal{T}_2$ , expressed in frame  $\mathcal{T}_1$ . Similar expressions as in (3.80) can be obtained in terms of the reference and desired positions of the end-effectors, leading to the following three position constraints in the error space

$$\Delta \tilde{\chi}_1 + \Delta \tilde{R}_1 p_{12}^1 = \Delta \tilde{\chi}_2 \quad (3.81)$$

where  $\Delta \tilde{\chi}_i = \chi_{id} - \chi_{ir}$  and  $\Delta \tilde{R}_1 = R_{1d} - R_{1r}$ . An important property of  $\Delta \tilde{R}_1$  is that it is not of full rank, but has rank 2 (see Appendix E). Since the position and orientation of the grasp of the object by the manipulators is the same for the actual, reference and desired trajectories, it follows that  $p_{12}^1 = p_{1r2r}^{1r} = p_{1d2d}^{1d}$ .

The other three constraints relate the orientations of the end-effectors. The end-effectors of the manipulators have a tight grasp on the rigid object. Therefore, the rotation matrix  $R_2^1$ , describing the orientation of the second end-effector frame with respect to the first end-effector frame, is constant

$$R_2 = R_1 R_2^1 \quad \Rightarrow \quad R_2^1 = R_1^T R_2. \quad (3.82)$$

Since the grasp position and orientation of the object by the manipulators is independent of the actual, reference and desired trajectories, it follows that  $R_2^1 = R_{2r}^{1r} = R_{2d}^{1d}$ , and thus

$$R_{1r}^T R_{2r} = R_{2r}^{1r} = R_2^1, \quad R_{1d}^T R_{2d} = R_{2d}^{1d} = R_2^1. \quad (3.83)$$

Using (3.83) the following can be obtained

$$R_{1r}^T R_{2r} = R_{1d}^T R_{2d} \quad \Rightarrow \quad R_{1d} R_{1r}^T = R_{2d} R_{2r}^T \quad \Rightarrow \quad \tilde{R}_{e1} = \tilde{R}_{e2} \quad \Rightarrow \quad \tilde{\xi}_1 = \tilde{\xi}_2, \quad (3.84)$$

where  $\tilde{R}_{ei}$  represents the equivalent rotation between the desired and reference trajectories [29] from which the orientation error  $\tilde{\xi}_i$  can be extracted. It follows from (3.84) that the orientation errors of both end-effectors are equal. Equations (3.79), (3.81) and (3.84) form 12 equations with 12 unknowns ( $\Delta\tilde{x}_1$  and  $\Delta\tilde{x}_2$ ).

$$\begin{aligned} J_{o1,r}^T S_1 \Delta\tilde{x}_1 + J_{o2,r}^T S_2 \Delta\tilde{x}_2 &= 0 \\ \Delta\tilde{\chi}_1 - \Delta\tilde{\chi}_2 + \Delta\tilde{R}_1 p_{12}^1 &= 0 \\ \tilde{\xi}_1 - \tilde{\xi}_2 &= 0, \end{aligned} \quad (3.85)$$

or in matrix form

$$\begin{bmatrix} J_{o1,r}^T S_1 & J_{o2,r}^T S_2 \\ -I_6 & -I_6 \end{bmatrix} \begin{bmatrix} \Delta\tilde{x}_1 \\ \Delta\tilde{x}_2 \end{bmatrix} + \begin{bmatrix} 0_6 \\ \Delta\tilde{R}_1 p_{12}^1 \\ 0_3 \end{bmatrix} = 0_{12} \quad (3.86)$$

where the term  $\Delta\tilde{R}_1 p_{12}^1$  is a nonlinear function of the desired and reference orientations of the first end-effector. Due to this nonlinear term, in [23] asymptotic stability could only be proved for a point mass, so  $p_{12}^1 = 0$ , or when the orientation error  $\Delta\tilde{R}_1$  is zero. In that case, the second vector on the left hand side of (3.86) reduces to zero. Since the object Jacobians  $J_{oi,r}$  and desired stiffness matrices  $S_i$  are all positive definite, the matrix on the left hand side is invertible and  $[\Delta\tilde{x}_1^T, \Delta\tilde{x}_2^T]^T = 0$  is the unique solution. To prove asymptotic stability in the case of  $p_{12}^1 \neq 0$ , the result  $\Delta\tilde{R}_1 p_{12}^1 = 0$  of Lemma 3.5 is substituted into (3.86), resulting in

$$\begin{bmatrix} J_{o1,r}^T S_1 & J_{o2,r}^T S_2 \\ -I_6 & -I_6 \end{bmatrix} \begin{bmatrix} \Delta\tilde{x}_1 \\ \Delta\tilde{x}_2 \end{bmatrix} = 0_{12} \quad (3.87)$$

The matrix on the left hand side has full rank, since  $J_{oi,r}$  is a positive definite matrix and  $S_i$  is a symmetric positive definite matrix. Thus, the unique solution to (3.87) is

$$\Delta\tilde{x}_i = 0 \quad \Rightarrow \quad \Delta\tilde{x} = 0 \quad (3.88)$$

and the largest invariant set  $N_2$  in  $E_2$  becomes

$$N_2 = \{ \Delta x, \Delta\dot{x}, \Delta\tilde{x}, \Delta\dot{\tilde{x}} \in E_2 \mid \Delta x = \Delta\tilde{x} = 0 \}. \quad (3.89)$$

From LaSalle's invariance principle it can be concluded that for  $t \rightarrow \infty$ ,  $\Delta x, \Delta\tilde{x} \rightarrow 0$ , so the equilibrium point  $\Delta x = \Delta\dot{x} = \Delta\tilde{x} = \Delta\dot{\tilde{x}} = 0$  is asymptotically stable. Consequently, for  $t \rightarrow \infty$ , the end-effectors of the manipulators asymptotically track their desired trajectory  $x_d$ . From the impedance relationship (3.61) it follows that since  $\Delta\tilde{x}_i$  and time derivatives are equal to zero, we also have  $\Delta h_{Ii} = 0$  for  $t \rightarrow \infty$ . This means that the contribution of the manipulators to the internal force of the object  $h_I$  asymptotically tracks the desired internal force  $h_{Id}$ , so the desired compression, extension, torsion and bending can be achieved.  $\square$

The following Lemma 3.5 is used in the proof of Proposition 3.4.

**Lemma 3.5.** *Consider the desired and reference orientation of the end-effector of manipulator 1, defined by  $R_{1d}$  and  $R_{1r}$  respectively. Let the constant vector from frame  $\mathcal{T}_1$  to frame  $\mathcal{T}_2$ , expressed in frame  $\mathcal{T}_1$  (see Figure 3.2), be denoted by  $p_{12}^1 \neq 0$ . Under the assumption that it is possible to find a combination of gains  $S_{it}$ ,  $S_{i\alpha}$  and  $S_{ic}$  for  $i = \{1, 2\}$  such that the following matrices  $\Gamma, \Psi \in \mathbb{R}^{3 \times 3}$ ,*

$$\Gamma = - (S_{1c}^T - \Lambda(R_{1r}p_{12}^1)S_{1t} - S_{2c}^T S_{2t}^{-1} S_{1t}) (S_{1t} + S_{2t})^{-1} S_{2t} \quad (3.90)$$

$$\Psi = [S_{1\alpha} + S_{2\alpha} - \Lambda(R_{1r}p_{12}^1)S_{1c} - S_{2c}^T S_{2t}^{-1} (S_{1c} + S_{2c}) \\ - (S_{1c}^T - \Lambda(R_{1r}p_{12}^1)S_{1t} - S_{2c}^T S_{2t}^{-1} S_{1t}) (S_{1t} + S_{2t})^{-1} (S_{1c} + S_{2c})] \quad (3.91)$$

are of full rank (i.e. rank 3), if the difference matrix is defined as  $\Delta\tilde{R}_1 = R_{1d} - R_{1r}$ , then the vector  $p_{12}^1$  is projected onto the null space of  $\Delta\tilde{R}_1$ , so that  $\Delta\tilde{R}_1 p_{12}^1 = 0$ .

*Proof.* Equation (3.79) can be written in matrix form

$$\begin{bmatrix} I_3 & O_3 \\ -\Lambda(p_{1r}) & I_3 \end{bmatrix} \begin{bmatrix} S_{1t} & S_{1c} \\ S_{1c}^T & S_{1\alpha} \end{bmatrix} \begin{bmatrix} \Delta\tilde{\chi}_1 \\ \tilde{\xi}_1 \end{bmatrix} + \begin{bmatrix} I_3 & O_3 \\ -\Lambda(p_{2r}) & I_3 \end{bmatrix} \begin{bmatrix} S_{2t} & S_{2c} \\ S_{2c}^T & S_{2\alpha} \end{bmatrix} \begin{bmatrix} \Delta\tilde{\chi}_2 \\ \tilde{\xi}_2 \end{bmatrix} = \begin{bmatrix} 0_3 \\ 0_3 \end{bmatrix} \quad (3.92)$$

where  $S_{it}, S_{i\alpha}, S_{ic} \in \mathbb{R}^{3 \times 3}$  represent the translational, rotational and coupling stiffnesses and  $\Lambda(p_{ir})$  a skew-symmetric matrix with  $p_{ir} = R_{ir} p_{ir}^r$ . Note that  $p_i^i = p_{ir}^r = p_{id}^d$ , because the grasp position and orientation of the object by the manipulators is independent of the actual, reference and desired trajectories. From (3.92), it follows that

$$S_{1t}\Delta\tilde{\chi}_1 + S_{1c}\tilde{\xi}_1 + S_{2t}\Delta\tilde{\chi}_2 + S_{2c}\tilde{\xi}_2 = 0 \quad (3.93)$$

$$(S_{1c}^T - \Lambda(p_{1r})S_{1t})\Delta\tilde{\chi}_1 + (S_{1\alpha} - \Lambda(p_{1r})S_{1c})\tilde{\xi}_1 + (S_{2c}^T - \Lambda(p_{2r})S_{2t})\Delta\tilde{\chi}_2 \\ + (S_{2\alpha} - \Lambda(p_{2r})S_{2c})\tilde{\xi}_2 = 0. \quad (3.94)$$

In [123] the authors investigated asymptotic stability from equations (3.93) and (3.94) for an  $n$ -manipulator system where the coupling stiffness  $S_{ic} = 0$ . In that case equations (3.93) and (3.94) reduce to

$$\sum_{i=1}^n S_{it}\Delta\tilde{\chi}_i = 0 \\ \sum_{i=1}^n -\Lambda(p_{ir})S_{it}\Delta\tilde{\chi}_i + \sum_{i=1}^n S_{i\alpha}\tilde{\xi}_i = 0.$$

Since the desired stiffness matrices are positive definite, their submatrices  $S_{it}$  and  $S_{i\alpha}$  are as well. From the first equation the authors of [123] conclude that  $\Delta\tilde{\chi}_i = 0$  and then from the second equation that  $\tilde{\xi}_i = 0$  is the unique solution to this set of equations. However, it can easily be seen that for example for  $n = 2$ ,  $\Delta\tilde{\chi}_1 = -S_{1t}^{-1}S_{2t}\Delta\tilde{\chi}_2$  is always a solution to the first equation, even when  $\Delta\tilde{\chi}_1$  and  $\Delta\tilde{\chi}_2$  are unequal to zero. Since  $\Delta\tilde{\chi}_i = \tilde{\xi}_i = 0$  is not the unique solution, asymptotic stability is wrongly concluded in [123]. Apparently, the authors did not take into account that (3.93) and (3.94) have 12 unknowns, but consists of only 6 equations.

To prove that  $\Delta\tilde{\chi}_i = \tilde{\xi}_i = 0$  is the unique solution of (3.86), independent of the dimensions of object and without any restrictions on the desired stiffness matrix (such as being diagonal or block diagonal), (3.93) is pre-multiplied with  $\Lambda(p_{2r})$

$$\Lambda(p_{2r})S_{2t}\Delta\tilde{\chi}_2 + \Lambda(p_{2r})S_{2c}\tilde{\xi}_2 = -\Lambda(p_{2r})S_{1t}\Delta\tilde{\chi}_1 - \Lambda(p_{2r})S_{1c}\tilde{\xi}_1 \quad (3.95)$$

and then substituted into (3.94)

$$\begin{aligned} (S_{1c}^T - \Lambda(p_{1r})S_{1t})\Delta\tilde{\chi}_1 + (S_{1\alpha} - \Lambda(p_{1r})S_{1c})\tilde{\xi}_1 + S_{2c}^T\Delta\tilde{\chi}_2 + \Lambda(p_{2r})S_{1t}\Delta\tilde{\chi}_1 \\ + S_{2\alpha}\tilde{\xi}_2 + \Lambda(p_{2r})S_{1c}\tilde{\xi}_1 = 0 \\ (S_{1c}^T - (\Lambda(p_{1r}) - \Lambda(p_{2r}))S_{1t})\Delta\tilde{\chi}_1 + (S_{1\alpha} - (\Lambda(p_{1r}) - \Lambda(p_{2r}))S_{1c})\tilde{\xi}_1 \\ + S_{2c}^T\Delta\tilde{\chi}_2 + S_{2\alpha}\tilde{\xi}_2 = 0. \end{aligned} \quad (3.96)$$

This expression consists of 12 unknowns and 3 separate equations. An expression for  $\Delta\tilde{\chi}_2$  is obtained from (3.93)

$$\Delta\tilde{\chi}_2 = -S_{2t}^{-1} \left( S_{1t}\Delta\tilde{\chi}_1 + S_{1c}\tilde{\xi}_1 + S_{2c}\tilde{\xi}_2 \right) \quad (3.97)$$

and substituted into (3.96) to eliminate the three unknowns of  $\Delta\tilde{\chi}_2$

$$\begin{aligned} (S_{1c}^T - (\Lambda(p_{1r}) - \Lambda(p_{2r}))S_{1t})\Delta\tilde{\chi}_1 + (S_{1\alpha} - (\Lambda(p_{1r}) - \Lambda(p_{2r}))S_{1c})\tilde{\xi}_1 \\ - S_{2c}^T S_{2t}^{-1} \left( S_{1t}\Delta\tilde{\chi}_1 + S_{1c}\tilde{\xi}_1 + S_{2c}\tilde{\xi}_2 \right) + S_{2\alpha}\tilde{\xi}_2 = 0 \\ (S_{1c}^T - (\Lambda(p_{1r}) - \Lambda(p_{2r}))S_{1t} - S_{2c}^T S_{2t}^{-1} S_{1t})\Delta\tilde{\chi}_1 \\ + (S_{1\alpha} - (\Lambda(p_{1r}) - \Lambda(p_{2r}))S_{1c} - S_{2c}^T S_{2t}^{-1} S_{1c})\tilde{\xi}_1 + (-S_{2c}^T S_{2t}^{-1} S_{2c} + S_{2\alpha})\tilde{\xi}_2 = 0. \end{aligned} \quad (3.98)$$

This results in 3 separate equations with 9 unknowns. Using  $\tilde{\xi}_1 = \tilde{\xi}_2$  from the orientation error constraint of (3.84), the three unknowns of  $\tilde{\xi}_2$  can be eliminated

$$\begin{aligned} (S_{1c}^T - (\Lambda(p_{1r}) - \Lambda(p_{2r}))S_{1t} - S_{2c}^T S_{2t}^{-1} S_{1t})\Delta\tilde{\chi}_1 \\ + (S_{1\alpha} + S_{2\alpha} - (\Lambda(p_{1r}) - \Lambda(p_{2r}))S_{1c} - S_{2c}^T S_{2t}^{-1} (S_{1c} + S_{2c}))\tilde{\xi}_1 = 0, \end{aligned} \quad (3.99)$$

resulting in 3 separate equations with 6 unknowns ( $\Delta\tilde{\chi}_1$  and  $\tilde{\xi}_1$ ). Substituting the expression obtained for  $\Delta\tilde{\chi}_2$  from (3.97) into the position error constraint of (3.81) and rewriting, results in the following expression for  $\Delta\tilde{\chi}_1$

$$\Delta\tilde{x}_{1t} = -(S_{1t} + S_{2t})^{-1} \left( S_{2t}\Delta\tilde{R}_1 p_{12}^1 + (S_{1c} + S_{2c})\tilde{\xi}_1 \right). \quad (3.100)$$

Substituting this expression into (3.99) to eliminate the 3 unknowns of  $\Delta\tilde{x}_{1t}$  gives

$$\begin{aligned} & - (S_{1c}^T - (\Lambda(p_{1r}) - \Lambda(p_{2r}))S_{1t} - S_{2c}^T S_{2t}^{-1} S_{1t}) (S_{1t} + S_{2t})^{-1} S_{2t}\Delta\tilde{R}_1 p_{12}^1 \\ & + [S_{1\alpha} + S_{2\alpha} - (\Lambda(p_{1r}) - \Lambda(p_{2r}))S_{1c} - S_{2c}^T S_{2t}^{-1} (S_{1c} + S_{2c}) \\ & - (S_{1c}^T - (\Lambda(p_{1r}) - \Lambda(p_{2r}))S_{1t} - S_{2c}^T S_{2t}^{-1} S_{1t}) (S_{1t} + S_{2t})^{-1} (S_{1c} + S_{2c})] \tilde{\xi}_1 = 0. \end{aligned} \quad (3.101)$$

This expression consists of 3 separate equations and only the 3 unknowns of  $\tilde{\xi}_1$  ( $\Delta\tilde{R}_1 = \Delta\tilde{R}_1(\tilde{\xi}_1)$ ). The difference between the skew symmetric matrices  $\Lambda(p_{1r}) - \Lambda(p_{2r})$  can be expressed as

$$\begin{aligned} \Lambda(p_{1r}) - \Lambda(p_{2r}) &= \Lambda(R_{1r}p_{1r}^{1r}) - \Lambda(R_{2r}p_{2r}^{2r}) \\ &= \Lambda(R_{1r}p_{1r}^{1r} - R_{2r}p_{2r}^{2r}) \\ &= \Lambda(R_{1r}p_{1r}^{1r} - R_{1r}R_{2r}^{1r}p_{2r}^{2r}) \\ &= \Lambda(R_{1r}p_{1r}^{1r} - R_{1r}p_{2r}^{1r}) \\ &= \Lambda(R_{1r}p_{1r2r}^{1r}) \end{aligned} \quad (3.102)$$

where  $p_{1r2r}^{1r} = p_{1r}^{1r} - p_{2r}^{1r}$ . Here,  $p_{1r2r}^{1r} = p_{12}^1$  (see Figure 3.2) and  $R_{2r}^{1r} = R_2^1$  similar to the cases in (3.81) and (3.83). Substituting this result into (3.101)

$$\begin{aligned} & - (S_{1c}^T - \Lambda(R_{1r}p_{12}^1)S_{1t} - S_{2c}^T S_{2t}^{-1} S_{1t}) (S_{1t} + S_{2t})^{-1} S_{2t}\Delta\tilde{R}_1 p_{12}^1 \\ & + [S_{1\alpha} + S_{2\alpha} - \Lambda(R_{1r}p_{12}^1)S_{1c} - S_{2c}^T S_{2t}^{-1} (S_{1c} + S_{2c}) \\ & - (S_{1c}^T - \Lambda(R_{1r}p_{12}^1)S_{1t} - S_{2c}^T S_{2t}^{-1} S_{1t}) (S_{1t} + S_{2t})^{-1} (S_{1c} + S_{2c})] \tilde{\xi}_1 = 0, \end{aligned} \quad (3.103)$$

or

$$\begin{aligned} \Gamma\Delta\tilde{R}_1 p_{12}^1 + \Psi\tilde{\xi}_1 &= 0 \\ \tilde{\xi}_1 + \Psi^{-1}\Gamma\Delta\tilde{R}_1 p_{12}^1 &= 0 \end{aligned} \quad (3.104)$$

with

$$\Gamma = - (S_{1c}^T - \Lambda(R_{1r}p_{12}^1)S_{1t} - S_{2c}^T S_{2t}^{-1} S_{1t}) (S_{1t} + S_{2t})^{-1} S_{2t} \quad (3.105)$$

$$\begin{aligned} \Psi &= [S_{1\alpha} + S_{2\alpha} - \Lambda(R_{1r}p_{12}^1)S_{1c} - S_{2c}^T S_{2t}^{-1} (S_{1c} + S_{2c}) \\ & - (S_{1c}^T - \Lambda(R_{1r}p_{12}^1)S_{1t} - S_{2c}^T S_{2t}^{-1} S_{1t}) (S_{1t} + S_{2t})^{-1} (S_{1c} + S_{2c})]. \end{aligned} \quad (3.106)$$



Here, it is assumed that a combination of  $S_{it}$ ,  $S_{i\alpha}$  and  $S_{ic}$  can be found which results in full rank of the square matrices  $\Gamma$  and  $\Psi$ . It should be emphasized that, this assumption may not always be fulfilled.

By using the orthogonality of  $\Delta\tilde{R}_1 = R_{1d} - R_{1r}$  to  $\tilde{\xi}_1$  (see Lemma E.1 in Appendix E) and by premultiplying (3.104) with  $\Delta\tilde{R}_1^T$  results in

$$\begin{aligned} \underbrace{\Delta\tilde{R}_1^T \tilde{\xi}_1}_{=0} + \Delta\tilde{R}_1^T \Psi^{-1} \Gamma \Delta\tilde{R}_1 p_{12}^1 &= 0 \\ \Rightarrow \Delta\tilde{R}_1^T \Psi^{-1} \Gamma \Delta\tilde{R}_1 p_{12}^1 &= 0. \end{aligned} \quad (3.107)$$

Since  $\Delta\tilde{R}_1$  has rank 2, the expression (3.107) consists of only two independent equations (the third equation depends on the other two). Therefore,  $\tilde{\xi}_1 = 0$  is not the unique solution to (3.107). A third independent equation can be obtained, using the following property of a skew symmetric matrix  $\Lambda(\cdot) \in \mathbb{R}^{3 \times 3}$

$$a^T \Lambda(\cdot) a = 0 \quad (3.108)$$

with  $a \in \mathbb{R}^3$  an arbitrary vector. Thus, the third independent equation reads

$$(p_{12}^1)^T \Delta\tilde{R}_1^T \Lambda(R_{1r} p_{12}^1) \Delta\tilde{R}_1 p_{12}^1 = 0. \quad (3.109)$$

The two independent rows of (3.107) and (3.109) can be combined into

$$\underbrace{\begin{bmatrix} (n_{1d} - n_{1r})^T \Psi^{-1} \Gamma \\ (s_{1d} - s_{1r})^T \Psi^{-1} \Gamma \\ (p_{12}^1)^T \Delta\tilde{R}_1^T \Lambda(R_{1r} p_{12}^1) \end{bmatrix}}_W \Delta\tilde{R}_1 p_{12}^1 = 0. \quad (3.110)$$

It can be shown that  $\Delta\tilde{R}_1 p_{12}^1 = 0$  is the unique solution of (3.110). If  $\Delta\tilde{R}_1 p_{12}^1 \neq 0$  it can be shown that with a proper choice of  $\Gamma$  and  $\Psi$ , matrix  $W$  has full rank (see Appendix E), so it is invertible. Then, from (3.110) it follows that

$$\Delta\tilde{R}_1 p_{12}^1 = 0. \quad (3.111)$$

□

**Remark 3.6.** *The assumption in Lemma 3.5 may not always be fulfilled. Indeed, if  $S_i$  is selected as a block diagonal matrix, i.e.  $S_{ic} = 0$ , then  $\Psi = S_{1\alpha} + S_{2\alpha}$  and  $\Gamma = \Lambda(R_{1r} p_{12}^1) S_{1t} (S_{1t} + S_{2t})^{-1} S_{2t}$ , where  $\Gamma$  is of rank 2 since  $\Lambda(R_{1r} p_{12}^1)$  is a  $3 \times 3$  skew-symmetric matrix, which is always rank deficient. This is also the case if the gains are selected as  $S_1 = S_2$ , then  $\Gamma = \frac{1}{2} \Lambda(R_{1r} p_{12}^1) S_{1t}$  and  $\Psi = 2S_{1\alpha}$ .*

### 3.3.3 External force-based impedance control

Contact of the object with the environment can cause large contact forces if they are not controlled which can result in the damage of the object, the manipulators or the environment. This can be insured if the following object impedance relationship, to control the object/environment contact forces, is used

$$D_o \Delta \ddot{x}_{ocd} + B_o \Delta \dot{x}_{ocd} + S_o \Delta x_{ocd} = \Delta h_{ext,cd} \quad (3.II2)$$

with  $D_o, B_o, S_o \in \mathbb{R}^{6 \times 6}$  the desired object inertia, damping and stiffness matrices and  $\Delta x_{ocd}$  the position and orientation error between the commanded and desired object trajectories  $\Delta x_{ocd} = x_{oc} - x_{od}$ . The commanded  $x_{oc} \in \mathbb{R}^6$  and desired  $x_{od} \in \mathbb{R}^6$  object trajectories are defined as

$$x_{oc} = \begin{bmatrix} \chi_{oc} \\ \phi_{oc} \end{bmatrix}, \quad x_{od} = \begin{bmatrix} \chi_{od} \\ \phi_{od} \end{bmatrix} \quad (3.II3)$$

with  $\chi_{oc} \in \mathbb{R}^3$  the position and  $\phi_{oc} \in \mathbb{R}^3$  the orientation part of the *commanded* object trajectory and  $\chi_{od} \in \mathbb{R}^3$  the position and  $\phi_{od} \in \mathbb{R}^3$  the orientation part of the *desired* object trajectory. Here, the commanded trajectory is a time-varying signal which is determined by the required task (e.g. transportation of the grasped object from one position to another). Any minimal set of parameters can be used to define the orientations (for example Euler angles,  $\phi = [\varphi \ \vartheta \ \psi]^T$  [29]). The commanded object velocity  $\dot{x}_{oc} \in \mathbb{R}^6$  and acceleration  $\ddot{x}_{oc} \in \mathbb{R}^6$  are defined as

$$\dot{x}_{oc} = \begin{bmatrix} \dot{\chi}_{oc} \\ \dot{\phi}_{oc} \end{bmatrix}, \quad \ddot{x}_{oc} = \begin{bmatrix} \ddot{\chi}_{oc} \\ \ddot{\phi}_{oc} \end{bmatrix} \quad (3.II4)$$

and the desired object velocity  $\dot{x}_{od} \in \mathbb{R}^6$  and acceleration  $\ddot{x}_{od} \in \mathbb{R}^6$  are defined as

$$\dot{x}_{od} = \begin{bmatrix} \dot{\chi}_{od} \\ \dot{\phi}_{od} \end{bmatrix}, \quad \ddot{x}_{od} = \begin{bmatrix} \ddot{\chi}_{od} \\ \ddot{\phi}_{od} \end{bmatrix}. \quad (3.II5)$$

Note that the time derivatives of the Euler angles are used and not the angular velocities and accelerations. The relationship between the time derivative of the Euler angles and the angular velocity is given by

$$\omega_{oc} = T(\phi_{oc}) \dot{\phi}_{oc} \quad (3.II6)$$

$$\omega_{od} = T(\phi_{od}) \dot{\phi}_{od} \quad (3.II7)$$

where the transformation matrix  $T(\cdot) \in \mathbb{R}^{3 \times 3}$  depends on the choice of angular parametrization and becomes rank deficient at representation singularities [131].

The object/environment contact force and moment error  $\Delta h_{ext,cd} \in \mathbb{R}^6$  is defined as difference between commanded  $h_{ext,c}$  and desired  $h_{ext,d}$  contact forces and moments

$$\Delta h_{ext,cd} = h_{ext,c} - h_{ext,d} = \begin{bmatrix} f_{ext,c} \\ \mu_{ext,c} \end{bmatrix} - \begin{bmatrix} f_{ext,d} \\ \mu_{ext,d} \end{bmatrix} \quad (3.118)$$

with  $f_{ext,c} \in \mathbb{R}^3$  and  $\mu_{ext,c} \in \mathbb{R}^3$  the commanded contact forces and moments and  $f_{ext,d} \in \mathbb{R}^3$  and  $\mu_{ext,d} \in \mathbb{R}^3$  the desired contact forces and moments.

The object/environment contact forces  $f_{ext} \in \mathbb{R}^3$  and moments  $\mu_{ext} \in \mathbb{R}^3$  are modeled as mechanical springs and dampers

$$h_{ext} = \Sigma S_{env} (x_o - x_{env}) + \Sigma B_{env} (\dot{x}_o - \dot{x}_{env}) \quad (3.119)$$

with  $S_{env} \in \mathbb{R}^{6 \times 6}$  the stiffness and  $B_{env} \in \mathbb{R}^{6 \times 6}$  the damping matrix of the environment. The diagonal selection matrix  $\Sigma$  has diagonal elements being either 1 in the directions of contact or 0 in the directions without contact. It is assumed that these three matrices are known. The vector  $x_{env} = [\chi_{env}^T \ \phi_{env}^T]^T$  contains the position  $\chi_{env}$  and orientation  $\phi_{env}$  (Euler angles) of the environment and  $\dot{x}_{env} = [\dot{\chi}_{env}^T \ \dot{\phi}_{env}^T]^T$  contains the translation  $\dot{\chi}_{env}$  and orientation  $\dot{\phi}_{env}$  velocities of the environment. Again, the time derivatives of the Euler angles are used to express the rotational velocities. The commanded  $h_{ext,c}$  and desired  $h_{ext,d}$  object/environment contact forces are modeled in a similar way as  $h_{ext}$  in (3.119)

$$h_{ext,c} = \Sigma S_{env} (x_{oc} - x_{env}) + \Sigma B_{env} (\dot{x}_{oc} - \dot{x}_{env}) \quad (3.120)$$

$$h_{ext,d} = \Sigma S_{env} (x_{od} - x_{env}) + \Sigma B_{env} (\dot{x}_{od} - \dot{x}_{env}). \quad (3.121)$$

Using equations (3.118), (3.120) and (3.121), the external forces and moments error  $\Delta h_{ext}$  can be written as

$$\begin{aligned} \Delta h_{ext} &= \Sigma S_{env} (x_{oc} - x_{env}) + \Sigma B_{env} (\dot{x}_{oc} - \dot{x}_{env}) - \Sigma S_{env} (x_{od} - x_{env}) \\ &\quad - \Sigma B_{env} (\dot{x}_{od} - \dot{x}_{env}) \\ &= \Sigma S_{env} (x_{oc} - x_{od}) + \Sigma B_{env} (\dot{x}_{oc} - \dot{x}_{od}) \\ &= \Sigma S_{env} \Delta x_{ocd} + \Sigma B_{env} \Delta \dot{x}_{ocd}. \end{aligned} \quad (3.122)$$

Substituting this expression into the object impedance relationship (3.112) gives

$$D_o \Delta \ddot{x}_{ocd} + (B_o - \Sigma B_{env}) \Delta \dot{x}_{ocd} + (S_o - \Sigma S_{env}) \Delta x_{ocd} = 0. \quad (3.124)$$

**Remark 3.7.** *An advantage over the object impedance controller of [28, 126] is that the actual contact force is not required for the controller. The idea is that when  $x_d$  is tracked by the internal force-based impedance controller (3.61) and the motion controller (3.42),  $h_{ext}$  converges to  $h_{ext,c}$ . Furthermore, we can specify a commanded contact force and aim to apply any force on the environment, rather than controlling the contact force to zero as in [28, 126].*

The main result of this subsection can be presented with the following Proposition.

**Proposition 3.8.** *If Proposition 3.4 is satisfied and the matrices  $D_o$ ,  $B_o - \Sigma B_{env}$  and  $S_o - \Sigma S_{env}$  are designed positive definite, then the system, described by (3.5), (3.42), (3.61), (3.112), is asymptotically stable, i.e.  $\Delta x, \Delta \tilde{x}, \Delta x_{ocd} \rightarrow 0$  for  $t \rightarrow \infty$ .*

*Proof.* Stability of the controlled system, consisting of multiple manipulators, the rigid object, motion controller (3.42)-(3.49), internal force-based impedance controller (3.61) and external force-based impedance controller (3.124), is investigated with the candidate Lyapunov function

$$V_3 = V_2 + \frac{1}{2} \Delta \dot{x}_{ocd}^T D_o \Delta \dot{x}_{ocd} + \frac{1}{2} \Delta x_{ocd}^T (S_o - \Sigma S_{env}) \Delta x_{ocd} \quad (3.125)$$

where  $D_o$  is positive definite and  $S_o$  should be designed to make  $S_o - \Sigma S_{env}$  positive definite. Calculating the time derivative  $\dot{V}_3$  results in

$$\dot{V}_3 = \dot{V}_2 + \Delta \dot{x}_{ocd}^T [D_o \Delta \ddot{x}_{ocd} + (S_o - \Sigma S_{env}) \Delta x_{ocd}] \quad (3.126)$$

and using the object impedance relationship of (3.124)

$$\dot{V}_3 = \underbrace{-\Delta \dot{x}^T K_v \Delta \dot{x}}_{\leq 0} - \underbrace{\Delta \tilde{x}^T B \Delta \dot{\tilde{x}}}_{\leq 0} - \underbrace{\Delta \dot{x}_{ocd}^T (B_o - \Sigma B_{env}) \Delta \dot{x}_{ocd}}_{\leq 0} \leq 0 \quad (3.127)$$

where it is assumed that with a proper tuning of  $B_o$  the matrix  $B_o - \Sigma B_{env}$  is positive definite. The matrices  $K_v$  and  $B$  are also positive definite, so from (3.127) stability of the complete system can be concluded: for  $t \rightarrow \infty$ ,  $\Delta \dot{x}, \Delta \dot{\tilde{x}}, \Delta \dot{x}_{ocd} \rightarrow 0$ . Thus for  $t \rightarrow \infty$ ,  $\Delta x \rightarrow c_1$ ,  $\Delta \tilde{x} \rightarrow c_2$  and  $\Delta x_{ocd} \rightarrow c_3$ , with  $c_1, c_2$  and  $c_3$  constant parameters. Note that the system is stable, even when the object is in contact with the environment.

In sections 3.3.1 and 3.3.2 it was shown that the system with motion and internal force-based impedance controller is asymptotically stable ( $\Delta x, \Delta \tilde{x} \rightarrow 0$  for  $t \rightarrow \infty$ ). Asymptotic stability of the external force-based impedance controller (3.124) is investigated with LaSalle's invariance principle. The radially unbounded set  $\Omega_3$  is defined as

$$\Omega_3 = \left\{ \Delta x, \Delta \dot{x}, \Delta \tilde{x}, \Delta \dot{\tilde{x}} \in \mathbb{R}^{6n}, \Delta x_{ocd}, \Delta \dot{x}_{ocd} \in \mathbb{R}^6 \mid V_3(\Delta x, \Delta \dot{x}, \Delta \tilde{x}, \Delta \dot{\tilde{x}}, \Delta x_{ocd}, \Delta \dot{x}_{ocd}) \leq \infty \right\}. \quad (3.128)$$

The set  $E_3$  in  $\Omega_3$  is defined as

$$\begin{aligned} E_3 &= \left\{ \Delta x, \Delta \dot{x}, \Delta \tilde{x}, \Delta \dot{\tilde{x}}, \Delta x_{ocd}, \Delta \dot{x}_{ocd} \in \Omega_3 \mid \dot{V}_3 = 0 \right\}, \\ &= \left\{ \Delta x, \Delta \dot{x}, \Delta \tilde{x}, \Delta \dot{\tilde{x}}, \Delta x_{ocd}, \Delta \dot{x}_{ocd} \in \Omega_3 \mid \Delta \dot{x} = \Delta \dot{\tilde{x}} = \Delta \dot{x}_{ocd} = 0 \right\}. \end{aligned} \quad (3.129)$$

The set  $N_3$  is defined as the largest invariant set in  $E_3$ . The set  $N_3$  is obtained by substituting  $\Delta\dot{x}_{ocd} = \Delta\ddot{x}_{ocd} = 0$  in (3.124)

$$(S_o - \Sigma S_{env}) \Delta x_{ocd} = 0. \quad (3.130)$$

The matrix  $S_o - \Sigma S_{env}$  is positive definite, so the unique solution to (3.130) is

$$\Delta x_{ocd} = 0. \quad (3.131)$$

Thus, the largest invariant set  $N_3$  in  $E_3$  is

$$N_3 = \{ \Delta x, \Delta \dot{x}, \Delta \tilde{x}, \Delta \dot{\tilde{x}}, \Delta x_{ocd}, \Delta \dot{x}_{ocd} \in E_3 \mid \Delta x = \Delta \tilde{x} = \Delta x_{ocd} = 0 \}. \quad (3.132)$$

From LaSalle's invariance principle it can be concluded that  $\Delta x, \Delta \tilde{x}, \Delta x_{ocd} \rightarrow 0$ , for  $t \rightarrow \infty$ , so the equilibrium point  $\Delta x = \Delta \dot{x} = \Delta \tilde{x} = \Delta \dot{\tilde{x}} = \Delta x_{ocd} = \Delta \dot{x}_{ocd} = 0$  is asymptotically stable. Thus with the control structure of Figure 3.4 the motion of the object can be controlled, together with the internal forces and moments of the object and the contact forces and moments between the object and the environment.  $\square$

**Remark 3.9.** *In case  $S_{env}$  and  $B_{env}$  are not known exactly, an over approximation can be used to guarantee asymptotic stability. As long as  $B_o - \Sigma B_{env}$  and  $S_o - \Sigma S_{env}$  are positive definite, a desired trajectory  $x_{od}$  will be computed that reduces  $\Delta h_{ext,c}$ .*

## 3.4 Numerical simulations

In this section, first, the simulation results are presented for the cooperative manipulators rigidly grasping an object using the controller represented by Figure 3.4. Then, simulation results for the case of cooperative manipulators concerning non-rigid grasps introduced in Section 3.2.2 are presented.

### 3.4.1 Fixed grasp

For the fixed grasp case, first a way to tune the impedance parameters of (3.61) is discussed. Tuning these parameters by hand can be difficult and time consuming. Instead, the procedure of [4] is followed. Here, the desired inertia matrix  $D_i$  is chosen to represent the mass and mass moments of inertia felt at the end-effector

$$D_i(q_i) = (J_i(q_i)M_i(q_i)^{-1}J_i(q_i)^T)^{-1} \quad (3.133)$$

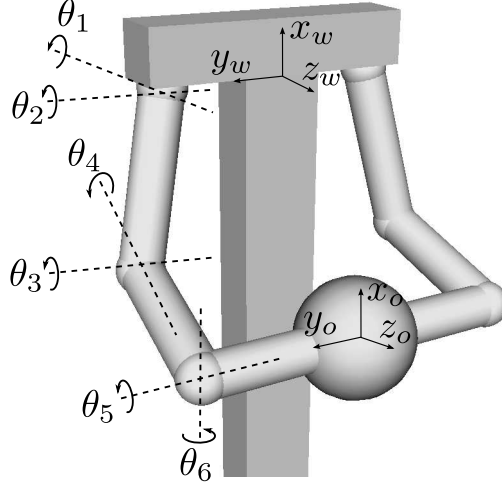


Figure 3.5 Cooperative manipulator system.

such that convergence to zero is assured with equal rate for all 6 directions of  $\Delta \tilde{x}_i$  and  $\Delta h_{I_i}$ . The desired stiffness  $S_i$  and damping  $B_i$  matrices are based on  $D_i$  via

$$S_i = Q_i S_{i0} Q_i^T \quad (3.134)$$

$$B_i = 2Q_i B_{i0} S_{i0}^{1/2} Q_i^T \quad (3.135)$$

where  $S_{i0}$  is the diagonal stiffness matrix and  $B_{i0}$  is a diagonal matrix containing the damping coefficients ( $B_{i0} = I_6$  represents critical damping). These matrices can be tuned such as to achieve the required response. The matrix  $Q_i$  follows from  $D_i = Q_i Q_i^T$ . Note that for the stability analysis of Section 3.3.2, the matrices  $D_i$ ,  $B_i$  and  $S_i$  should be computed once and kept constant during the task.

In our simulation case-study, the cooperative manipulator system consists of two identical 6 DOF manipulators, handling a spherical, rigid object, as shown in Figure 3.5. The manipulators have dimensions similar to an arm of an average adult human. The object has radius  $r_o = 0.1$  m and mass  $m_o = 0.1$  kg. In order to simulate the cooperative manipulator system, the dynamics of the manipulators (3.5) and the object (3.8) are combined with the velocity constraints by following a procedure presented in [23].

The commanded task consists of free motion and constrained motion. During the free motion phase (0-0.5 s), the object is simultaneously rotated and translated to the environment (see top plots of Figure 3.6;  $\vartheta_{oc}$  is a rotation about  $y_w$ , and  $\chi_{oc,z}$  is a translation in  $z_w$  of Figure 3.5) and compressed with a desired internal force of 5 N (see the top plot in Figure 3.7). At  $t = 0.5$  s the object makes contact with

the environment, which is located at position  $z_{env} = 0.4$  m, and characterized by the stiffness  $s_{env} = 1 \cdot 10^4$  N/m and damping constant  $b_{env} = 1$  Ns/m. During the constrained motion (0.5-1 s), an external force of 5 N is commanded (second plot of Figure 3.7). The motion control gains are selected as  $K_{pi} = 50^2 I_6 = 2500 I_6$  and  $K_{vi} = 2 \times 1 \times 50 I_6 = 100 I_6$  to obtain a critically damped response with a natural frequency of 50 [rad/s]. The gains of the internal impedance controllers are  $S_{i0} = 100 I_6$  and  $B_{i0} = I_6$  and the gains of the external impedance controller are  $D_o = 0.1 I_6$ ,  $B_o - \Sigma B_{env} = 2 \times 0.1 \times 1 \times 10\pi I_6 = 6.28 I_6$  and  $S_o - \Sigma S_{env} = 0.1 \times (10\pi)^2 I_6 = 98.70 I_6$ . Note that due to the structure of  $M_i$ , the matrices  $D_i$ ,  $B_i$  and  $S_i$  have nonzero coupling matrices. The internal impedance controller gains are selected to ensure a critically damped response assuming that  $M_i$  in (3.133) is slowly varying in time. The external impedance controller gains are selected to obtain a critically damped contact force response between the environment and the object.

The motion errors between the commanded and the actual object trajectories,  $\Delta\phi_{oc,a} = \phi_{oc} - \phi_o$  and  $\Delta\chi_{oc,a} = \chi_{oc} - \chi_o$ , are shown in bottom plots of Figure 3.6, and they converge to zero. In bottom plots of Figure 3.7, the internal force  $\Delta f_I$  and moment  $\Delta\mu_I$  errors are shown. These errors also converge to zero, thus desired compression of the object is achieved. The small transients at  $t = 0.5$  s are due to the damping components in (3.120) and (3.121): impact of the object with the environment at nonzero velocity results in a discontinuous change of  $h_{ext}$ . The commanded and actual external force between object and environment are shown in the second plot of Figure 3.7. After contact with the environment is made, the commanded contact force of 5 N is obtained. Note that the contact dynamics is shaped by tuning the impedance parameters in (3.112).

### 3.4.2 Non-fixed grasp

The modelling approach presented in Section 3.2.2 is investigated in a planar case where two 2 d.o.f. manipulators suspended from a ceiling grasp a disk shaped object. Each manipulator is controlled using the following PD plus gravity compensation controller,

$$\tau_i = K_{pi} (q_{ref_i} - q_i) + K_{di} (\dot{q}_{ref_i} - \dot{q}_i) + g_i (q_i) \quad (3.136)$$

where  $i \in \{1, 3\}$  is the index for the corresponding manipulator,  $q_{ref_i}$  is the reference joint angle,  $q_i$  is the actual joint angle and  $g_i (q_i)$  is the gravity torque,  $K_{pi}$  and  $K_{di}$  are the PD controller gains respectively. The following simulation is done to show the transition between rolling and sliding contacts. A perfectly inelastic collision is assumed, thus the coefficient of restitution is zero both in normal and tangential directions (i.e.  $e_{N_i} = 0$  and  $e_{T_i} = 0$  in (3.38)). A constant time step

size of  $\Delta t = 4 \cdot 10^{-5}$  seconds have been used during the simulations. Initially the disk shaped object starts from the contact phase and a step reference has been applied to the second link of the first manipulator. The reference and actual robot motions are displayed in Figure 3.8. It can be observed from Figure 3.8 that the actual robot joint angles reach constant values at the end of the simulation, even though tracking is not achieved. The object position in  $x$  and  $y$  coordinates and its orientation  $\phi$  are shown in Figure 3.9. It can be observed from Figure 3.9 that the object coordinates also reach constant values at the end of the simulation, and since no reference object trajectory is defined tracking is out of question. The normal and tangential contact velocities for both contact points are presented in Figure 3.10. The normal and tangential contact impulses for both contact points are presented in Figure 3.11. When Figures 3.10 and 3.11 are compared it can be realized that when the tangential component of the relative velocity is zero, the magnitude of the tangential impulse  $\Lambda_T$  is less than  $\mu \cdot \Lambda_N$ , thus the contact is rolling (remember that only one friction coefficient is modeled here, not two different coefficients such as static and kinetic). Moreover, when the tangential contact velocity is different than zero, then the magnitude of the tangential impulse  $\Lambda_T$  equals to  $\mu \cdot \Lambda_N$ . In each case the normal contact velocity is zero (or nearly zero since time-stepping algorithm terminates at a predefined tolerance, which is  $10^{-9}$  in all the simulation results) since contact with the object is maintained. The results for the simulations which involve transition from non-contact to contact phase are given in Appendix F. The effect of bouncing is highlighted in these results, since the collisions are modelled to be elastic.

### 3.5 Concluding remarks

Cooperative manipulators are modelled in two different cases, fixed and non-fixed grasps. A cascade control algorithm is introduced for the case of fixed grasps. With the proposed control algorithm for cooperative manipulation, the motion, internal and external forces of the object can be controlled. Using impedance relationships, a commanded object trajectory is converted into reference trajectories for the motion controllers of the manipulators such that the desired internal and contact forces can be achieved. In contrast to previously published results, criteria for each controller are determined to guarantee asymptotically stable behavior of the cooperative manipulator system. Guidelines are presented for the internal impedance relationships to compute the control parameters. As a result, all control parameters can be tuned intuitively. The implementation of the control algorithm is illustrated with simulations. The simulations done for the non-fixed grasp case show that the Lagrangian complementarity framework is a suitable approach to represent friction and impacts between the manipulators and the object.



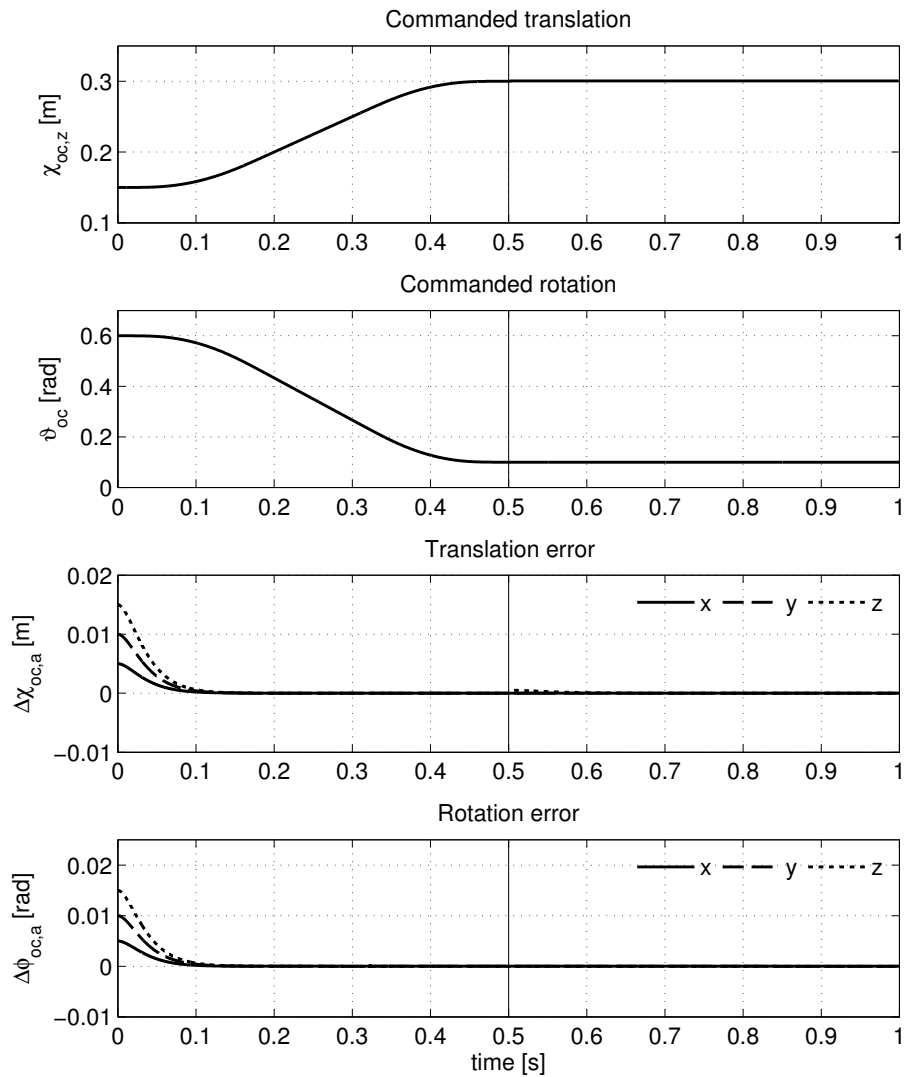


**Figure 3.6** Object position and orientation. Top two plots: commanded trajectories. Bottom two plots: motion errors. The solid vertical lines at  $t = 0.5$  s indicate the time of contact with the environment.

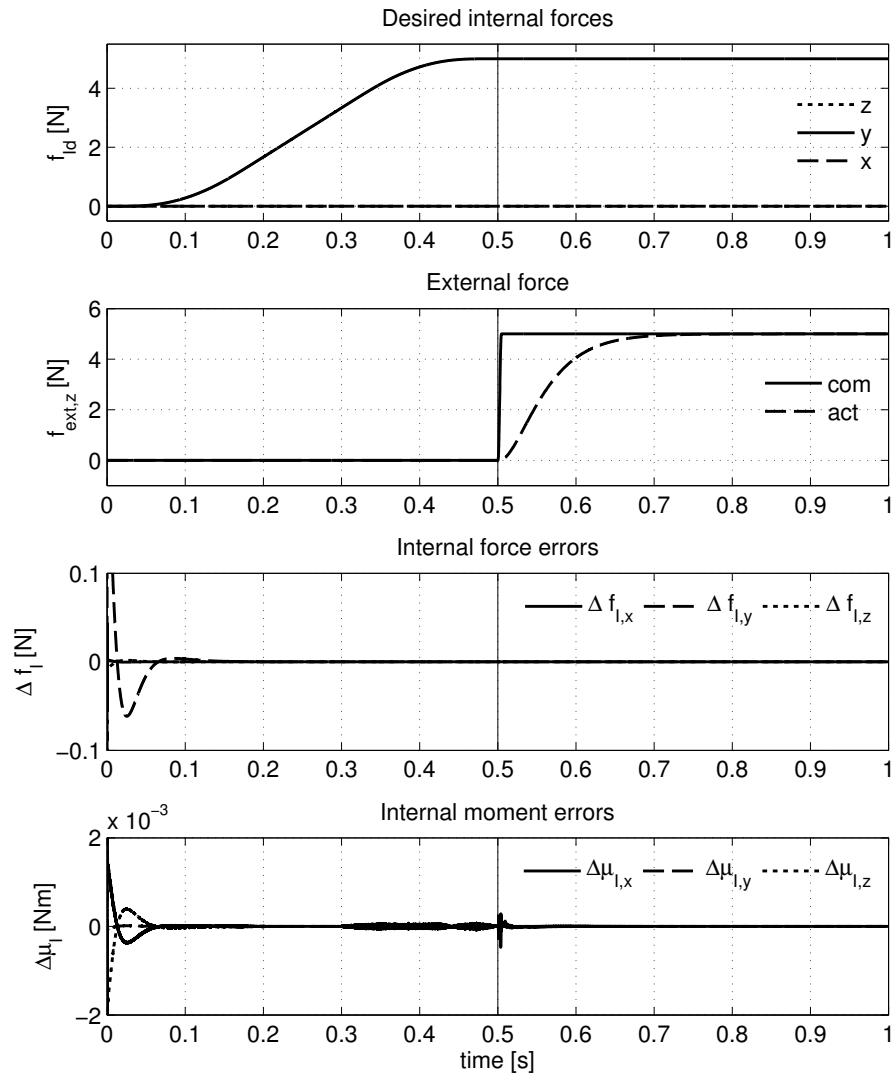


**Figure 3.7** Object internal and external forces. Top two plots: desired internal and external forces. Bottom two plots: internal force and moment errors. The solid vertical lines at  $t = 0.5$  s indicate the time of contact with the environment.

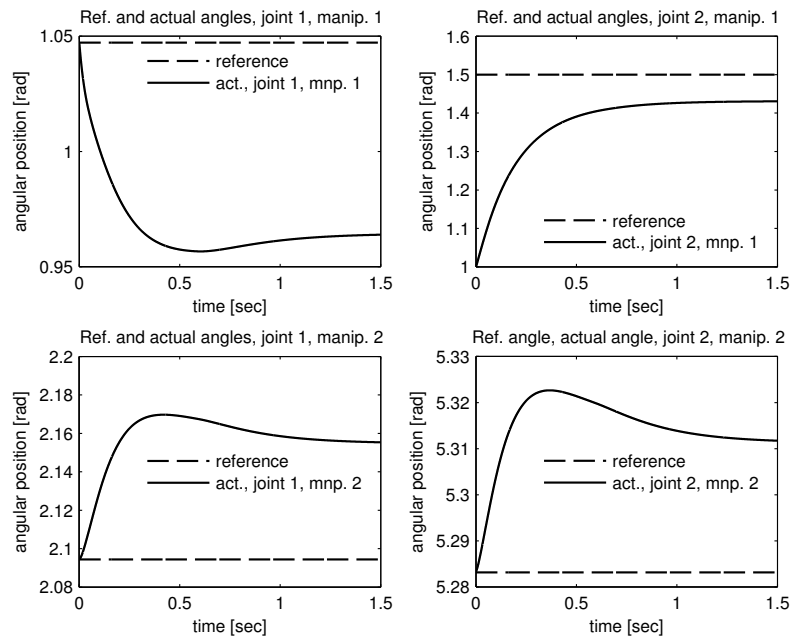


**Figure 3.8** Reference and actual robot motions

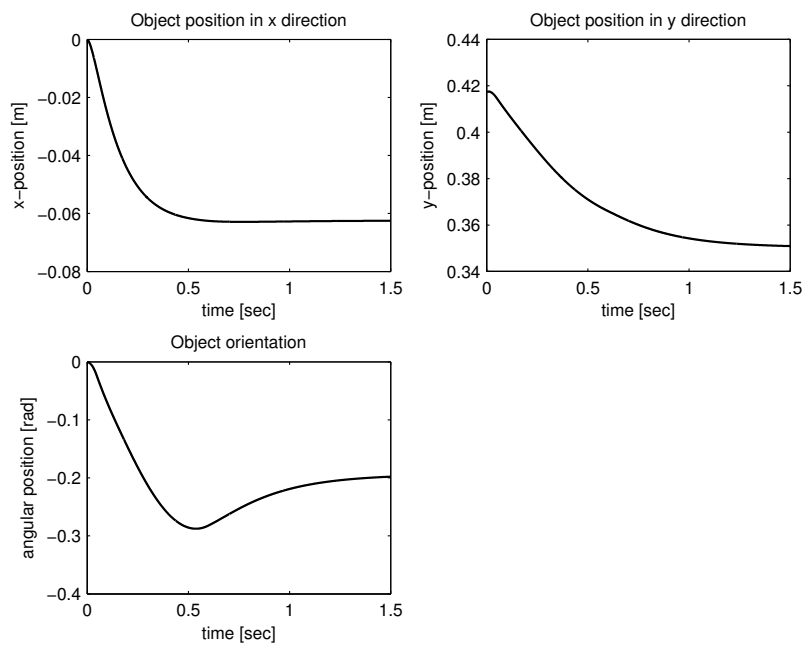


**Figure 3.9** Object position and orientation

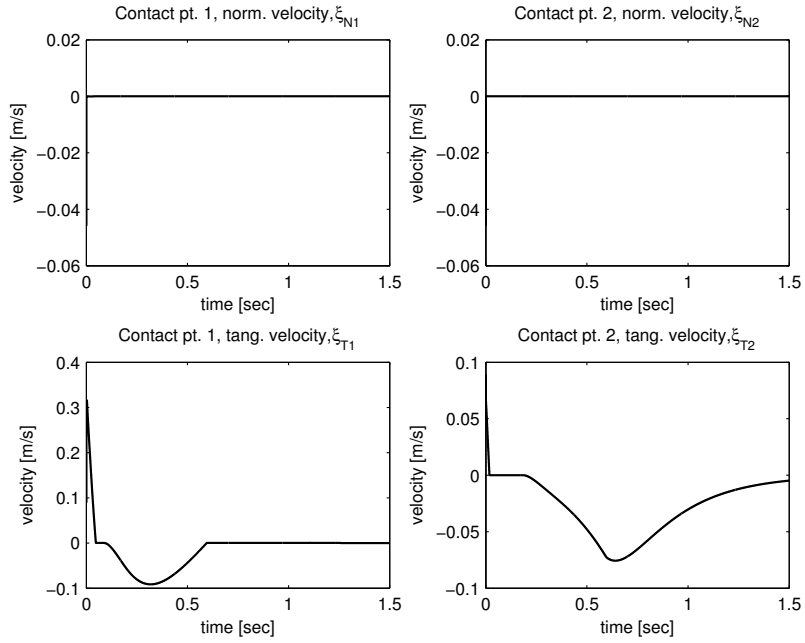


Figure 3.10 Normal and tangential contact velocities

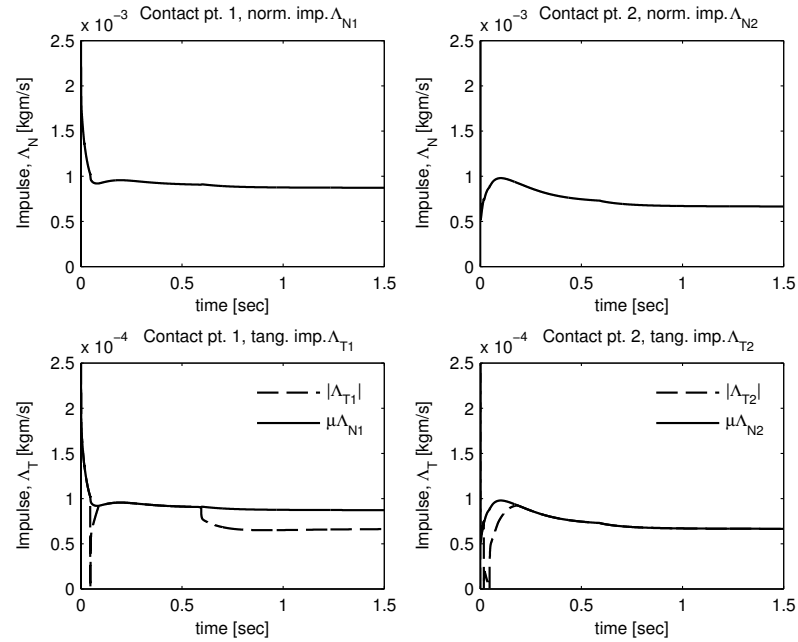


Figure 3.11 Normal and tangential contact impulses

# Chapter 4

## Time-delay compensation using Internal Model Principle and Control Together<sup>1</sup>

**Abstract** Teleoperated systems may be subject to destabilizing and performance degrading effects due to time delays. An appealing remedy for these effects is the application of the Internal Model Principle And Control Together (IMPACT) structure to the position error based bilateral teleoperation. The IMPACT algorithm proposed in this chapter allows time-delay compensation and rejection of disturbances from a known class that act at the output of the slave manipulator. Simulation and experimental results illustrate the effectiveness of the algorithm.

### 4.1 Introduction

Teleoperated systems have been a popular research subject in the robotics community for several decades. They are utilized in applications that take place in hazardous environments such as nuclear power plants for nuclear waste disposal, in hospitals to perform minimally invasive surgery, in space to perform repair of orbital modules, e.g. [67, 107]. The teleoperated tasks are carried out by a slave manipulator located at a remote environment. The slave receives commands sent by a human operator through a communication channel. Depending on the direction of information flow between the master and the slave, a teleoperation scheme can either be unilateral or bilateral. A unilateral teleoperation architecture can be considered as a cascaded system, where only operator commands are sent to the slave to be followed. In the case of bilateral teleoperations, the sensor data from the slave is also sent back to the operator through the same or a different commu-

---

<sup>1</sup>Parts of this chapter have been published in [43, 44]

nication channel, thus forming an internal closed-loop. The control problem in this case is more challenging due to the fact that the master and slave manipulators are coupled by a control algorithm implemented in the software.

An important issue that complicates the design of control algorithms for bilateral teleoperated systems is the time delays in the communication channel. Long distances or communication media such as the Internet can lead to time-delayed responses of the slave manipulator to the commands sent by the operator. Furthermore, the sensor data sent from the slave to the master can also be delayed, which can lead to delayed corrective actions of the operator. The time delays can hamper the performance of teleoperations or even destabilize the complete system. One of the early studies on the performance of telerobotic systems was conducted by Sheridan and Farrell [129]. They found out that whenever the communication loop features time-delays, the operator adopts a move and wait strategy from which it can be deduced that the task completion time is linear with respect to the induced time-delay in the loop. A comparative study on teleoperation control schemes in the presence of time delays is performed by Arcara et. al. [8]. That comparison considers five different aspects: stability as a function of time delay, perceived inertia and damping in free motion, position tracking performance, perceived stiffness in the case of interaction with a structured environment, and position drift between master and slave manipulators.

Among the available approaches, a possible remedy for time-delays is the use of Smith predictors in the control scheme. The main purpose of a Smith predictor is to render the control system virtually free from time delays. An overview of Smith predictor based control architectures for time-delayed teleoperations is given in [134]. There, a force-position type predictive control architecture is proposed which combines two neural networks to online estimate and map the slave and environment dynamics at the master side. A nonlinear extension of the Smith predictor is developed by Wong et. al. in [161]. In [82], a time-delay compensation method is applied to control systems with nonlinear dynamics and process dead-time. Normay-Rico et. al. give a broad review of dead-time compensators in [108], where they analyze the basic Smith predictor and propose design of suitable dead-time compensators for unstable systems. Scattering (or wave variables) is another common technique which aims to passify the communication channel. In [97], Miyoshi et. al. modified the approach by introducing wave filters in the scattering variables, designed by  $H_\infty$  method.

It is pointed out by Matijević et. al., in [96] that Smith predictor type control architectures are characterized by limited robustness and disturbance rejection capabilities. A new control architecture for systems with Smith predictors is proposed by Stojić et. al. to improve their robustness and performance of disturbance rejection [137]. This architecture is based on the internal model principle and con-

trol together (IMPACT) approach. This approach was introduced in [146] as a way to combine the internal model principle (IMP) and internal model control (IMC). IMP is used to cope with the disturbances that affect the plant, and is also known as the absorption principle [162]. The absorption principle considers including a model of or an estimator for the disturbance within the controller structure. The effect of immeasurable external disturbances can be suppressed or even eliminated by using IMP. The IMC structure is shown in Figure 4.1, where  $\tilde{P}$  refers to a model of the true process  $P$ , and  $Q$  refers to the IMC controller.

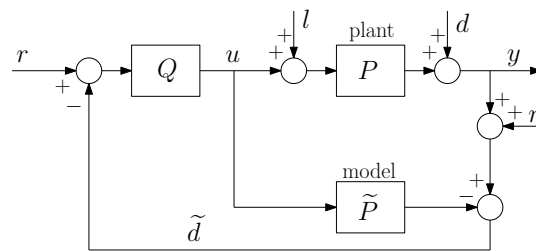


**Figure 4.1** Internal Model Control (IMC) structure.

IMC includes a nominal model of the plant in the controller structure in order to incorporate modeling uncertainty into the control system [100, 133]. The Smith predictor and IMC structures are equivalent to each other [24]. The advantage of IMPACT structure over IMC is that it provides a systematic and intuitive way to separate the problems of predictor design and the disturbance rejection [146].

There exist different types of control architectures in bilateral teleoperation systems. They can be categorized based on the exchanged sensory information between the master and slave manipulators. Among them, the most common are position error, kinesthetic force feedback and 4-channel control architectures.

In this chapter, we address time-delay compensation and disturbance rejection in position error (PERR) based bilateral teleoperation. We employ the benefits of the IMPACT structure for this purpose and apply it to the position error based bilateral teleoperation problem. These are robustness against uncertainties and external disturbances. The master and slave manipulators are modelled by means of a feedback connection of a linear dynamical system and a nonlinear element. By doing so, incorporating nonlinear compensators into the local feedback controllers is possible. This allows us to deal with some practical issues such as friction or gravity compensation. Furthermore, a pragmatic rational is applied in the design of local controllers which is based on frequency response function (FRF) measurements and a pole placement method. Keeping the number of controller parameters small leads to an easy and straightforward way of tuning the controller. The robust stability of the designed controller is analyzed by means of the Nyquist

criterion. The effectiveness of the approach is demonstrated through extensive experimentation. The results presented in this chapter are based on the publication [44]. A preliminary version of this work appears in [43].

This chapter is organized as follows. A general introduction to the classification of bilateral teleoperation architectures is presented in Section 4.2. In Section 4.3, a time-delay compensation scheme for the PERR based bilateral teleoperations employing the IMPACT structure to increase robustness, disturbance rejection, and trajectory tracking performance is presented. Numerical experiments illustrating the disturbance compensation capabilities of the approach are presented in Section 4.4. In Section 4.5, the experimental setup is introduced and the approach is validated by experiments. Conclusions and final remarks are given in Section 4.6.

## 4.2 Bilateral teleoperation architectures

The information flow within and between the master and slave sides can be represented as in Figure 4.2 [77]. The vectors  $\vec{X}_i$  for  $i = \{m, s\}$ , respectively for the

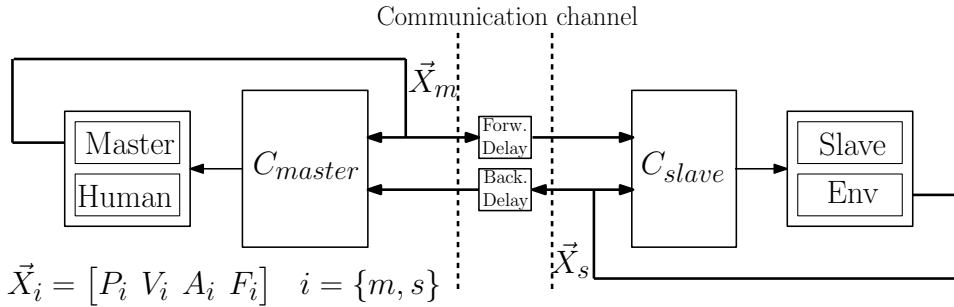


**Figure 4.2** A teleoperated system from the perspective of information flow.

master and the slave consist of all the possible sensor information, namely:

- $P_i$  : Position information,
- $V_i$  : Velocity information,
- $A_i$  : Acceleration information,
- $F_i$  : Force information.

Leaving aside setup specific control actions (e.g. gravity/friction compensation) or filtering of sensor data, a control architecture can be described systematically by the following notation.

### Controller notation

- $x_b$  : Variable only used in a local feedback loop,
- $X$  : Variable sent to the other device,



$X_b$  : Variable used in a local feedback loop and sent to the other device,  
 $\hat{X}$  : Estimated/observed variable.

All the basic control architectures in the literature can be presented as shown in Figure 4.3 using a combination of ports from  $a$  to  $h$ . Here, the term "basic" means that no signal is estimated or advanced methods such as adaptive control are used. This figure is a simplification of the previously introduced general no-

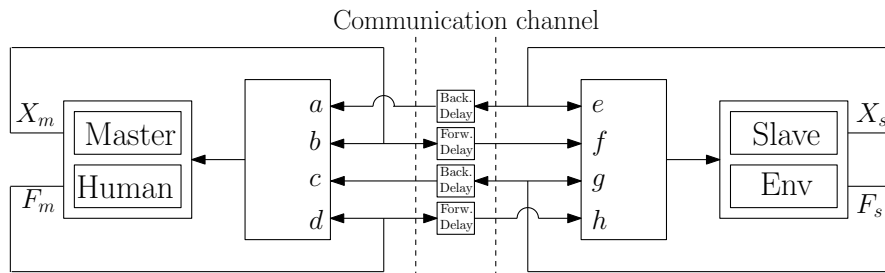


**Figure 4.3** Channel definition for a basic architecture.

tation. Since in many practical situations position is measured, it is used instead of velocity or acceleration in this figure. There are  $2^8 - 1 = 255$  possible combinations of architectures in total, since any of the eight ports can be enabled or disabled. This means each side (master/slave) can send or not the position and/or force to the other and at each side it is possible to use or not the local position and/or force feedback. By imposing several constraints, regarding whether the architectures are meaningful and satisfy the bilateral constraint, this number can be reduced to 21. Here, the bilateral constraint means that a possible architecture must at least send information from the master to the slave, and vice versa. In the next section, a few of the common basic architectures that exist in the literature are discussed together with their respective advantages and disadvantages. Before this discussion, the term "transparency" is described. Transparency describes how close the remote operation and interaction of the slave device with the remote environment are recreated to the operator.

#### 4.2.1 Position error, ( $P_b - P_b$ )

Position error, ( $P_b - P_b$ ) teleoperation architecture only sends position information between master and slave, and uses the position error as reference trajectory in both master and slave. In [5], it is concluded that its main advantage is that no force sensors are required. However, it is unable to offer light maneuverability and large force reflection at the same time. Performance can be improved by increasing the gains of the controller. Furthermore, in [8] it is shown that in the absence of time delays, by choosing a specific optimal set of gains, the inertia and damping

perceived by operator are doubled with respect to the inertia and damping of master, a low tracking error, an almost correct stiffness perception and negligible position drift can be achieved. Although time delays can still cause instability, the maximum amount of this delay can analytically be derived. The scheme of this architecture can be obtained by enabling the ports  $\{a, b, e, f\}$  and disabling the ports  $\{c, d, g, h\}$  in Figure 4.3. In Section 4.3, this control architecture's scheme is reorganized such that the design of the IMPACT structure can be explained.

#### 4.2.2 Kinesthetic force feedback, (P- $p_b$ F)

Kinesthetic force feedback,  $(P - p_b F)$  teleoperation architecture requires position sensors at both the master and the slave side and also requires a force sensor at the slave side. The force sensor at the slave side makes it possible to use an inverse dynamics based impedance controller to decrease the apparent inertia of the slave robot, therefore it increases the force reflection ratio. Although this is a widely used control architecture, many researchers report stability issues, unless the force feedback gain is attenuated [5, 83].

#### 4.2.3 Four channel, (P $_b$ F $_b$ -P $_b$ F $_b$ )

Lawrence [83] concludes that for perfect transparency, the use of all four communication channels is required. The system block diagram is illustrated in Figure 4.4. Lawrence called this system the "Transparency Optimized Controller". Hashtrudi-Zaad and Salcudean [61] included local force feedback at the master and the slave sides, to improve system performance and stability. The 4-channel architecture can provide perfect transparency in theory, but stability and performance can be compromised by time delays and human and environmental uncertainties. Although in the absence of time delays the 4-channel architecture theoretically can achieve perfect transparency, recent literature has shown results of obtaining (almost) perfect transparency using 3-channel and even 2-channel architectures.

### 4.3 Internal Model Principle and Control Together (IMPACT)

Before detailing the derivation of the IMPACT algorithm for the position error based teleoperation architecture, its block diagram is reorganized. Furthermore, the modelling of the master and slave devices is introduced and the compensation of some typical nonlinear effects such as friction is presented. In the PERR based teleoperation scheme shown in Figure 4.5, the slave manipulator is required to follow the commands sent from the master device handled by the operator [107].  $Q_m(s)$  denotes the position of the master,  $Q_s(s)$  the position of the slave, and  $T_d$

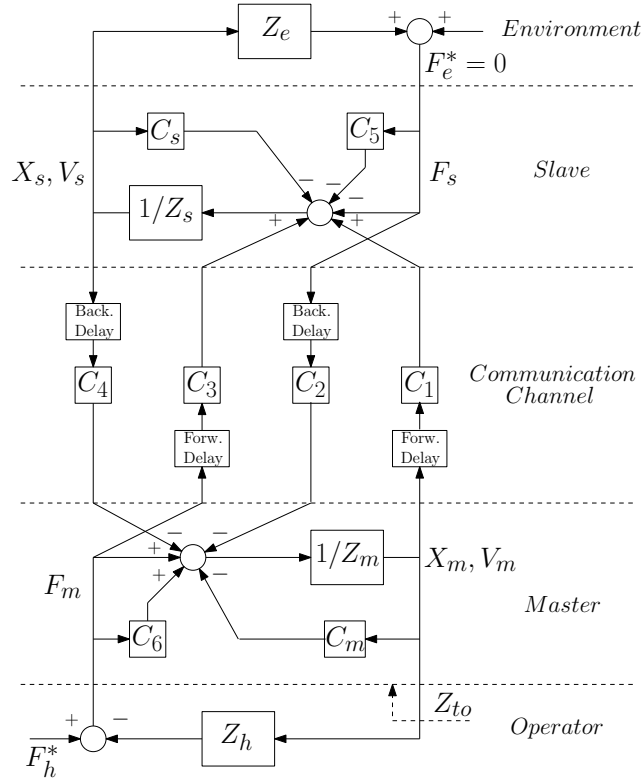


**Figure 4.4** 4-Channel control architecture by Lawrence [83], updated by Hashtrudi-Zaad and Salcudean [61].

represents the time delay in the communication channel. Only position information is exchanged between the master and slave manipulators as presented in Figure 4.5. In Figure 4.6,  $G_m(s)$  and  $G_s(s)$  denote the transfer functions of the master and slave manipulators, respectively.  $\varphi_m(\cdot)$ ,  $\varphi_s(\cdot)$  are the nonlinear terms such as friction or cogging torques/forces and  $\hat{\varphi}_m(\cdot)$ ,  $\hat{\varphi}_s(\cdot)$  are the suitable nonlinear compensation torques/forces for the master and slave manipulators, respectively. The master and slave controllers are given by

$$U_m(s) = K_{m,1}(s)(Q_{ref}(s) - Q_m(s)) + K_{m,2}(s)(Q_s(s)e^{-T_d s} - Q_m(s)), \quad (4.1)$$

$$U_s(s) = K_s(s)(Q_m(s)e^{-T_d s} - Q_s(s)), \quad (4.2)$$

where  $K_{m,2}(s)$  and  $K_s(s)$  are local controllers for the master and slave manipulators, respectively.  $K_{m,1}(s)$  can either represent the human dynamics or another local controller which can replace the human when the task is supposed to be performed automatically. The master device is commanded to track the position reference trajectory  $Q_{ref}(s)$  in the latter case.

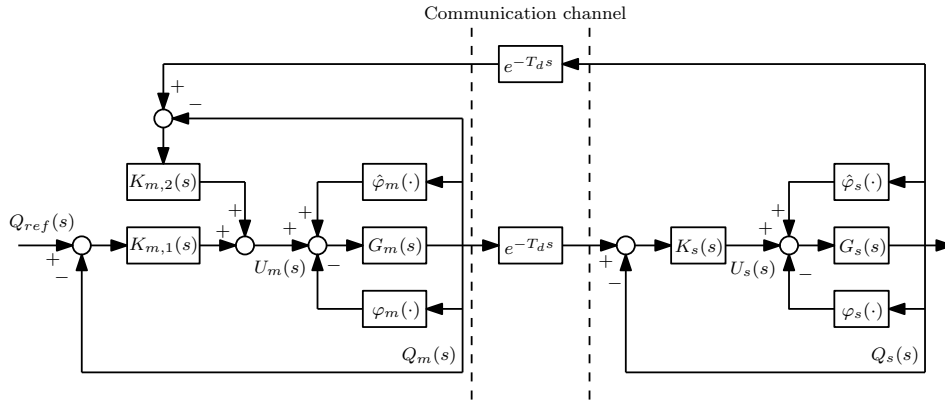


Figure 4.5 Position error based teleoperation scheme redrawn.

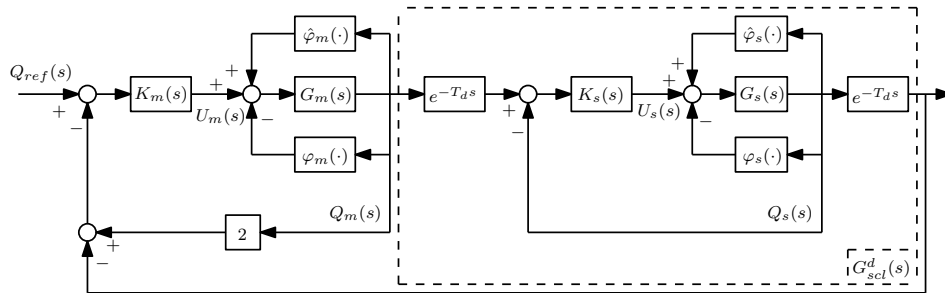


Figure 4.6 Position error based teleoperation scheme reorganized.

**Remark 4.1.** In the remainder of this chapter, it is assumed that a local controller executes the required task instead of the human operator, therefore,  $K_{m,1}(s)$  is considered as a local controller. It should be mentioned that, in (4.1) using two different control laws for the two different kind of errors,  $Q_{ref}(s) - Q_m(s)$  and  $Q_s(s)e^{-T_d s} - Q_m(s)$ , provides extra degrees of freedom for tuning and higher performance, eventually. Keeping that in mind, we should emphasize that, for the sake of easy tuning, the local controllers  $K_{m,1}(s)$  and  $K_{m,2}(s)$  are selected identical to each other (i.e.  $K_{m,1}(s) = K_{m,2}(s) = K_m(s)$ ). Therefore, the design and stability analysis of the teleoperated system is performed for the case  $K_{m,1}(s) = K_{m,2}(s) = K_m(s)$ .

In this chapter, single degree-of-freedom manipulators are considered at the master and slave sides. Furthermore, the nonlinear terms which we are interested in, are related to the friction torques/forces. The dynamics of these manipulators in time

domain, that apply as they conduct free motions, are given by

$$J_m \ddot{q}_m + \tau_{f,m}(\dot{q}_m) + C_m q_m = \tau_m, \quad (4.3)$$

$$J_s \ddot{q}_s + \tau_{f,s}(\dot{q}_s) + C_s q_s = \tau_s, \quad (4.4)$$

where  $J_m$ ,  $\tau_{f,m}(\dot{q}_m)$ ,  $C_m$  and  $J_s$ ,  $\tau_{f,s}(\dot{q}_s)$ ,  $C_s$  are the masses (for translational dynamics)/mass moments of inertia (for rotational dynamics), the friction forces/torques and the stiffness coefficient of master and slave manipulators, respectively, while  $\tau_m$  and  $\tau_s$  are the input forces/torques. Appropriate parameters and their respective units are selected depending on whether the dynamics is translational or rotational.

There are many different models in the literature to represent the friction phenomena that exist in robotic systems [22]. The complexity of these models depends on the velocity regime at which the system operates. In this chapter, we concentrate on a relatively simple friction model which is comprised of Coulomb friction and viscous friction terms:

$$\tau_{f,m}(\dot{q}_m) = \tau_{c,m} \text{sgn}(\dot{q}_m) + B_m \dot{q}_m, \quad (4.5)$$

$$\tau_{f,s}(\dot{q}_s) = \tau_{c,s} \text{sgn}(\dot{q}_s) + B_s \dot{q}_s, \quad (4.6)$$

where  $\text{sgn}(\cdot)$  is the signum function and  $\tau_{c,m}$ ,  $B_m$  and  $\tau_{c,s}$ ,  $B_s$  are the Coulomb friction and viscous friction coefficients of the master and slave manipulators, respectively. The effect of Coulomb friction can be compensated by using Coulomb friction compensation, if the inputs to the master and slave robots are taken as,

$$\tau_m = \hat{\tau}_{c,m} \text{sgn}(\dot{q}_m) + u_m, \quad (4.7)$$

$$\tau_s = \hat{\tau}_{c,s} \text{sgn}(\dot{q}_s) + u_s, \quad (4.8)$$

where  $\hat{\tau}_{c,m}$ ,  $\hat{\tau}_{c,s}$  are Coulomb friction compensation coefficients and  $u_m$ ,  $u_s$  are the new control inputs. These new control inputs can be used to design suitable control laws such as (4.1) and (4.2). From (4.3), (4.4), (4.5) and (4.6), we can determine the transfer functions of two manipulators as

$$G_m(s) = \frac{1}{J_m s^2 + B_m s + C_m}, \quad (4.9)$$

$$G_s(s) = \frac{1}{J_s s^2 + B_s s + C_s}. \quad (4.10)$$

In the following, we assume that the Coulomb friction is exactly compensated.

### 4.3.1 Control structure

This section describes an IMPACT structure which is suitable for the considered PERR teleoperation problem. The block diagram of the IMPACT structure is

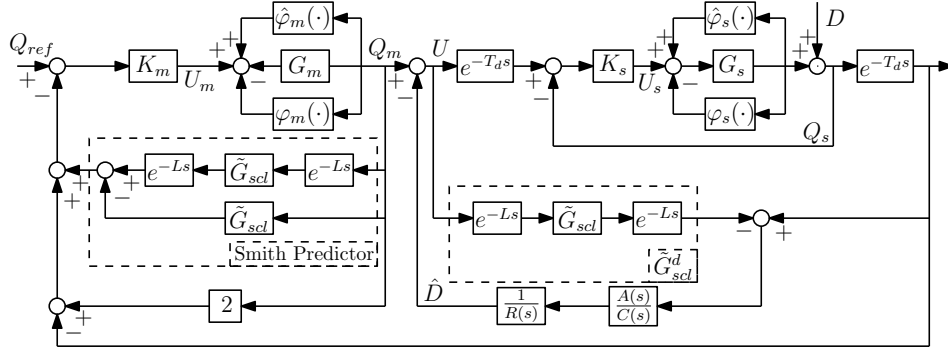


**Figure 4.7** IMPACT structure for PERR based teleoperation system.

shown in Figure 4.7. Here,  $D$  denotes a disturbance at the slave side of the telemanipulation system, such as undesired vibrations acting at the output of the slave manipulator. The structure shown in Figure 4.7 implements a Smith predictor at the master side, while at the slave side  $\tilde{G}_{scld}^d$  is the internal nominal plant model and  $A(s)/C(s)$  is the transfer function representing an internal model of the disturbances. The difference between the outputs of the actual and nominal plants are filtered by the transfer function  $(1/R(s))(A(s)/C(s))$ , where  $R(s)$  is a transfer function in the disturbance estimator whose design will be introduced in the next section. The resulting signal  $\hat{D}$  is the disturbance estimator. The nominal plant model is given by

$$\tilde{G}_{scld}^d(s) = \frac{K_s(s)\tilde{G}_s(s)}{1 + K_s(s)\tilde{G}_s(s)} e^{-2Ls}, \quad (4.11)$$

where  $\tilde{G}_s(s)$  is the nominal model of the slave manipulator and  $L$  is the nominal value of the time-delay  $T_d$  in a single direction of the communication channel. In our control design, the nominal value  $L$  is considered to be constant, known and same for both forward and backward directions; it can be determined by practical measurements, as an average of the actual time-delays. The influence of the perturbations on the nominal value of the time-delay,  $L$  is investigated via robustness analysis. The actual plant is given by,

$$G_{scld}^d(s) = \frac{K_s(s)G_s(s)}{1 + K_s(s)G_s(s)} e^{-2T_d s}, \quad (4.12)$$

where  $G_s(s)$  represents the actual transfer function of the slave manipulator.

### 4.3.2 Controller design

This section presents the design of local s controllers for master and slave manipulators and describes a method for disturbance absorption. Following the rationale

given in [82], the local feedback controllers  $K_m(s)$  and  $K_s(s)$  for the master and slave manipulators, respectively, are designed based on the inverse plant model

$$K_m(s) = \frac{1}{W(s) - 1} \frac{1}{\tilde{G}_m(s)}, \quad (4.13)$$

$$K_s(s) = \frac{1}{W(s) - 1} \frac{1}{\tilde{G}_s(s)}, \quad (4.14)$$

where  $\tilde{G}_m(s)$  and  $\tilde{G}_s(s)$  are the nominal models of master and slave manipulators, respectively, and  $W(s)$  is the characteristic polynomial describing the desired location of closed-loop poles for the local feedback loops at master and slave sides

$$W(s) = (\epsilon s + 1)^r. \quad (4.15)$$

Here,  $\epsilon > 0$  and  $r$  is the relative order of the nominal models of the master and slave manipulators. Polynomial (4.15) is selected such as to keep the number of tuning parameters small. We assume that the dynamics of the master and slave manipulators described by (4.9) and (4.10) are known and given by

$$\tilde{G}_m(s) = \frac{1}{\tilde{J}_m s^2 + \tilde{B}_m s + \tilde{C}_m}, \quad (4.16)$$

$$\tilde{G}_s(s) = \frac{1}{\tilde{J}_s s^2 + \tilde{B}_s s + \tilde{C}_s}, \quad (4.17)$$

where  $\tilde{J}_m$ ,  $\tilde{J}_s$ ,  $\tilde{B}_m$ ,  $\tilde{B}_s$ ,  $\tilde{C}_m$  and  $\tilde{C}_s$  are the nominal model parameters that are determined, for instance, using system identification. For the manipulator dynamics of the second order,  $r$  equals to 2 in (4.15).

**Remark 4.2.** *The local control laws (4.13) and (4.14) may or may not have integral action depending on the nominal master/slave manipulator models (4.16)-(4.17). For example, when the nominal models do not have stiffness terms (i.e.  $\tilde{C}_m = \tilde{C}_s = 0$ ), the local control laws can be written as,*

$$K_m(s) = \frac{\tilde{J}_m s + \tilde{B}_m}{\epsilon^2 s + 2\epsilon}, \quad K_s(s) = \frac{\tilde{J}_s s + \tilde{B}_s}{\epsilon^2 s + 2\epsilon} \quad (4.18)$$

*which are of lead or lag type depending on the location of their poles/zeros. In the case when the stiffness terms of the nominal models are nonzero (i.e.  $\tilde{C}_m \neq 0$  and  $\tilde{C}_s \neq 0$ ), we obtain the following local control laws,*

$$K_m(s) = \frac{\tilde{J}_m s^2 + \tilde{B}_m s + \tilde{C}_m}{s(\epsilon^2 s + 2\epsilon)}, \quad K_s(s) = \frac{\tilde{J}_s s^2 + \tilde{B}_s s + \tilde{C}_s}{s(\epsilon^2 s + 2\epsilon)} \quad (4.19)$$

*that have an integral action in their structure.*

In addition to the feedback controllers (4.13) and (4.14), the tracking performance can be improved by adding the feedforward terms related to the velocity and acceleration profiles of the reference trajectory for the master manipulator. From (4.11), (4.14) and (4.15), the nominal plant model is given by

$$\tilde{G}_{scl}^d(s) = \frac{1}{(\epsilon s + 1)^2} e^{-2Ls}. \quad (4.20)$$

Referring to Figure 4.7, we can determine the closed-loop transfer functions, based on the nominal plant between the inputs  $Q_{ref}^d(s)$  and  $D(s)$  and the output  $Q_s(s)$ :

$$N(s) = \frac{Q_s(s)}{Q_{ref}^d(s)} = \frac{K_m(s)\tilde{G}_m(s)K_s(s)\tilde{G}_s(s)}{(1 + K_s(s)\tilde{G}_s(s))(1 + K_m(s)\tilde{G}_m(s)) + K_m(s)\tilde{G}_m(s)}, \quad (4.21)$$

$$\frac{Q_s(s)}{D(s)} = (1 + N(s)e^{-2Ls}) \left( \frac{1}{1 + K_s(s)\tilde{G}_s(s)} \right) \left( 1 - \frac{A(s)}{R(s)C(s)} \frac{K_s(s)\tilde{G}_s(s)e^{-2Ls}}{1 + K_s(s)\tilde{G}_s(s)} \right), \quad (4.22)$$

where  $Q_{ref}^d(s) = Q_{ref}(s)e^{-Ls}$  represents the delayed reference signal. When (4.13)-(4.15) and (4.16)-(4.17) are substituted into (4.21) and (4.22), we obtain:

$$N(s) = \frac{Q_s(s)}{Q_{ref}^d(s)} = \frac{1}{\epsilon^4 s^4 + 4\epsilon^3 s^3 + 7\epsilon^2 s^2 + 6\epsilon s + 1}, \quad (4.23)$$

$$\frac{Q_s(s)}{D(s)} = (1 + N(s)e^{-2Ls}) \left( \frac{\epsilon(\epsilon s + 2)}{(\epsilon s + 1)^2} \right) \left( 1 - \frac{A(s)}{R(s)C(s)} \frac{e^{-2Ls}}{(\epsilon s + 1)^2} \right). \quad (4.24)$$

The stability of the closed-loop system described by the transfer function (4.23) can be evaluated using the Routh's stability criterion [51]. It can be shown that the elements in the first column of the Routh's table are positive, since by definition,  $\epsilon > 0$ . According to the Routh criterion, this implies that the poles of the closed-loop are all in the left half of the complex plane.

By applying the final value theorem to (4.24), it can be shown that the effect of disturbance  $D$  on the steady-state motion of the slave manipulator diminishes if

$$\lim_{s \rightarrow 0} s \left( (1 + N(s)e^{-2Ls}) s \left( \frac{\epsilon(\epsilon s + 2)}{(\epsilon s + 1)^2} \right) \left( 1 - \frac{A(s)}{R(s)C(s)} \frac{e^{-2Ls}}{(\epsilon s + 1)^2} \right) D(s) \right) = 0. \quad (4.25)$$

Since

$$\lim_{s \rightarrow 0} (1 + N(s)e^{-2Ls}) = 2, \quad \lim_{s \rightarrow 0} \left( \frac{\epsilon(\epsilon s + 2)}{(\epsilon s + 1)^2} \right) = 2\epsilon, \quad (4.26)$$



to have (4.25) achieved, the following should hold:

$$\lim_{s \rightarrow 0} s^2 \left( 1 - \frac{A(s)}{R(s)C(s)} \frac{e^{-2Ls}}{(\epsilon s + 1)^2} \right) D(s) = 0. \quad (4.27)$$

The polynomial  $A(s)$  can be selected as any stable polynomial. Here it is selected as

$$A(s) = (\epsilon s + 1)^2 A_0(s), \quad (4.28)$$

where  $A_0(s)$  is a disturbance absorption polynomial whose design is explained in detail in the remaining part of this subsection. To guarantee stability of the disturbance estimator, polynomials  $R(s)$  and  $C(s)$  should have stable zeros. A simple way to select  $R(s)$  and  $C(s)$ , which decreases the number adjustable parameters, is proposed in [137]:

$$R(s) = 1, \quad C(s) = (T_0 s + 1)^n, \quad (4.29)$$

where  $T_0$  is a time constant and  $n$  is an order of the filter. The design parameters  $T_0$  and  $n$  determine the speed of the disturbance absorption process. The disturbance is absorbed more quickly if lower values are selected for  $T_0$  and  $n$ . For the particular choice of (4.28) and (4.29), condition (4.27) can be rewritten as,

$$\lim_{s \rightarrow 0} s^2 (C(s) - A_0(s)e^{-2Ls}) D(s) = 0. \quad (4.30)$$

It can be realized from (4.30) that the absorption of a step disturbance (i.e.  $D(s) = 1/s$ ) can be achieved for any  $A_0(s)$  and  $C(s)$ . For a class of polynomial disturbances  $d(t) = \sum_{i=0}^m d_i t^i$ , after application of the L'Hôpital rule, we can uniquely determine the polynomial  $A_0(s)$  using the following expression,

$$\lim_{s \rightarrow 0} \frac{d^k}{ds^k} (C(s) - A_0(s)e^{-2Ls}) = 0, \quad 0 \leq k < m. \quad (4.31)$$

As an example, for a ramp disturbance (i.e.  $D(s) = 1/s^2$ ) by using (4.28), (4.31)

$$A_0(0) = 1, \quad \text{for } k = 0 \quad (4.32)$$

is obtained. In the case of a disturbance that can be represented as a second order function of time (i.e.  $d(t) = t^2/2$ , thus  $D(s) = 1/s^3$ ), we determine

$$A_0(0) = 1 \quad \text{for } k = 0, \quad (4.33)$$

$$A_0(s) = (nT_0 + 2L)s + A_0(0) \quad \text{for } k = 1. \quad (4.34)$$

For an arbitrary disturbance described by its Laplace transform  $D(s) = N_d(s)/D_d(s)$ , such as a sinusoid function (i.e.  $D(s) = 1/(s^2 + \omega^2)$  for  $d(t) = \sin \omega t$ ), the following condition is induced from (4.30),

$$C(s) - A_0(s)e^{-2Ls} = \Phi(s)B(s), \quad (4.35)$$

where  $\Phi(s)$  represents the absorption polynomial determined by  $\Phi(s) \equiv D_d(s)$  which is the denominator of Laplace transform of the disturbance. In order to solve equation (4.35) for  $A_0(s)$  which is used in the design of disturbance estimator, the exponential term  $e^{-2Ls}$  can be approximated by Taylor series as

$$e^{-2Ls} \cong \sum_{k=0}^N \frac{(-2Ls)^k}{k!}, \quad (4.36)$$

with  $N$  being the number of terms used in the approximation and then substituted into (4.35) which leads to the Diophantine equation given by

$$A_0(s) \sum_{k=0}^N \frac{(-2Ls)^k}{k!} + B(s) \Phi(s) = C(s). \quad (4.37)$$

Padé method could be another way to approximate the exponential term  $e^{-2Ls}$  in (4.35). The obtained relation does not have a unique solution in terms of  $A_0(s)$  (cf. [11]). A solution procedure for the Diophantine equation is given in [109]. The only constraint is due to causality, i.e.

$$\deg(A(s)) = 2 + \deg(A_0(s)) \leq \deg(C(s)). \quad (4.38)$$

The solution procedure roughly works as follow. First select  $C(s)$ ,  $N$  and the degree of the polynomials  $A_0(s)$  and  $B(s)$ , and then substitute the corresponding absorption polynomial  $\Phi(s)$  for the disturbance. After that, equation (4.37) can be solved for the polynomials  $A_0(s)$  and  $B(s)$ , by equating the coefficients of the terms of equal order on both sides.

### 4.3.3 Robustness analysis

Since the control design is based on nominal plant model  $\tilde{G}_{scl}^d(s)$ , it should be investigated how uncertainties in plant parameters and unmodeled dynamics influence stability and control performance of the considered teleoperated system. As the starting point of robustness analysis, we assume that real plant  $G_{scl}^d(s)$  belongs to the set  $\Pi$  of plants that deviate from nominal plant due to unmodelled dynamics and uncertainties and/or perturbations of plant parameters. Here, this deviation is represented by an additive uncertainty. Note that, multiplicative uncertainty could be used for the same purpose. In the following analysis, the frequency response functions are used therefore the variable  $s$  is replaced by  $j\omega$  where  $j$  is the complex variable. Mathematically, the set  $\Pi$  can be defined as follows

$$\Pi = \left\{ G_{scl}^d : \left| G_{scl}^d(j\omega) - \tilde{G}_{scl}^d(j\omega) \right| \leq \bar{l}_a(\omega), \quad \forall \omega \in \mathbb{R} \right\} \quad (4.39)$$

where  $\bar{l}_a(\omega)$  is the worst-case bound on the additive uncertainty. Thus, each member of this set satisfies:

$$G_{scl}^d(j\omega) = \tilde{G}_{scl}^d(j\omega) + l_a(j\omega), \quad (4.40)$$

where  $l_a(j\omega)$  is the additive uncertainty and  $|l_a(j\omega)| \leq \bar{l}_a(\omega)$ . According to [100], [11], in order to have all elements of the set  $\Pi$  stable, it is sufficient that,

$$|l_a(j\omega)| < \beta(\omega) \quad (4.41)$$

holds. Here,  $\beta(\omega)$  is given by

$$\beta(\omega) = \left| \frac{\tilde{G}_{scl}^d(j\omega)}{G_{cl,des}(j\omega)} \right| \left| \frac{G_{ff}(j\omega)}{G_{fb}(j\omega)} \right|, \quad (4.42)$$

where  $G_{cl,des}(j\omega)$  is the frequency response function of the desired closed-loop transfer function,  $G_{cl,des}(s)$  given by (4.23). In (4.42), the terms  $G_{ff}(j\omega)$  and  $G_{fb}(j\omega)$  are defined by

$$U(j\omega) = G_{ff}(j\omega)Q_{ref}(j\omega) - G_{fb}(j\omega)Q_s(j\omega), \quad (4.43)$$

with  $G_{ff}(j\omega)$  and  $G_{fb}(j\omega)$  being the frequency response of the transfer functions  $G_{ff}(s)$  and  $G_{fb}(s)$  representing the feedforward and feedback parts of the overall control structure in Figure 4.7, respectively (see [11] for more details). The robust stability condition (4.41) can be derived by rewriting the overall control structure in a more compact form and then by applying the Nyquist stability criterion. The frequency response of the transfer function of the overall control structure can be derived using (4.15), (4.28) and (4.29) after substituting  $s = j\omega$  as,

$$U(j\omega) = \frac{(\epsilon j\omega + 1)^2 C(j\omega)}{C(j\omega) - A_0(j\omega)e^{-2Lj\omega}} \left[ \frac{1}{(\epsilon j\omega + 1)^4 + \epsilon j\omega(\epsilon j\omega + 2) + e^{-2Lj\omega}} Q_{ref}(j\omega) \right. \\ \left. + \frac{C(j\omega) - A_0(j\omega) \left( (\epsilon j\omega + 1)^4 + \epsilon j\omega(\epsilon j\omega + 2) + e^{-2Lj\omega} \right)}{C(j\omega) \left( (\epsilon j\omega + 1)^4 + \epsilon j\omega(\epsilon j\omega + 2) + e^{-2Lj\omega} \right)} Q_s(j\omega) e^{-Lj\omega} \right]. \quad (4.44)$$

By using (4.15), (4.28) and (4.29), robust stability bound (4.42) is rewritten as

$$\beta(\omega) = \left| \frac{\Gamma(j\omega)}{(\epsilon j\omega + 1)^2} \right| \left| \frac{C(j\omega)}{C(j\omega) - A_0(j\omega)(\Gamma(j\omega) + e^{-2Lj\omega})} \right| \quad (4.45)$$

where  $\Gamma(j\omega) = (\epsilon j\omega + 1)^4 + \epsilon j\omega(\epsilon j\omega + 2)$ . Inclusion of the disturbance estimator within the IMPACT structure can increase robustness of the system to uncertainties in the plant parameters. At high frequencies,  $\beta(\omega)$  converges to a constant

value if  $C(j\omega)$ ,  $A_0(j\omega)$  and  $A(j\omega)$  are selected such that their transfer functions satisfy  $\deg C(s) = \deg A(s) = 2 + \deg A_0(s)$ . This can be shown by selecting  $C(s) = (T_0s + 1)^n$  and  $A_0(s) = a_{n-2}s^{n-2} + a_{n-3}s^{n-3} + \dots + a_1s + a_0$ , and after substituting for  $s = j\omega$  since

$$\lim_{\omega \rightarrow \infty} \beta(\omega) = \frac{T_0^n}{\epsilon^2 a_{n-2}}. \quad (4.46)$$

In the case when  $C(j\omega)$  and  $A(j\omega)$  are selected such that their transfer functions satisfy  $\deg C(s) > \deg A(s)$ ,  $\beta(\omega)$  goes to infinity at high frequencies, i.e.

$$\lim_{\omega \rightarrow \infty} \beta(\omega) \rightarrow \infty. \quad (4.47)$$

Another observation is that selecting a lower value for  $\epsilon$ , in order to reduce the transient in setpoint tracking, reduces the robustness of the system. Thus, there exists a tradeoff between performance and robustness.

## 4.4 Numerical simulations

In this section we present a simulation case-study which illustrates application of the proposed IMPACT structure to the PERR based bilateral teleoperation problem. The absorption of two types of disturbances is considered. The first is a second order function of time, whereas the second one is a harmonic function which can represent undesired vibrations acting at the slave side. The parameters of the master and slave manipulators are given in Table 4.1, together with real  $T_d$  and nominal  $L$  time-delays. For simplicity, we have considered only inertia and viscous friction terms in both the real and nominal manipulator dynamics used in simulations. In all simulations, the reference is selected as a Heaviside step-function  $q_{ref}(t) = h(t)$  [1] defined as,

$$h(t) = \begin{cases} 1, & t \geq 0 \\ 0, & t < 0 \end{cases}. \quad (4.48)$$

The first case-study is related to absorption of a parabolic disturbance. The corresponding results are shown in Figure 4.8. The two plots at the top of this figure show the reference  $q_{ref}$ , position  $q_m$  of the master manipulator, and the difference (error) between them. The position  $q_s$  of the slave manipulator, the reference delayed by  $T_d$ , and the scaled disturbance (with a scaling factor of 0.01, being scaled for the ease of plotting) are shown in the two plots at the bottom of Figure 4.8. The disturbance absorption polynomial is given by (4.34), with  $n = 3$  and  $T_0 = 2$ . The local controller parameter is selected as  $\epsilon = 0.25$ . It can be observed from Figure 4.8 that the influence of the disturbance is absorbed reasonably fast and that

**Table 4.1** Parameters used in numerical experiments

Parameter	Master	Slave
Sampling time [s]	0.001	
Real inertia, $J_m$ & $J_s$ [kgm <sup>2</sup> ]	1	1
Modeled inertia, $\tilde{J}_m$ & $\tilde{J}_s$ [kgm <sup>2</sup> ]	1.1	1.1
Real viscous friction, $B_m$ & $B_s$ [kgm <sup>2</sup> ]	0.1	0.1
Modeled viscous friction, $\tilde{B}_m$ & $\tilde{B}_s$ [kgm <sup>2</sup> ]	0.11	0.11
Time delay, $T_d$ [s]	1	
Modeled time delay, $L$ [s]	1.25	

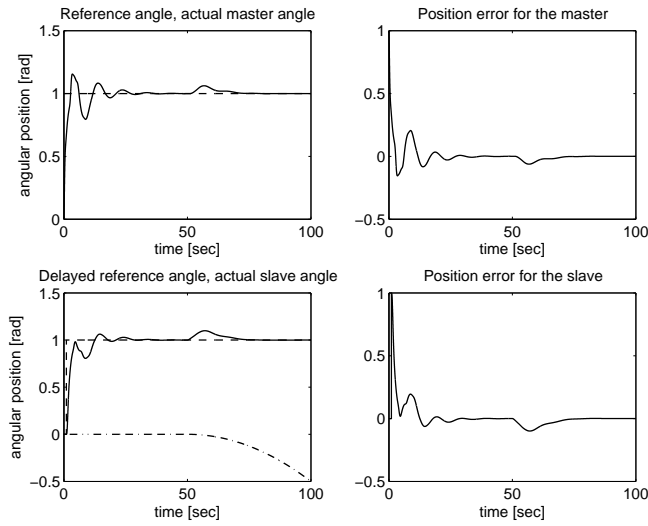


**Figure 4.8** Results for disturbance absorption of a parabolic disturbance. Reference (---) and actual (—) master angles are shown in the upper left part of the figure. Delayed reference (---), actual slave (—) angles and the disturbance (— · —) are shown in the lower left part.

the steady-state value of the output remains the same as before the disturbance has been applied.

In the second case-study, we consider the following periodic disturbance function:

$$d(t) = \sin(0.1(t - 50))h(t - 50) + 0.5 \sin(0.25(t - 50))h(t - 50). \quad (4.49)$$

The disturbance absorption polynomial in this case is obtained by solving the

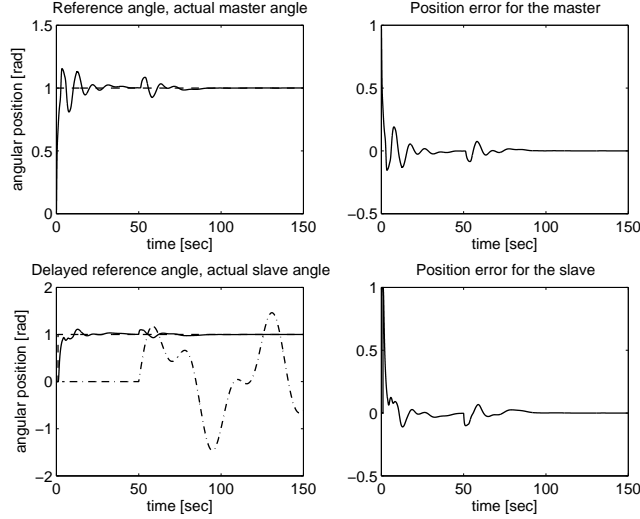


**Figure 4.9** Results for disturbance absorption of sinusoidal disturbance. Reference (---) and actual (—) master angles are shown in the upper left part of the figure. Delayed reference (---), actual slave (—) angles and the disturbance (— · —) are shown in the lower left part.

Diophantine equation given by (4.37). The resulting absorption polynomial is:

$$\Phi(s) = (s^2 + 0.1^2)(s^2 + 0.25^2). \quad (4.50)$$

The polynomial  $A_0(s)$  which solves (4.37) is obtained using (4.50) and selecting  $N = 4$ ,  $n = 5$  and  $T_0 = 3$ . The obtained result is

$$A_0(s) = 383.9s^3 + 41.2s^2 + 16.1s + 0.2. \quad (4.51)$$

As in the first case-study, the local controller parameter is selected as  $\epsilon = 0.25$ . It can be observed from Figure 4.9 that the influence of the disturbance is absorbed reasonably fast and the steady-state value of the output remains the same as before the disturbance is applied.

From both case-studies it can be observed that the master-manipulator is also affected by the disturbances, however the influences vanish after the transients. In both cases, smaller values for  $\epsilon$ ,  $n$  and  $T_0$  can be selected to improve the control performance, however at the cost of decreasing the robustness property. In Figure 4.10 and Figure 4.11, we show results of the robustness analysis when (4.34) is used as the disturbance absorption polynomial. The local controller parameter is selected as  $\epsilon = 0.1$ . The additive uncertainty bounds  $|l_a(j\omega)|$  together with the robust stability bounds  $\beta(\omega)$  are depicted in these figures. The robust stability bounds are plotted in Figure 4.10 for  $T_0 = 1$  and for three values of  $n$ :

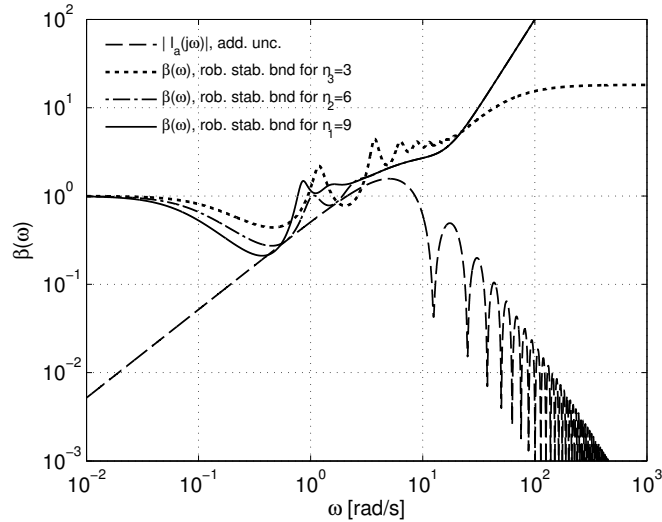


**Figure 4.10** Robustness analysis for different  $n$  values.

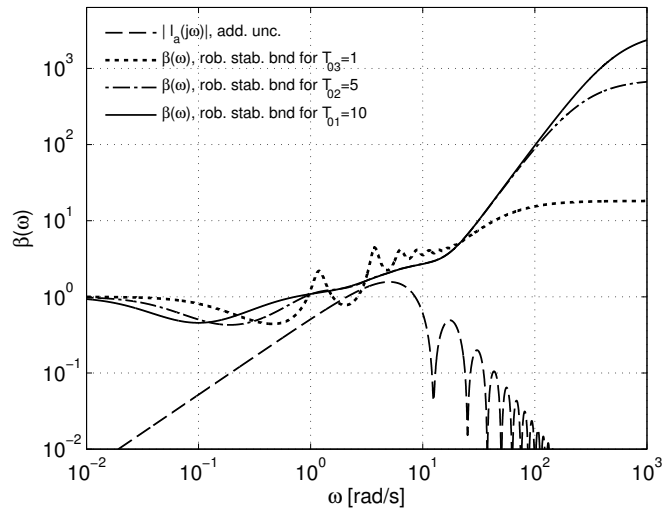


**Figure 4.11** Robustness analysis for different  $T_0$  values.

$(n_1, n_2, n_3) = (9, 6, 3)$ . It can be observed from this figure that the robustness of the system improves if  $n$  is increased. The robust stability bounds are plotted in Figure 4.11 for  $n = 3$  and for three values of  $T_0$ :  $(T_{01}, T_{02}, T_{03}) = (10, 5, 1)$ . It can be observed from this figure that the robustness of the system improves for higher values of  $T_0$ . The fluctuations observed in Figures 4.10 and 4.11 at frequen-

cies higher than  $\omega = 10$  rad/s are caused by the mismatch between the real and nominal values of the time-delay.

## 4.5 Experiments

In this section, our experimental setup is introduced. Then, simulation results based on the identified model of the setup are given. Finally, experimental results are presented.

### 4.5.1 Experimental setup

The experiments are conducted on two similar 4 degree-of-freedom manipulators, fabricated by the Centre for Manufacturing Technology (CFT) Philips Laboratory. The experimental setup is shown in Figure 4.12(a) with its schematic representation shown in Figure 4.12(b), respectively. During the experiments, the horizontal degree-of-freedom marked with number 1, shown in Figure 4.12(b), is used in both manipulators. Two manipulators are connected to the same PC via ethernet connection and control software is implemented in Matlab/Simulink 2006a. The sampling frequency of the controller is 500 Hz. The time delay  $T_d$  due to commu-

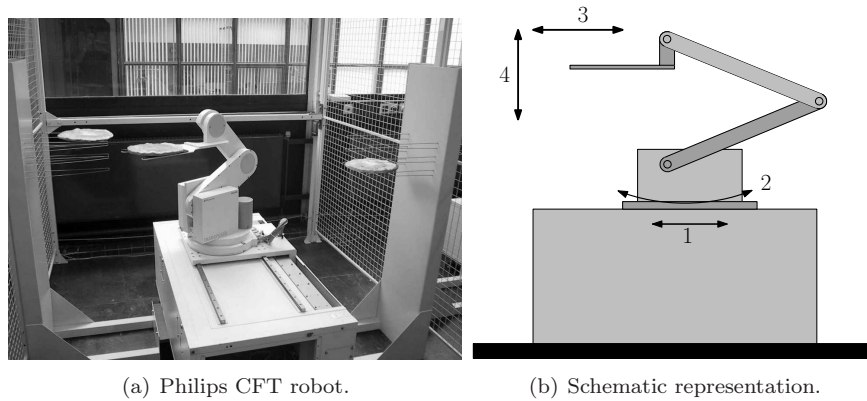


**Figure 4.12** Philips CFT robot and its schematic representation

nication between the master and slave robots is introduced by control software. In all experiments, the following smooth Coulomb friction compensation law is used,

$$\tau_m = \hat{\tau}_{c,m} \tanh(\alpha_m \dot{q}_m) + u_m, \quad (4.52)$$

$$\tau_s = \hat{\tau}_{c,s} \tanh(\alpha_s \dot{q}_s) + u_s, \quad (4.53)$$



for the master and slave robots respectively. The Coulomb friction compensation coefficients, obtained by means of an empirical estimation procedure, are  $\alpha_m = \alpha_s = 50$ ,  $\hat{\tau}_{c,m} = 1$  and  $\hat{\tau}_{c,s} = 0.6$  for the master and slave robots, respectively [22]. The nominal transfer functions,  $\tilde{G}_m(s)$  and  $\tilde{G}_s(s)$  for the master and slave robots, respectively, are obtained using frequency response function (FRF) measurements, with a multisine excitation signal [154]. For simplicity, we consider only inertia and viscous friction terms for the nominal manipulator dynamics. Therefore, the following second order transfer functions are fitted to the frequency response measurements of the master and slave manipulators,

$$\tilde{G}_m(s) = \frac{0.0641}{s^2 + 1.005s} = \frac{1}{15.601s^2 + 15.673s}, \quad (4.54)$$

$$\tilde{G}_s(s) = \frac{0.1013}{s^2 + 0.2325s} = \frac{1}{9.871s^2 + 2.295s} \quad (4.55)$$

respectively. In all experiments, the local controllers are designed in continuous time using (4.13),(4.14) and then discretized using Tustin approximation. Furthermore, the tuning of controllers is performed for optimal tracking error performance.

**Remark 4.3.** *The master and slave manipulators are subject to nonlinear effects such as stick-slip friction, which are not identified using dedicated identification experiments. Therefore, these nonlinear phenomena would influence the frequency response measurements. Although the inertial and kinematic properties of both manipulators are similar, the same cannot be said for the nonlinear effects and consequently their influence on the frequency response measurements. Furthermore, the numerical artifacts of the transfer function fitting process together with the frequency range emphasized (using a suitable weighting function) during this process may cause this difference [113, 114].*

## 4.5.2 Illustrative simulations

In this section we present results of a simulation case-study using the identified model of the experimental setup. First, the absorption of a ramp type of disturbance is considered. Then, robustness of the closed-loop system dynamics against parametric uncertainties is analysed. Finally, we compare the performance of our algorithm with a filtered (see  $W_m(s)$  and  $W_s(s)$  in Figure 4.16(a)) scattering based approach introduced in [97]. The master and slave models that are used during simulations are given by the transfer functions (4.54) and (4.55), respectively. The parameters of the master and slave manipulators are given in Table 4.2. These parameters are obtained by fitting (4.16) and (4.17) to the transfer functions (4.54) and (4.55). For simplicity, in simulations we consider only inertia and viscous friction terms in both the real and nominal manipulator dynamics. The modeled

values of the inertias and viscous friction coefficients correspond to 50% level of uncertainty. The first case-study is related to absorption of a ramp disturbance. The

**Table 4.2** Parameters used in illustrative simulations

Quantity/Cont.	IMPACT	Quantity/Cont.	Wave filter
$J_m$	15.601 [kg]	$k_m$	0.0641 [(m/s)/N]
$\tilde{J}_m$	7.801 [kg]	$b_m$	1.005
$J_s$	9.871 [kg]	$k_s$	0.1013 [(m/s)/N]
$\tilde{J}_s$	4.935 [kg]	$b_s$	0.2325
$B_m$	15.673 [N/(m/s)]	$K_h$	600 [N/m]
$\tilde{B}_m$	23.51 [N/(m/s)]	$D_h$	90 [N/(m/s)]
$B_s$	2.295 [N/(m/s)]	$k_p$	250000
$\tilde{B}_s$	3.443 [N/(m/s)]	$k_d$	20000
$T_d$	0.2 [s]	$T_1$	0.2 [s]
$L$	0.25 [s]	$T_2$	0.2 [s]
$\epsilon$	0.0165	$W_m(s)$	1
$n$	2	$W_s(s)$	$\frac{1}{(0.02s+1)^2}$
$T_0$	0.65	$b$	20
$A_0(s)$	1	$\varpi$	0.001
		$a$	2

corresponding results are shown in Figure 4.13. In this simulation, the reference is a step-function  $q_{ref}(t) = h(t)$ , defined as,

$$h(t) = \begin{cases} 0.1, & t \geq 0 \\ 0, & t < 0 \end{cases}. \quad (4.56)$$

The two plots at the top of this figure show the reference  $q_{ref}$ , position  $q_m$  of the master manipulator, and the difference (error) between them. The position  $q_s$  of the slave manipulator, the reference delayed by  $T_d$ , and the scaled disturbance (with a scaling factor of 0.01, being scaled for the ease of plotting) are shown in the two plots at the bottom of Figure 4.13. The disturbance absorption polynomial is selected as  $A_0(s) = 1$  and the lowpass filter parameters are  $n = 3$  and  $T_0 = 2$ . The local controller parameter is selected as  $\epsilon = 0.045$ . The actual time delay is  $T_d = 0.25$  [s] and the modeled time-delay is  $L = 0.3125$  [s] corresponding to an uncertainty of 25%. It can be observed from Figure 4.13 that the influence of the disturbance is absorbed reasonably fast and that the steady-state value of the output remains the same as before the disturbance is applied. Furthermore, it can be observed that the master-manipulator is also affected by the disturbance, however its influence vanishes after the transients. Smaller values for  $\epsilon$ ,  $n$  and  $T_0$  can be selected to improve the control performance, however at the cost of decreasing stability margins.

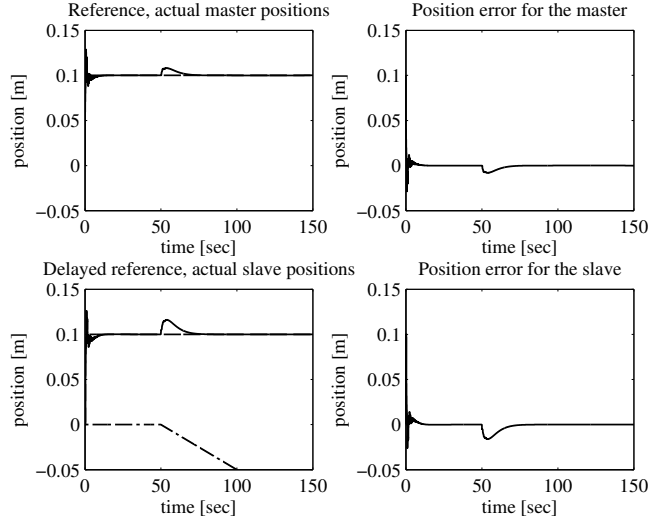


**Figure 4.13** Results for disturbance absorption of a ramp disturbance. Reference (- -) and actual (-) master angles are shown in the upper left part of the figure. Delayed reference (- -), actual slave (-) angles and the disturbance (- · -) are shown in the lower left part.

In Figures 4.14 and 4.15, we show results of the robustness analysis when the disturbance absorption polynomial is  $A_0(s) = 1$ . The local controller parameter is selected as  $\epsilon = 0.03$ . The modeled and actual time delays are the same as in the previous case. The additive uncertainty bounds  $|l_a(j\omega)|$  together with the robust stability bounds  $\beta(\omega)$  are depicted in these figures. The robust stability bounds are plotted in Figure 4.14 for  $T_0 = 0.15$  and for three values of  $n$ :  $(n_1, n_2, n_3) = (15, 8, 3)$ . It can be observed from this figure that the robustness of the system improves if  $n$  is increased. The robust stability bounds are plotted in Figure 4.15 for  $n = 3$  and for three values of  $T_0$ :  $(T_{01}, T_{02}, T_{03}) = (10, 5, 0.15)$ . It can be observed from this figure that the robustness of the system improves for higher values of  $T_0$ . The fluctuations observed in Figures 4.14 and 4.15 at frequencies higher than  $\omega = 100$  rad/s are caused by the mismatch between the real and nominal values of the time-delay.

A block diagram of the teleoperation scheme considered in [97] are shown in Figure 4.16 together with a detailed representation of the remote and local sides. Here,  $G_m(s)$ ,  $G_s(s)$  represent the transfer functions of the master and slave manipulators with their respective local controllers. The transfer functions,  $W_m(s)$ ,  $W_s(s)$  are the wave filters and  $b$  is the scattering parameter. In Figure 4.16(b),  $K_h$  and  $D_h$  are the stiffness and damping coefficients of the human and  $G_{cm}(s)$  is a phase-lead

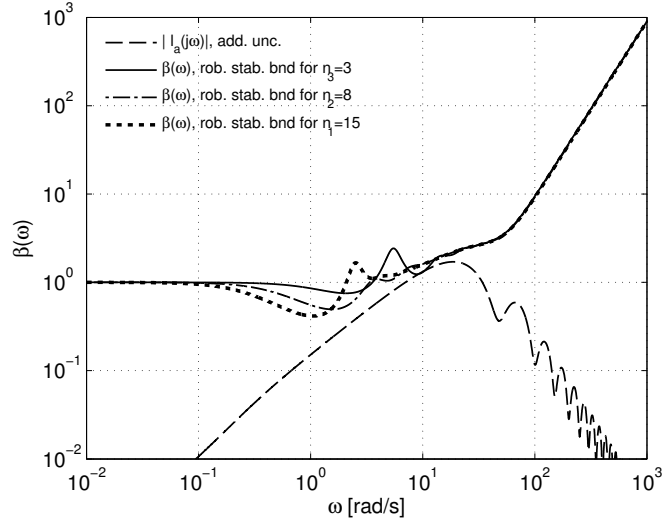


Figure 4.14 Robustness analysis for different  $n$  values.

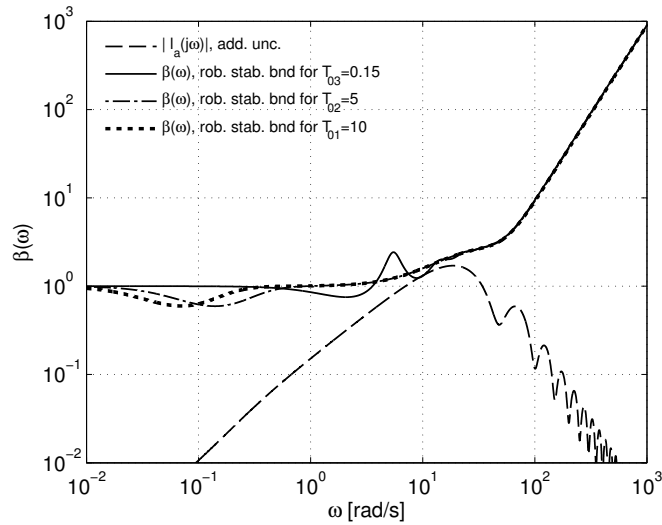


Figure 4.15 Robustness analysis for different  $T_0$  values.

compensator. In Figure 4.16(c),  $K_{env}$  and  $D_{env}$  are the stiffness and damping coefficients of the environment,  $\alpha$  is a transformation coefficient from the external force to corresponding motor voltage, and  $G_{cs}$  is a phase-lag compensator. In order to make a fair comparison of our algorithm with the one given in [97], we tested both algorithms in a free motion task. Therefore, the environment

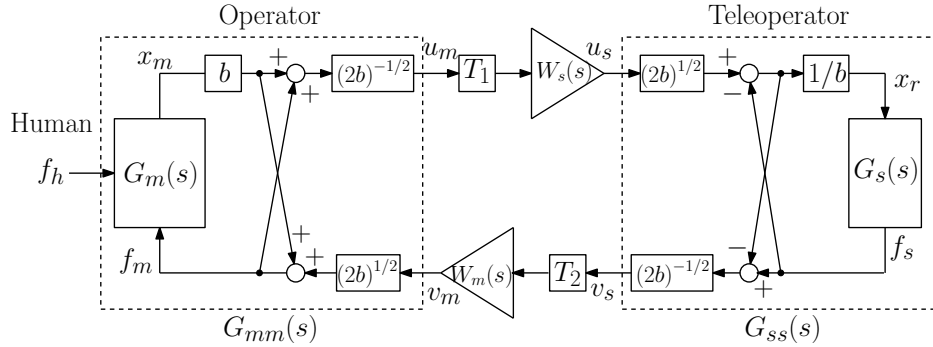
stiffness and damping coefficients and  $\alpha$  are set to zero (i.e.  $K_{env} = D_{env} = 0$ ,  $\alpha = 0$ ). The same master and slave manipulator dynamics are used in both algorithms. We tuned both control laws heuristically such as to achieve a tracking error as low as possible. The simulation results which compare IMPACT and the modified scattering based approach are shown in Figure 4.17. The control input forces of both approaches are shown in Figure 4.18. The parameters used in both control laws are reported in Table 4.2. A more quantitative comparison based on the maximum absolute error, averaged integrated absolute error (IAE), averaged integrated square error (ISE) and the maximum value of the control inputs are summarized in Table 4.3. The mass and damping parameters used in the IMPACT algorithm correspond to 50% uncertainty, whereas there is 25% uncertainty in the delay model. It can be realized from the results given in Figure 4.17 and Table 4.3 that the tracking error performance of both control algorithms are comparable. The considered uncertainty in the master/slave dynamics and the time-delay used in the simulations is large enough to be encountered in practice. However, for higher uncertainty especially in the modeled time-delay, the tracking performance of the IMPACT algorithm would likely become worse. However, it is also a well known fact that the performance of teleoperated systems with wave variables deteriorates rapidly with increasing communication delay. For a detailed analysis please see Munir et. al. [101].

**Table 4.3** Comparison of errors and inputs of the control laws

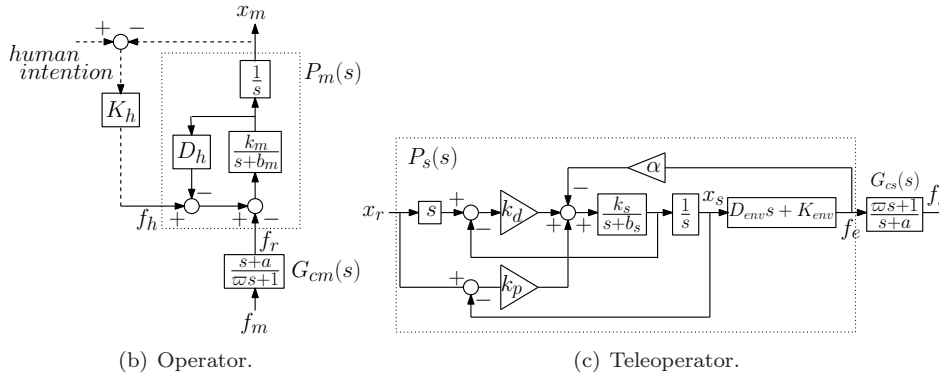
Quantity/Cont.	IMPACT		Wave filter	
	Master	Slave	Master	Slave
Max. abs. error [m]	0.0530	0.0825	0.1608	0.0575
IAE error [m]	0.0263	0.0148	0.0892	0.0196
ISE error [m]	0.001	0.00038	0.0111	0.0006
Max. abs. cont. inp. [N]	38.1137	13.24	24.5452	11.6963

### 4.5.3 Experimental results

In this section, first experimental results are given to demonstrate the tracking error performance of the local controllers. Then, tracking performance is presented in the case of bilateral teleoperations. Finally, robustness of the IMPACT structure to uncertainties in time-delay and its disturbance rejection performance are shown. A repetitive second order reference trajectory, which takes approximately 6 seconds, is used during the experiments whose details are given in the Appendix G. The individual tracking error performance of each manipulator is shown in Figure 4.19 for the local control laws given by (4.13)-(4.14). The local controller parameter for this experiment is selected as  $\epsilon = 0.04$ . This figure reveals the



(a) Block diagram of teleoperation system with time-delay.



(b) Operator.

(c) Teleoperator.

**Figure 4.16** Teleoperation system with modified wave variables.

steady state errors for both the master and slave robots, since the local controllers are only of the lead filter type with no integral action included. The absence of the integral action in the local control laws is due to the structure of the nominal transfer functions of the master and slave robots, (4.54) and (4.55), respectively, as explained in the Remark 4.2.

The results for the case when no IMPACT structure is applied and no time-delay is present ( $T_d = 0$ ), are shown in Figure 4.20. In this experiment, the teleoperation scheme shown in Figure 4.6 is implemented with only local controllers given by equation (4.13). The local controller parameter for this experiment is  $\epsilon = 0.045$ . It can be observed from Figure 4.20 that, even when time-delays are not present in the teleoperated system, an offset is present in the tracking errors and now also affecting the master. The results when IMPACT structure is not applied and a time-delay of  $T_d = 0.25$  seconds is introduced, are shown in Figure 4.21. The local controller parameter for this experiment is  $\epsilon = 0.09$ . It can be observed that the

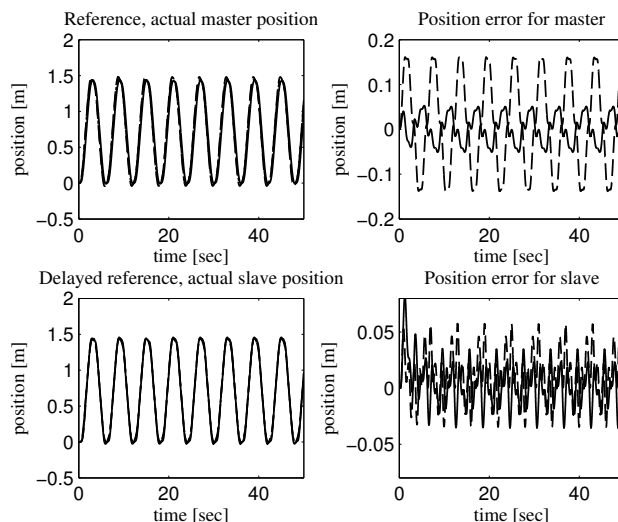


**Figure 4.17** Tracking errors for master and slave achieved using IMPACT and scattering approaches. Reference (— · —) and actual master positions (IMPACT (— · —), scattering (—)) are shown in the upper left. Delayed reference (— · —) and actual slave positions (IMPACT (— · —), scattering (—)) are shown in the lower left. The tracking errors for the master and the slave (IMPACT (— · —), scattering (—)) are shown in the upper right and lower right, respectively.

position errors of both master and slave manipulators are quite high (at the level of 50%) and fluctuate around a non-zero value.

The results when the IMPACT structure is applied are presented in Figure 4.22, with the local controller parameter,  $\epsilon = 0.045$ . The parameters of the lowpass filter  $C(s)$  are selected as  $T_0 = 2$  and  $n = 3$ . It can be observed that the offset in the error, which can be thought as a constant output disturbance, is mostly reduced and the tracking error is significantly improved (the maximum after the transient vanishes, is below 5%). The remaining peaks in the error occur when the position signal changes direction, which can be due to imperfect cancellation of friction at low velocities. The results with the IMPACT structure when a time-delay of  $T_d = 0.5$  seconds is introduced, are shown in Figure 4.23. For this experiment, the values of the parameters of the local control laws and the low-pass filter  $C(s)$  are,  $\epsilon = 0.0535$ ,  $T_0 = 3$  and  $n = 3$ , respectively.

Finally, the results with the IMPACT structure in situation when there are mismatches in time-delay and disturbances are presented. The results of the experiment for a virtual ramp disturbance acting at the output of the slave are shown in

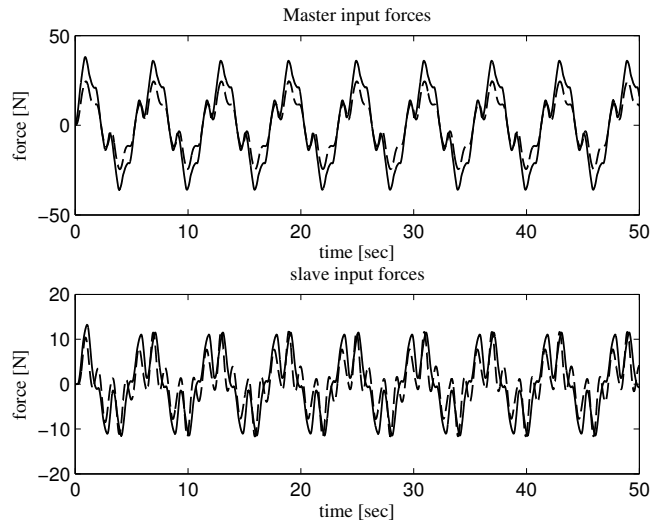


**Figure 4.18** Control inputs for the master and slave using IMPACT and scattering approaches. The master and slave control signals are shown in the top and bottom parts, respectively (IMPACT (—), scattering (---)).

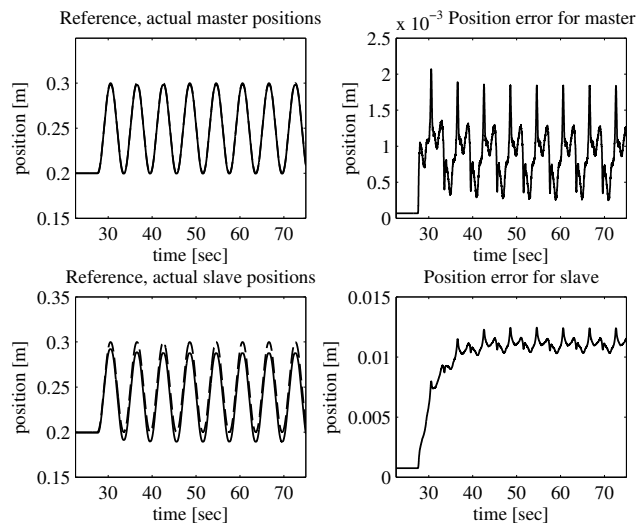


**Figure 4.19** Individual tracking performance of master and slave manipulators using the local control laws. Reference (---) and actual (—) master and slave positions.



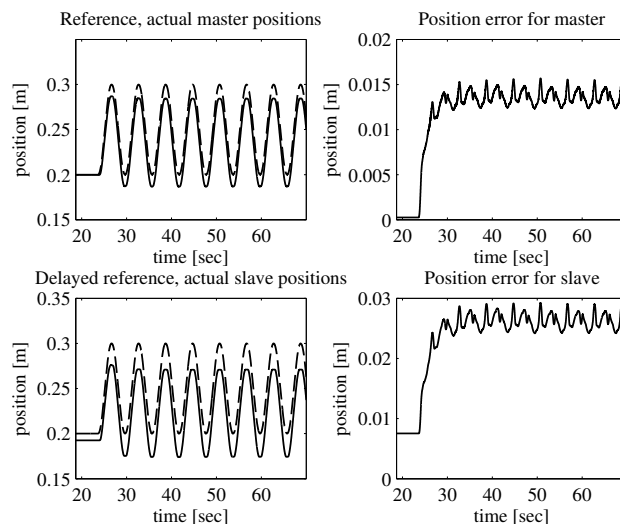


**Figure 4.20** Results for bilateral teleoperation without the IMPACT structure and without any time-delay. Reference (---) and actual (—) master positions are shown in upper left part of the figure. Delayed reference (---), actual slave (—) positions are shown in lower left part.

Figure 4.24. After the system is settled, approximately at 85 seconds, the disturbance is added to the output of the slave. The local controller parameter is selected as  $\epsilon = 0.05$ . The parameters of the lowpass filter  $C(s)$  are selected as  $T_0 = 2$  and  $n = 2$ . It can be observed that the effect of the additional virtual disturbance is mostly absorbed and only a small amount of steady-state error remains (at the level of 2%). Finally, the effect of a mismatch in the modeled time-delay is investigated, where  $T_d = 0.25$  and  $L = 0.275$  correspond to a perturbation of 10%. The results of this experiment are presented in Figure 4.25. For this experiment, the values of the parameters of the local control laws and the low-pass filter  $C(s)$  are,  $\epsilon = 0.0675$ ,  $T_0 = 6$  and  $n = 4$ , respectively. It can be observed in Figure 4.25 that the tracking error increases since the controller parameter is higher. However, the system is still stable in spite of the mismatch in the time-delay, which illustrates the robustness of the IMPACT scheme to uncertainties in the plant model and unmodeled dynamics.

**Remark 4.4.** For the level of uncertainty considered in the results, the tracking performance of the IMPACT algorithm is comparable to approaches such as scattering [97]. However, for higher level of uncertainty especially in the time-delay, the tracking performance of the IMPACT algorithm would likely be worse. Therefore, from the results obtained in this chapter, the IMPACT algorithm can be considered as an alternative to such approaches.

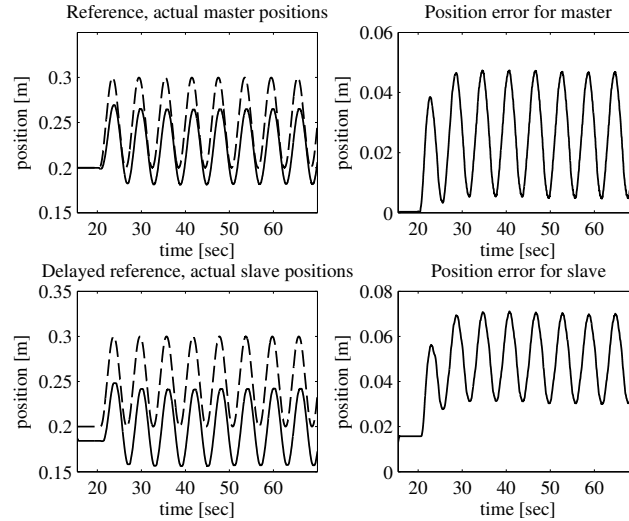


**Figure 4.21** Results for bilateral teleoperation without the IMPACT structure for 0.25 second time delay. Reference (---) and actual (—) master positions are shown in upper left part of the figure. Delayed reference (---), actual slave (—) positions are shown in lower left part.

## 4.6 Concluding remarks

An IMPACT structure to compensate for time-delays and disturbances affecting a bilateral teleoperation system is presented in this chapter. It incorporates a Smith predictor and a disturbance estimator designed for an expected class of disturbances. Both the Smith predictor and the disturbance estimator are implemented at the master side of the teleoperated system. We design local controllers for the master and slave manipulators by means of frequency response measurements and a suitable pole placement criterion. Coulomb friction is compensated by means of a suitable nonlinear feedback term in the local controllers. For formal stability analysis, the Nyquist criterion is used. There is a significant improvement in the tracking performance of the bilateral teleoperation system compared to the case when the IMPACT structure is not applied. The presented simulation results verify disturbance rejection capabilities and robustness to parametric uncertainties using our control approach. Moreover, the experimental results confirm the benefits of the algorithm against the aforementioned issues.

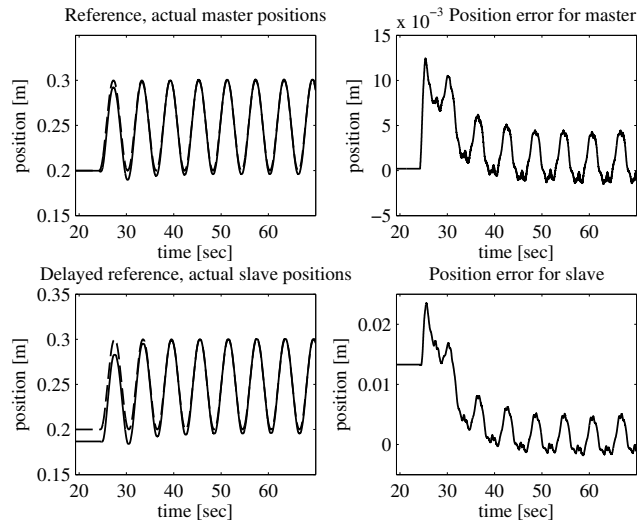


**Figure 4.22** Results for bilateral teleoperation with the IMPACT structure with  $T_d = 0.25$  seconds. Reference (- -) and actual (-) master positions are shown in the upper left part of the figure. Delayed reference (- -), actual slave (-) positions are shown in the lower left part.

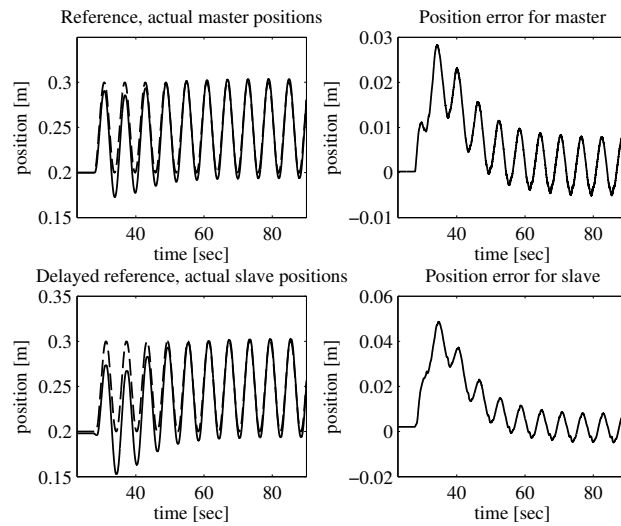


**Figure 4.23** Results for bilateral teleoperation with the IMPACT structure with  $T_d = 0.5$  seconds. Reference (- -) and actual (-) master positions are shown in the upper left part of the figure. Delayed reference (- -), actual slave (-) positions are shown in the lower left part.

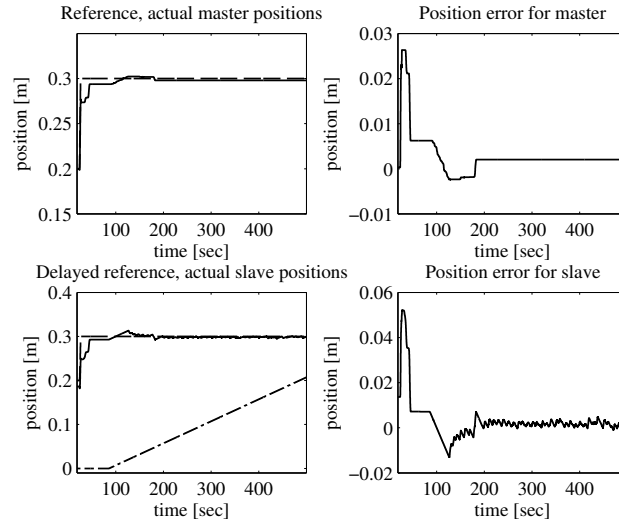


**Figure 4.24** Results for disturbance absorption of a ramp disturbance. Reference (- -) and actual (-) master positions are shown in the upper left part of the figure. Delayed reference (- -), actual slave (-) positions and the disturbance (- · -) are shown in the lower left part.

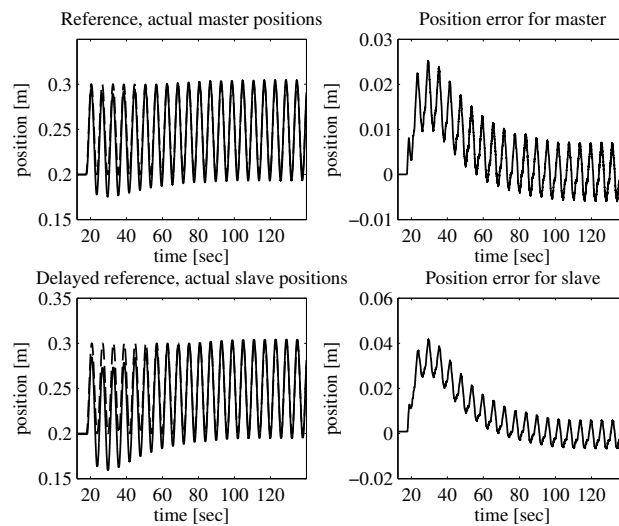


**Figure 4.25** Results for bilateral teleoperation with the IMPACT structure with  $T_d = 0.25$  and  $L = 0.275$  seconds. Reference (- -) and actual (-) master positions are shown in the upper left part of the figure. Delayed reference (- -), actual slave (-) positions are shown in the lower left part.

# Chapter 5

## Conclusions and recommendations

**Abstract** The main contributions and results of this thesis are summarized in this chapter. Furthermore, some recommendations for future research directions are provided in the last section.

### 5.1 Conclusions

In this thesis, the robot-environment interaction problems are addressed for single and multiple robots as well as the teleoperation of robots. Control strategies that guarantee stability and performance in the presence of uncertainties are proposed. The main contributions and results for these problems are explained in greater detail in the remainder of this section.

#### **A hybrid impedance controller with finite-time stability characteristics**

In Chapter 2, a model based hybrid impedance controller for robotic manipulators is proposed with finite-time stability characteristics. The design of the controller is inspired by the homogeneity principle for vector fields. The controller is designed in task space coordinates such that suitable impedance characteristics in accordance with the constraints of the environment can be assigned in order to track the desired position and force trajectories. Contrarily to sliding mode controllers that achieve finite time convergence by means of a discontinuous control, the controller designed in this work is continuous and achieves finite time convergence without leading to chattering. The controller can operate even if the stiffness coefficient and the undeformed position of the environment are unknown. It can also handle transitions from free motion to contact motion phase without switching. The controller contains model based compensation terms incorporating the terms of the manipulator dynamic model. The rotational part of the controller is designed using the vector part of the unit quaternions. Stability of the closed-loop system subject to this controller is analyzed assuming that the manipulator

dynamic model is exactly known (i.e. the nominal case). Guidelines to investigate the ultimate bound on error trajectories of the closed-loop system are provided for the case when the manipulator dynamics are not perfectly known. The position, orientation and force tracking performance of the algorithm in the presence of uncertainties is investigated in simulations of a Puma 560 manipulator. Furthermore, experimental results are provided that are obtained on a three degrees-of-freedom robotic manipulator. From the simulation results, it can be concluded that for a similar amplitude of control signals, a much better position and orientation tracking error is obtained with the finite-time stable hybrid impedance controller as compared to the linear one, whereas this difference is not high for force tracking errors. Experimental results further demonstrate the tracking performance of the designed controller. It can be observed from experimental results that the controller can handle uncertainties in the manipulator dynamics, environment dynamics and geometry. Furthermore, contact instability in the form of continuous bouncing is not present in experiments.

### **Impedance controller for cooperative manipulation**

In Chapter 3, cooperative manipulators are modelled in two different cases, depending on whether the grasp points are fixed or non-fixed. A cascade control algorithm is introduced for the case of fixed grasps. With the proposed control algorithm for cooperative manipulation, the motion, internal and external forces of the object can be controlled. Using impedance relationships, a commanded object trajectory is converted into reference trajectories for the motion controllers of the manipulators such that the desired internal and contact forces can be achieved. In contrast to previously published results, criteria for each controller are determined to guarantee asymptotically stable behavior of the cooperative manipulator system. Guidelines are presented for the internal impedance relationships to compute the control parameters. As a result, all control parameters can be tuned intuitively. The implementation of the control algorithm is illustrated with simulations. The simulations done for the non-fixed grasp case show that the Lagrangian complementarity framework is a suitable approach to represent friction and impacts between the manipulators and the object.

### **Time-delay compensation using Internal Model Principle and Control Together**

In Chapter 4, an internal model principle and control together (IMPACT) structure is proposed to compensate for time-delays and disturbances affecting a bilateral teleoperation system. The proposed controller is integrated into the position error based bilateral teleoperation architecture to achieve position synchronization between master and slave robots. A Smith predictor constitutes the internal

model control part whereas a disturbance estimator represents the internal model principle part of the algorithm. Both the Smith predictor and the disturbance estimator are implemented at the master side of the teleoperated system. The local controllers of the teleoperation architecture for the master and slave manipulators are designed with the help of frequency response measurements and a suitable pole placement criterion. Coulomb friction is compensated by means of a suitable nonlinear feedback term in the local controllers. For formal stability analysis, the Nyquist criterion is used. There is a significant improvement in the position synchronization performance of the bilateral teleoperation system compared to the case when the IMPACT structure is not applied. The presented simulation results verify disturbance rejection capabilities and robustness to parametric uncertainties using our control approach. Moreover, the experimental results confirm the benefits of the algorithm against the aforementioned issues.

## 5.2 Recommendations

Possible future research directions are introduced in this section.

### **A hybrid impedance controller with finite-time stability characteristics**

The robust stability analysis should be completed by finding a Lyapunov function with a strictly negative definite time derivative since in Section 2.6.2 it has only been conjectured that the error trajectory of the uncertain system is uniformly ultimately bounded. Although the representation singularity associated with the rotational part of the controller can be dealt with an ad hoc approach, it influences the robustness analysis. Therefore, a finite-time stable rotational controller that does not suffer from representation singularities should be derived. The approach should be extended to the case when there is no knowledge about the environment dynamics and geometry. The adaptive approaches such as [72] that estimate local geometry of the environment can be used for this purpose. Investigating the applicability of the approach on perfectly rigid environments can be another possible future research direction. Although the controller is shown to handle contact transitions in simulations and experiments, the stability of the closed-loop system for the contact transition phase should formally be analyzed. The controller should be tested in more complex manipulation tasks such as opening a door, inserting a peg into a hole, etc. For such tasks, the rotational impedance stiffness parameters should be selected in consistence with the task geometry (see [47] for more details). The performance of the controller with nonlinear terms can be compared with a piecewise linear controller which has a very high gain close to zero and low gain away from it. Such a comparison can help to distinguish whether nons-

moothness or the infinite slope of the nonlinear terms at zero improve performance.

### **Impedance controller for cooperative manipulation**

The cascade controller proposed for the fixed grasp case should be tested on an experimental setup comprised of multiple, not necessarily identical, robot arms cooperating in different tasks. The performance of the inverse dynamics controllers that constitute the lowest level of the proposed controller can degrade if the dynamic models of the manipulators are not known accurately enough. The stability of the closed-loop system in the presence of such perturbations and uncertainties should be investigated. Furthermore, robust or adaptive control or their combination can be used to deal with perturbations. A controller for the case of non-fixed grasps should be designed that can handle transitions between different modes, such as between free and constrained motions and between rolling and sliding contacts. The controller proposed for the case of fixed grasps may be a starting point, however, care should be taken due to the force feedback terms in the controller which can feed back impulsive forces in the case of non-fixed grasps. The part of the cascade controller responsible to regulate the external forces acting on the object requires accurate knowledge of the environment dynamics, which is seldom available in practice. The technique used in chapter 2 might be a possible way to cope with this issue, however, the accurate estimation of the external forces on the object might be required. The proposed controller can also be investigated in a wider scope of cooperative manipulation systems, for instance, involving redundant or mobile manipulators.

### **Time-delay compensation using Internal Model Principle and Control Together**

The IMPACT approach should be extended to teleoperated systems featuring manipulators of nonlinear dynamics with multiple degrees-of-freedom. For this purpose, nonlinear internal model control and different type of disturbance observers can further be investigated. It could be beneficial to investigate the compensation of more complicated low velocity friction effects by means of friction observers. Furthermore, the robustness and disturbance rejection capabilities of the IMPACT approach should be investigated in other bilateral teleoperation architectures, such as kinesthetic force feedback and 4-channel control architectures. The uncertain constant (or slowly time-varying) time delay considered in this work may be less suitable to applications involving different communication links (e.g. wireless communication) where significantly time-varying delays and packet dropouts come into play. The techniques from the Networked Control Systems literature can be investigated to handle these communication constraints [64].



# Appendix **A**

## Proofs for hybrid impedance control with finite-time stability characteristics

### A.1 Proof of Proposition 2.14

Consider the following  $C^1$  candidate Lyapunov function,

$$\begin{aligned}
 V(e_r, \dot{e}_r, \epsilon_{de}, \dot{\epsilon}_{de}) &= \frac{1}{2} \dot{e}_r^T \dot{e}_r + \frac{1}{\alpha_1 + 1} \sum_{i=1}^3 \frac{\bar{k}_{d,r,i}}{m_{d,r,i}} |e_{r,i}|^{\alpha_1+1} + \frac{1}{2} e_r^T M_{d,r}^{-1} K_e e_r \\
 &+ \frac{1}{2} \dot{\epsilon}_{de}^T \dot{\epsilon}_{de} + \frac{1}{\alpha_1 + 1} \sum_{i=1}^3 \frac{\bar{k}_{d,\phi,i}}{m_{d,\phi,i}} |\epsilon_{de,i}|^{\alpha_1+1} \\
 &= \frac{1}{2} \dot{e}_r^T \dot{e}_r + \frac{1}{\alpha_1 + 1} e_r^T M_{d,r}^{-1} \bar{K}_{d,r} \text{Sig}(e_r)^{\alpha_1} + \frac{1}{2} e_r^T M_{d,r}^{-1} K_e e_r \\
 &+ \frac{1}{2} \dot{\epsilon}_{de}^T \dot{\epsilon}_{de} + \frac{1}{\alpha_1 + 1} \epsilon_{de}^T M_{d,\phi}^{-1} K_{d,\phi} \text{Sig}(\epsilon_{de})^{\alpha_1} \tag{A.1}
 \end{aligned}$$

which is a positive definite and radially unbounded function that satisfies  $V(0) = 0$ . The time derivative of this Lyapunov function is computed as

$$\begin{aligned}
 \dot{V} &= \dot{e}_r^T \ddot{e}_r + \dot{e}_r^T M_{d,r}^{-1} \bar{K}_{d,r} \text{Sig}(e_r)^{\alpha_1} + \dot{e}_r^T M_{d,r}^{-1} K_e e_r + \dot{\epsilon}_{de}^T \ddot{\epsilon}_{de} + \dot{\epsilon}_{de}^T M_{d,\phi}^{-1} K_{d,\phi} \text{Sig}(\epsilon_{de})^{\alpha_1} \\
 &= -\dot{e}_r^T M_{d,r}^{-1} B_{d,r} \text{Sig}(\dot{e}_r)^{\alpha_2} - \dot{\epsilon}_{de}^T M_{d,\phi}^{-1} B_{d,\phi} \text{Sig}(\dot{\epsilon}_{de})^{\alpha_2} \leq 0 \tag{A.2}
 \end{aligned}$$

which is negative semi-definite, implying  $\dot{e}_r, \dot{\epsilon}_{de} \rightarrow 0$  as  $t \rightarrow \infty$ . In order to investigate the asymptotic stability of (2.55) and (2.59) LaSalle's invariance principle is employed. Let the region in which the manipulator operates, be a subset of the finite workspace from which kinematic and representation singularities are removed, be denoted by  $\mathcal{W}$ . Then, the state-space is given by  $\mathfrak{C}_s := \mathcal{W} \times \mathbb{R}^6$  where  $\mathbb{R}^6$  is included for end-effector velocities. Let  $\Omega \subset \mathfrak{C}_s$  be a compact set that is positively invariant with respect to (2.59). It can be realized that (A.1) is a continuously

differentiable function (i.e.  $C^1$ ) such that  $\dot{V} \leq 0$  in  $\Omega$ . Let  $\mathcal{E}$  be the set of all points in  $\Omega$  such that  $\dot{V} = 0$ , i.e.

$$\mathcal{E} = \{(e_r, \dot{e}_r, \epsilon_{de}, \dot{\epsilon}_{de}) \in \mathfrak{C}_s \mid \dot{V} = 0\} = \{(e_r, \dot{e}_r, \epsilon_{de}, \dot{\epsilon}_{de}) \in \mathfrak{C}_s \mid \dot{e}_r = 0, \dot{\epsilon}_{de} = 0\}. \quad (\text{A.3})$$

The largest invariant set in  $\mathcal{E}$  can be determined from (2.55) and (2.59) using  $\dot{e}_r \equiv 0$ ,  $\ddot{e}_r \equiv 0$  and  $\dot{\epsilon}_{de} \equiv 0$ ,  $\ddot{\epsilon}_{de} \equiv 0$  as

$$\bar{K}_{d,r} \text{Sig}(e_r)^{\alpha_1} + K_e e_r = 0, \quad K_{d,\phi} \text{Sig}(\epsilon_{de})^{\alpha_1} = 0 \quad (\text{A.4})$$

or equivalently

$$|e_{r,n}|^{\alpha_1} \text{sgn}(e_{r,n}) \left( k_{f,r} k_e^{\alpha_1} + k_e |e_{r,n}|^{1-\alpha_1} \right) = 0 \quad (\text{A.5})$$

$$k_{d,t,i} |e_{r,t,i}|^{\alpha_1} \text{sgn}(e_{r,t,i}) = 0 \quad \text{for } i = 1, 2 \quad (\text{A.6})$$

$$k_{d,\phi,i} |\epsilon_{de,i}|^{\alpha_1} \text{sgn}(\epsilon_{de,i}) = 0 \quad \text{for } i = 1, 2, 3 \quad (\text{A.7})$$

whose unique solution is  $\epsilon_{de} = 0$  and  $e_r = 0$ , since  $k_{f,r} k_e^{\alpha_1} + k_e |e_{r,n}|^{1-\alpha_1} > 0$  for all  $e_{r,n}$ . Therefore, the largest invariant set contained in  $\mathcal{E}$  becomes

$$\mathcal{M} = \{(e_r, \dot{e}_r, \epsilon_{de}, \dot{\epsilon}_{de}) \in \Omega \mid (e_r, \dot{e}_r, \epsilon_{de}, \dot{\epsilon}_{de}) = (0, 0, 0, 0)\} \quad (\text{A.8})$$

hence local asymptotic stability follows. After proving the local asymptotic stability, the next step is to prove the local finite-time convergence of the closed-loop dynamics which could be done by using the Lemma's 2.6 and 2.9. The closed-loop system given by (2.55) and (2.59) is represented in state-space form by selecting the states  $x_1 = e_r$ ,  $x_2 = \dot{e}_r$ ,  $x_3 = \epsilon_{de}$ ,  $x_4 = \dot{\epsilon}_{de}$  and  $x = [x_1^T x_2^T x_3^T x_4^T]^T$  as follows,

$$\dot{x}_1 = x_2 \quad (\text{A.9})$$

$$\dot{x}_2 = M_{d,r}^{-1} \left( -\bar{K}_{d,r} \text{Sig}(x_1)^{\alpha_1} - B_{d,r} \text{Sig}(x_2)^{\alpha_2} - K_e x_1 \right) \quad (\text{A.10})$$

$$\dot{x}_3 = x_4 \quad (\text{A.11})$$

$$\dot{x}_4 = M_{d,\phi}^{-1} \left( -K_{d,\phi} \text{Sig}(x_3)^{\alpha_1} - B_{d,\phi} \text{Sig}(x_4)^{\alpha_2} \right) \quad (\text{A.12})$$

which in accordance with Lemma 2.9 can be rewritten as,

$$\dot{x} = f(x) + \hat{f}(x) \quad (\text{A.13})$$

where

$$f(x) = \begin{bmatrix} f_1(x) \\ f_2(x) \\ f_3(x) \\ f_4(x) \end{bmatrix} = \begin{bmatrix} x_2 \\ M_{d,r}^{-1} \left( -\bar{K}_{d,r} \text{Sig}(x_1)^{\alpha_1} - B_{d,r} \text{Sig}(x_2)^{\alpha_2} \right) \\ x_4 \\ M_{d,\phi}^{-1} \left( -K_{d,\phi} \text{Sig}(x_3)^{\alpha_1} - B_{d,\phi} \text{Sig}(x_4)^{\alpha_2} \right) \end{bmatrix}, \quad (\text{A.14})$$

$$\hat{f}(x) = \begin{bmatrix} \hat{f}_1(x) \\ \hat{f}_2(x) \\ \hat{f}_3(x) \\ \hat{f}_4(x) \end{bmatrix} = \begin{bmatrix} 0 \\ -M_{d,r}^{-1} K_e x_1 \\ 0 \\ 0 \end{bmatrix} \quad (\text{A.15})$$

are the homogeneous part and the perturbation which satisfies  $\widehat{f}(0) = 0$ , respectively. Using the Definition 2.3, the dilation mapping for the system is given by

$$\Delta_\lambda^r(x) = [\lambda^{r_{11}}x_{11}, \lambda^{r_{12}}x_{12}, \lambda^{r_{13}}x_{13}, \lambda^{r_{21}}x_{21}, \lambda^{r_{22}}x_{22}, \lambda^{r_{23}}x_{23}, \lambda^{r_{31}}x_{31}, \lambda^{r_{32}}x_{32}, \lambda^{r_{33}}x_{33}, \lambda^{r_{41}}x_{41}, \lambda^{r_{42}}x_{42}, \lambda^{r_{43}}x_{43}]^T \quad (\text{A.16})$$

which is used to investigate the homogeneity of the vectorfield  $f(x)$  by writing,

$$f_1(\Delta_\lambda^r(x)) = \begin{bmatrix} \lambda^{r_{21}}x_{21} \\ \lambda^{r_{22}}x_{22} \\ \lambda^{r_{23}}x_{23} \end{bmatrix} = \begin{bmatrix} \lambda^{\kappa+r_{11}}x_{21} \\ \lambda^{\kappa+r_{12}}x_{22} \\ \lambda^{\kappa+r_{13}}x_{23} \end{bmatrix} \quad (\text{A.17})$$

$$\begin{aligned} f_2(\Delta_\lambda^r(x)) &= \begin{bmatrix} (-b_{d,n}\lambda^{r_{21}\alpha_2}\text{sig}(x_{21})^{\alpha_2} - k_{f,r}k_e^{\alpha_1}\lambda^{r_{11}\alpha_1}\text{sig}(x_{11})^{\alpha_1})/m_{d,n} \\ (-b_{d,t}\lambda^{r_{22}\alpha_2}\text{sig}(x_{22})^{\alpha_2} - k_{d,t}\lambda^{r_{12}\alpha_1}\text{sig}(x_{12})^{\alpha_1})/m_{d,t} \\ (-b_{d,t}\lambda^{r_{23}\alpha_2}\text{sig}(x_{23})^{\alpha_2} - k_{d,t}\lambda^{r_{13}\alpha_1}\text{sig}(x_{13})^{\alpha_1})/m_{d,t} \end{bmatrix} \\ &= \begin{bmatrix} \lambda^{\kappa+r_{21}}(-b_{d,n}\text{sig}(x_{21})^{\alpha_2} - k_{f,r}k_e^{\alpha_1}\text{sig}(x_{11})^{\alpha_1})/m_{d,n} \\ \lambda^{\kappa+r_{22}}(-b_{d,t}\text{sig}(x_{22})^{\alpha_2} - k_{d,t}\text{sig}(x_{12})^{\alpha_1})/m_{d,t} \\ \lambda^{\kappa+r_{23}}(-b_{d,t}\text{sig}(x_{23})^{\alpha_2} - k_{d,t}\text{sig}(x_{13})^{\alpha_1})/m_{d,t} \end{bmatrix} \end{aligned} \quad (\text{A.18})$$

$$f_3(\Delta_\lambda^r(x)) = \begin{bmatrix} \lambda^{r_{41}}x_{41} \\ \lambda^{r_{42}}x_{42} \\ \lambda^{r_{43}}x_{43} \end{bmatrix} = \begin{bmatrix} \lambda^{\kappa+r_{31}}x_{41} \\ \lambda^{\kappa+r_{32}}x_{42} \\ \lambda^{\kappa+r_{33}}x_{43} \end{bmatrix} \quad (\text{A.19})$$

$$\begin{aligned} f_4(\Delta_\lambda^r(x)) &= \begin{bmatrix} (-b_{d,\phi}\lambda^{r_{41}\alpha_2}\text{sig}(x_{41})^{\alpha_2} - k_{d,\phi}\lambda^{r_{31}\alpha_1}\text{sig}(x_{31})^{\alpha_1})/m_{d,\phi} \\ (-b_{d,\phi}\lambda^{r_{42}\alpha_2}\text{sig}(x_{42})^{\alpha_2} - k_{d,\phi}\lambda^{r_{32}\alpha_1}\text{sig}(x_{32})^{\alpha_1})/m_{d,\phi} \\ (-b_{d,\phi}\lambda^{r_{43}\alpha_2}\text{sig}(x_{43})^{\alpha_2} - k_{d,\phi}\lambda^{r_{33}\alpha_1}\text{sig}(x_{33})^{\alpha_1})/m_{d,\phi} \end{bmatrix} \\ &= \begin{bmatrix} \lambda^{\kappa+r_{41}}(-b_{d,\phi}\text{sig}(x_{41})^{\alpha_2} - k_{d,\phi}\text{sig}(x_{31})^{\alpha_1})/m_{d,\phi} \\ \lambda^{\kappa+r_{42}}(-b_{d,\phi}\text{sig}(x_{42})^{\alpha_2} - k_{d,\phi}\text{sig}(x_{32})^{\alpha_1})/m_{d,\phi} \\ \lambda^{\kappa+r_{43}}(-b_{d,\phi}\text{sig}(x_{43})^{\alpha_2} - k_{d,\phi}\text{sig}(x_{33})^{\alpha_1})/m_{d,\phi} \end{bmatrix} \end{aligned} \quad (\text{A.20})$$

from which the following

$$\begin{aligned} r_{2i} &= \kappa + r_{1i}, & r_{2i}\alpha_2 &= r_{1i}\alpha_1 = \kappa + r_{2i}, \\ r_{4i} &= \kappa + r_{3i}, & r_{4i}\alpha_2 &= r_{3i}\alpha_1 = \kappa + r_{4i}, \end{aligned} \quad \text{for } i = 1, 2, 3 \quad (\text{A.21})$$

can be deduced. From here, it can be found that the system  $\dot{x} = f(x)$  is homogeneous of degree  $\kappa = \alpha_1 - 1 < 0$ , w.r.t. the dilation (A.16) with  $r_{1i} = r_{3i} = 2$  and  $r_{2i} = r_{4i} = \alpha_1 + 1$  for  $i = 1, 2, 3$ . In order to prove finite-time stability, according to Lemma 2.6 the asymptotic stability of the system  $\dot{x} = f(x)$  with (A.14) should be investigated. This is done using the following Lyapunov function candidate,

$$V_2 = \frac{1}{2}x_2^T x_2 + \frac{1}{\alpha_1 + 1} \sum_{i=1}^3 \frac{\bar{k}_{d,r,i}}{m_{d,r,i}} |x_{1,i}|^{\alpha_1+1} + \frac{1}{2}x_4^T x_4 + \frac{1}{\alpha_1 + 1} \sum_{i=1}^3 \frac{k_{d,\phi,i}}{m_{d,\phi,i}} |x_{3,i}|^{\alpha_1+1} \quad (\text{A.22})$$

which satisfies  $V_2(0) = 0$ . The time derivative of (A.22) is calculated as,

$$\dot{V}_2 = -x_2^T M_{d,r}^{-1} B_{d,r} \text{Sig}(x_2)^{\alpha_2} - x_4^T M_{d,\phi}^{-1} B_{d,\phi} \text{Sig}(x_4)^{\alpha_2} \leq 0 \quad (\text{A.23})$$

$x_2, x_4 \rightarrow 0$  as  $t \rightarrow \infty$ . LaSalle's invariance principle is used to prove asymptotic stability. Let  $\Omega_2 \subset \mathcal{D}$  be a compact set that is positively invariant w.r.t.  $\dot{x} = f(x)$  and let the set  $\mathcal{E}_2 \subset \Omega_2$  be defined as  $\mathcal{E}_2 = \{x \in \Omega_2 \mid \dot{V}_2(x) = 0\}$ . It can be shown that the largest invariant set in  $\mathcal{E}_2$  is given by  $\mathcal{M}_2 = \{x \in \Omega_2 \mid x = 0\}$  as follows. It can be realized that when  $x_2(t) \equiv 0$  and  $x_4(t) \equiv 0$ , then  $\dot{x}_2(t) \equiv 0$  and  $\dot{x}_4(t) \equiv 0$ . When this is substituted into  $\dot{x} = f(x)$  with  $f(x)$  as in (A.14), we obtain,

$$\bar{K}_{d,r} \text{Sig}(x_1)^{\alpha_1} = 0, \quad K_{d,\phi} \text{Sig}(x_3)^{\alpha_1} = 0 \quad (\text{A.24})$$

from where it can be seen that  $x_1 = 0$  and  $x_3 = 0$  is the unique solution. Thus,  $x = 0$  is the only solution contained in the set  $\Omega_2$ , and it is locally asymptotically stable. According to Lemma 2.6, the system  $\dot{x} = f(x)$  with (A.14) is finite-time stable. The last item that should be checked in Lemma 2.9 is whether the perturbed part  $\hat{f}(x)$  satisfies (2.10). This is done by calculating the following limits,

$$\lim_{\lambda \rightarrow 0} \frac{\hat{f}_{1i}(\Delta_\lambda^r(x))}{\lambda^{\kappa+r_{1i}}} = 0, \quad \text{for } i = 1, 2, 3 \quad (\text{A.25})$$

$$\lim_{\lambda \rightarrow 0} \frac{\hat{f}_{21}(\Delta_\lambda^r(x))}{\lambda^{\kappa+r_{21}}} = \lim_{\lambda \rightarrow 0} \frac{-k_e \lambda^{r_{11}} x_{11}}{m_{d,r,n} \lambda^{\kappa+r_{21}}} = -\frac{k_e x_{11}}{m_{d,r,n}} \lim_{\lambda \rightarrow 0} \lambda^{2-2\alpha_1} = 0 \quad (\text{A.26})$$

$$\lim_{\lambda \rightarrow 0} \frac{\hat{f}_{2i}(\Delta_\lambda^r(x))}{\lambda^{\kappa+r_{2i}}} = 0, \quad \text{for } i = 2, 3 \quad (\text{A.27})$$

$$\lim_{\lambda \rightarrow 0} \frac{\hat{f}_{3i}(\Delta_\lambda^r(x))}{\lambda^{\kappa+r_{3i}}} = 0, \quad \text{for } i = 1, 2, 3 \quad (\text{A.28})$$

$$\lim_{\lambda \rightarrow 0} \frac{\hat{f}_{4i}(\Delta_\lambda^r(x))}{\lambda^{\kappa+r_{4i}}} = 0, \quad \text{for } i = 1, 2, 3 \quad (\text{A.29})$$

since  $0 < \alpha_1 < 1$ . Thus, local finite-time stability of the closed-loop system is proven.

## A.2 Derivation of the bound $\rho(x, t)$ in (2.90)

The norm bound on the uncertainty term (2.75) can be computed as follows,

$$\begin{aligned} \|\tilde{\Xi}\| &\leq \|\mathfrak{T} M_c^{-1}(\theta) \delta M_c(\theta) u\| + \|\mathfrak{T} M_c^{-1}(\theta) \delta C_c(\theta, \dot{\theta}) v\| + \|\mathfrak{T} M_c^{-1}(\theta) \delta F_f(\theta, \dot{\theta})\| \\ &\quad + \|\mathfrak{T} M_c^{-1}(\theta) \delta g_c(\theta)\| \end{aligned} \quad (\text{A.30})$$

which using the Property 2.18 can be rewritten as

$$\|\tilde{\Xi}\| \leq \|\mathfrak{T}\| \|M_c^{-1}(\theta) \delta M_c(\theta) u\| + \|\mathfrak{T}\| \|M_c^{-1}(\theta) \delta C_c(\theta, \dot{\theta}) v\|$$

$$\begin{aligned}
& + \|\mathfrak{T}\| \left\| M_c^{-1}(\theta) \delta F_f(\theta, \dot{\theta}) \right\| + \|\mathfrak{T}\| \left\| M_c^{-1}(\theta) \delta g_c(\theta) \right\| \\
& \leq \left\| M_c^{-1}(\theta) \delta M_c(\theta) u \right\| + \left\| M_c^{-1}(\theta) \delta C_c(\theta, \dot{\theta}) v \right\| + \left\| M_c^{-1}(\theta) \delta F_f(\theta, \dot{\theta}) \right\| \\
& + \left\| M_c^{-1}(\theta) \delta g_c(\theta) \right\| \tag{A.31}
\end{aligned}$$

where a norm bound for each term on the right-hand side is computed using aforementioned properties and remarks. The bound on the first term is given as

$$\left\| M_c^{-1}(\theta) \delta M_c(\theta) u \right\| \leq \max(J_{r,M}, 1) \alpha_M \tilde{J}_M \tilde{J}_{r,M} \|u\|. \tag{A.32}$$

By denoting  $v_d = [\dot{r}_d^T \ \omega_d^T]^T$  and using the matrices defined for (2.74) and Property 2.18 and substituting (2.53) and (2.56), (A.32) is written as

$$\begin{aligned}
& \leq \max(J_{r,M}, 1) \alpha_M \tilde{J}_M \tilde{J}_{r,M} \\
& \cdot \left\| \mathfrak{T}^{-1} \left( \mathfrak{T}^T \dot{v}_d + \dot{\mathfrak{T}}^T v_d - \dot{\mathfrak{T}} v + M_d^{-1} (B_d \text{Sig}(\dot{e})^{\alpha_2} + K_d \text{Sig}(e)^{\alpha_1} + K_E e) \right) \right\| \\
& \leq \max(J_{r,M}, 1) \alpha_M \tilde{J}_M \tilde{J}_{r,M} \left\| \mathfrak{T}^{-1} \right\| \left( \|\dot{v}_d\| + \|\dot{\mathfrak{T}}\| (\|v_d\| + \|v\|) + 6^{\frac{1-\alpha_2}{2}} \right. \\
& \cdot \max_{i=1,\dots,6} \left( \frac{b_{d,i}}{m_{d,i}} \right) \|\dot{e}\|^{\alpha_2} + 6^{\frac{1-\alpha_1}{2}} \max_{i=1,\dots,6} \left( \frac{k_{d,i}}{m_{d,i}} \right) \|e\|^{\alpha_1} \\
& \left. + k_{f,r} (k_e)^{\alpha_1} \max_{i=1,\dots,6} \left( \frac{1}{m_{d,i}} \right) \|e\| \right) \tag{A.33}
\end{aligned}$$

where the inequality (2.11) in Lemma 2.11 is used. By rewriting  $v$ ,

$$v = \begin{bmatrix} \dot{r}_e \\ \omega_e \end{bmatrix} = \begin{bmatrix} \dot{r}_d - \dot{e}_r \\ 2E^{-T} \left( \frac{1}{2} E \omega_d - \dot{e}_{de} \right) \end{bmatrix} = \mathfrak{T}^{-1} (\mathfrak{T}^T v_d - \dot{e}) \tag{A.34}$$

where the error variables  $e$  and  $\dot{e}$  are used, we obtain

$$\begin{aligned}
& \leq \max(J_{r,M}, 1) \alpha_M \tilde{J}_M \tilde{J}_{r,M} \left\| \mathfrak{T}^{-1} \right\| \left( \sqrt{\mathcal{A}_M^2 + \mathfrak{K}_M^2} + \|\dot{\mathfrak{T}}\| \left( \sqrt{\mathcal{V}_M^2 + \Omega_M^2} \right. \right. \\
& \left. \left. + \|\mathfrak{T}^{-1}\| \left( \sqrt{\mathcal{V}_M^2 + \Omega_M^2} + \|e\| \right) \right) + 6^{\frac{1-\alpha_2}{2}} \max_{i=1,\dots,6} \left( \frac{b_{d,i}}{m_{d,i}} \right) \|\dot{e}\|^{\alpha_2} \right. \\
& \left. + 6^{\frac{1-\alpha_1}{2}} \max_{i=1,\dots,6} \left( \frac{k_{d,i}}{m_{d,i}} \right) \|e\|^{\alpha_1} + k_{f,r} (k_e)^{\alpha_1} \max_{i=1,\dots,6} \left( \frac{1}{m_{d,i}} \right) \|e\| \right). \tag{A.35}
\end{aligned}$$

The bound on the second term of (A.31) is obtained using Property 2.18 and (A.34)

$$\begin{aligned}
& \left\| M_c^{-1}(\theta) \delta C_c(\theta, \dot{\theta}) v \right\| \\
& = \left\| (\mathbb{J}^{-T}(\theta) M(\theta) \mathbb{J}^{-1}(\theta))^{-1} \mathbb{J}^{-T}(\theta) \left( \delta C(\theta, \dot{\theta}) - \delta M(\theta) \mathbb{J}^{-1}(\theta) \dot{\mathbb{J}}(\theta) \right) \mathbb{J}^{-1}(\theta) v \right\| \\
& = \left\| \mathbb{J}(\theta) M(\theta) \left( \delta C(\theta, \dot{\theta}) - \delta M(\theta) \mathbb{J}^{-1}(\theta) \dot{\mathbb{J}}(\theta) \right) \mathbb{J}^{-1}(\theta) v \right\| \\
& \leq \left\| \mathbb{J}(\theta) M(\theta) \delta C(\theta, \dot{\theta}) \mathbb{J}^{-1}(\theta) v \right\| + \left\| \mathbb{J}(\theta) M(\theta) \delta M(\theta) \mathbb{J}^{-1}(\theta) \dot{\mathbb{J}}(\theta) \mathbb{J}^{-1}(\theta) v \right\|. \tag{A.36}
\end{aligned}$$

By using (2.39) and (2.40), (A.36) is rewritten as

$$\begin{aligned}
&\leq \max(J_{r,M}, 1) J_M M_M C_M \|\mathbb{J}^{-1}(\theta)v\|^2 + \\
&\quad \max(J_{r,M}, 1) J_M \alpha_M \tilde{J}_M \tilde{J}_{r,M} (\bar{J}_{r,M} J_M + \max(J_{r,M}, 1) \bar{J}_M) \|\mathbb{J}^{-1}(\theta)v\|^2 \\
&\leq \max(J_{r,M}, 1) J_M \left( M_M C_M + \alpha_M \tilde{J}_M \tilde{J}_{r,M} (\bar{J}_{r,M} J_M \right. \\
&\quad \left. + \max(J_{r,M}, 1) \bar{J}_M) \right) \tilde{J}_M \tilde{J}_{r,M} \|v\|^2 \\
&\leq \max(J_{r,M}, 1) J_M \left( M_M C_M + \alpha_M \tilde{J}_M \tilde{J}_{r,M} (\bar{J}_{r,M} J_M + \max(J_{r,M}, 1) \bar{J}_M) \right) \cdot \\
&\quad \cdot \tilde{J}_M \tilde{J}_{r,M} \|\mathfrak{I}^{-1}\|^2 \left( \mathcal{V}_M^2 + \Omega_M^2 + 2\sqrt{\mathcal{V}_M^2 + \Omega_M^2} \|e\| + \|e\|^2 \right) \tag{A.37}
\end{aligned}$$

where (A.34) is used. The bound on the third term is computed as

$$\begin{aligned}
\|M_c^{-1}(\theta)\delta F_f(\theta, \dot{\theta})\| &\leq \|(\mathbb{J}^{-T}(\theta)M(\theta)\mathbb{J}^{-1}(\theta))^{-1} \mathbb{J}^{-T}(\theta)\delta\tau_f(\dot{\theta})\| \\
&\leq \|\mathbb{J}(\theta)\| \|M^{-1}(\theta)\| \|\delta\tau_f(\dot{\theta})\| \\
&\leq \max(J_{r,M}, 1) \frac{J_M}{M_m} \left( \mathcal{F}_1 + \hat{\mathcal{F}}_1 + (\mathcal{F}_2 + \hat{\mathcal{F}}_2) \|\dot{\theta}\| \right) \\
&\leq \max(J_{r,M}, 1) \frac{J_M}{M_m} \left( \mathcal{F}_1 + \hat{\mathcal{F}}_1 + (\mathcal{F}_2 + \hat{\mathcal{F}}_2) \|\mathbb{J}^{-1}(\theta)v\| \right) \\
&\leq \max(J_{r,M}, 1) \frac{J_M}{M_m} \left( \mathcal{F}_1 + \hat{\mathcal{F}}_1 + (\mathcal{F}_2 + \hat{\mathcal{F}}_2) \tilde{J}_M \tilde{J}_{r,M} \cdot \right. \\
&\quad \left. \cdot \|\mathfrak{I}^{-1}\| \left( \sqrt{\mathcal{V}_M^2 + \Omega_M^2} + \|e\| \right) \right) \tag{A.38}
\end{aligned}$$

where (A.34) is used. The bound on the last term is obtained using Property 2.17

$$\begin{aligned}
\|M_c^{-1}(\theta)\delta g_c(\theta)\| &\leq \|(\mathbb{J}^{-T}(\theta)M(\theta)\mathbb{J}^{-1}(\theta))^{-1} \mathbb{J}^{-T}(\theta)\delta g(\theta)\| \\
&\leq \|\mathbb{J}(\theta)\| \|M^{-1}(\theta)\| \|\delta g(\theta)\| \leq \max(J_{r,M}, 1) \frac{J_M}{M_m} \left( G_M + \hat{G}_M \right). \tag{A.39}
\end{aligned}$$

By using (A.35), (A.37), (A.38) and (A.39) the bound  $\varrho(x, t)$  is obtained as

$$\|\tilde{\Xi}\| \leq \varrho(x, t) = \rho_4 \|x\|^2 + \rho_3 \|x\| + \rho_2 \|x\|^{\alpha_2} + \rho_1 \|x\|^{\alpha_1} + \rho_0 \tag{A.40}$$

where  $\rho_0, \rho_1, \rho_2, \rho_3$  and  $\rho_4$  are given by,

$$\begin{aligned}
\rho_0 &= \max(J_{r,M}, 1) \alpha_M \tilde{J}_M \tilde{J}_{r,M} \|\mathfrak{I}^{-1}\| \left( \sqrt{\mathcal{A}_M^2 + \mathfrak{N}_M^2} + \|\dot{\mathfrak{I}}\| \sqrt{\mathcal{V}_M^2 + \Omega_M^2} (1 \right. \\
&\quad \left. + \|\mathfrak{I}^{-1}\|) \right) + \max(J_{r,M}, 1) \frac{J_M}{M_m} \left( G_M + \hat{G}_M \right) + \max(J_{r,M}, 1) \frac{J_M}{M_m} \left( \mathcal{F}_1 + \hat{\mathcal{F}}_1 \right)
\end{aligned}$$

$$\begin{aligned}
& + \left( \mathcal{F}_2 + \widehat{\mathcal{F}}_2 \right) \tilde{J}_M \tilde{J}_{r,M} \cdot \|\mathfrak{T}^{-1}\| \sqrt{\mathcal{V}_M^2 + \Omega_M^2} \\
& + \max(J_{r,M}, 1) J_M \left( M_M C_M + \alpha_M \tilde{J}_M \tilde{J}_{r,M} (\bar{J}_{r,M} J_M \right. \\
& \quad \left. + \max(J_{r,M}, 1) \bar{J}_M) \right) \tilde{J}_M \tilde{J}_{r,M} \|\mathfrak{T}^{-1}\|^2 \mathcal{V}_M^2 + \Omega_M^2
\end{aligned} \tag{A.41}$$

$$\rho_1 = 6^{\frac{1-\alpha_1}{2}} \max(J_{r,M}, 1) \alpha_M \tilde{J}_M \tilde{J}_{r,M} \|\mathfrak{T}^{-1}\| \max_{i=1,\dots,6} \left( \frac{k_{d,i}}{m_{d,i}} \right) \tag{A.42}$$

$$\rho_2 = 6^{\frac{1-\alpha_2}{2}} \max(J_{r,M}, 1) \alpha_M \tilde{J}_M \tilde{J}_{r,M} \|\mathfrak{T}^{-1}\| \max_{i=1,\dots,6} \left( \frac{b_{d,i}}{m_{d,i}} \right) \tag{A.43}$$

$$\begin{aligned}
\rho_3 = & \max(J_{r,M}, 1) \alpha_M \tilde{J}_M \tilde{J}_{r,M} \|\mathfrak{T}^{-1}\| \left( \|\mathfrak{I}\| \|\mathfrak{T}^{-1}\| + k_{f,r} (k_e)^{\alpha_1} \max_{i=1,\dots,6} \left( \frac{1}{m_{d,i}} \right) \right) \\
& + \max(J_{r,M}, 1) \frac{J_M}{M_m} \left( \mathcal{F}_1 + \widehat{\mathcal{F}}_1 + \left( \mathcal{F}_2 + \widehat{\mathcal{F}}_2 \right) \tilde{J}_M \tilde{J}_{r,M} \|\mathfrak{T}^{-1}\| \right) \\
& + 2 \max(J_{r,M}, 1) J_M \left( M_M C_M + \alpha_M \tilde{J}_M \tilde{J}_{r,M} (\bar{J}_{r,M} J_M \right. \\
& \quad \left. + \max(J_{r,M}, 1) \bar{J}_M) \right) \tilde{J}_M \tilde{J}_{r,M} \|\mathfrak{T}^{-1}\|^2 \sqrt{\mathcal{V}_M^2 + \Omega_M^2}
\end{aligned} \tag{A.44}$$

$$\begin{aligned}
\rho_4 = & \max(J_{r,M}, 1) J_M \left( M_M C_M + \alpha_M \tilde{J}_M \tilde{J}_{r,M} (\bar{J}_{r,M} J_M \right. \\
& \quad \left. + \max(J_{r,M}, 1) \bar{J}_M) \right) \tilde{J}_M \tilde{J}_{r,M} \|\mathfrak{T}^{-1}\|^2.
\end{aligned} \tag{A.45}$$

### A.3 Investigation of a strict Lyapunov function for (2.97)

The positive definiteness and radial unboundedness of (2.98) can be shown either using Young's inequality or Lemma 2.8 that is justified by the following remark.

**Remark A.1.** Let  $S = \{x \in \mathbb{R}^n : \|x\|_{r,m} = 1\}$ , where  $\|x\|_{r,m}$  is the homogeneous norm according to the Definition 2.5, which may be viewed as a generalized unit sphere. Note that equations or inequalities consisting of homogeneous (w.r.t. the same dilations) functions are valid if and only if they are valid on  $S$ . This is a crucial property facilitating the analysis of homogeneous systems (see [68]).

It can be realized that the homogeneous norm for the system (2.97) is given as,

$$\|x\|_{r,m} = \left( |x_1|^{\frac{m}{r_1}} + |x_2|^{\frac{m}{r_2}} \right)^{\frac{1}{m}} \tag{A.46}$$

where  $m > \max\{r_1, r_2\} = \max\left\{\frac{2}{1+\alpha_1}, 1\right\} = \frac{2}{1+\alpha_1}$  with  $r_1 = 2$ ,  $r_2 = 1 + \alpha_1$  being the weights of the states. Denote  $\xi_1 = \text{sig}(x_1)^{\frac{1+\alpha_1}{2}}$  and  $\xi_2 = x_2$ , then the following

can be obtained from (2.98),

$$\begin{aligned} V(\xi_1, \xi_2) &= \underbrace{\begin{bmatrix} \text{sig}(\xi_1)^{\frac{3+\alpha_1}{2(1+\alpha_1)}} \\ \text{sig}(\xi_2)^{\frac{3+\alpha_1}{2(1+\alpha_1)}} \end{bmatrix}^T}_{\zeta^T} \underbrace{\begin{bmatrix} \frac{2}{3+\alpha_1}c_1 & 0 \\ 0 & \frac{1+\alpha_1}{3+\alpha_1}c_2 \end{bmatrix}}_P \underbrace{\begin{bmatrix} \text{sig}(\xi_1)^{\frac{3+\alpha_1}{2(1+\alpha_1)}} \\ \text{sig}(\xi_2)^{\frac{3+\alpha_1}{2(1+\alpha_1)}} \end{bmatrix}}_{\zeta} + c_3 \underbrace{\text{sig}(\xi_1)^{\frac{2}{1+\alpha_1}} \xi_2}_{f_1(\xi_1, \xi_2)} \\ &= \zeta^T P \zeta + c_3 f_1(\xi_1, \xi_2) \end{aligned} \quad (\text{A.47})$$

and the values it takes on the circle  $\mathbb{S} = \{(\xi_1, \xi_2) : \xi_1^2 + \xi_2^2 = 1\}$  (obtained by setting  $m = 2$  in (A.46)) can be investigated. Then, Lemma 2.11 is used to upper and lower bound the first term of (A.47). Using Lemma 2.8 and by taking  $y_1 = \text{sig}(\xi_1)^{\frac{3+\alpha_1}{1+\alpha_1}}$ ,  $y_2 = \text{sig}(\xi_2)^{\frac{3+\alpha_1}{1+\alpha_1}}$  and  $m = \frac{3+\alpha_1}{2(1+\alpha_1)}$ , the following can be obtained,

$$\left( |\xi_1|^{\frac{3+\alpha_1}{1+\alpha_1}} + |\xi_2|^{\frac{3+\alpha_1}{1+\alpha_1}} \right)^{\frac{2(1+\alpha_1)}{3+\alpha_1}} \leq |\xi_1|^2 + |\xi_2|^2 \leq 2^{1-\frac{2(1+\alpha_1)}{3+\alpha_1}} \left( |\xi_1|^{\frac{3+\alpha_1}{1+\alpha_1}} + |\xi_2|^{\frac{3+\alpha_1}{1+\alpha_1}} \right)^{\frac{2(1+\alpha_1)}{3+\alpha_1}} \quad (\text{A.48})$$

which can be used to upper and lower bound the first term of (A.47) as,

$$\lambda_{\min}(P) 2^{\frac{\alpha_1-1}{2(1+\alpha_1)}} \leq \lambda_{\min}(P) \zeta^T \zeta \leq \zeta^T P \zeta \leq \lambda_{\max}(P) \zeta^T \zeta \leq \lambda_{\max}(P) \quad (\text{A.49})$$

where  $\lambda_{\min}(P) = \min\left(\frac{2}{3+\alpha_1}c_1, \frac{1+\alpha_1}{3+\alpha_1}c_2\right)$  and  $\lambda_{\max}(P) = \max\left(\frac{2}{3+\alpha_1}c_1, \frac{1+\alpha_1}{3+\alpha_1}c_2\right)$ . The upper and lower bounds on the second term of (A.47) are obtained with the help of Lemma 2.23 in Section 2.6.2 similar to Lemma 1 in [15]. Consequently, upper and lower bounds on the circle,  $\mathbb{S} = \{(\xi_1, \xi_2) : \xi_1^2 + \xi_2^2 = 1\}$  for the candidate Lyapunov function are obtained using the inequalities (A.49) and (2.100). The time derivative of the Lyapunov function,  $V(x_1, x_2)$  given by (2.98), along the solutions of (2.97) can be computed as,

$$\begin{aligned} \dot{V}(x) &= -c_3 l_1 |x_1|^{1+\alpha_1} - (c_2 l_2 - c_3) x_2^2 + c_1 x_2 \text{sig}(x_1)^{\frac{1+\alpha_1}{2}} - c_2 l_1 \text{sig}(x_1)^{\alpha_1} \text{sig}(x_2)^{\frac{2}{1+\alpha_1}} \\ &\quad - c_3 l_2 x_1 \text{sig}(x_2)^{\frac{2\alpha_1}{1+\alpha_1}} \end{aligned} \quad (\text{A.50})$$

which can be rewritten as follows,

$$\begin{aligned} \dot{V}(\xi_1, \xi_2) &= \underbrace{\begin{bmatrix} \xi_1 \\ \xi_2 \end{bmatrix}^T}_{\xi^T} \underbrace{\begin{bmatrix} -c_3 l_1 & \frac{c_1}{2} \\ \frac{c_1}{2} & -(c_2 l_2 - c_3) \end{bmatrix}}_Q \underbrace{\begin{bmatrix} \xi_1 \\ \xi_2 \end{bmatrix}}_{\xi} - c_2 l_1 \underbrace{\text{sig}(\xi_1)^{\frac{2\alpha_1}{1+\alpha_1}} \text{sig}(\xi_2)^{\frac{2}{1+\alpha_1}}}_{f_2(\xi_1, \xi_2)} \\ &\quad - c_3 l_2 \underbrace{\text{sig}(x_1)^{\frac{2}{1+\alpha_1}} \text{sig}(\xi_2)^{\frac{2\alpha_1}{1+\alpha_1}}}_{f_3(\xi_1, \xi_2)} \end{aligned} \quad (\text{A.51})$$



where the eigenvalues of the matrix  $Q$  given in (A.51) are given as,

$$\begin{aligned}\lambda_{\min}(Q) &= \frac{-(c_3l_1 + c_2l_2 - c_3) - \sqrt{(c_3l_1 + c_2l_2 - c_3)^2 - 4\left((c_2l_2 - c_3) - \frac{c_1^2}{4}\right)}}{2} \\ &= \frac{-(c_3l_1 + c_2l_2 - c_3) - \sqrt{(c_2l_2 - c_3l_1 - c_3)^2 + c_1^2}}{2}\end{aligned}\quad (\text{A.52})$$

$$\begin{aligned}\lambda_{\max}(Q) &= \frac{-(c_3l_1 + c_2l_2 - c_3) + \sqrt{(c_3l_1 + c_2l_2 - c_3)^2 - 4\left((c_2l_2 - c_3) - \frac{c_1^2}{4}\right)}}{2} \\ &= \frac{-(c_3l_1 + c_2l_2 - c_3) + \sqrt{(c_2l_2 - c_3l_1 - c_3)^2 + c_1^2}}{2}\end{aligned}\quad (\text{A.53})$$

which are negative if,

$$-c_3l_1 - (c_2l_2 - c_3) < 0, \quad c_3l_1(c_2l_2 - c_3) - \frac{1}{4}c_1^2 > 0 \quad (\text{A.54})$$

The bounds on the second and third terms in (A.50) on the circle can be obtained with the help of the Lemma 2.24. Consequently, the values the time derivative of (2.98) given by (A.50) takes on the circle  $\mathbb{S} = \{(\xi_1, \xi_2) : \xi_1^2 + \xi_2^2 = 1\}$  vary between

$$\begin{aligned}-\frac{(c_3l_1 + c_2l_2 - c_3) - \sqrt{(c_2l_2 - c_3l_1 - c_3)^2 + c_1^2} - 2M_2(c_2l_1 + c_3l_2)}{2} &\leq \dot{V}(\xi_1, \xi_2) \leq \\ \frac{-(c_3l_1 + c_2l_2 - c_3) + \sqrt{(c_2l_2 - c_3l_1 - c_3)^2 + c_1^2} + 2M_2(c_2l_1 + c_3l_2)}{2}\end{aligned}\quad (\text{A.55})$$

where lower bound can easily be made negative, however, the same is not true for upper bound. Thus, the function (2.98) proposed in [71] is not a strict Lyapunov function. The second candidate for strict Lyapunov function is proposed in [15] as given in (2.99). The time derivative of the function (2.99) is computed as,

$$\begin{aligned}\dot{V}(x_1, x_2) &= c_1x_1\dot{x}_1 + c_2\text{sig}(x_2)^{\frac{3-\alpha_1}{1+\alpha_1}}\dot{x}_2 + c_3\dot{x}_1\text{sig}(x_2)^{\frac{2-\alpha_1}{1+\alpha_1}} + c_3x_1\dot{x}_2|x_2|^{\frac{1-\alpha_1}{1+\alpha_1}} \\ &= |x_2|^{\frac{1-\alpha_1}{1+\alpha_1}} \left[ -c_3l_1|x_1|^{1+\alpha_1} - (c_2l_2 - c_3)x_2^2 + (c_1 - c_3l_2)x_1\text{sig}(x_2)^{\frac{2\alpha_1}{1+\alpha_1}} \right. \\ &\quad \left. - c_1l_1\text{sig}(x_1)^{\alpha_1}\text{sig}(x_2)^{\frac{2}{1+\alpha_1}} \right]\end{aligned}\quad (\text{A.56})$$

for which conditions are derived on the control gains of the system (2.97) in [15] to conclude finite-time stability (see Theorem 4 of [15]). However, for  $(x_1, x_2) = (x_1^*, 0)$  the time derivative (A.56) becomes equal to 0. This means that it is negative semi-definite. Therefore, this cannot be a strict Lyapunov function either, since its time derivative should only be 0 when  $(x_1, x_2) = (0, 0)$ .

## A.4 Proof of Lemma 2.23

It can be realized that due to symmetry of the circle, the value of the function would be positive on the I<sup>st</sup> and III<sup>rd</sup> quadrants and negative on the II<sup>nd</sup> and IV<sup>th</sup>

quadrants. Therefore, it suffices to check only two quadrants, for example,  $I^{st}$  and  $II^{nd}$ . On the  $I^{st}$  quadrant both  $\xi_1, \xi_2 > 0$  and by taking  $\xi_2 = \sqrt{1 - \xi_1^2}$ , we obtain,

$$f_1(\xi_1) = \xi_1^{\frac{2}{1+\alpha_1}} \sqrt{1 - \xi_1^2} \quad (\text{A.57})$$

whose stationary points can be found by calculating its derivative as,

$$\begin{aligned} \frac{df_1}{d\xi_1} &= \frac{2}{1 + \alpha_1} \xi_1^{\frac{1-\alpha_1}{1+\alpha_1}} (1 - \xi_1^2)^{\frac{1}{2}} + \xi_1^{\frac{2}{1+\alpha_1}} \frac{(-2\xi_1)}{2(1 - \xi_1^2)^{\frac{1}{2}}} = 0 \\ &= \frac{\xi_1^{\frac{1-\alpha_1}{1+\alpha_1}}}{(1 - \xi_1^2)^{\frac{1}{2}}} \left( \frac{2}{1 + \alpha_1} (1 - \xi_1^2) - \xi_1^2 \right) = 0 \end{aligned} \quad (\text{A.58})$$

whose solutions are  $\xi_1^* = 0$  and  $\xi_1^* = \pm \sqrt{\frac{2}{3+\alpha_1}}$ . Since we are working on the  $I^{st}$  quadrant, we are interested in the solution  $\xi_1^* = \sqrt{\frac{2}{3+\alpha_1}}$ ,  $\xi_2^* = \sqrt{\frac{1+\alpha_1}{3+\alpha_1}}$  which leads to the maximum,  $f_1(\xi_1^*, \xi_2^*) = \left(\frac{2}{3+\alpha_1}\right)^{\frac{1}{1+\alpha_1}} \left(\frac{1+\alpha_1}{3+\alpha_1}\right)^{\frac{1}{2}}$ . On the  $II^{nd}$  quadrant,  $\xi_1 < 0$  and  $\xi_2 > 0$  and by taking  $\xi_2 = \sqrt{1 - \xi_1^2}$ , we obtain,

$$f_1(\xi_1) = -(-\xi_1)^{\frac{2}{1+\alpha_1}} \sqrt{1 - \xi_1^2} \quad (\text{A.59})$$

whose stationary points can be found by calculating its derivative as,

$$\begin{aligned} \frac{df_1}{d\xi_1} &= -\frac{2}{1 + \alpha_1} (-1) (-\xi_1)^{\frac{1-\alpha_1}{1+\alpha_1}} (1 - \xi_1^2)^{\frac{1}{2}} - (-\xi_1)^{\frac{2}{1+\alpha_1}} \frac{(-2\xi_1)}{2(1 - \xi_1^2)^{\frac{1}{2}}} = 0 \\ &= \frac{1}{(1 - \xi_1^2)^{\frac{1}{2}}} \left( \frac{2}{1 + \alpha_1} (-\xi_1)^{\frac{1-\alpha_1}{1+\alpha_1}} (1 - \xi_1^2) + (-\xi_1)^{\frac{2}{1+\alpha_1}} \xi_1 \right) = 0 \\ &= \frac{(-\xi_1)^{\frac{1-\alpha_1}{1+\alpha_1}}}{(1 - \xi_1^2)^{\frac{1}{2}}} \left( \frac{2}{1 + \alpha_1} (1 - \xi_1^2) - \xi_1^2 \right) = 0 \end{aligned} \quad (\text{A.60})$$

whose solutions are  $\xi_1^* = 0$  and  $\xi_1^* = \pm \sqrt{\frac{2}{3+\alpha_1}}$ . Since we are working in the  $II^{nd}$  quadrant, we are interested in the solution  $\xi_1^* = -\sqrt{\frac{2}{3+\alpha_1}}$ ,  $\xi_2^* = \sqrt{\frac{1+\alpha_1}{3+\alpha_1}}$  which leads to the minimum,  $f_1(\xi_1^*, \xi_2^*) = -\left(\frac{2}{3+\alpha_1}\right)^{\frac{1}{1+\alpha_1}} \left(\frac{1+\alpha_1}{3+\alpha_1}\right)^{\frac{1}{2}}$ .

## A.5 Proof of Lemma 2.24

The proof is similar to that of the Lemma 2.23 given in Appendix A.4.

# Appendix **B**

## Additional simulation and experimental results for hybrid impedance control with finite-time stability characteristics

### **B.1 Additional simulation results**

In this section, additional simulation results are presented in the case when the manipulator dynamics is perfectly known (i.e. no uncertainties) and actuator saturation is not included as mentioned in Section 2.7. This is done to confirm the theoretical results obtained in Chapter 2. The setpoint regulation and contact transition performance (i.e. when the manipulator is not in contact with the environment) of the hybrid impedance controller with finite-time stability characteristics are investigated. The end-effector is initially located at  $[0.17 \quad -0.55 \quad 0.014]^T$ . The results for the case of a linear hybrid impedance controller are also presented for comparison purposes (e.g. like in [20]). This can be achieved by setting the exponential powers in the feedback terms of (2.47) and (2.53) to  $\alpha_1 = 1$  and consequently  $\alpha_2 = 1$ . A constant desired contact force of  $f_{d,n} = -10$  [N] is used in the normal direction. The final desired quaternion for the rotational part of the closed-loop is selected randomly while satisfying the unit norm constraint. The effect of actuator saturation is also present in the simulation model where the numerical values of the limits are taken from [9]. All of the parameters for both control laws are selected the same as in Section 2.7. The initial value of the actual end-effector quaternion vector and the desired one are the same as in Section 2.7. The results are shown in Figure B.1 and Figure B.3 where the linear hybrid impedance controller is used and in Figure B.2 and B.4 where the finite-time stable hybrid impedance controller is used. It can be observed from Figure B.1 and Figure B.2 that perfect tracking (i.e. zero steady-state error) is achieved when there is no uncertainty in the manipulator dynamical model. Furthermore, the finite-time convergent controller converges faster compared to the linear one.

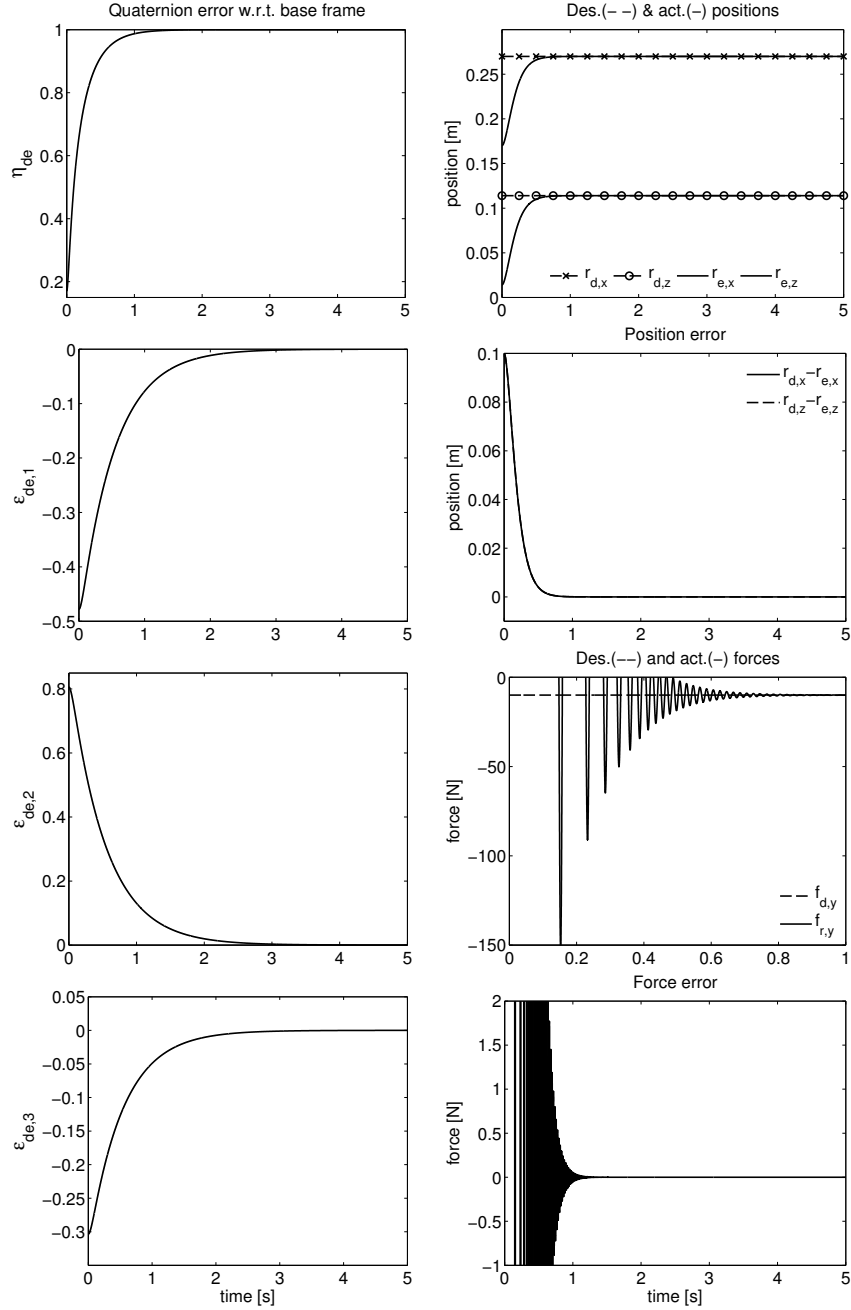


**Figure B.1** Quaternion error ( $\eta_{de}, \epsilon_{de,1}, \epsilon_{de,2}, \epsilon_{de,3}$ ) expressed w.r.t. base frame (left), desired  $r_{d,t}$  and actual  $r_{e,t}$  tangential end-effector positions (top right), and their difference (2<sup>nd</sup> from right), desired  $f_{d,n}$  and actual  $f_{r,n}$  normal contact forces (3<sup>rd</sup> from right) and their difference (bottom right) with the linear hybrid impedance controller.

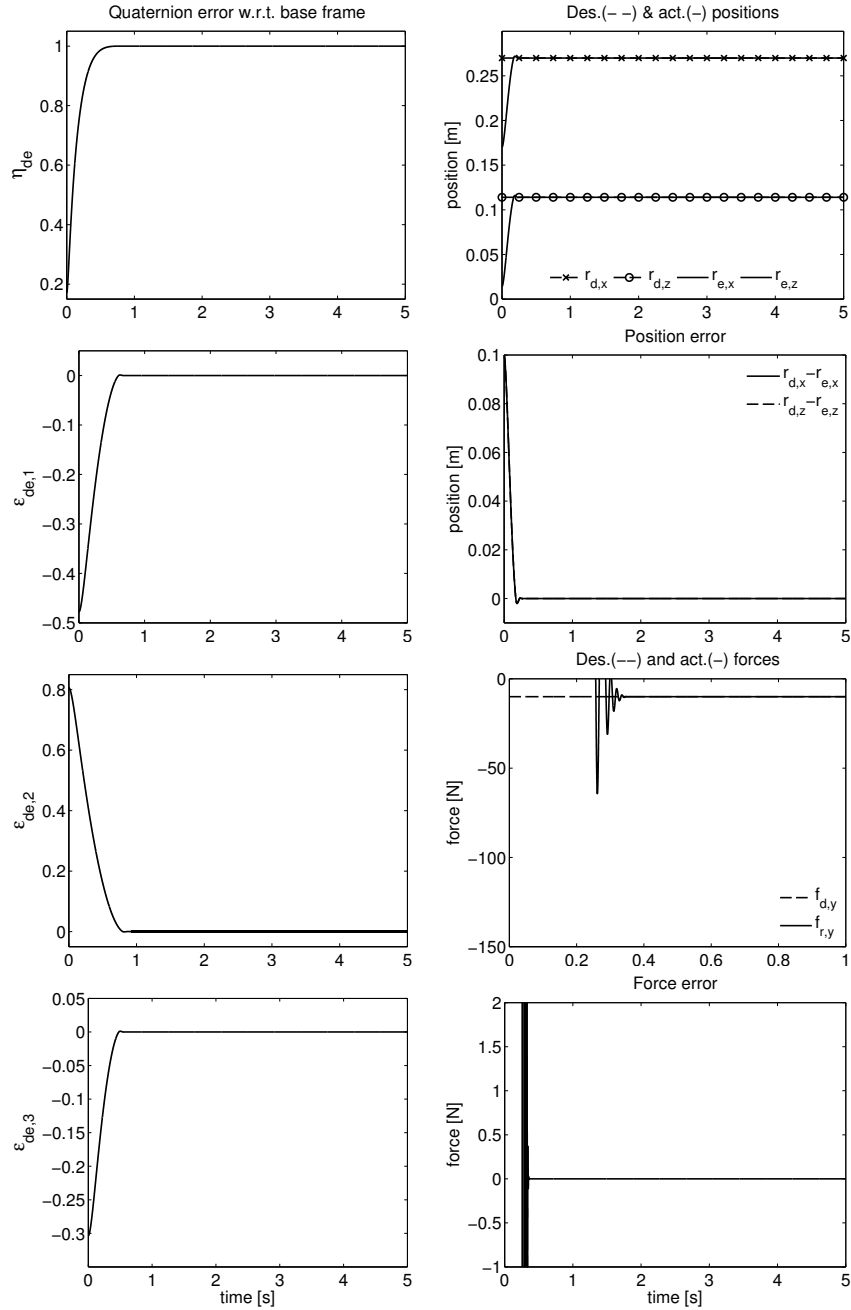


**Figure B.2** Quaternion error ( $\eta_{de}, \epsilon_{de,1}, \epsilon_{de,2}, \epsilon_{de,3}$ ) expressed w.r.t. base frame (left), desired  $r_{d,t}$  and actual  $r_{e,t}$  tangential end-effector positions (top right), and their difference (2<sup>nd</sup> from right), desired  $f_{d,n}$  and actual  $f_{r,n}$  normal contact forces (3<sup>rd</sup> from right) and their difference (bottom right) with the finite-time stable hybrid impedance controller.

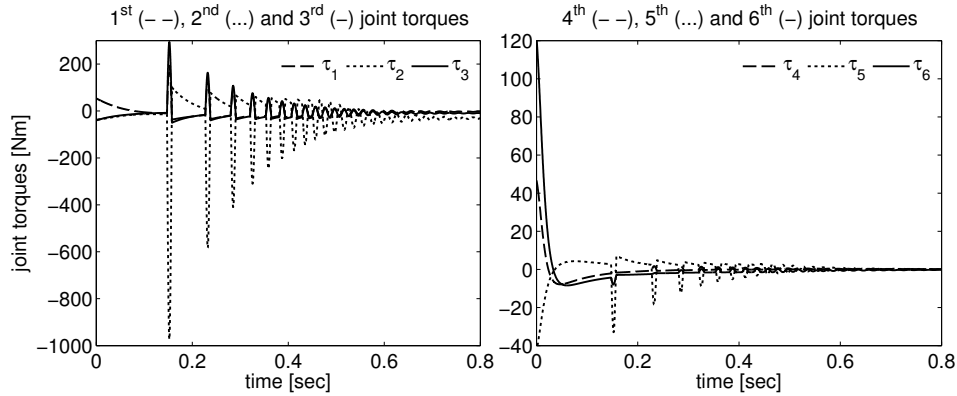


**Figure B.3** Joint torques when the linear hybrid impedance controller is used.

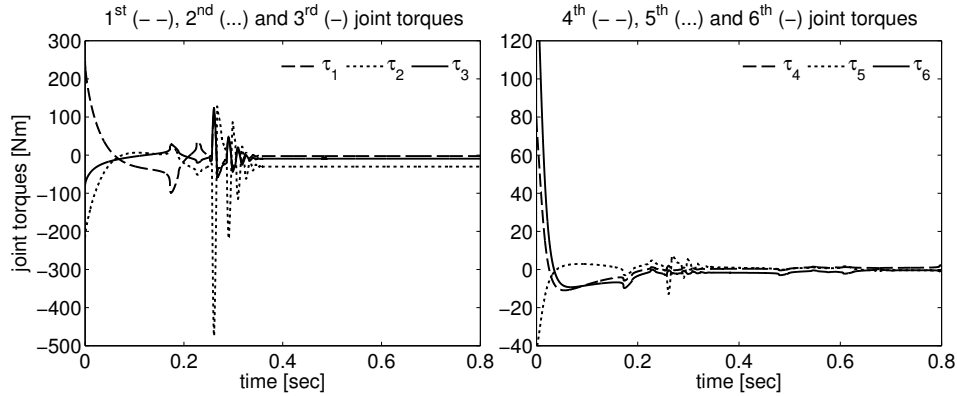


**Figure B.4** Joint torques when the finite-time stable hybrid impedance controller is used.

## B.2 Additional experimental results

In this section, additional experimental results are presented when the desired half circle trajectory in the contact phase is designed to be executed faster than the one given in Section 2.8.2. This is done in order to highlight the effect of stick-slip friction phenomena in the experiments. By moving the manipulator faster, it is expected to reduce the effect of combined effects of joint and contact friction. The parts of the additional experiment excluding the time interval where the manipulator draws a half circle twice on the whiteboard are the same with the experiment introduced in Section 2.8.2. Since the plots related to the first part of the experiment for bringing the manipulator to the vicinity of the whiteboard are similar to Figure 2.11, they are not shown here for brevity. The total duration of the half circle trajectory presented in this section is 8.958 [s] which is less than the one used in Section 2.8.2 (i.e. faster desired trajectory). First of all, it

can be seen from Figure B.6 that the forces in the tangential directions (i.e. x- and z-) during the time interval between  $t = 18$  [s] and  $t = 26.958$  [s] are lower compared to the plots shown in Figure 2.13. Furthermore, from Figure B.8 it can be observed that the position tracking errors in the tangential directions has also slightly reduced as compared to the plots shown in Figure 2.15. This can be due to the manipulator moving faster and consequently operating away from the region where the stick-slip friction phenomena is present at the joints of the manipulator and at the contact point with the whiteboard. The aforementioned reduction in the position tracking errors can also be observed when Figure 2.17 and Figure B.10 are compared. The vibrations visible at the contact force plots in y-direction due to stick-slip friction has also reduced as can be seen in Figure B.7. Similar to the experiment presented in Section 2.8.2, it can be noticed from Figure B.5 that no chattering phenomenon is present in the joint torques sent to the actuators since the control law is continuous.

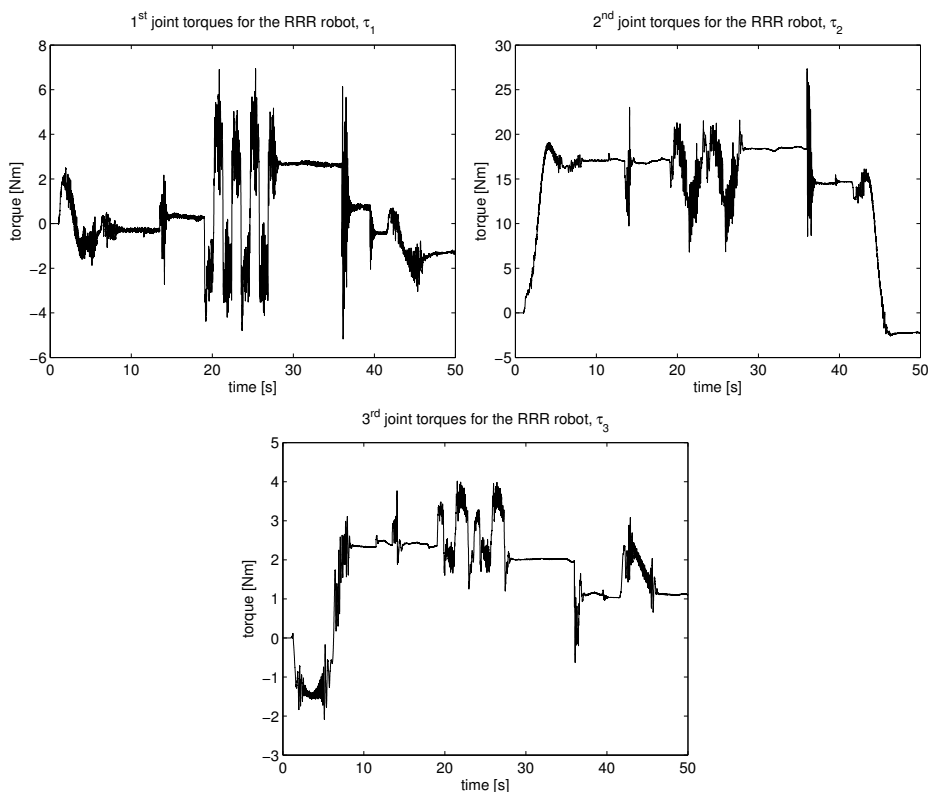


**Figure B.5** Joint torques for the finite-time stable hybrid impedance controller.

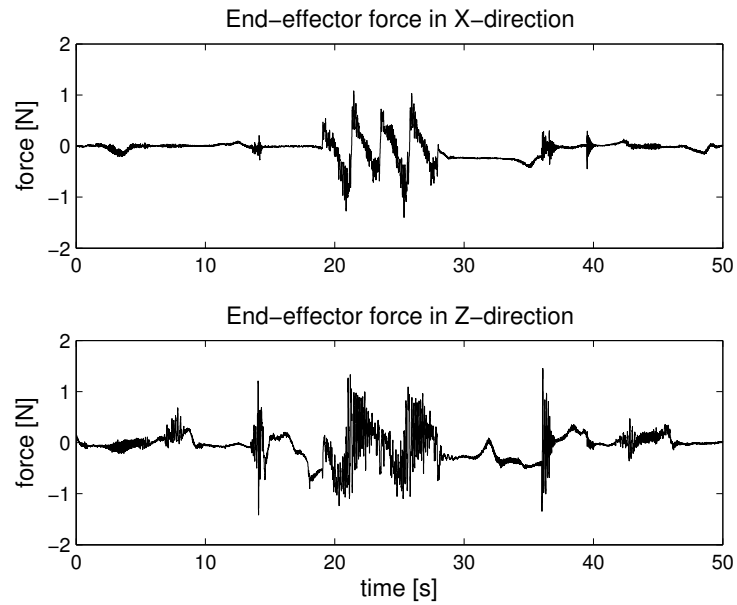


Figure B.6 End-effector forces in tangential x-(top) and z-(bottom) directions.

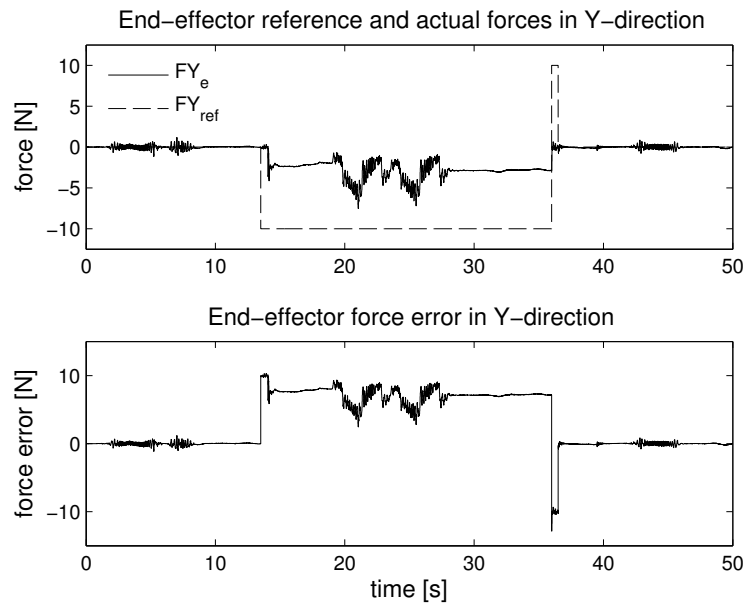
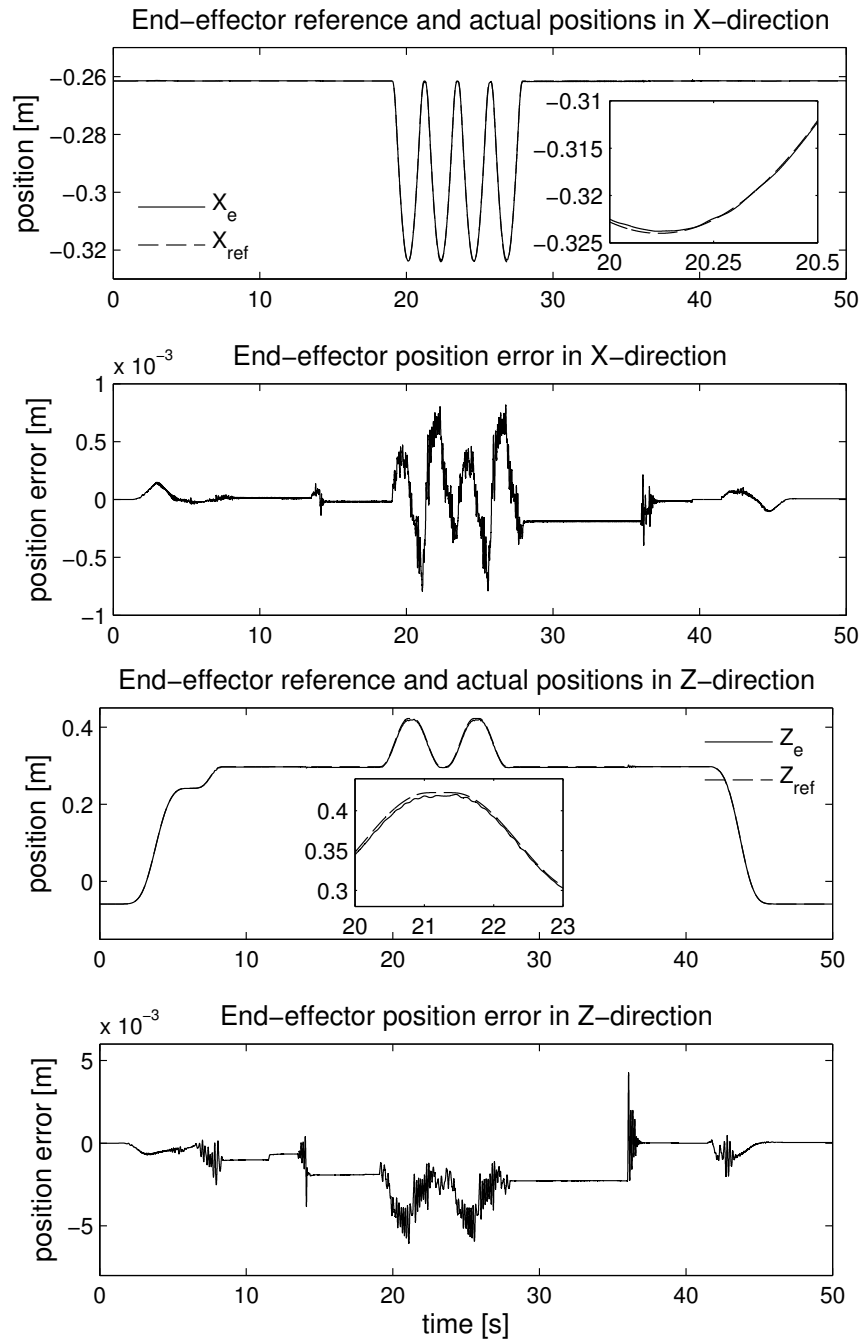


Figure B.7 Reference (- -), actual (-) end-effector forces in normal (y-) direction.





**Figure B.8** Reference (- -) and actual (-) positions and error in tangential (x-,z-) directions.

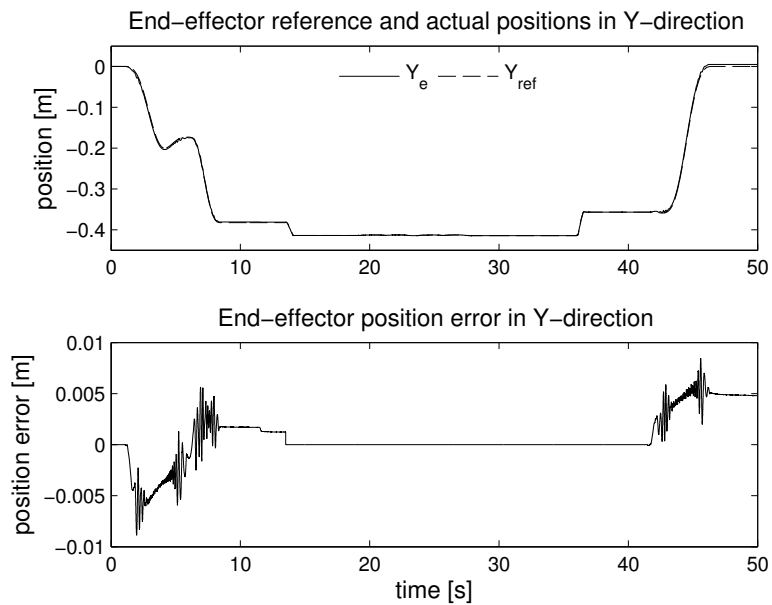


Figure B.9 Reference (- -), actual (-) positions in normal (y-) direction.

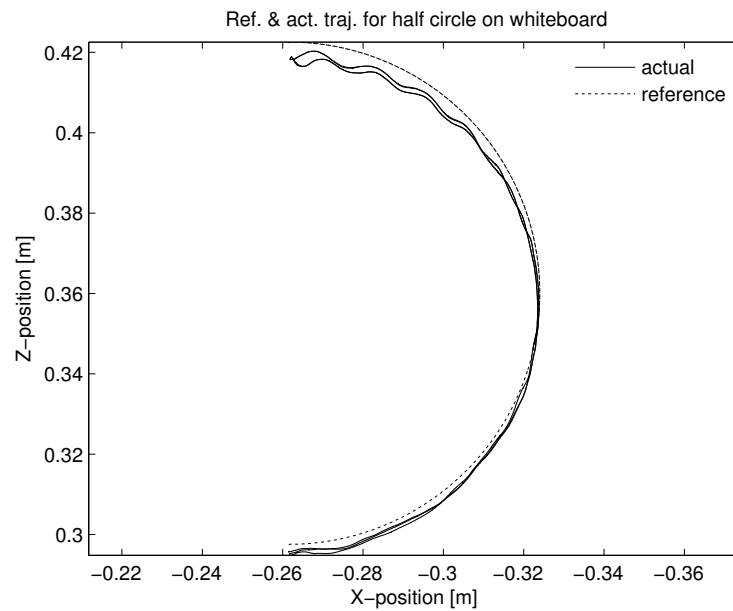


Figure B.10 Reference ( $\cdots$ ), actual (-) positions for half circle part of trajectory.

# Appendix C

## Technical drawings and force sensor calibration

### C.1 Force sensor calibration

In this section, the calibration procedure for the sensor is introduced which is based on [145]. The force sensor attached to the robot's elbow provides the force and torque measurements to be used for feedback in a control loop. The main problem with this sensor is that it is affected by factors other than the contact force. Therefore, the sensor needs to be calibrated to obtain actual contact force readings. When the sensor is initialized an offset value appears. This initial offset can be removed by averaging a few samples of sensor readings, however such a correction is only valid if the sensor is not reoriented. The probe attached to the flange is considered as part of the offset so it is initially deleted but, when the elbow is moved, the effect of the weight appears in the sensor readings distorting the measurement. If there is no contact with the environment the force and torque reading is due to the weight of the tool (probe) and sensor. It can be considered as a force pointing to the floor applied at the center of gravity of the union of probe/sensor, so the sensor registers the projection of this magnitude on its axes. The procedure to compute the weight of the union of probe/sensor, places the  $X$ -axis of the sensor frame parallel to the floor and then rotates the elbow (or the third joint) with constant velocity several times in both directions. This way the load vector is perpendicular to the floor and at some points coincides with  $Y$  and  $Z$  axes. Plots with the results of the experiment are shown in Figure C.1, where it can be seen that the  $X$ -forces are roughly zero and  $Y$  and  $Z$  forces record the effect of the weight. By fitting a circle to the recorded  $Y$ - $Z$  force data as shown in Figure C.1, the weight of the probe/sensor and the offsets for  $Y$  and  $Z$  directions can be obtained from the radius and the center coordinates.

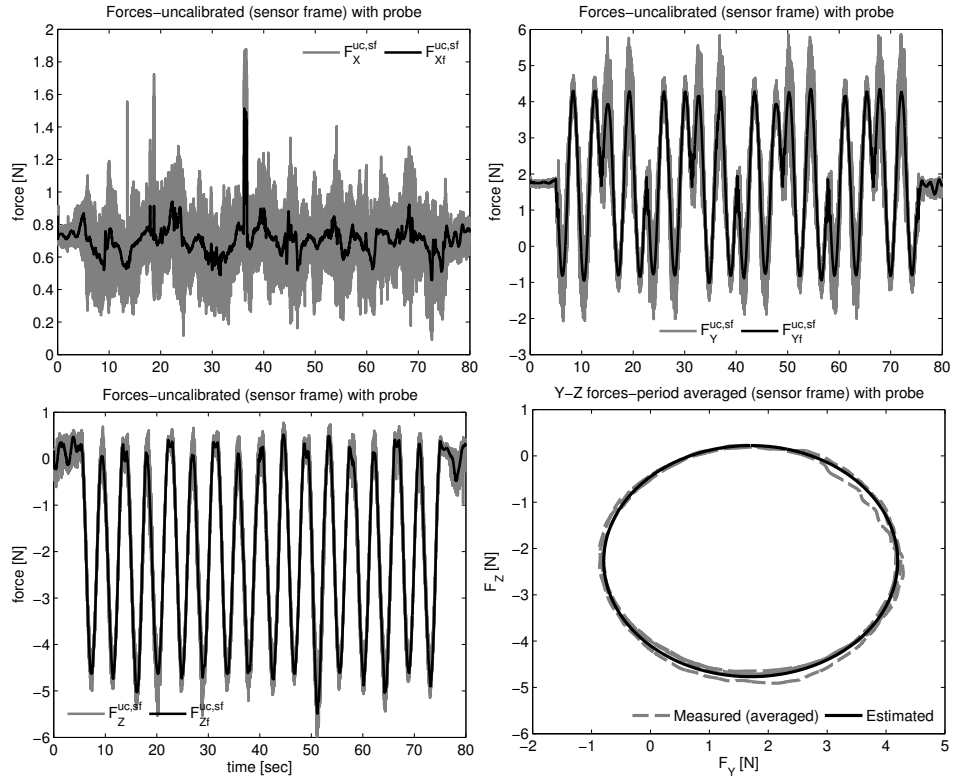


**Figure C.1** Forces recorded in the sensor frame in the experiment to estimate the weight of the probe and sensor. Forces in  $X$  and  $Y$  directions (top), in  $Z$  direction (bottom left), (gray-measured,black-lowpass filtered).  $Y$  and  $Z$  forces plotted together (bottom right) and circle fitted to it.

## C.2 Technical drawings for mechanical interface

In this section, the technical drawings for the mechanical interface designed to hold the force sensor and the probe assembly that makes contact with the whiteboard shown in Figure 2.10 are introduced. In Figure C.2, the probe with a hemispherical tip which makes contact with the whiteboard is shown. In Figure C.4, the last link which attaches the force sensor to the RRR robot arm is shown. The mechanical assembly of each of these parts can be seen in Figure C.5.



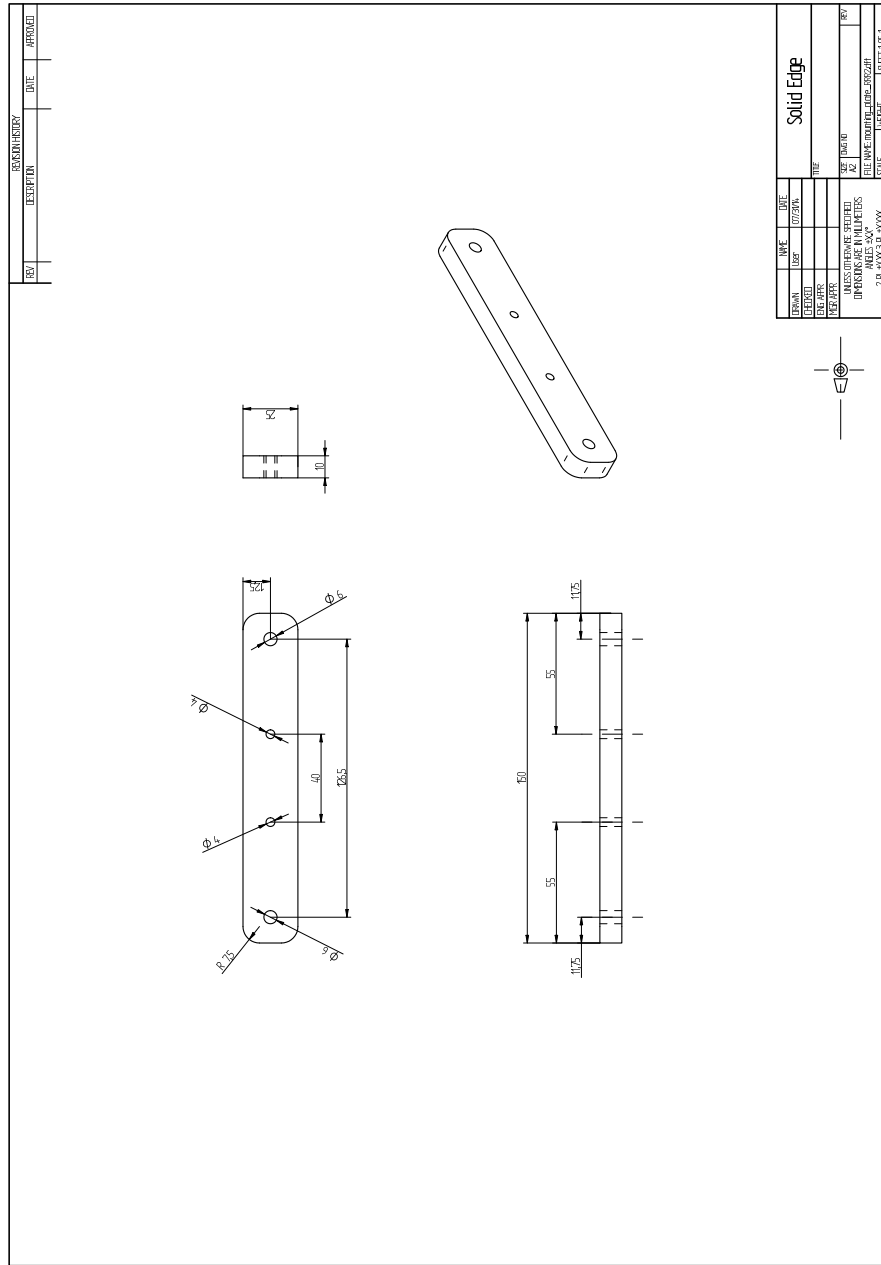


Figure C.3 2D drawing for the mounting plate.

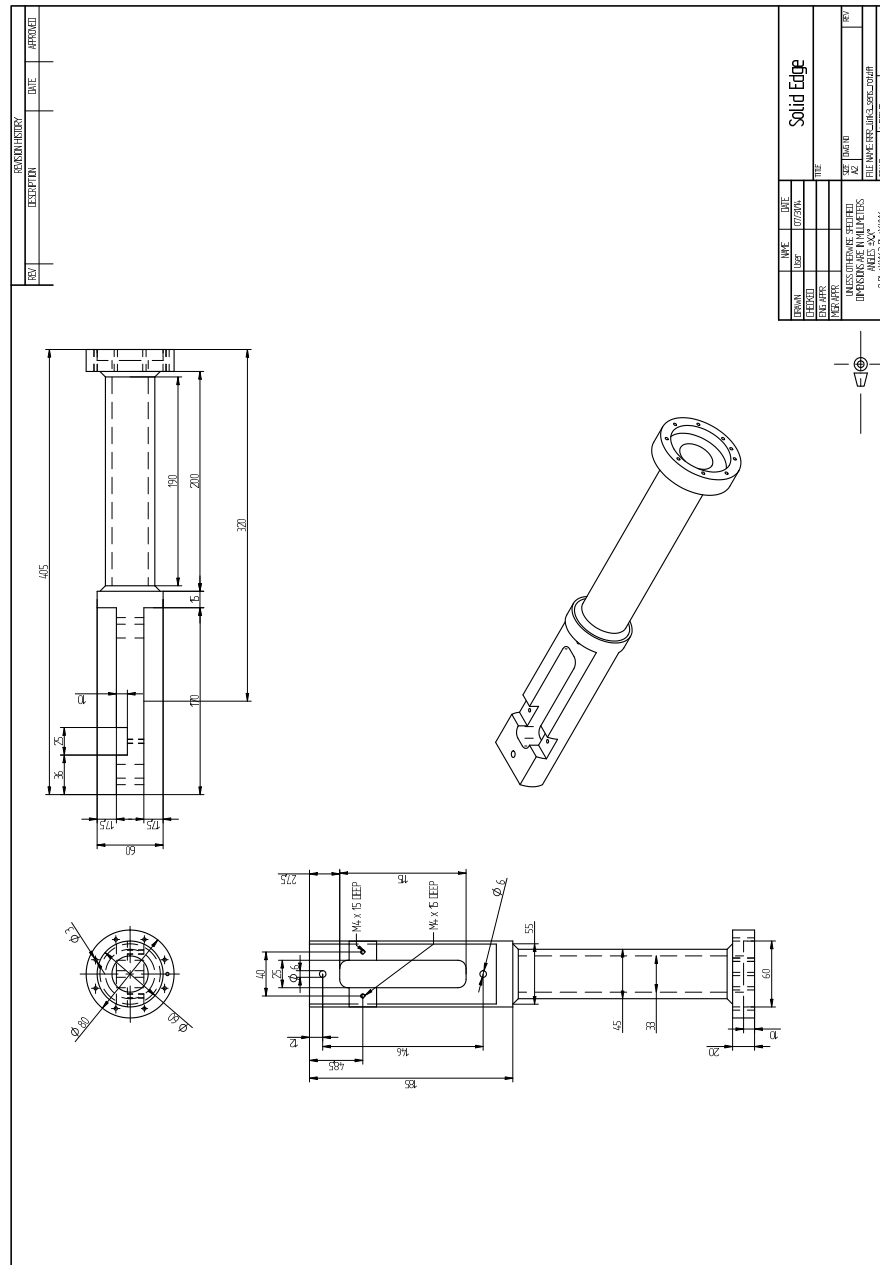


Figure C.4 2D drawing for mechanical interface (i.e. last link).



**Figure C.5** CAD rendering of the mechanical assembly.



# Appendix **D**

## Further information about unilateral constraints

### **D.1 Set-valued force laws for frictional contact**

In this section, the constitutive laws for frictional unilateral contact formulated as set-valued force laws are given (see [56] for an extensive treatise on the subject). The formulation here is taken from [56, 85, 86]. Normal contact between rigid bodies is described by a set-valued force law called Signorini's law. Consider two convex rigid bodies at a relative distance  $g_N$  from each other. The normal contact distance  $g_N$  is uniquely defined for convex bodies and is such, that the points 1 and 2 have parallel tangent planes (shown as light gray planes in Figure 3.3). The normal contact distance  $g_N$  is non-negative since the bodies do not penetrate into each other. The bodies touch when  $g_N = 0$ . The normal contact force  $\lambda_N$  between the bodies is non-negative because the bodies can exert only repelling forces on each other, i.e. the constraint is unilateral. The normal contact force vanishes when there is no contact ( $g_N > 0$ ), and is positive when contact is present ( $g_N = 0$ ). Under the assumption of impenetrability, expressed by  $g_N \geq 0$  and no adhesion ( $\lambda_N \geq 0$ ), only two situations may occur:

$$\begin{aligned} g_N = 0 \wedge \lambda_N \geq 0 & \quad \text{contact,} \\ g_N > 0 \wedge \lambda_N = 0 & \quad \text{no contact.} \end{aligned} \tag{D.1}$$

From (D.1), we see that the normal contact law shows a complementarity behavior: the product of the contact force and normal contact distance is always zero, i.e.  $g_N \lambda_N = 0$ . The relationship between the normal contact force and the normal contact distance is therefore described by

$$g_N \geq 0, \quad \lambda_N \geq 0, \quad g_N \lambda_N = 0, \tag{D.2}$$

which is the complementarity condition between  $g_N$  and  $\lambda_N$ . The inequality complementarity of normal contact law depicted in Figure D.1(a) shows a set-valued graph of admissible combinations of  $g_N$  and  $\lambda_N$ . The normal contact law can also be expressed by the subdifferential of a non-smooth conjugate potential  $\Psi_{C_N}^*(g_N)$

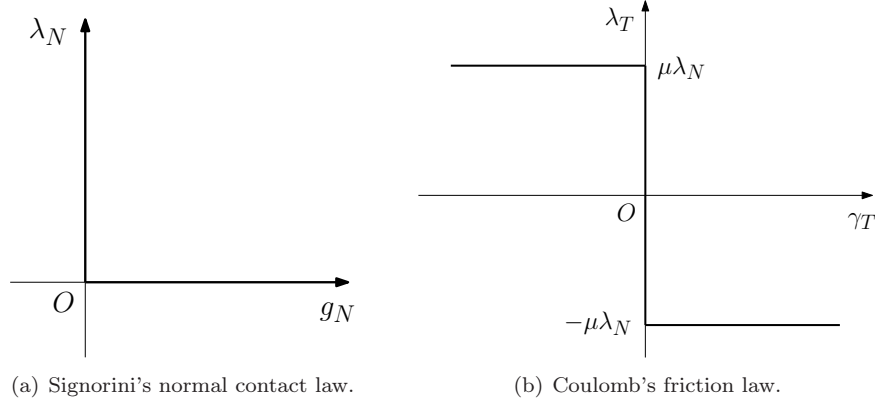


**Figure D.1** Signorini's normal contact law and Coulomb's friction law

$$-\lambda_N \in \partial\Psi_{C_N^*}, \quad (\text{D.3})$$

where  $C_N$  is the admissible set of negative contact forces  $-\lambda_N$ ,

$$C_N = \{-\lambda_N \in \mathbb{R} \mid \lambda_N \geq 0\} = \mathbb{R}^- \quad (\text{D.4})$$

and  $\Psi_{C_N}$  is the indicator function of  $C_N$ . Alternatively, we can formulate the contact law in a compact form by means of the normal cone of  $C_N$ :

$$g_N \in N_{C_N}(-\lambda_N). \quad (\text{D.5})$$

The potential  $\Psi_{C_N}$  is depicted in Figure D.2(a) and it is the indicator function of  $C_N = \mathbb{R}^-$ . Taking the subdifferential of the indicator function gives the set-valued relation  $g_N \in \partial\Psi_{C_N}(-\lambda_N)$ , depicted in Figure D.2(c). Interchanging the axis gives the Figure D.2(d) which expresses (D.3) and is equivalent to the Figure D.1(a). Integration of the latter relation gives the support function  $\Psi_{C_N^*}(g_N)$ , which is the conjugate of the indicator function on  $C_N$ . The normal contact law, also called Signorini's law, expresses impenetrability of contact and can formally be stated for a number of contact points  $i = 1, \dots, n_C$ ,

$$g_N \in N_{C_N}(-\lambda_N), \quad C_N = \{-\lambda_N \in \mathbb{R}^n \mid \lambda_N \geq 0\}, \quad (\text{D.6})$$

where  $\lambda_N$  is the vector of normal contact forces  $\lambda_{N_i}$  and  $g_N$  is the vector of normal contact distances  $g_{N_i}$ . Signorini's law, a set-valued normal contact law on displacement level, can be expressed on velocity level for closed contacts

$$\gamma_N \in N_{C_N}(-\lambda_N), \quad g_N = 0, \quad (\text{D.7})$$

where  $\gamma_N$  is the relative normal contact velocity, i.e.  $\gamma_N = \dot{g}_N$  for non-impulsive motion. Coulomb's friction law is another example of a force law that can be

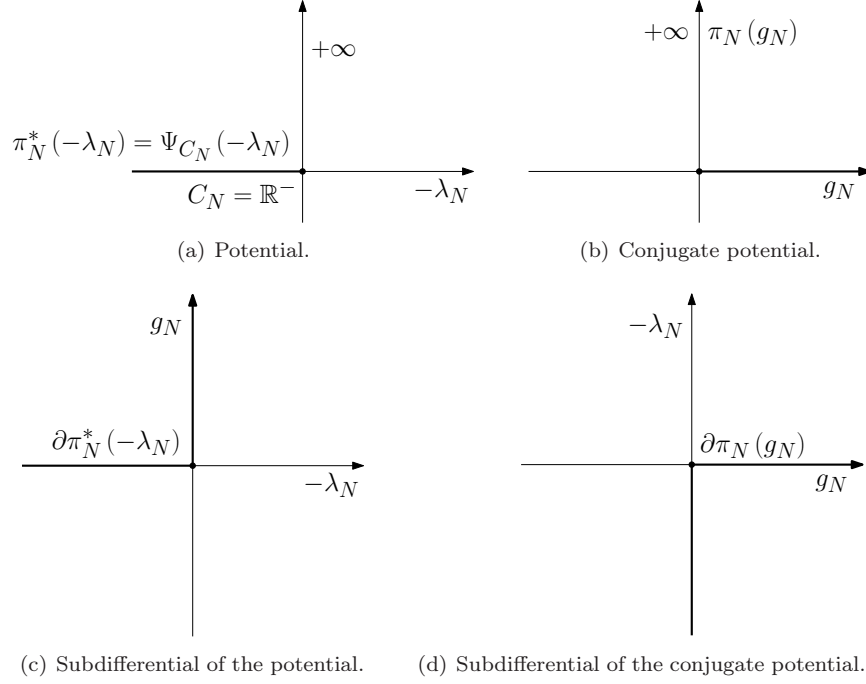


**Figure D.2** Potential, conjugate potential and subdifferential of the normal contact problem  $C = C_N = \mathbb{R}^-$

described by a non-smooth potential. Consider the contact pair 1-2 shown in Figure 3.3 with Coulomb friction at the contact point. We denote the relative velocity of point 1 w.r.t. point 2 along their tangent plane by  $\gamma_T$ . If the bodies are in contact, i.e.  $g_N = 0$ , then the friction between them imposes a force  $\lambda_T$  along the tangent plane of the contact point. If the bodies are sliding over each other, then the friction force  $\lambda_T$  has magnitude  $\mu\lambda_N$  and acts in the direction of  $-\lambda_T$

$$-\lambda_T = \mu\lambda_N \text{sign}(\gamma_T), \quad \gamma_T \neq 0, \quad (\text{D.8})$$

where  $\mu$  is the friction coefficient and  $\lambda_N$  is the normal contact force. If the relative tangential velocity vanishes, i.e.  $\lambda_T = 0$ , then the bodies purely roll over each other without slip. Pure rolling, or no slip for locally flat objects, is denoted by *stick*. If the bodies stick, then the friction force must lie in the interval  $-\mu\lambda_N \leq \lambda_T \leq \mu\lambda_N$ . For unidirectional friction, i.e. for planar contact problems, the following three cases are possible:

$$\begin{aligned} \gamma_T = 0 &\Rightarrow |\lambda_T| \leq \mu\lambda_N && \text{sticking,} \\ \gamma_T < 0 &\Rightarrow \lambda_T \leq -\mu\lambda_N && \text{negative sliding,} \\ \gamma_T > 0 &\Rightarrow \lambda_T \leq \mu\lambda_N && \text{positive sliding.} \end{aligned}$$

We can express the friction force by a potential  $\pi_T(\gamma_T)$ , which we mechanically interpret as a dissipation function,

$$-\lambda_T \in \partial\pi_T(\gamma_T), \quad \pi_T(\gamma_T) = \mu\lambda_N |\gamma_T|, \quad (\text{D.9})$$

from which follows the set-valued force law

$$-\lambda_T \in \begin{cases} \mu\lambda_N, & \gamma_T > 0, \\ [-1, 1]\mu\lambda_N, & \gamma_T = 0 \\ -\mu\lambda_N, & \gamma_T < 0. \end{cases} \quad (\text{D.10})$$

A non-smooth convex potential therefore leads to a maximal monotone set-valued force law. The admissible values of the negative tangential force  $\lambda_T$  form a convex set  $C_T$  that is bounded by the values of the normal force:

$$C_T = \{-\lambda_T \mid -\mu\lambda_N \leq \lambda_T \leq +\mu\lambda_N\}. \quad (\text{D.11})$$

Coulomb's law can be expressed with the aid of the indicator function of  $C_T$  as

$$\gamma_T \in \partial\Psi_{C_T}(-\lambda_T) \Leftrightarrow \gamma_T \in N_{C_T}(-\lambda_T), \quad (\text{D.12})$$

where the indicator function  $\Psi_{C_T}$  is the conjugate potential of the support function  $\pi_T(C_T) = \Psi_{C_T}^*(C_T)$  see Figure D.3. The Coulomb's friction law for spatial contact formulates a two-dimensional friction force  $\lambda_T \in \mathbb{R}^2$  which lies in the tangent-plane of the contacting bodies. The set of negative admissible friction forces is a convex set  $C_T \subset \mathbb{R}^2$  that is a disk for isotropic Coulomb friction:

$$C_T = \{-\lambda_T \mid \|\lambda_T\| \leq \mu\lambda_N\}. \quad (\text{D.13})$$

Using the set  $C_T$ , the spatial Coulomb friction law can be formulated as

$$\begin{aligned} \gamma_T \in \partial\Psi_{C_T}(-\lambda_T) &\Leftrightarrow -\lambda_T \in \partial\Psi_{C_T}^*(\gamma_T) \\ &\Leftrightarrow \gamma_T \in N_{C_T}(-\lambda_T), \end{aligned}$$

in which  $\gamma_T \in \partial\Psi_{C_T}(-\lambda_T)$  is the relative sliding velocity. Similarly, an elliptic choice of  $C_T$  would result in an orthotropic Coulomb friction law. A combined friction law, which takes into account sliding friction as well as pivoting (or drilling) friction, can be formulated using a three-dimensional set of admissible (generalised) friction forces and is called the spatial Coulomb-Contensou friction law. The function  $\gamma_T$  is the relative velocity of the bodies at the contact point.

## D.2 Impact

Signorini's law and Coulomb's friction law are set-valued force laws for non-impulsive forces. In order to describe impact, we need to introduce impact laws for the contact impulses. We will consider a Newton type of restitution law,

$$\gamma_N^+ = -\epsilon_N \gamma_N^-, \quad g_N = 0, \quad (\text{D.14})$$

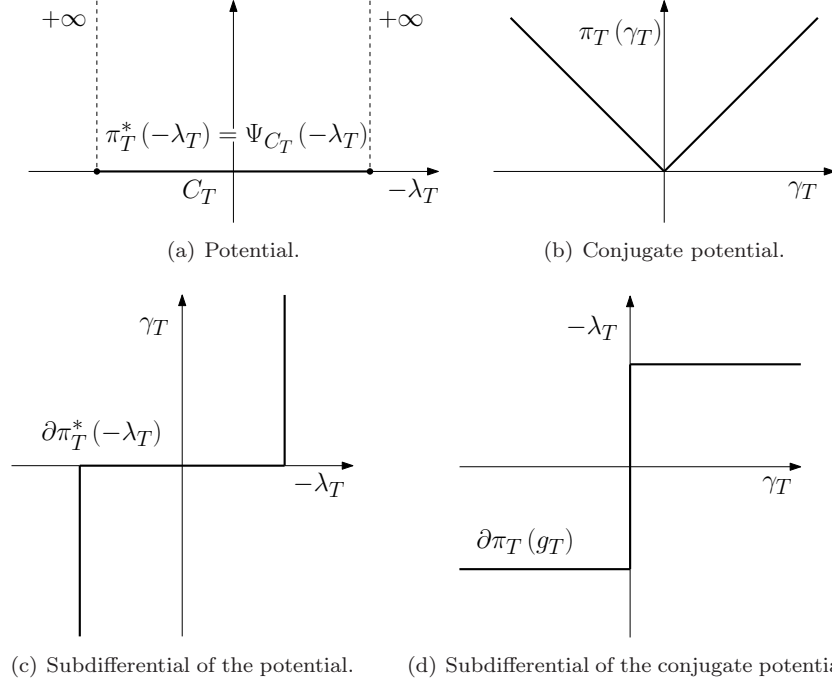


**Figure D.3** Potential, conjugate potential and subdifferential of the tangential contact problem  $C = C_T$

which relates the post-impact velocity  $\gamma_N^+$  of a contact point to the pre-impact velocity  $\gamma_N^-$  by Newton's coefficient of restitution  $e_N$ . The case  $e_N = 1$  corresponds to a completely elastic contact, whereas  $e_N = 0$  corresponds to a completely inelastic contact. The impact, which causes the sudden change in relative velocity, is accompanied by a normal contact impulse  $\Lambda_N > 0$ . Following [55], suppose that, for any reason, the contact does not participate in the impact, i.e. that the value of the normal contact impulse  $\Lambda_N$  is zero, although the contact is closed. This happens normally for multicontact situations. For this case, we allow the postimpact relative velocities to be higher than the value prescribed by Newton's impact law,  $\gamma_N^+ > -e_N \gamma_N^-$ , in order to express that the contact is superfluous and could be removed without changing the contact-impact process. We can therefore express the impact law as an inequality complementarity on velocity-impulse level:

$$\Lambda_N \geq 0, \quad \xi_N \geq 0, \quad \Lambda_N \xi_N = 0, \quad (\text{D.15})$$

with  $\xi_N = \gamma_N^+ + e_N \gamma_N^-$  (see [55]). Similarly to Signorini's law on velocity level, we can write the impact law in normal direction as

$$\xi_N \in N_{C_N}(-\Lambda_N), \quad g_N = 0, \quad (\text{D.16})$$

or by using the support function

$$-\Lambda_N \in \partial\Psi_{C_N}^*(\xi_N), \quad g_N = 0. \quad (\text{D.17})$$

A normal contact impulse  $\Lambda_N$  at a frictional contact leads to a tangential contact impulse  $\Lambda_T$  with  $\|\Gamma_T\| \leq \mu\Lambda_N$ . We thus have to specify a tangential impact law which can be formulated similarly as has been done for the normal impact law:

$$-\Lambda_T \in \partial\Psi_{C_T(\Lambda_N)}(\xi_T), \quad g_T = 0, \quad (\text{D.18})$$

with  $\xi_T = \gamma_T^+ + e_T\gamma_T^-$ . Tangential restitution coefficient  $e_T$  is often taken as zero.

### D.3 Modelling nonlinear mechanical systems with dry friction and impact using measure differential inclusions

In this section, the class of nonlinear time-autonomous mechanical systems with unilateral frictional contact is defined. First a measure differential inclusion is derived that describes the temporal dynamics of mechanical systems with discontinuities in the velocity. It is assumed that these mechanical systems exhibit only bilateral holonomic frictionless constraints and unilateral constraints in which dry friction can be present. We also assume that a set of independent generalised coordinates,  $q \in \mathbb{R}^n$ , for which these bilateral constraints are eliminated from the formulation of the dynamics of the system, is known. The generalised coordinates  $q(t)$  are assumed to be absolutely continuous functions of time  $t$ . Also, we assume the generalised velocities,  $u(t) = \dot{q}(t)$  for almost all  $t$ , to be functions of locally bounded variation. Thus, at each time-instant a left limit  $u^-$  and a right limit  $u^+$  of the velocity can be defined and the generalised accelerations  $\dot{u}$  are not defined for all  $t$ . The set of discontinuity points  $\{t_j\}$  for which  $\dot{u}$  is not defined is assumed to have Lebesgue measure zero. We formulate the dynamics of the system using a Lagrangian approach, resulting in

$$\left( \frac{d}{dt} \left( \frac{\partial T}{\partial u} \right) - \frac{\partial T}{\partial q} + \frac{\partial U}{\partial q} \right)^T = f^{nc}(q, u) + W_N(q)\lambda_N + W_T(q)\lambda_T, \quad (\text{D.19})$$

or, alternatively,

$$M(q)\dot{u} - h(q, u) = W_N(q)\lambda_N + W_T(q)\lambda_T, \quad (\text{D.20})$$

which is a differential equation for the non-impulsive part of the motion. Herein,  $M(q) = M^T(q) > 0$  is the mass-matrix. The scalars  $T$  and  $U$  are the kinetic and potential energies and it is assumed that  $T$  can be written as  $T = \frac{1}{2}u^T M(q)u$ . The vector  $f^{nc}$  in (D.19) represents all smooth generalised non-conservative forces. The

state-dependent vector  $h(q, u)$  in (D.20) contains all differentiable forces (both conservative and non-conservative), such as spring forces, gravitation, smooth damper forces and gyroscopic terms. We introduce the following index sets:

$$\begin{aligned} I_G &= \{1, \dots, n_C\} && \text{the set of all contacts,} \\ I_N &= \{i \in I_G \mid g_{N_i}(q) = 0\} && \text{the set of all closed contacts,} \end{aligned} \quad (\text{D.21})$$

and set up the force laws and impact laws of each contact as has been elaborated in Sections D.1 and D.2. The normal contact distances  $g_{N_i}(q)$  depend on the generalised coordinates  $q$  and are gathered in a vector  $g_N(q)$ . During a non-impulsive part of the motion, the normal contact force  $-\lambda_{N_i} \in C_N$  and friction force  $-\lambda_{T_i} \in C_{T_i}$  of each closed contact  $i \in I_N$ , are assumed to be associated with a non-smooth potential, being the support function of a convex set, i.e.

$$-\lambda_{N_i} \in \partial\Psi_{C_N}^*(\gamma_{N_i}), \quad -\lambda_{T_i} \in \partial\Psi_{C_{T_i}}^*(\gamma_{T_i}) \quad (\text{D.22})$$

where  $C_N = R^-$  and the set  $C_{T_i}$  can depend on normal contact force  $\lambda_{N_i}$ . The normal and tangential contact forces of all  $n_C$  contacts are gathered in columns  $\lambda_N = \{\lambda_{N_i}\}$  and  $\lambda_T = \{\lambda_{T_i}\}$  and corresponding normal and tangential relative velocities are gathered in columns  $\gamma_N = \{\gamma_{N_i}\}$  and  $\lambda_T = \{\lambda_{T_i}\}$ , for  $i \in I_G$ . We assume that these contact velocities are related to generalised velocities through:

$$\gamma_N(q, u) = W_N^T(q)u, \quad \gamma_T(q, u) = W_T^T(q)u. \quad (\text{D.23})$$

It should be noted that  $W_X^T(q) = \frac{\partial \gamma_X}{\partial u}$  for  $X = \{N, T\}$ . This assumption is very important as it excludes rheonomic contacts. Equation (D.20) together with the set-valued force laws (D.22) form a differential inclusion

$$M(q)\dot{u} - h(q, u) \in - \sum_{i \in I_N} W_{N_i}(q)\partial\Psi_{C_N}^*(\gamma_{N_i}) - W_{T_i}(q)\partial\Psi_{C_{T_i}}^*(\gamma_{T_i}) \quad (\text{D.24})$$

for almost all  $t$ . Differential inclusions of this type are called Filippov systems. The differential inclusion (D.24) only holds for impact free motion. Subsequently, we define for each contact point the constitutive impact laws

$$\Lambda_{N_i} \in \partial\Psi_{C_N}^*(\xi_{N_i}), \quad \Lambda_{T_i} \in \partial\Psi_{C_{T_i}}^*(\xi_{T_i}), \quad i \in I_N, \quad (\text{D.25})$$

with

$$\xi_{N_i} = \gamma_{N_i}^+ + e_{N_i}\gamma_{N_i}^-, \quad \xi_{T_i} = \gamma_{N_i}^+ + e_{N_i}\gamma_{N_i}^- \quad (\text{D.26})$$

in which  $e_{N_i}$  and  $e_{T_i}$  are the normal and tangential restitution coefficients, respectively. The inclusions (D.25) form very complex set-valued mappings representing the contact laws at the impulse level. The force laws for non-impulsive motion can

be put in the same form because  $u^+ = u^-$  holds in the absence of impacts and because of the positive homogeneity of the support function

$$\lambda_{N_i} \in \partial\Psi_{C_N}^*(\xi_{N_i}), \quad \lambda_{T_i} \in \partial\Psi_{C_{T_i}}^*(\xi_{T_i}), \quad i \in I_N. \quad (\text{D.27})$$

We now replace the differential inclusion (D.24), which holds for almost all  $t$ , by an equality of measures

$$M(q)du - h(q, u)dt = W_N(q)d\Lambda_N + W_T(q)d\Lambda_T \quad \forall t, \quad (\text{D.28})$$

which holds for all time-instances  $t$ . The differential measure of contact impulses  $d\Lambda_N$  and  $d\Lambda_T$  contains a Lebesgue measurable part  $\lambda dt$  and an atomic part  $\Lambda d\eta$

$$d\Lambda_N = \lambda_N dt + \Lambda_N d\eta, \quad d\Lambda_T = \lambda_T dt + \Lambda_T d\eta, \quad (\text{D.29})$$

which can be expressed as inclusions

$$\begin{aligned} -d\Lambda_{N_i} &\in \partial\Psi_{C_N}^*(\xi_{N_i})(dt + d\eta), \\ -d\Lambda_{T_i} &\in \partial\Psi_{C_{T_i}(\lambda_{N_i})}^*(\xi_{T_i})dt + \partial\Psi_{C_{T_i}(\Lambda_{N_i})}^*(\xi_{T_i})d\eta. \end{aligned} \quad (\text{D.30})$$

As an abbreviation we write

$$M(q)du - h(q, u)dt = W(q)d\Lambda \quad \forall t, \quad (\text{D.31})$$

using short-hand notation

$$\lambda = \begin{bmatrix} \lambda_N \\ \lambda_T \end{bmatrix}, \quad \Lambda = \begin{bmatrix} \Lambda_N \\ \Lambda_T \end{bmatrix}, \quad W = [W_N W_T], \quad \gamma = \begin{bmatrix} \gamma_N \\ \gamma_T \end{bmatrix}. \quad (\text{D.32})$$

Furthermore we introduce the quantities

$$\xi \equiv \gamma^+ + E\gamma^-, \quad \delta \equiv \gamma^+ - \gamma^-, \quad (\text{D.33})$$

with  $E = \text{diag}(\{e_{N_i}, e_{T_i}\})$  from which we deduce

$$\gamma^+ = \{I + E\}^{-1} \{\xi + E\delta\}, \quad \gamma^- = \{I + E\}^{-1} \{\xi - \delta\}. \quad (\text{D.34})$$

The equality of measures (D.31) together with the set-valued force laws (D.30) form a measure differential inclusion that describes the time-evolution of a mechanical system with discontinuities in the generalised velocities. Such a measure differential inclusion does not necessarily have existence and uniqueness of solutions for all admissible initial conditions. Indeed, if the friction coefficient is large, then the coupling between motion normal to the constraint and tangential to the constraint can cause existence and uniqueness problems (known as the Painlevé problem [26, 84]). In the following, we will assume existence and uniqueness of solutions in forward time. The contact laws guarantee that the generalised positions  $q(t)$  are such that penetration is avoided ( $g_{N_i} > 0$ ) and the generalised positions therefore remain within the admissible set

$$\mathcal{K} = \{q \in \mathbb{R}^n \mid g_{N_i}(q) \geq 0 \quad \forall i \in I_G\} \quad \text{for all } t. \quad (\text{D.35})$$

The condition  $q(t) \in \mathcal{K}$  follows from the assumption on existence of solutions.



# Appendix E

## Impedance controller for cooperative manipulation: Lemmas

**Lemma E.1.** *Consider two rotation matrices  $R_1 = [n_1 \ s_1 \ a_1] \in SO(3)$  and  $R_2 = [n_2 \ s_2 \ a_2] \in SO(3)$ ,  $R_1 \neq R_2$  where  $n_i, s_i, a_i$  for  $i = 1, 2$  are orthogonal unit vectors. Then, the matrix  $\Delta R_{21} := R_2 - R_1 \neq 0$  is always of rank 2. Furthermore, orientation error between these two matrices defined according to angle/axis representation,  $\xi_{21} = \frac{1}{2}(n_1 \times n_2 + s_1 \times s_2 + a_1 \times a_2) \neq 0$  satisfies  $(\Delta R_{21})^T \xi_{21} = 0$ .*

*Proof.* The determinant of  $\Delta R_{21}$  is computed to check whether it has full rank. The determinant of a matrix  $N$  can be computed using its columns  $a$ ,  $b$  and  $c$  as,

$$\det N = a \cdot (b \times c) = c \cdot (a \times b) = b \cdot (c \times a) \quad (\text{E.1})$$

where "." and " $\times$ " are dot and vector products, respectively. The determinant of  $\Delta R_{21}$  is computed as,

$$\begin{aligned} \det(R_2 - R_1) &= (n_2 - n_1) \cdot [(s_2 - s_1) \times (a_2 - a_1)] \\ &= (n_2 - n_1) \cdot [(s_2 - s_1) \times a_2 - (s_2 - s_1) \times a_1] \\ &= (n_2 - n_1) \cdot [-a_2 \times (s_2 - s_1) + a_1 \times (s_2 - s_1)] \\ &= (n_2 - n_1) \cdot [-a_2 \times s_2 + a_2 \times s_1 + a_1 \times s_2 - a_1 \times s_1] \\ &= (n_2 - n_1) \cdot [n_2 + a_2 \times s_1 + a_1 \times s_2 + n_1] \\ &= n_2 \cdot n_2 - n_1 \cdot n_2 + n_2 \cdot (a_2 \times s_1) - n_1 \cdot (a_2 \times s_1) + n_2 \cdot (a_1 \times s_2) \\ &\quad - n_1 \cdot (a_1 \times s_2) + n_2 \cdot n_1 - n_1 \cdot n_1 \\ &= n_2 \cdot n_2 - n_1 \cdot n_2 + s_1 \cdot (n_2 \times a_2) - a_2 \cdot (s_1 \times n_1) + a_1 \cdot (s_2 \times n_2) \\ &\quad - s_2 \cdot (n_1 \times a_1) + n_2 \cdot n_1 - n_1 \cdot n_1 \\ &= n_2 \cdot n_2 - n_1 \cdot n_2 - s_1 \cdot s_2 + a_2 \cdot a_1 - a_1 \cdot a_2 + s_2 \cdot s_1 \\ &\quad + n_2 \cdot n_1 - n_1 \cdot n_1 = 0. \end{aligned} \quad (\text{E.2})$$

This implies that  $\Delta R_{21}$  is not full rank and can only have rank 1 or 2. To determine the rank of  $\Delta R_{21}$ , the dimension of its kernel should be determined, that is the space of vectors  $v$  for which

$$(R_2 - R_1)v = 0 \quad (\text{E.3})$$

which can be rewritten as,

$$\begin{aligned} R_2 v &= R_1 v \\ v &= R_2^{-1} R_1 v \end{aligned} \quad (\text{E.4})$$

since rotation matrices are invertible. However,  $R_2^{-1} R_1$  is again a rotation matrix and for rotations in  $SO(3)$  there is always a one-dimensional subspace of vectors that are not changed (i.e. the rotation axis) which follows from Euler's rotation theorem. Therefore, the rank of  $\Delta R_{21} = R_2 - R_1$  is 2. The orientation error between  $R_2$  and  $R_1$  can be expressed as

$$\xi_{21} = r_{21} \sin(\theta_{21}) \quad (\text{E.5})$$

where  $\theta_{21}$  and  $r_{21}$  are the angle and axis of the equivalent rotation  $R_2 R_1^T$  which is a unique relation for  $-\frac{\pi}{2} < \theta_{21} < \frac{\pi}{2}$ . An equivalent representation for (E.5) is given by,

$$\xi_{21} = \frac{1}{2}(n_1 \times n_2 + s_1 \times s_2 + a_1 \times a_2) \quad (\text{E.6})$$

which is unique for  $n_1^T n_2 \geq 0$ ,  $s_1^T s_2 \geq 0$  and  $a_1^T a_2 \geq 0$ . Since,  $R_2^T$  and  $R_1^T$  are again two rotation matrices, the kernel of  $\Delta R_{21}^T$  can be determined from the vectors satisfying,

$$(R_2 - R_1)^T v = 0 \quad (\text{E.7})$$

which can be rewritten as,

$$\begin{aligned} R_2^T v &= R_1^T v \\ v &= R_2 R_1^T v. \end{aligned} \quad (\text{E.8})$$

Since, the rotation axis  $r_{21}$  satisfies this relation, it follows that

$$(R_2 - R_1)^T r_{21} = 0 \quad \rightarrow \quad (R_2 - R_1)^T r_{21} \sin(\theta_{21}) = 0 \quad \rightarrow \quad (R_2 - R_1)^T \xi_{21} = 0 \quad (\text{E.9})$$

by post multiplication with  $\sin(\theta_{21})$ .  $\square$

### Rank of $W$ in (3.110)

The matrix  $W$  in equation (3.110) reads

$$W = \begin{bmatrix} (n_{1d} - n_{1r})^T \Psi^{-1} \Gamma \\ (s_{1d} - s_{1r})^T \Psi^{-1} \Gamma \\ p_{12}^1{}^T \Delta \tilde{R}_1^T \Lambda(R_{1r} p_{12}^1) \end{bmatrix}$$

where  $\Gamma$  and  $\Psi$  are defined in equations (3.105) and (3.106) and  $\Delta \tilde{R}_1 = R_{1d} - R_{1r}$ . The columns  $n_{1d} - n_{1r}$  and  $s_{1d} - s_{1r}$  are the two independent columns of  $\Delta \tilde{R}_1$ . It is assumed that  $\Delta \tilde{R}_1 p_{12}^1 \neq 0$ , so  $\Delta \tilde{R}_1 \neq 0 \rightarrow n_{1d} - n_{1r} \neq 0$  and  $s_{1d} - s_{1r} \neq 0$ . The third row of  $W$  can be rewritten to

$$\begin{aligned} p_{12}^1{}^T \Delta \tilde{R}_1^T \Lambda(R_{1r} p_{12}^1) &= p_{12}^1{}^T (R_{1d}^T - R_{1r}^T) \Lambda(R_{1r} p_{12}^1) \\ &= -\Lambda(R_{1r} p_{12}^1) (R_{1d} - R_{1r}) p_{12}^1 \\ &= -(R_{1r} p_{12}^1) \times ((R_{1d} - R_{1r}) p_{12}^1) \\ &= (R_{1d} p_{12}^1) \times (R_{1r} p_{12}^1). \end{aligned}$$

The third row of  $W$  is only equal to zero when the vectors  $R_{1d} p_{12}^1$  and  $R_{1r} p_{12}^1$  are parallel. Assuming small orientation errors and  $\Delta \tilde{R}_1 = R_{1d} - R_{1r} \neq 0$ , it can be concluded that the third row of  $W$  is nonzero. The rank of  $W$  is investigated by calculation of the determinant using the scalar triple product (E.1). Using the property of the cross product under a matrix transformation

$$(Ma) \times (Mb) = \det(M) M^{-T} (a \times b)$$

with  $M \in \mathbb{R}^{3 \times 3}$ ,  $M^{-T}$  the transpose of the inverse and  $a, b \in \mathbb{R}^3$ , the determinant of  $W$  reads

$$\begin{aligned} \det(W) &= \det(W^T) \\ &= ((R_{1d} p_{12}^1) \times (R_{1r} p_{12}^1)) \cdot ((\Gamma^T \Psi^{-T} (n_{1d} - n_{1r})) \times (\Gamma^T \Psi^{-T} (s_{1d} - s_{1r}))) \\ &= ((R_{1d} p_{12}^1) \times (R_{1r} p_{12}^1)) \cdot \left( \det(\Psi^{-1} \Gamma) (\Gamma^T \Psi^{-T})^{-T} (n_{1d} - n_{1r}) (s_{1d} - s_{1r}) \right) \\ &= \det(\Psi^{-1} \Gamma) \Lambda(R_{1d} p_{12}^1) R_{1r} p_{12}^1 \cdot \left( (\Gamma^T \Psi^{-T})^{-T} \Lambda(n_{1d} - n_{1r}) (s_{1d} - s_{1r}) \right) \\ &= -\det(\Psi^{-1} \Gamma) \underbrace{(s_{1d} - s_{1r})^T \Lambda(n_{1d} - n_{1r})}_{\neq 0} (\Gamma^T \Psi^{-T})^{-1} \underbrace{\Lambda(R_{1d} p_{12}^1) R_{1r} p_{12}^1}_{\neq 0} \end{aligned}$$

with  $\Lambda(x) \in \mathbb{R}^{3 \times 3}$  a skew symmetric matrix of the vector  $x \in \mathbb{R}^3$ . The matrices  $\Gamma$  and  $\Psi$  are designed to have full rank, so  $\det(\Psi^{-1} \Gamma) \neq 0$  and  $\Gamma^T \Psi^{-T}$  is invertible. The columns  $n_{1d} - n_{1r}$  and  $s_{1d} - s_{1r}$  are independent, so  $(s_{1d} - s_{1r})^T \Lambda(n_{1d} - n_{1r}) \neq 0$  and since  $\Delta \tilde{R}_1 \neq 0$ , the vector  $\Lambda(R_{1d} p_{12}^1) R_{1r} p_{12}^1 \neq 0$ . With a proper choice of

$\Gamma^T \Psi^{-T}$  (thus of the submatrices of the desired stiffness matrix  $S_i$ ) it is assumed that the vectors  $(s_{1d} - s_{1r})^T \Lambda (n_{1d} - n_{1r})$  and  $(\Gamma^T \Psi^{-T})^{-1} \Lambda (R_{1d} p_{12}^1) R_{1r} p_{12}^1$  are not parallel, so that  $\det(W) \neq 0$ . Then, the matrix  $W$  has full rank.

# Appendix **F**

## Impedance controller for cooperative manipulation: Additional Simulations

In this section, additional simulation results are presented related to the non-fixed grasp case introduced in Section 3.2.2. The circular disk in the simulations presented in this section is initially not in contact contrary to the results shown in Section 3.4.2 and its transition from non-contact to contact is introduced. An elastic collision is assumed and the coefficient of restitution in the normal direction is selected as  $e_{N_i} = 0.99$  whereas in the tangential direction it is kept at  $e_{T_i} = 0$  in (D.26). It can be observed from Figure F.1 that the actual robot joint angles reach a constant value at the end of the simulation, even though tracking is not achieved. The object position in  $x$  and  $y$  coordinates and its orientation  $\phi$  is shown in Figure F.2. It can be observed from Figure F.2 that the object coordinates also reach a constant value at the end of the simulation, and since no reference object trajectory is defined tracking is out of question. The normal and tangential contact velocities for both contact points are presented in Figure F.3. The normal and tangential contact impulses for both contact points are presented in Figure F.4. When Figures F.3 and F.4 are inspected it can be realized that initially normal components of the relative velocities are non-zero whereas the normal impulses are zero. This implies that the bodies are initially not in contact and they made contact after some time and the complementarity condition presented in Section 3.2.2 is satisfied. The effect of bouncing due to elastic collisions can further be observed from the Figure F.5 which is a zoomed version of Figure F.3.

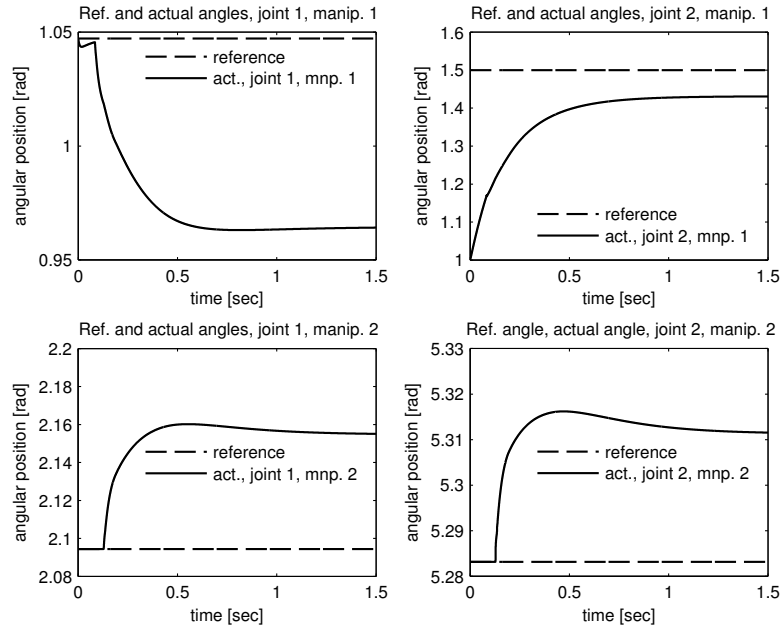


Figure F.1 Reference and actual robot motions

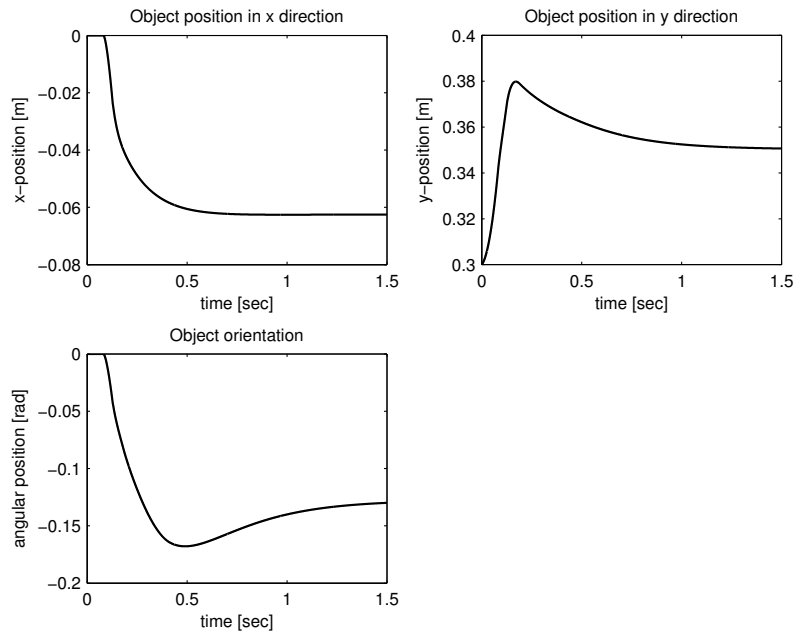


Figure F.2 Object position and orientation

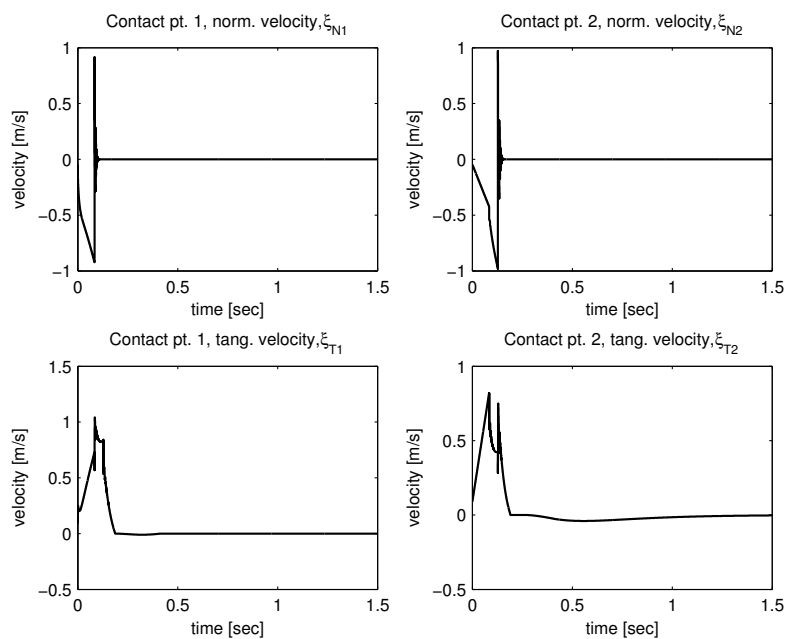


Figure F.3 Normal and tangential contact velocities

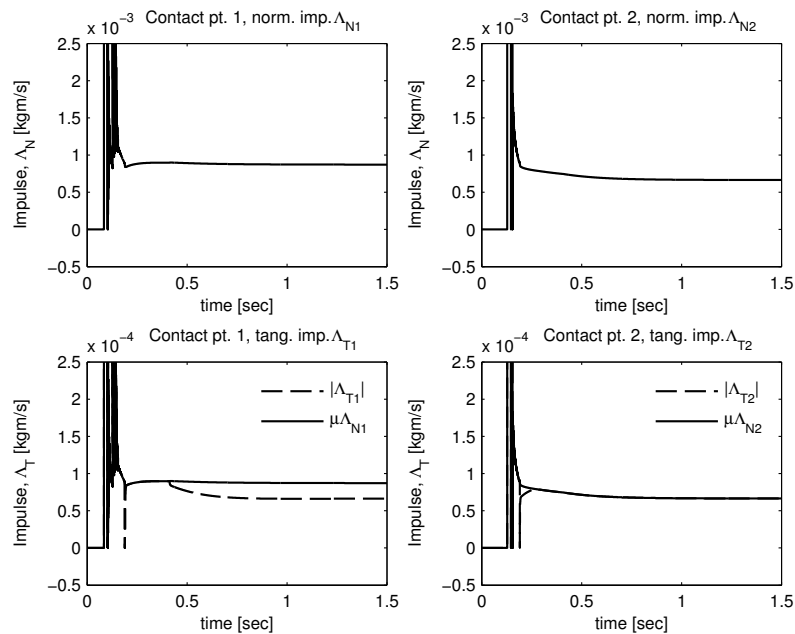
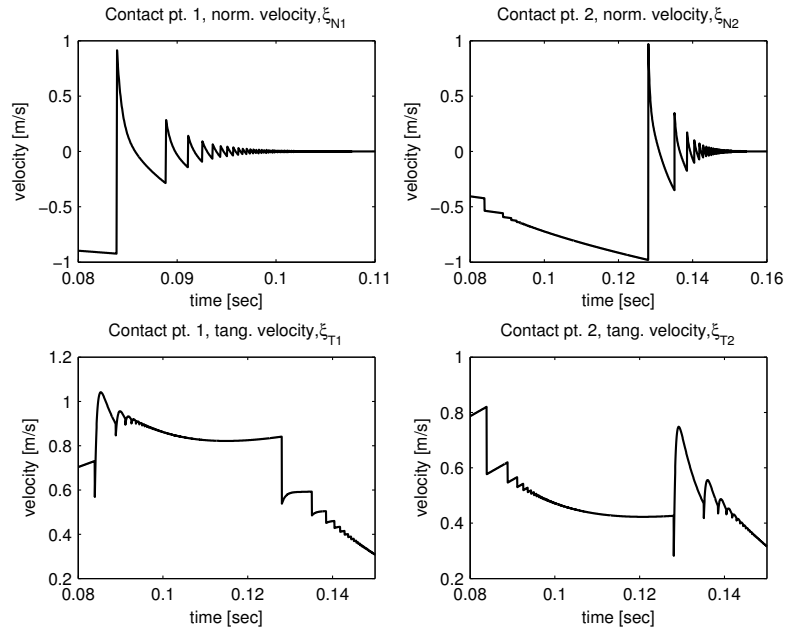


Figure F.4 Normal and tangential contact impulses



**Figure F.5** Normal and tangential contact velocities zoomed



# Appendix G

## Reference trajectory

The equations of the repetitive third order reference trajectory mentioned in Section 2.8.2 and Section 4.5.3 are introduced in this appendix. The acceleration of the reference trajectory is comprised of segments which are piecewise linear w.r.t. time. The equation of the reference position is given as follows,

$$q_{ref}(t) = \begin{cases} q_{0,1}(t), & t_0 \leq t \leq t_1 \\ q_{1,2}(t), & t_1 < t \leq t_2 \\ q_{2,3}(t), & t_2 < t \leq t_3 \\ q_{3,4}(t), & t_3 < t \leq t_4 \\ q_{4,5}(t), & t_4 < t \leq t_5 \\ q_{5,6}(t), & t_5 < t \leq t_6 \\ q_{6,7}(t), & t_6 < t \leq t_7 \end{cases} \quad (\text{G.1})$$

with

$$\begin{aligned} q_{0,1}(t) &= \frac{1}{6}\bar{j}(t^3 - t_0^3) + p_0, \\ q_{1,2}(t) &= \frac{1}{2}\bar{a}(\Delta t_1)^2 + v_1\Delta t_1 + p_1, \\ q_{2,3}(t) &= -\frac{1}{6}\bar{j}(t^3 - t_2^3) + \frac{1}{2}\bar{a}(\Delta t_2)^2 + v_2\Delta t_2 + p_2, \\ q_{3,4}(t) &= \bar{v}\Delta t_3 + p_3, \\ q_{4,5}(t) &= -\frac{1}{6}\bar{j}(t^3 - t_4^3) + \bar{v}\Delta t_4 + p_4, \\ q_{5,6}(t) &= -\frac{1}{2}\bar{a}(\Delta t_5)^2 + v_5\Delta t_5 + p_5, \\ q_{6,7}(t) &= \frac{1}{6}\bar{j}(t^3 - t_6^3) - \frac{1}{2}\bar{a}(\Delta t_6)^2 + v_6\Delta t_6 + p_6, \\ \Delta t_i &= t - t_i \quad \text{for } i = 1, \dots, 6 \end{aligned}$$

where  $\bar{v}$ ,  $\bar{a}$  and  $\bar{j}$  represent the selected bounds on the maximum velocity, acceleration and jerk of the trajectory respectively. Furthermore, the positions  $p_i = q_{ref}(t_i)$  and the velocities  $v_i = \dot{q}_{ref}(t_i)$  for  $i = 1, \dots, 6$  are given as,

$$\begin{aligned} p_1 &= \frac{1}{6}\bar{j}t_{\bar{j}}^3 + p_0, & p_2 &= \frac{1}{2}\bar{a}t_{\bar{a}}^2 + v_1t_{\bar{a}} + p_1, \\ p_3 &= -\frac{1}{6}\bar{j}t_{\bar{j}}^3 + \frac{1}{2}\bar{a}t_{\bar{j}}^2 + v_2t_{\bar{j}} + p_2, & p_4 &= \bar{v}t_{\bar{v}} + p_3 \end{aligned} \quad (\text{G.2})$$

$$\begin{aligned} p_5 &= -\frac{1}{6}\bar{j}t_{\bar{j}}^3 + \bar{v}t_{\bar{j}} + p_4, & p_6 &= -\frac{1}{2}\bar{a}t_{\bar{a}}^2 + v_5t_{\bar{a}} + p_5, \\ p_7 &= \frac{1}{6}\bar{j}t_{\bar{j}}^3 - \frac{1}{2}\bar{a}t_{\bar{j}}^2 + v_6t_{\bar{j}} + p_6 \end{aligned} \quad (\text{G.3})$$

$$\begin{aligned} v_1 &= \frac{1}{2}\bar{j}t_{\bar{j}}^2, & v_2 &= \bar{a}t_{\bar{a}} + v_1, & v_3 &= \bar{v} = -\frac{1}{2}\bar{j}t_{\bar{j}}^2 + \bar{a}t_{\bar{j}} + v_2, \\ v_5 &= -\frac{1}{2}\bar{j}t_{\bar{j}}^2, & v_6 &= -\bar{a}t_{\bar{a}} + v_5 \end{aligned} \quad (\text{G.4})$$

where  $p_0 = q_{ref}(t_0)$  is the initial position, with

$$t_{\bar{j}} = t_1 - t_0 = t_3 - t_2 = t_5 - t_4 = t_7 - t_6 = \frac{\bar{a}}{\bar{j}}, \quad (\text{G.5})$$

$$t_{\bar{a}} = t_2 - t_1 = t_6 - t_5 = \frac{v_2 - v_1}{\bar{a}}, \quad (\text{G.6})$$

$$t_{\bar{v}} = t_4 - t_3 = \frac{p_4 - p_3}{\bar{v}} \quad (\text{G.7})$$

which can be calculated using (G.2), (G.3) and (G.4). For the experimental results introduced in Section 4.5.3,  $p_0 = 0.2[\text{m}]$ ,  $\bar{v} = 0.05[\text{m/s}]$ ,  $\bar{a} = 0.05[\text{m/s}^2]$ , and  $\bar{j} = 10[\text{m/s}^3]$ , respectively. Once, the algorithm is started at  $t_0$  (i.e.  $t_0$  is given), then the switching time instances  $t_i$  for  $i = 1, \dots, 7$  are calculated accordingly.

# Bibliography

- [1] M. Abramowitz and I. A. Stegun. *Handbook of Mathematical Functions, With Formulas, Graphs, and Mathematical Tables*. Dover Publications, Incorporated, 1974.
- [2] R.P. Agarwal and V. Lakshmikantham. *Uniqueness and Nonuniqueness Criteria for Ordinary Differential Equations*. Ser. Real Anal. 6. World Scientific, 1993.
- [3] F. Al-Bender, V. Lampaert, and J. Swevers. The generalized maxwell-slip model: a novel model for friction simulation and compensation. *IEEE Transactions on Automatic Control*, 50(11):1883–1887, 2005.
- [4] A. Albu-Schaffer, C. Ott, U. Frese, and G. Hirzinger. Cartesian impedance control of redundant robots: recent results with the dlr-light-weight-arms. In *Proceedings of IEEE International Conference on Robotics and Automation (ICRA)*, pages 3704–3709 vol.3, 2003.
- [5] I. Aliaga, A. Rubio, and E. Sanchez. Experimental quantitative comparison of different control architectures for master-slave teleoperation. *IEEE Transactions on Control Systems Technology*, 12(1):2–11, 2004.
- [6] F. Alonge, A. Bruno, and F. D’Ippolito. Adaptive interaction robot control with estimation of contact force. In *17<sup>th</sup> World Congress of the International Federation of Automatic Control (IFAC)*, 2008.
- [7] R. Anderson and M.W. Spong. Hybrid impedance control of robotic manipulators. *IEEE Journal of Robotics and Automation*, 4(5):549–556, 1988.
- [8] P. Arcara and C. Melchiorri. Control schemes for teleoperation with time delay: A comparative study. *Robotics and Autonomous Systems*, 38(1):49–64, 2002.

- 
- [9] B. Armstrong, O. Khatib, and J. Burdick. The explicit dynamic model and inertial parameters of the puma 560 arm. In *Proceedings of IEEE International Conference on Robotics and Automation (ICRA)*, volume 3, pages 510–518, 1986.
- [10] H. Asada and K. Youcef-Toumi. *Direct-drive Robots: Theory and Practice*. MIT Press, Cambridge, MA, USA, 1987.
- [11] K. J. Åström and B. Wittenmark. *Computer-Controlled Systems: theory and design*. Prentice-Hall, Upper Saddle River, NJ, 3rd edition, 1997.
- [12] ATI Industrial Automation, Apex, North Carolina USA. *F/T Data Acquisition (DAQ) Six-Axis Force/Torque Sensor System Installation and Operation Manual*, April 2012.
- [13] L. Bascetta and P. Rocco. Revising the robust-control design for rigid robot manipulators. *IEEE Transactions on Robotics*, 26(1):180–187, 2010.
- [14] C. Bechlioulis, Z. Doulgeri, and G. Rovithakis. Model free force/position robot control with prescribed performance. In *18<sup>th</sup> Mediterranean Conference on Control Automation (MED)*, pages 377–382, 2010.
- [15] E. Bernuau, W. Perruquetti, D. Efimov, and E. Moulay. Finite-time output stabilization of the double integrator. In *IEEE 51<sup>st</sup> Annual Conference on Decision and Control (CDC)*, pages 5906–5911, 2012.
- [16] S.P. Bhat and D.S. Bernstein. Finite-time stability of homogeneous systems. In *Proceedings of the American Control Conference*, volume 4, pages 2513–2514, 1997.
- [17] S.P. Bhat and D.S. Bernstein. Continuous finite-time stabilization of the translational and rotational double integrators. *IEEE Transactions on Automatic Control*, 43(5):678–682, 1998.
- [18] S.P. Bhat and D.S. Bernstein. Finite-time stability of continuous autonomous systems. *SIAM J. Control Optim.*, 38:751–766, 2000.
- [19] S.P. Bhat and D.S. Bernstein. Geometric homogeneity with applications to finite-time stability. *Mathematics of Control, Signals, and Systems (MCSS)*, 17:101–127, 2005.
- [20] R. Bickel, M. Tomizuka, and W. Chung. Hybrid impedance control in constraint coordinates using a disturbance observer. In *Proceedings of 35<sup>th</sup> IEEE Decision and Control*, volume 2, pages 1974–1979, 1996.
- [21] A. Bolognoni and S. Regnier. A review of haptic feedback teleoperation systems for micromanipulation and microassembly. *IEEE Transactions on Automation Science and Engineering*, 10(3):496–502, 2013.

- [22] B. Bona and M. Indri. Friction compensation in robotics: an overview. In *Proceedings of the Joint 44<sup>th</sup> IEEE Conference on Decision and Control and European Control Conference (CDC/ECC)*, pages 4360–4367, 2005.
- [23] R.G. Bonitz and T.C. Hsia. Internal force-based impedance control for co-operating manipulators. *IEEE Transactions on Robotics and Automation*, 12(1):78–89, 1996.
- [24] R. D. Braatz. Internal model control. In William S. Levine, editor, *The Control Handbook, Volume I*, pages 215–224. CRC Press, 1996.
- [25] B. Brogliato. Feedback control. In *Nonsmooth Mechanics*, Communications and Control Engineering, pages 397–461. Springer London, 1999.
- [26] B. Brogliato. *Nonsmooth mechanics: models, dynamics, and control*. Springer Verlag, 1999.
- [27] B. Brogliato and J.-M. Bourgeot. Tracking control of complementarity lagrangian systems. *International Journal of Bifurcation and Chaos*, 15(6):1839–1866, 2005.
- [28] F. Caccavale, P. Chiacchio, A. Marino, and L. Villani. Six-dof impedance control of dual-arm cooperative manipulators. *IEEE/ASME Transactions on Mechatronics*, 13(5):576–586, 2008.
- [29] F. Caccavale, C. Natale, B. Siciliano, and L. Villani. Resolved-acceleration control of robot manipulators: A critical review with experiments. *Robotica*, 16:565–573, 1998.
- [30] F. Caccavale, C. Natale, B. Siciliano, and L. Villani. Six-dof impedance control based on angle/axis representations. *IEEE Transactions on Robotics and Automation*, 15(2):289–300, 1999.
- [31] F. Caccavale and M. Uchiyama. Cooperative manipulators. In B. Siciliano and O. Khatib, editors, *Springer Handbook of Robotics*, pages 701–718. Springer Berlin Heidelberg, 2008.
- [32] F. Caccavale and L. Villani. Impedance control of cooperative manipulators. *Machine, Intelligence and Robotic Control*, 2:51–57, 2000.
- [33] S.P. Chan, B. Yao, W.B. Gao, and M. Cheng. Robust impedance control of robot manipulators. *International Journal of Robotics and Automation*, 6(4):220–227, 1991.
- [34] K.-S. Chang, R. Holmberg, and O. Khatib. The augmented object model: cooperative manipulation and parallel mechanism dynamics. In *Proceedings of IEEE International Conference on Robotics and Automation (ICRA)*, pages 470–475 vol.1, 2000.

- 
- [35] S. Chiaverini and L. Sciavicco. The parallel approach to force/position control of robotic manipulators. *IEEE Transactions on Robotics and Automation*, 9(4):361–373, 1993.
- [36] C.-S. Chiu, K.-Y. Lian, and T.-C. Wu. Robust adaptive motion/force tracking control design for uncertain constrained robot manipulators. *Automatica*, 40(12):2111–2119, 2004.
- [37] E. A. Coddington and N. Levinson. *Theory of Ordinary Differential Equations*. Robert E. Krieger, Malabar, Florida, 1984.
- [38] R. Colbaugh and K. Glass. Adaptive compliant motion control of manipulators without velocity measurements. *Journal of Robotic Systems*, 14(7):513–527, 1997.
- [39] R. Colbaugh and K. Glass. Adaptive task-space control of flexible-joint manipulators. *Journal of Intelligent and Robotic Systems*, 20(2-4):225–249, 1997.
- [40] R. Colbaugh, K. Glass, and K. Wedeward. Adaptive compliance control of electrically-driven manipulators. In *Proceedings of 35<sup>th</sup> IEEE Conference on Decision and Control*, pages 394–399 vol.1, 1996.
- [41] J. de Schutter and H. Van Brussel. Compliant robot motion ii. a control approach based on external control loops. *The International Journal of Robotics Research*, 7(4):18–33, 1988.
- [42] C.C. de Wit, H. Olsson, K.J. Astrom, and P. Lischinsky. A new model for control of systems with friction. *IEEE Transactions on Automatic Control*, 40(3):419–425, 1995.
- [43] A. Denasi, D. Kostić, and H. Nijmeijer. An application of impact structure to bilateral teleoperations. In *49<sup>th</sup> IEEE Conference on Decision and Control (CDC)*, pages 1985–1990, 2010.
- [44] A. Denasi, D. Kostić, and H. Nijmeijer. Time delay compensation in bilateral teleoperations using impact. *IEEE Transactions on Control Systems Technology*, 21(3):704–715, 2013.
- [45] Z. Doulgeri and Y. Karayiannidis. Force/position control self-tuned to unknown surface slopes using motion variables. *Robotica*, 26:703–710, 2008.
- [46] J. Duffy. The fallacy of modern hybrid control theory that is based on "orthogonal complements" of twist and wrench spaces. *Journal of Robotic Systems*, 7(2):139–144, 1990.
- [47] E.D. Fasse and J.F. Broenink. A spatial impedance controller for robotic manipulation. *IEEE Transactions on Robotics and Automation*, 13(4):546–556, 1997.

- [48] A. F. Filippov. *Differential equations with discontinuous righthand sides*, volume 18 of *Mathematics and its Applications (Soviet Series)*. Kluwer Academic Publishers Group, Dordrecht, 1988.
- [49] O.-E. Fjellstad. *Control of Unmanned Underwater Vehicles in Six Degrees of Freedom: A Quaternion Feedback Approach*. PhD thesis, The Norwegian Institute of Technology University of Trondheim, November 1994.
- [50] T.I. Fossen. *Marine control systems: guidance, navigation and control of ships, rigs and underwater vehicles*. Marine Cybernetics AS, 2002.
- [51] G.F. Franklin, J.D. Powell, and A. Emami-Naeini. *Feedback control of dynamic systems*. Prentice-Hall, Upper Saddle River, NJ 07458, USA, 4th edition, 2002.
- [52] L.-G. Garcia-Valdovinos, V. Parra-Vega, and M.A. Arteaga. Observer-based sliding mode impedance control of bilateral teleoperation under constant unknown time delay. *Robotics and Autonomous Systems*, 55(8):609–617, 2007.
- [53] G. Gilardi and I. Sharf. Literature survey of contact dynamics modelling. *Mechanism and Machine Theory*, 37(10):1213 – 1239, 2002.
- [54] C. Glocker. Formulation of spatial contact situations in rigid multibody systems. *Computer Methods in Applied Mechanics and Engineering*, 177(3-4):199 – 214, 1999.
- [55] C. Glocker. On frictionless impact models in rigid-body systems. *Philosophical Transactions of the Royal Society of London. Series A: Mathematical, Physical and Engineering Sciences*, 359(1789):2385–2404, 2001.
- [56] C. Glocker. *Set-Valued Force Laws, Dynamics of Non-Smooth Systems*, volume 1 of *Lecture Notes in Applied Mechanics*. Springer-Verlag, Berlin, 2001.
- [57] P. B. Goldsmith, B.A. Francis, and A.A. Goldenberg. The cause of kinematic instability in hybrid position/force control: contact compliance. In *Proceedings of Intelligent Information Systems (IIS)*, pages 594–598, 1997.
- [58] V.T. Haimo. Finite time controllers. *SIAM J. Control Optim.*, 24:760–770, 1986.
- [59] H.-Y. Han and S. Kawamura. Analysis of stiffness of human fingertip and comparison with artificial fingers. In *Proceedings of IEEE International Conference on Systems, Man, and Cybernetics (SMC)*, pages 800–805 vol.2, 1999.
- [60] G.H. Hardy, J.E. Littlewood, and G. Pólya. *Inequalities*. Cambridge Mathematical Library. Cambridge University Press, 1952.

- [61] K. Hastrudi-Zaad and S.E. Salcudean. On the use of local force feedback for transparent teleoperation. In *Proceedings of IEEE International Conference on Robotics and Automation*, pages 1863–1869 vol.3, 1999.
- [62] S. Hayati. Hybrid position/force control of multi-arm cooperating robots. In *Proceedings of IEEE International Conference on Robotics and Automation*, volume 3, pages 82–89, 1986.
- [63] D.J.F. Heck, D. Kostić, A. Denasi, and H. Nijmeijer. Internal and external force-based impedance control for cooperative manipulation. In *Proceedings of the European Control Conference (ECC), July 17-19*, pages 2299–2304, 2013.
- [64] W.P.M.H. Heemels, A.R. Teel, N. van de Wouw, and D. Nesic. Networked control systems with communication constraints: Tradeoffs between transmission intervals, delays and performance. *IEEE Transactions on Automatic Control*, 55(8):1781–1796, 2010.
- [65] Y.K. Ho, D. Wang, and Y.C. Soh. Modelling of constrained robot system with constraint uncertainties. *Journal of Robotic Systems*, 17(1):53–61, 2000.
- [66] N. Hogan. Impedance control: An approach to manipulation: Part i-theory. *Journal of Dynamic Systems, Measurement, and Control*, 107(1):1–7, 1985.
- [67] P.F. Hokayem and M.W. Spong. Bilateral teleoperation: An historical survey. *Automatica*, 42(12):2035 – 2057, 2006.
- [68] Y. Hong.  $H_\infty$  control, stabilization, and input-output stability of nonlinear systems with homogeneous properties. *Automatica*, 37(6):819 – 829, 2001.
- [69] Y. Hong, J. Huang, and Y. Xu. On an output feedback finite-time stabilisation problem. In *Proceedings of 38<sup>th</sup> IEEE Conference on Decision and Control*, pages 1302–1307 vol.2, 1999.
- [70] Y. Hong, J. Huang, and Y. Xu. On an output feedback finite-time stabilization problem. *IEEE Transactions on Automatic Control*, 46(2):305–309, 2001.
- [71] Y. Hong, J. Huang, and Y. Xu. Finite-time control for robot manipulators. *Systems & Control Letters*, 46(4):243–253, 2002.
- [72] Y. Karayiannidis and Z. Doulgeri. Robot contact tasks in the presence of control target distortions. *Robotics and Autonomous Systems*, 58(5):596–606, 2010.
- [73] H.K. Khalil. *Nonlinear Systems*. Prentice Hall, 3<sup>rd</sup> edition, 2002.
- [74] O. Khatib. Object manipulation in a multi-effector robot system. In *Proc. 4<sup>th</sup> Int. Symp. on Robotics Research*, pages 137–144. The MIT Press, Cambridge, MA, USA, 1988.



- [75] O. Khatib. Inertial properties in robotic manipulation: An object-level framework. *The International Journal of Robotics Research*, 14(1):19–36, 1995.
- [76] J.-S. Kim, K. Suzuki, A. Konno, and M. Uchiyama. Force control of constrained flexible manipulators. In *Proceedings of IEEE International Conference on Robotics and Automation*, pages 635–640 vol.1, 1996.
- [77] F.M. Klomp. Haptic control for dummies, an introduction and analysis. Master’s thesis, Eindhoven University of Technology, August 2006.
- [78] M. Koga, K. Kosuge, K. Furuta, and K. Nosaki. Coordinated motion control of robot arms based on the virtual internal model. *IEEE Transactions on Robotics and Automation*, 8(1):77–85, 1992.
- [79] A. J. Koivo and M.A. Unseren. Reduced order model and decoupled control architecture for two manipulators holding a rigid object. *Journal of Dynamic System, Measurement, and Control*, 113(4):646–654, 1991.
- [80] M. Koot. Identification and control of the rrr-robot. Dct report no. 2001.48, Department of Mechanical Engineering, Technische Universiteit Eindhoven, Eindhoven, The Netherlands, 2001.
- [81] D. Kostić. *Data-driven Robot Motion Control Design*. PhD thesis, Technische Universiteit Eindhoven, 2004.
- [82] C. Kravaris and R. A. Wright. Deadtime compensation for nonlinear processes. *AIChE Journal*, 35(9):1535–1542, 1989.
- [83] D.A. Lawrence. Stability and transparency in bilateral teleoperation. *IEEE Transactions on Robotics and Automation*, 9(5):624–637, 1993.
- [84] R.I. Leine, B. Brogliato, and H. Nijmeijer. Periodic motion and bifurcations induced by the painlevé paradox. *European Journal of Mechanics - A/Solids*, 21(5):869 – 896, 2002.
- [85] R.I. Leine and N. van de Wouw. *Stability and convergence of mechanical systems with unilateral constraints*. Lecture notes in applied and computational mechanics. Springer, Berlin, 2008.
- [86] R.I. Leine and N. van de Wouw. Stability properties of equilibrium sets of non-linear mechanical systems with dry friction and impact. *Nonlinear Dynamics*, 51(4):551–583, 2008.
- [87] A.C. Leite, F. Lizarralde, and L. Hsu. Hybrid adaptive vision-force control for robot manipulators interacting with unknown surfaces. *The International Journal of Robotics Research*, 28(7):911–926, 2009.

- [88] S. Li and Y.-P. Tian. Finite-time stability of cascaded time-varying systems. *International Journal of Control*, 80(4):646–657, 2007.
- [89] S.-K. Lin. Euler parameters in robot cartesian control. In *Proceedings of IEEE International Conference on Robotics and Automation*, pages 1676–1681 vol.3, 1988.
- [90] S.-K. Lin. Singularity of nonlinear feedback control scheme for robots. *IEEE Transactions on Systems, Man and Cybernetics*, 19(1):134–139, 1989.
- [91] V. Lippiello, B. Siciliano, and L. Villani. Robot force/position control with force and visual feedback. In *European Control Conference (ECC)*, pages 3790–3795, 2007.
- [92] G.J. Liu and A.A. Goldenberg. Robust hybrid impedance control of robot manipulators. In *Proceedings of IEEE International Conference on Robotics and Automation*, volume 1, pages 287–292, 1991.
- [93] J. Y S Luh, M. W. Walker, and R. P C Paul. Resolved-acceleration control of mechanical manipulators. *IEEE Transactions on Automatic Control*, 25(3):468–474, 1980.
- [94] R. Mahony and T. Hamel. Robust trajectory tracking for a scale model autonomous helicopter. *International Journal of Robust and Nonlinear Control*, 14(12):1035–1059, 2004.
- [95] J. Maitin-Shepard, M. Cusumano-Towner, J. Lei, and P. Abbeel. Cloth grasp point detection based on multiple-view geometric cues with application to robotic towel folding. In *IEEE International Conference on Robotics and Automation (ICRA)*, pages 2308–2315, 2010.
- [96] M.S. Matijević, M.R. Stojić, and K. Schlacher. Absorption principle in process control applications. *Electrical Engineering*, 89(7):577–584, 2007.
- [97] T. Miyoshi, K. Terasima, and M. Buss. A design method of wave filter for stabilizing non-passive operating system. In *IEEE International Conference on Control Applications*, pages 1318–1324, 2006.
- [98] D.J. Montana. The kinematics of contact and grasp. *The International Journal of Robotics Research*, 7(3):17–32, 1988.
- [99] S.A.A. Moosavian and E. Papadopoulos. Multiple impedance control for object manipulation. In *Proceedings of IEEE/RSJ International Conference on Intelligent Robots and Systems*, pages 461–466 vol.1, 1998.
- [100] M. Morari and E. Zafiriou. *Robust Process Control*. Prentice-Hall, 1989.
- [101] S. Munir and W.J. Book. Internet-based teleoperation using wave variables with prediction. *IEEE/ASME Transactions on Mechatronics*, 7(2):124–133, 2002.

- [102] R.M. Murray, S.S. Sastry, and Z. Li. *A Mathematical Introduction to Robotic Manipulation*. CRC Press, Inc., Boca Raton, FL, USA, 1<sup>st</sup> edition, 1994.
- [103] M. Namvar and F. Aghili. Adaptive force-motion control of coordinated robots interacting with geometrically unknown environments. *IEEE Transactions on Robotics*, 21(4):678–694, 2005.
- [104] NASA. Robonaut 1. <http://robonaut.jsc.nasa.gov/R1/sub/software.asp>, March 2008.
- [105] C. Natale and L. Villani. Adaptive control of a robot manipulator in contact with a curved compliant surface. In *Proceedings of American Control Conference*, pages 288–292 vol.1, 1999.
- [106] Technology Research News. Cooperative robots share the load, February 2002. [http://www.trnmag.com/Stories/2002/021302/Cooperative\\_robots\\_share\\_the\\_load\\_021302.html](http://www.trnmag.com/Stories/2002/021302/Cooperative_robots_share_the_load_021302.html).
- [107] G. Niemeyer, C. Preusche, and G. Hirzinger. Telerobotics. In B. Siciliano and O. Khatib, editors, *Springer Handbook of Robotics*, pages 741–757. Springer Berlin Heidelberg, 2008.
- [108] J.E. Normey-Rico and E.F. Camacho. Dead-time compensators: A survey. *Control Engineering Practice*, 16(4):407–428, 2008. Special Section on Manoeuvring and Control of Marine Craft.
- [109] K. Ogata. *Discrete-time control systems (2nd ed.)*. Prentice-Hall, Inc., Upper Saddle River, NJ, USA, 1995.
- [110] P.R. Paglia. Control of contact problem in constrained euler-lagrange systems. *IEEE Transactions on Automatic Control*, 46(10):1595–1599, 2001.
- [111] P.R. Pagilla and M. Tomizuka. Contact transition control of nonlinear mechanical systems subject to a unilateral constraint. *J. Dyn. Sys., Meas., Control*, 119(4):749–759, 1997.
- [112] V. Parra-Vega, A. Rodriguez-Angeles, and G. Hirzinger. Perfect position/force tracking of robots with dynamical terminal sliding mode control. *Journal of Robotic Systems*, 18(9):517–532, 2001.
- [113] R. Pintelon, P. Guillaume, Y. Rolain, J. Schoukens, and H. Van Hamme. Parametric identification of transfer functions in the frequency domain—a survey. *IEEE Transactions on Automatic Control*, 39(11):2245–2260, 1994.
- [114] R. Pintelon and J. Schoukens. *System Identification: A Frequency Domain Approach*. Wiley, 2<sup>nd</sup> edition, 2012.
- [115] Quanser Consulting, Markham, Ontario, Canada. *MultiQ-PCI Data Acquisition System: user’s guide V1.0*, 2000.

- 
- [116] Quanser Consulting, Markham, Ontario, Canada. *WinCon 5.0: user's guide V1.1*, 2002.
- [117] M. H. Raibert and J.J. Craig. Hybrid position/force control of manipulators. *Journal of Dynamics Systems, Measurement, and Control*, 103(2):126–133, 1981.
- [118] J. Pena Ramirez, A. Denasi, A. Rodriguez-Angeles, J. Alvarez, H. Nijmeijer, and K. Aihara. Controlled synchronization: A huygens' inspired approach. In *19<sup>th</sup> World Congress of the International Federation of Automatic Control (IFAC)*, 2014.
- [119] E. Rang. Isochrone families for second-order systems. *IEEE Transactions on Automatic Control*, 8(1):64–65, 1963.
- [120] Yaskawa Motoman Robotics. Motoman sda10 assembling a chair. <http://www.motoman.com/industries/furniture-fixtures.php>.
- [121] Robot Rose. Robot rose media footage. <http://robot-rose.com/media/>.
- [122] L. Rosier. Homogeneous lyapunov function for homogeneous continuous vector field. *Systems & Control Letters*, 19(6):467 – 473, 1992.
- [123] N. Sadati and A. Ghaffarkhah. Decentralized impedance control of nonredundant multi-manipulator systems. In *IEEE International Conference on Networking, Sensing and Control (ICNSC)*, pages 206–211, 2008.
- [124] J.K. Salisbury. Active stiffness control of a manipulator in cartesian coordinates. In *19<sup>th</sup> IEEE Conference on Decision and Control including the Symposium on Adaptive Processes*, volume 19, pages 95–100, 1980.
- [125] N. Sarkar, X. Yun, and V. Kumar. Dynamic control of 3-d rolling contacts in two-arm manipulation. *IEEE Transactions on Robotics and Automation*, 13(3):364–376, 1997.
- [126] S.A. Schneider and Jr. Cannon, R.H. Object impedance control for cooperative manipulation: theory and experimental results. *IEEE Transactions on Robotics and Automation*, 8(3):383–394, 1992.
- [127] H. Seraji. Adaptive force and position control of manipulators. *Journal of Robotic Systems*, 4(4):551–578, 1987.
- [128] T.B. Sheridan. *Telerobotics, automation, and human supervisory control*. MIT Press, Cambridge, MA, USA, 1992.
- [129] T.B. Sheridan and W.R. Ferrell. Remote manipulative control with transmission delay. *IEEE Transactions on Human Factors in Electronics*, 4(1):25–29, 1963.

- [130] R. Shoureshi, M.E. Momot, and M.D. Roesler. Robust control for manipulators with uncertain dynamics. *Automatica*, 26(2):353 – 359, 1990.
- [131] B. Siciliano, L. Sciavicco, L. Villani, and G. Oriolo. *Robotics: Modelling, Planning and Control*. Springer Verlag, 2009.
- [132] B. Siciliano and L. Villani. *Robot Force Control*, volume 540 of *The Springer International Series in Engineering and Computer Science*. Springer US, 1999.
- [133] S. Skogestad and I. Postlethwaite. *Multivariable Feedback Control: Analysis and Design*. John Wiley & Sons, 2005.
- [134] A.C. Smith and K. Hashtrudi-Zaad. Smith predictor type control architectures for time delayed teleoperation. *The International Journal of Robotics Research*, 25(8):797–818, 2006.
- [135] C. Smith, Y. Karayiannidis, L. Nalpantidis, X. Gratal, P. Qi, D.V. Dimarogonas, and D. Kragic. Dual arm manipulation—a survey. *Robotics and Autonomous Systems*, 60(10):1340–1353, 2012.
- [136] M.W. Spong, S. Hutchinson, and M. Vidyasagar. *Robot Modeling and Control*. John Wiley & Sons, Inc, 2006.
- [137] M.R. Stojić, M.S. Matijević, and L.S. Draganović. A robust smith predictor modified by internal models for integrating process with dead time. *IEEE Transactions on Automatic Control*, 46(8):1293–1298, 2001.
- [138] J. Stuelpnagel. On the parametrization of the three-dimensional rotation group. *SIAM Review*, 6(4):pp. 422–430, 1964.
- [139] C.-Y. Su and Y. Stepanenko. Adaptive sliding mode coordinated control of multiple robot arms handling one constrained object. In *American Control Conference*, pages 1406–1413, 1993.
- [140] Y. Su. Global continuous finite-time tracking of robot manipulators. *International Journal of Robust and Nonlinear Control*, 19(17):1871–1885, 2009.
- [141] Y. Su and C. Zheng. A simple nonlinear pid control for finite-time regulation of robot manipulators. In *IEEE International Conference on Robotics and Automation (ICRA)*, pages 2569–2574, 2009.
- [142] S. Tafazoli, S.E. Salcudean, K. Hashtrudi-Zaad, and P.D. Lawrence. Impedance control of a teleoperated excavator. *IEEE Transactions on Control Systems Technology*, 10(3):355–367, 2002.
- [143] T.-J. Tarn, A.K. Bejczy, and X. Yun. Design of dynamic control of two cooperating robot arms: Closed chain formulation. In *Proceedings of IEEE International Conference on Robotics and Automation*, volume 4, pages 7–13, 1987.

- [144] T.-J. Tarn, Y. Wu, N. Xi, and A. Isidori. Force regulation and contact transition control. *IEEE Control Systems*, 16(1):32–40, 1996.
- [145] A.G. Torres. From cad-design to force controlled robot manufacturing. Master thesis, Lund University, Department of Automatic Control, September 2010.
- [146] Ya.Z. Tsympkin and U. Holmberg. Robust stochastic control using the internal mode principle and internal model control. *International Journal of Control*, 61(4):809–822, 1995.
- [147] M. Uchiyama. Chapter 1 multi-arm robot systems: A survey. In Pasquale Chiacchio and Stefano Chiaverini, editors, *Complex Robotic Systems*, volume 233 of *Lecture Notes in Control and Information Sciences*, pages 1–31. Springer Berlin Heidelberg, 1998.
- [148] M. Uchiyama and P. Dauchez. A symmetric hybrid position/force control scheme for the coordination of two robots. In *Proceedings of IEEE International Conference on Robotics and Automation*, pages 350–356 vol.1, 1988.
- [149] M. Uchiyama and P. Dauchez. Symmetric kinematic formulation and non-master/slave coordinated control of two-arm robots. *Advanced Robotics*, 7(4):361–383, 1992.
- [150] M. Uchiyama, N. Iwasawa, and K. Hakomori. Hybrid position/force control for coordination of a two-arm robot. In *Proceedings of IEEE International Conference on Robotics and Automation*, volume 4, pages 1242–1247, 1987.
- [151] Stanford University. The stanford assistant mobile manipulator (samm). <http://robotics.stanford.edu/~ruspini/samm.html>.
- [152] H. Urbanek, A. Albu-Schaffer, and P. Van Der Smagt. Learning from demonstration: repetitive movements for autonomous service robotics. In *Proceedings of IEEE/RSJ International Conference on Intelligent Robots and Systems (IROS)*., pages 3495–3500 vol.4, 2004.
- [153] A.M. van Beek. Rrr-robot: instruction manual. Technical Report WFW report 98.012, Faculty of Mechanical Engineering, Technische Universiteit Eindhoven, Eindhoven, The Netherlands, 1998.
- [154] E. van den Ouderaa, J. Schoukens, and J. Renneboog. Peak factor minimization, using time-frequency domain swapping algorithm. *IEEE Trans. Instrum. Meas.*, 37(1):144–147, 1988.
- [155] B. Vanderborght, A. Albu-Schaeffer, A. Bicchi, E. Burdet, D.G. Caldwell, R. Carloni, M. Catalano, O. Eiberger, W. Friedl, G. Ganesh, M. Garabini, M. Grebenstein, G. Grioli, S. Haddadin, H. Hoppner, A. Jafari, M. Laf-franchi, D. Lefeber, F. Petit, S. Stramigioli, N. Tsagarakis, M. Van Damme,

- R. Van Ham, L.C. Visser, and S. Wolf. Variable impedance actuators: A review. *Robotics and Autonomous Systems*, 61(12):1601–1614, 2013.
- [156] L. Villani, C. Natale, B. Siciliano, and C. Canudas de Wit. An experimental study of adaptive force/position control algorithms for an industrial robot. *IEEE Transactions on Control Systems Technology*, 8(5):777–786, 2000.
- [157] L. Villani and J. de Schutter. Force control. In B. Siciliano and O. Khatib, editors, *Springer Handbook of Robotics*, pages 161–187. Springer, 2008.
- [158] K. Waldron and J. Schmiedeler. Kinematics. In B. Siciliano and O. Khatib, editors, *Springer Handbook of Robotics*, pages 9–33. Springer Berlin Heidelberg, 2008.
- [159] K. Wedeward, R. Colbaugh, and A. Engelmann. Adaptive explicit force control of position-controlled manipulators. *Journal of Robotic Systems*, 13(9):603–618, 1996.
- [160] T. Wimböck, C. Ott, and G. Hirzinger. Impedance behaviors for two-handed manipulation: Design and experiments. In *IEEE International Conference on Robotics and Automation*, pages 4182–4189, 2007.
- [161] S.K.P. Wong and D.E. Seborg. Control strategy for single-input single-output non-linear systems with time delays. *International Journal of Control*, 48:2303 – 2327, 1988.
- [162] W.M. Wonham. *Linear multivariable control: A Geometric Approach*. Springer-Verlag, Berlin; New York, 1974.
- [163] C.-h. Wu, J.C. Houk, K.-Y. Young, and L.E. Miller. Nonlinear damping of limb motion. In J.M. Winters and S.L.-Y. Woo, editors, *Multiple Muscle Systems*, pages 214–235. Springer New York, 1990.
- [164] Di Xiao, B.K. Ghosh, Ning Xi, and T.J. Tarn. Sensor-based hybrid position/force control of a robot manipulator in an uncalibrated environment. *IEEE Transactions on Control Systems Technology*, 8(4):635–645, 2000.
- [165] B. Yao, S.P. Chan, and D. Wang. Unified formulation of variable structure control schemes for robot manipulators. *IEEE Transactions on Automatic Control*, 39(2):371–376, 1994.
- [166] B. Yao, S.P. Chan, and D. Wang. Variable structure adaptive motion and force control of robot manipulators. *Automatica*, 30(9):1473 – 1477, 1994.
- [167] B. Yao, S.P. Chan, and D. Wang. Vsc motion and force control of robot manipulators in the presence of environmental constraint uncertainties. *Journal of Robotic Systems*, 11(6):503–515, 1994.

- 
- [168] B. Yao, W.B. Gao, S.P. Chan, and M. Cheng. Vsc coordinated control of two manipulator arms in the presence of environmental constraints. *IEEE Transactions on Automatic Control*, 37(11):1806–1812, 1992.
- [169] B. Yao and M. Tomizuka. Adaptive robust motion and force tracking control of robot manipulators in contact with compliant surfaces with unknown stiffness. *ASME J. of Dynamic Systems, Measurement, and Control*, 120(2):232–240, 1998.
- [170] T. Yoshikawa. Force control of robot manipulators. In *Proceedings of IEEE International Conference on Robotics and Automation (ICRA)*, pages 220–226 vol.1, 2000.
- [171] T. Yoshikawa and A. Sudou. Dynamic hybrid position/force control of robot manipulators-on-line estimation of unknown constraint. *IEEE Transactions on Robotics and Automation*, 9(2):220–226, 1993.
- [172] V.I. Zubov. Systems of ordinary differential equations with generalized-homogeneous right-hand sides. *Izv. Vyssh. Uchebn. Zaved., Mat.*, 1958(1(2)):80–88, 1958.



# Samenvatting

Dit proefschrift behandelt twee belangrijke onderzoeksgebieden van robotica, namelijk interactie controle en tele-robotica. De interactie controle is bestudeerd in twee verschillende instellingen, waar een robot wordt gebruikt in de eerste een of meerdere robots worden gebruikt in het tweede. Dat laatste is ook wel bekend als de coöperatieve manipulatie probleem. Telebesturing systemen zijn een populair onderzoeksobject in de robotica gemeenschap voor tientallen jaren. Ze worden gebruikt in toepassingen die plaatsvinden in risicovolle omgevingen zoals kerncentrales voor verwijdering van nucleair afval, in ziekenhuizen voor uitvoering minimaal invasieve chirurgie, in de ruimte te kunnen repareren van orbitale modules. Onlangs, bij het snel vergrijzende samenleving is er ook een grotere inspanning op het gebied van de integratie robots in huishoudelijke omgevingen. Coöperatieve manipulatie, aan de andere kant gaat met taken zoals montage, transport van grote of zware voorwerpen die enkel manipulators waarschijnlijk niet uitvoeren.

Het probleem van eindige time interactie controletaken is gericht in het eerste deel van dit proefschrift. Gerobotiseerde taken zoals coöperatieve manipulatie bestaat uit meerdere sub-taken zoals benaderen van een bepaald object en vastpakken. Een geschikte referentie signaal is zodanig ontworpen dat elke fase voor het uitvoeren van de volledige taak. Goede maatregelen van prestaties voor de sub-taken zijn de convergentie snelheid van de werkelijke signalen naar de gewenste signalen en de uiteindelijke fout. Afhankelijk van de kenmerken van de gesloten-lus vergelijking, verschillende stabilisatietijden kan worden verkregen. Een specifiek geval is wanneer deze stabilisatietijd is eindig en dus de fout verdwijnt in eindige-tijd. Een dergelijke strategie kan nuttig zijn, omdat het garandeert dat de taak wordt uitgevoerd zoals het is opgedragen. Voor dit doel, een continue eindige-tijd stabiele werking tracking impedantie regelalgoritme wordt voorgesteld. De manipulator rotationele beweging wordt beschreven met behulp van een daarvoor geschikte quaternion vertegenwoordiging. Wanneer de omgeving kan worden gemodelleerd als een lineaire veer met onbekende constante stijfheid coëfficiënt en rust positie,

is onderzocht. De robuustheid van het algoritme tegen onzekerheden in de robot dynamische model wordt geanalyseerd.

In het tweede deel van het proefschrift, coöperatieve manipulatie van een stijf object behandeld door niet-redundante robots, starre links en niet-flexibele joints op een vaste basis, is onderzocht. Controle ontwerp voor dergelijke coöperatieve systemen ingewikkelder is in vergelijking met het bedienen van een enkel manipulator, omdat de wisselwerking tussen het object, manipulators, en de omgeving waar het object in aanraking komt, moeten eveneens in aanmerking worden genomen. Voor een veilige en succesvolle uitvoering van de taak, naast de bewegingsrichting van het object en neem contact op met krachten die veroorzaakt worden door de omgeving, de interne krachten die een goede maatregel van de mechanische belastingen, moet worden ondergebracht. Twee verschillende modellering methoden worden onderzocht. In de eerste methode de manipulators houdt het object via vaste contactpunten, waar er wordt aangenomen dat er geen relatieve beweging tussen het object en de manipulators. De tweede methode wordt rekening gehouden met de relatieve beweging tussen de manipulators en het object op de contactpunten. Een cascade-regelaar, bestaat uit motion control, interne en object impedantie regelkringen is ontworpen voor het eerste geval. Er zijn richtlijnen gegeven voor het afstemmen van de parameters van de interne en object impedantie relaties. Speciale aandacht is geschonken aan de uniciteit van de oplossingen van het gesloten-lus systeem onderzoeken zijn asymptotische stabiliteit.

Het laatste deel van dit proefschrift richt zich op tijdsvertraging compensatie en verstoring afwijzing in een veelgebruikte bilaterale tele-operatie architectuur. In een afstand bestuurbare scenario, de eigenlijke taak wordt uitgevoerd door een slave manipulator zich op een externe omgeving waar zij ontvangt opdrachten die afkomstig zijn van een menselijke operator via een communicatie kanaal. Hoewel tele-operatie is nuttig voor het verwijderen van de aanwezigheid van de operator uit de omgeving, komt met een prijs voor betalen. Aangezien de operator de opdrachten en signalen van het sensoren van de externe robot voor verbetering van zijn/haar bewustzijn worden doorgegeven door een communicatiekanaal, zij zouden worden onderworpen aan de tijdsvertraging. Tijdsvertragingen kunnen belemmeren de stabiliteit van de telerobotic systeem, als niet verantwoord in het ontwerp van de bediening. Voor dit doel, een prediction-based algoritme, dat is robuust met betrekking tot model onzekerheid en externe verstoringen, is ontworpen. Het ontwerp is gebaseerd op de combinatie van een intern model controle en interne model principe. Een pragmatische methode is toegepast in het ontwerp van lokaal controllers die gebaseerd is op frequentierespons functie metingen en een pool plaatsing methode. De methode is gevalideerd experimenteel op een setup bestaat uit twee industriële robots.

# Acknowledgements

After some years of hard work and constant struggle with textbooks, scientific articles and experimental setups, I can finally complete this book. Many people have contributed and supported me in this long and difficult quest without whom I wouldn't be able to accomplish this task. First and foremost, I express my deepest and most sincere gratitude to my parents and my sister. Tüm yaşantım boyunca manevi, maddi her türlü desteklerini sonuna kadar benim için kullanan, bugünlere gelmemde çok büyük emeği gegen ve hakkını asla ödeyemeyeceğim canım annem, babam ve sevgili ablama sonsuz teşekkür ederim.

Next, I would like to thank my promotor during the PhD, Professor Henk Nijmeijer. Dear Henk, I am grateful for your trust, constant encouragement, guidance, patience and valuable advice throughout this research. I enjoyed all our discussions and all our countless meetings.

I extend my gratitude to my co-supervisors Dragan Kostić and Alessandro Saccon. Dear Dragan, thanks for your guidance and valuable suggestions during the first half of my PhD research and during my graduation. I am grateful for your constant support and confidence in me. I have benefited greatly from your robotics and experimental knowledge. Dear Alessandro, I would like to thank you for your critical reading of my thesis. Despite the fact that we have only worked for a short period of time together, I appreciate your valuable input.

I would like to thank the professors that participated in the committee, Sandra Hirche, Michel Kinnaert, Kees van Hee and Frans van der Helm for their critical reading and evaluation of my thesis and for their valuable comments and feedback.

Regarding the setup used during the experiments, I want to thank the help of Peter Hamels, Pieter van Hoof and Harrie van de Loo for the fabrication of the probe and mechanical interface and the instrumentation for the force sensor. Furthermore, I would like to thank Bram de Jager for letting me use his experimental platform (RRR robot) to conduct experiments. I would like to thank Dennis Heck for our collaboration on cooperative manipulation. Likewise, I would also express my gratitude to Tom van Tilburg and Nathan van de Wouw for our collaboration on force sensorless haptic feedback. Finally, I acknowledge the collaboration with Jarno van Wijk on cooperative manipulation and Thomas Theunisse for helping with the experiments on time-delay compensation in bilateral teleoperation.

Regarding administrative matters I want to express my gratitude to Thea Weijers and Hetty van Neerven. Likewise, I would like to thank Geertje Janssen-Dols and Petra Aspers for always solving my administrative problems in a friendly way.

Thanks to all the colleagues at the Eindhoven University of Technology, in the D&C and CST groups, with whom we had chats at the coffee corner during many small breaks. Likewise, I would like to extend this gratitude towards Alejandro Alvarez, Sisfarmanto Adinandra, Eric van den Hoven, Roel Pieters, Alejandro Rodriguez-Angeles, Zhenyu Ye, America Morales, Haitao Xing, César López, Laura Guerrero, Erandi Miranda and Bahadır Saltık with whom we shared lunch and coffee breaks and other memorable times including outside the work environment. Special thanks goes to my former neighbor Hilal Karatoy and Alain Ayemlong Fokem who share their friendship with me beyond the scientific environment. Next in line are my office-mates, who are also my friends. Dear Carlos and Isaac, thanks for our many discussions, for stimulating conversations and for all the fun we had at practising sports. This also applies to my former roommates and friends Jonatán Peña Ramírez, Leonardo de Novellis, Behnam Asadi and Sinan Öncü. Dear Jonatán, thank you for the good times we spent together and for your funny jokes and all the nicknames you gave me (especially Edgar Sanchez). Dear Leonardo (Leo), thank you for all the memorable moments and being a selfless friend. I truly value the friendship of Engin Nisso Maçoro (Engin baba), Fredi Ferit Arditti (Ferdı baba) and Ender Aydoğmuş (Ender insan) from Turkey, Avi Cohen from Sweden and Özgür Can Çelik (Özgür insan) from Germany and feel myself very fortunate to know them.

My family has always played an important role for providing me encouragement especially at very difficult times to strive towards my goal. In this regard, I am deeply grateful to my aunt Lisette, to my uncle Zafer, to my cousins Yves and Alex and to their uncle Albert Scialom from Belgium. Furthermore, I want to extend this gratitude towards my cousins from France, Samson Alev and especially Professor Jacques Alev for his interest on my academic development during my PhD. Finally, I would like to thank all my cousins and other family members from Turkey who were there for me at difficult times.

Sevgili anne ne yazık ki bu doktora tezini bitirdiğimi göremeden aramızdan ayrıldın, fakat sen her zaman benim yanımda, aklımda ve de kalbimde olacaksın. Bu doktora tezini bu dünyaya gelmiş tanıdığım en fedakâr insan olan anneme adıyorum.

*Alper Denasi  
Eindhoven, The Netherlands  
January 20, 2015.*

# Curriculum Vitae

Alper Denasi was born on May 11<sup>th</sup>, 1984 in Istanbul, Turkey. In September 2002, he started his undergraduate education at Istanbul Technical University (ITU), Istanbul, Turkey. He received his Bachelor of Science degree in Mechanical Engineering in 2006. His B.Sc. graduation project entitled “Delta Robot, design and manufacturing of a pick and place robot” was awarded the best graduation project award in the Mechanical Engineering Department among all graduation projects in 2006. He continued his education at Eindhoven University of Technology, where he obtained a Master’s degree in Mechanical Engineering in 2009, specializing in dynamics and control. His master’s thesis was entitled “Programming of Robotic Manipulation Tasks By Demonstration”.

In May 2009, Alper started his PhD research in the Dynamics and Control group at the Department of Mechanical Engineering of Eindhoven University of Technology, working on force control, cooperative manipulators and teleoperation. The main results of his PhD research are presented in this dissertation.

